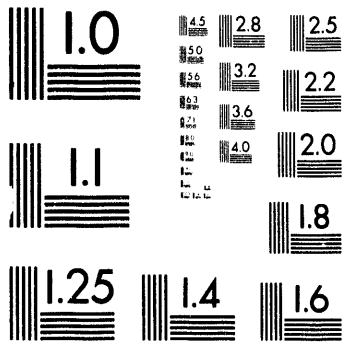
1.0
1.1
1.25
1.4
1.6
1.8
2.0
2.2
2.5
2.8
3.2
3.6
4.0
4.5
5.0
5.6
6.3
7.1
8.0
9.0

1 of 3

Distribution
Category UC-610

SAND93-1475
Unlimited Release
Printed October 1993

MELCOR 1.8.2 Assessment: IET Direct Containment Heating Tests

L. N. Kmetyk
Thermal/Hydraulic Analysis Department
Sandia National Laboratories
Albuquerque, NM 87185

Abstract

MELCOR is a fully integrated, engineering-level computer code, being developed at Sandia National Laboratories for the USNRC, that models the entire spectrum of severe accident phenomena in a unified framework for both BWRs and PWRs. As part of an ongoing assessment program, the MELCOR computer code has been used to analyze several of the IET direct containment heating experiments done at 1:10 linear scale in the Surtsey test facility at Sandia and at 1:40 linear scale in the corium-water thermal interactions (CWTI) COREXIT test facility at Argonne National Laboratory. These MELCOR calculations were done as an open post-test study, with both the experimental data and CONTAIN results available to guide the selection of code input.

Basecase MELCOR results are compared to test data in order to evaluate the new HPME DCH model recently added in MELCOR version 1.8.2. The effect of various user-input parameters in the HPME model, which define both the initial debris source and the subsequent debris interaction, were investigated in sensitivity studies. In addition, several other non-default input modelling changes involving other MELCOR code packages were required in our IET assessment analyses in order to reproduce the observed experiment behavior. Several calculations were done to identify whether any numeric effects exist in our DCH IET assessment analyses.

MASTER

DISTRIBUTION OF THIS DOCUMENT IS UNLIMITED

Contents

1 Introduction 1

2 Facility and Test Description 3

2.1 1:10 Linear Scale Surtsey DCH Test Facility 3

2.2 1:40 Linear Scale COREXIT/CWTI DCH Test Facility 12

3 MELCOR Computer Model 19

3.1 1:10-Scale Surtsey Test Facility MELCOR Model 19

3.2 1:40-Scale COREXIT Test Facility MELCOR Model 26

4 Reference Calculation Results 28

5 Experiment Uncertainty Studies 45

5.1 Steam Blowdown 45

5.2 Melt Injection Timing 48

5.3 Melt Injection Amount 51

5.4 Melt Injection Temperature 55

5.5 Melt Injection Distribution 55

6 DCH Modelling Studies 67

6.1 Airborne Debris Oxidation Characteristic Time 67

6.2 Airborne Debris Heat Transfer Characteristic Time 70

6.3 Airborne Debris Settling Characteristic Time 75

6.4 Deposited Debris Oxidation Characteristic Time 75

6.5 Deposited Debris Heat Transfer Coefficient 80

7 Other Modelling Studies 86

7.1 Hydrogen Combustion 86

7.2 Heat Transfer to Structures 90

7.3 Recirculation Flow 95

8 Scaling Sensitivity Study 104

8.1 Facility and Data Scaling Background Discussion 104

8.2 Scaling Facility Geometry and Test Conditions 109

8.3 Scaling Characteristic Interaction Times 111

8.4 Varying Hydrogen Combustion Parameters 119

8.5 Varying Convective Heat Transfer 120

8.6 Varying Recirculation Flow 123
9 Time Step Effects and Machine Dependency 127
9.1 Machine Dependencies 127
9.2 Time Step Effects 127
10 Comparison to CONTAIN 139
11 Code Problems Identified 144
11.1 Debris Material and Source Input 144
11.2 Debris Interaction with Structures 145
11.3 Hydrogen Combustion during DCH 145
11.4 Additional Output 146
11.5 Debris Heat Transfer 146
11.6 Cavity Condensate Water 148
12 Summary and Conclusions 149
Bibliography 157
A MELCOR FDI package HPME/DCH Model 161
B SNL/IET-1 Reference Calculation Input Deck 169

List of Figures

2.1.1 Surtsey Vessel, HPME Ejection System and Instrumentation Ports Used in the SNL/IET Experiments 4

2.1.2 HPME Ejection System (High-Pressure Steam Boiler, Steam Accumulator, Melt Generator), Cavity and Instrument Chute Used in the SNL IET Experiments 5

2.1.3 Cross-Sectional View of Subcompartments in Surtsey Vessel Used in the SNL/IET Experiments 6

2.1.4 Isometric View of Subcompartments in Surtsey Vessel Used in the SNL/IET Experiments 7

2.2.1 COREXIT Facility Used in the ANL/IET Experiments 13

2.2.2 HPME System, Cavity and Instrument Chute Used in the ANL/IET Experiments 14

2.2.3 Cross-Sectional Views of Subcompartments in ANL Vessel Used in the ANL/IET Experiments 15

3.1.1 Reference MELCOR Model for SNL/IET Experiment Analyses 20

4.1 Aluminum and Fe/Cr Masses Oxidized, and Oxygen and Steam Masses Reacted for SNL/IET Experiments – Reference Calculation 29

4.2 Hydrogen Production for SNL/IET Experiments – Reference Calculation . 32

4.3 Hydrogen Combustion for SNL/IET Experiments – Reference Calculation 33

4.4 Hydrogen Mole Fractions in the Subcompartments and Dome for SNL/IET Experiments – Reference Calculation 35

4.5 Oxygen Mole Fractions in the Subcompartments and Dome for SNL/IET Experiments – Reference Calculation 36

4.6 Vessel Pressures for SNL/IET Experiments – Reference Calculation 39

4.7 Subcompartment Temperatures for Experiments SNL/IET-1, SNL/IET-1R and SNL/IET-5 – Reference Calculation 41

4.8 Subcompartment Temperatures for Experiments SNL/IET-3, SNL/IET-4, SNL/IET-6 and SNL/IET-7 – Reference Calculation 42

4.9 Dome Temperatures for Experiments SNL/IET-1 and SNL/IET-5 – Reference Calculation 43

4.10 Dome Temperatures for Experiments SNL/IET-3, SNL/IET-4, SNL/IET-6 and SNL/IET-7 – Reference Calculation 44

5.1.1 Steam Accumulator Pressures for SNL/IET Experiments Using Valve Opening Times of 0.5s, 1s, 2s and 4s – Steam Blowdown Sensitivity Study . . . 46

5.1.2 Vessel Pressures for SNL/IET Experiments Using Valve Opening Times of 0.5s, 1s, 2s and 4s – Steam Blowdown Sensitivity Study 47

5.2.1 Vessel Pressures for SNL/IET Experiments Using Melt Injection Times of 0.1s, 0.5s, 1s and 2.5s – Melt Injection Timing Sensitivity Study 50

5.2.2 Subcompartment Temperatures for SNL/IET Experiments Using Melt Injection Times of 0.1s, 0.5s, 1s and 2.5s – Melt Injection Timing Sensitivity Study 53

5.3.1 Vessel Pressures for SNL/IET Experiments Using Melt Masses of 80%, 90%, 100% and 110% the Initial Charge – Melt Injection Amount Sensitivity Study 56

5.3.2 Subcompartment Temperatures for SNL/IET Experiments Using Melt Masses of 80%, 90%, 100% and 110% the Initial Charge – Melt Injection Amount Sensitivity Study 58

5.4.1 Vessel Pressures for SNL/IET Experiments Using Melt Temperatures of 2000K, 2300K, 2500K and 3000K – Melt Temperature Sensitivity Study . 59

5.4.2 Subcompartment Temperatures for SNL/IET Experiments Using Melt Temperatures of 2000K, 2300K, 2500K and 3000K – Melt Temperature Sensitivity Study 61

5.5.1 Vessel Pressures for SNL/IET Experiments Using Basecase Melt Distribution, Experimental Melt Distribution, Melt Mostly into Cavity and Melt Mostly into Dome – Melt Distribution Sensitivity Study 64

5.5.2 Subcompartment Temperatures for SNL/IET Experiments Using Basecase Melt Distribution, Experimental Melt Distribution, Melt Mostly into Cavity and Melt Mostly into Dome – Melt Distribution Sensitivity Study 66

6.1.1 Vessel Pressures for SNL/IET Experiments Using Airborne Debris Characteristic Oxidation Times of 0.5s, 0.1s, 0.05s and 0.01s – Airborne Debris Oxidation Characteristic Time Sensitivity Study 68

6.1.2 Subcompartment Temperatures for SNL/IET Experiments Using Airborne Debris Oxidation Characteristic Times of 0.5s, 0.1s, 0.05s and 0.01s – Airborne Debris Oxidation Characteristic Time Sensitivity Study 71

6.2.1 Vessel Pressures for SNL/IET Experiments Using Airborne Debris Characteristic Heat Transfer Times of 1s, 0.5s, 0.25s and 0.1s – Airborne Debris Heat Transfer Characteristic Time Sensitivity Study 72

6.2.2 Subcompartment Temperatures for SNL/IET Experiments Using Airborne Debris Characteristic Heat Transfer Times of 1s, 0.5s, 0.25s and 0.1s – Airborne Debris Heat Transfer Characteristic Time Sensitivity Study . . . 74

6.3.1 Vessel Pressures for SNL/IET Experiments Using Airborne Debris Characteristic Settling Times of 1s, 0.5s, 0.25s and 0.1s – Airborne Debris Settling Characteristic Time Sensitivity Study 76

6.3.2 Subcompartment Temperatures for SNL/IET Experiments Using Airborne Debris Characteristic Settling Times of 1s, 0.5s, 0.25s and 0.1s – Airborne Debris Settling Heat Transfer Characteristic Time Sensitivity Study 78

6.4.1 Vessel Pressures for SNL/IET Experiments Using Deposited Debris Characteristic Oxidation Times of 10s, 60s, 600s and 1800s – Deposited Debris Oxidation Characteristic Time Sensitivity Study 79

6.4.2 Subcompartment Temperatures for SNL/IET Experiments Using Deposited Debris Characteristic Oxidation Times of 10s, 60s, 600s and 1800s – Deposited Debris Oxidation Characteristic Time Sensitivity Study 82

6.5.1 Vessel Pressures for SNL/IET Experiments Using Deposited Debris Heat Transfer Coefficient of 1w/m^2-K, 10w/m^2-K, 100w/m^2-K and 1000w/m^2-K – Deposited Debris Heat Transfer Coefficient Sensitivity Study 83

6.5.2 Subcompartment Temperatures for SNL/IET Experiments Using Deposited Debris Heat Transfer Coefficient of 1w/m^2-K, 10w/m^2-K, 100w/m^2-K and 1000w/m^2-K – Deposited Debris Heat Transfer Coefficient Sensitivity Study 85

7.1.1 Vessel Pressures for SNL/IET Experiments with Default Burn Parameters, Basecase with Burn in the Dome Only with Zero Ignition Limit and Combustion Completeness of 0, with Burn in all Volumes with Zero Ignition Limit and Combustion Completeness of 0 and with Burn in the Dome Only with Zero Ignition Limit but Combustion Completeness of 1 – Hydrogen Combustion Sensitivity Study 87

7.1.2 Subcompartment Temperatures for SNL/IET Experiments with Default Burn Parameters, Basecase with Burn in the Dome Only with Zero Ignition Limit and Combustion Completeness of 0, with Burn in all Volumes with Zero Ignition Limit and Combustion Completeness of 0 and with Burn in the Dome Only with Zero Ignition Limit but Combustion Completeness of 1 – Hydrogen Combustion Sensitivity Study 89

7.2.1 Subcompartment Atmosphere-to-Structure Heat Transfer Coefficients for SNL/IET Experiments Using Default Volume Flow Areas/Velocities – Convective Heat Transfer Sensitivity Study 92

7.2.2 Subcompartment Atmosphere-to-Structure Heat Transfer Coefficients for SNL/IET Experiments Using Default Volume Flow Areas/Velocities, 0.1 × Volume Flow Areas, 0.01 × Volume Flow Areas and 0.001 × Volume Flow Areas – Convective Heat Transfer Sensitivity Study 94

7.2.3 Vessel Pressures for SNL/IET Experiments Using Default Volume Flow Areas/Velocities, 0.1 × Volume Flow Areas, 0.01 × Volume Flow Areas and 0.001 × Volume Flow Areas – Convective Heat Transfer Sensitivity Study 96

7.2.4 Subcompartment Temperatures for SNL/IET Experiments Using Default Volume Flow Areas/Velocities, 0.1 × Volume Flow Areas, 0.01 × Volume Flow Areas and 0.001 × Volume Flow Areas – Convective Heat Transfer Sensitivity Study 98

7.3.1 Vessel Pressures for SNL/IET Experiments for No Recirculation, 0.1 × Basecase, Basecase and 10 × Basecase – Recirculation Flow Sensitivity Study 99

7.3.2 Flows into and out of the Vessel Dome and Dome Inside Surface Heat Transfer Coefficients for SNL/IET Experiments for Basecase and 10 × Basecase – Recirculation Flow Sensitivity Study 101

7.3.3 Subcompartment Temperatures for SNL/IET Experiments for No Recirculation, 0.1 × Basecase, Basecase and 10 × Basecase – Recirculation Flow Sensitivity Study 103

8.1.1 Scaled, Measured Steam Accumulator Pressures for SNL and ANL Counterpart IET Experiments – Scaling Study 107

8.1.2 Scaled, Measured Vessel Pressures for SNL and ANL Counterpart IET Experiments – Scaling Study 108

8.2.1 Scaled Vessel Pressures for SNL and ANL Counterpart IET Experiments – Scaling Facility Geometry and Test Conditions 112

8.3.1 Scaled Vessel Pressures for SNL and ANL Counterpart IET Experiments – Scaling Airborne-Debris Settling Characteristic Interaction Times 113

8.3.2 Scaled Vessel Pressures for SNL and ANL Counterpart IET Experiments – Scaling Airborne-Debris Oxidation and Settling Characteristic Interaction Times 115

8.3.3 Scaled Vessel Pressures for SNL and ANL Counterpart IET Experiments – Scaling Airborne-Debris Heat Transfer and Settling Characteristic Interaction Times 116

8.3.4 Scaled Vessel Pressures for SNL and ANL Counterpart IET Experiments – Scaling All Characteristic Interaction Times 117

8.4.1 Scaled Vessel Pressures for SNL and ANL Counterpart IET Experiments Using Hydrogen Mole Fraction Ignition Limits of 0.01, 0.02, 0.03 and 0.04 for the ANL Experiment Simulations – Varying Hydrogen Combustion Parameters 121

8.5.1 Scaled Vessel Pressures for SNL and ANL Counterpart IET Experiments – Varying Convective Heat Transfer 124

8.6.1 Scaled Vessel Pressures for SNL and ANL Counterpart IET Experiments – Increasing and Reducing Recirculation Flow 126

9.1.1 Vessel Pressures for Experiments SNL/IET-1, SNL/IET-1R and SNL/IET-5 – Machine Dependency Sensitivity Study 128

9.1.2 Vessel Pressures for Experiments SNL/IET-3, SNL/IET-4, SNL/IET-6 and SNL/IET-7 – Machine Dependency Sensitivity Study 129

9.1.3 Total Run Times and Time Step Histories for SNL/IET-1 and SNL/IET-6 Experiment Analyses – Machine Dependency Sensitivity Study 131

9.2.1 Vessel Pressures for Experiments SNL/IET-1, SNL/IET-1R and SNL/IET-5 – Time Step Sensitivity Study 133

9.2.2 Vessel Pressures for Experiments SNL/IET-3, SNL/IET-4, SNL/IET-6 and SNL/IET-7 – Time Step Sensitivity Study 134

9.2.3 Hydrogen Combustion for Experiments SNL/IET-3, SNL/IET-4, SNL/IET-6 and SNL/IET-7 – Time Step Sensitivity Study 136

9.2.4 Total Run Times and Time Step Histories for SNL/IET-1 and SNL/IET-1R Experiment Analyses – Time Step Sensitivity Study 137

9.2.5 Total Run Times and Time Step Histories for SNL/IET-6 and SNL/IET-7 Experiment Analyses – Time Step Sensitivity Study 138

List of Tables

2.1.1 Common Initial Conditions for the SNL/IET Experiments 9

2.1.2 Individual Experiment Initial Conditions for the SNL/IET Experiments . 9

2.1.3 Debris Masses Recovered for the SNL/IET Experiments 11

2.1.4 Results Summary for the SNL/IET Experiments 11

2.2.1 Common Initial Conditions for the ANL/IET Experiments 17

2.2.2 Individual Experiment Initial Conditions for the ANL/IET Experiments . 17

2.2.3 Debris Masses Recovered for the ANL/IET Experiments 18

2.2.4 Results Summary for the ANL/IET Experiments 18

3.1.1 MELCOR FDI/HPME Debris Input Parameters Used for the SNL/IET Experiments 23

3.1.2 Characteristic Interaction Times Used in Reference MELCOR Model for SNL IET Experiment Analyses 24

4.1 Calculated HPME/DCH Mass Results Summary for the SNL/IET Experiments – Reference Calculation 31

4.2 Calculated Hydrogen Results Summary for the SNL/IET Experiments – Reference Calculation 31

4.3 Hydrogen Results for the SNL/IET Experiments – Reference Calculation . 38

4.4 Peak Pressures for the SNL/IET Experiments – Reference Calculation . . 38

5.1.1 Hydrogen Generation for the SNL/IET Experiments – Steam Blowdown Sensitivity Study 49

5.1.2 Hydrogen Combustion for the SNL/IET Experiments – Steam Blowdown Sensitivity Study 49

5.2.1 Hydrogen Generation for the SNL/IET Experiments – Melt Injection Timing Sensitivity Study 52

5.2.2 Hydrogen Combustion for the SNL/IET Experiments – Melt Injection Timing Sensitivity Study 52

5.3.1 Debris Masses for the SNL/IET Experiments – Melt Injection Amount Sensitivity Study 54

5.3.2 Hydrogen Generation for the SNL/IET Experiments – Melt Injection Amount Sensitivity Study 57

5.3.3 Hydrogen Combustion for the SNL/IET Experiments – Melt Injection Amount Sensitivity Study 57

5.4.1 Hydrogen Generation for the SNL/IET Experiments – Melt Temperature Sensitivity Study 60

5.4.2 Hydrogen Combustion for the SNL/IET Experiments – Melt Temperature Sensitivity Study 60
5.5.1 Debris Masses for the SNL/IET Experiments – Debris Distribution Sensitivity Study 62
5.5.2 Hydrogen Generation for the SNL/IET Experiments – Melt Distribution Sensitivity Study 65
5.5.3 Hydrogen Combustion for the SNL/IET Experiments – Melt Distribution Sensitivity Study 65
6.1.1 Hydrogen Generation for the SNL/IET Experiments – Airborne Debris Oxidation Characteristic Time Sensitivity Study 69
6.1.2 Hydrogen Combustion for the SNL/IET Experiments – Airborne Debris Oxidation Characteristic Time Sensitivity Study 69
6.2.1 Hydrogen Generation for the SNL/IET Experiments – Airborne Debris Heat Transfer Characteristic Time Sensitivity Study 73
6.2.2 Hydrogen Combustion for the SNL/IET Experiments – Airborne Debris Heat Transfer Characteristic Time Sensitivity Study 73
6.3.1 Hydrogen Generation for the SNL/IET Experiments – Airborne Debris Settling Characteristic Time Sensitivity Study 77
6.3.2 Hydrogen Combustion for the SNL/IET Experiments – Airborne Debris Settling Characteristic Time Sensitivity Study 77
6.4.1 Hydrogen Generation for the SNL/IET Experiments – Deposited Debris Oxidation Characteristic Time Sensitivity Study 81
6.4.2 Hydrogen Combustion for the SNL/IET Experiments – Deposited Debris Oxidation Characteristic Time Sensitivity Study 81
6.5.1 Hydrogen Generation for the SNL/IET Experiments – Deposited Debris Heat Transfer Coefficient Sensitivity Study 84
6.5.2 Hydrogen Combustion for the SNL/IET Experiments – Deposited Debris Heat Transfer Coefficient Sensitivity Study 84
7.1.1 Hydrogen Generation for the SNL/IET Experiments – Hydrogen Combustion Sensitivity Study 88
7.1.2 Hydrogen Combustion for the SNL/IET Experiments – Hydrogen Combustion Sensitivity Study 88
7.2.1 Hydrogen Generation for the SNL/IET Experiments – Convective Heat Transfer Sensitivity Study 97
7.2.2 Hydrogen Combustion for the SNL/IET Experiments – Convective Heat Transfer Sensitivity Study 97
7.3.1 Hydrogen Generation for the SNL/IET Experiments – Recirculation Flow Sensitivity Study 102

7.3.2 Hydrogen Combustion for the SNL/IET Experiments – Recirculation Flow Sensitivity Study 102
8.1.1 Facility Scaling for the SNL and ANL IET Experiments 106
8.1.2 Scaled, Measured Hydrogen Generation for SNL and ANL Counterpart IET Experiments – Scaling Study 110
8.1.3 Scaled, Measured Hydrogen Combustion for SNL and ANL Counterpart IET Experiments – Scaling Study 110
8.3.1 Hydrogen Generation for the ANL/IET Experiments – Scaling Facility Geometry and Test Conditions, and Characteristic Interaction Times 118
8.3.2 Hydrogen Combustion for the ANL/IET Experiments – Scaling Facility Geometry and Test Conditions, and Characteristic Interaction Times . . . 118
8.4.1 Hydrogen Generation for the ANL/IET Experiments – Varying Hydrogen Combustion Parameters 122
8.4.2 Hydrogen Combustion for the ANL/IET Experiments – Varying Hydrogen Combustion Parameters 122
9.1.1 Hydrogen Generation for the SNL/IET Experiments – Machine Dependency Sensitivity Study 130
9.1.2 Machine Dependency for the SNL/IET Experiments – Machine Dependency Sensitivity Study 130
9.2.1 Hydrogen Generation for the SNL/IET Experiments – Time Step Sensitivity Study 135
9.2.2 Hydrogen Combustion for the SNL/IET Experiments – Time Step Sensitivity Study 135
10.1 Peak Pressures for the SNL/IET Experiments – Code Comparison Study . 140
10.2 Hydrogen Generation for the SNL/IET Experiments – Code Comparison Study 141
10.3 Hydrogen Combustion for the SNL/IET Experiments – Code Comparison Study 142

Acknowledgements

The author would like to acknowledge a number of individuals who contributed significantly to this report. Mike Allen and the other experimenters provided high-quality, rapid and extensive documentation of the Sandia IET experiment results. Russ Smith of the MELCOR development team helped with both input model setup and code problem diagnosis and correction. Sam Thompson provided the code on various platforms on demand and friendly plot programs. Dave Williams and Richard Griffith provided information on the CONTAIN model and calculations, and Dave Williams provided copies of the ANL test data letter reports and the CONTAIN analysis letter reports. Susan Dingman and Dave Williams helped with interpretation of the results in many fruitful and informative discussions. Russ Smith and Dave Williams provided the final, formal technical review, which resulted in a large number of improvements and clarifications to the text; Sam Thompson, Randy Summers, Susan Dingman and Dr. Sud Basu of the NRC also reviewed the report and suggested a number of additional improvements, all of which were incorporated in the final product.

This work was funded by the Office of Research, U. S. Nuclear Regulatory Commission.

1 Introduction

MELCOR [1] is a fully integrated, engineering-level computer code, being developed at Sandia National Laboratories for the U. S. Nuclear Regulatory Commission (USNRC), that models the progression of severe accidents in light water reactor (LWR) nuclear power plants. The entire spectrum of severe accident phenomena, including reactor coolant system and containment thermal/hydraulic response, core heatup, degradation and relocation, and fission product release and transport, is treated in MELCOR in a unified framework for both boiling water reactors and pressurized water reactors.

The MELCOR computer code has been developed to the point that it is now being successfully applied in severe accident analyses. Some limited technical assessment activities were performed early in the MELCOR development process [2]; more recently, a more extensive, systematic program of verification and validation has been underway. To this end, a number of assessment calculations have been and are being done [3-9]. One of these assessment activities is analysis of some of the IET direct containment heating experiments done at 1:10 linear scale in the Surtsey test facility at Sandia [10-17] and at 1:40 linear scale in the corium-water thermal interactions (CWTI) test facility at Argonne National Laboratory (ANL) [18-24], to evaluate the new high-pressure melt ejection (HPME) direct containment heating (DCH) model [25] added to the Fuel Dispersal Interactions (FDI) package [26] in MELCOR 1.8.2. This report documents the results of those analyses. (This report assumes familiarity with the MELCOR FDI/HPME/DCH model, its terminology and modelling assumptions, and its input requirements. A brief description of the model, excerpted from [26], is included in Appendix A for the convenience of interested readers.)

Our original intent was to model three of the Sandia Surtsey experiments (SNL/IET-1, SNL/IET-3 and SNL/IET-6), together with one of the ANL counterpart experiments (ANL/IET-6). These particular tests were chosen to provide a base case (SNL/IET-1), to investigate the effects of hydrogen combustion in the presence of pre-existing oxygen (SNL/IET-3) and also pre-existing hydrogen (IET-6), and to investigate the effects of scaling (ANL/IET-6 at ANL). After we began work, we soon expanded our plans to include most of the Sandia Surtsey experiments (adding SNL/IET-1R, SNL/IET-4, SNL/IET-5 and SNL/IET-7) and the rest of the ANL counterpart experiments (ANL/IET-1RR and ANL/IET-3). This was done because the controlled variations done by the experimentalists in these tests (presence *vs* absence of pre-existing hydrogen and presence *vs* absence of basement condensate water) made little difference and required minor input changes, while the range of final melt distributions (*i.e.*, amounts of debris collected in various locations in the containment) observed in the tests created a significant uncertainty in specification of the MELCOR debris source. We chose to use reasonable, representative values for the debris mass and distribution for the Surtsey IET experiments, and address the variation in both total mass and distribution through sensitivity studies and analyses of more experiments.

We did not look at SNL/IET-2 in Surtsey because that was a set of separate-effects experiments on debris temperature measurements. We did not consider analyzing

SNL/IET-8 and SNL/IET-8B in Surtsey because this test pair involved significantly different phenomena due to the cavity being half filled with water. We did not consider any of the more recent Sandia IET experiments (SNL/IET-9 and SNL/IET-10) because they were done in a different facility at a different scale and for a different plant configuration, thus requiring major input modifications. We did not consider any of the early ANL tests (ANL/IET-1 and ANL/IET-1R) because of problems in the experimental procedure affecting steam/debris blowdown timing; we did not consider any of the later ANL tests (ANL/IET-7 and ANL/IET-8 which investigated variations initial atmosphere conditions and most recently U1A, U1B and U2 which evaluated the effects of using corium *vs* thermite melts) because of the different phenomena and more substantial input modifications required.

MELCOR version 1.8NN was used for all the calculations described in this report. (The release version of MELCOR 1.8.2 was MELCOR 1.8NM. The changes between the release version and version 1.8NN are discussed briefly in Section 11.) Note that these MELCOR calculations were done as an open post-test study, with both the experimental data and CONTAIN results [27-33] available to guide the selection of code input.

The Surtsey and CWTI test facilities, experimental configurations and experimental procedures are outlined in Section 2. Section 3 describes the input used for these MELCOR assessment analyses. The results of our reference calculations are given in Section 4. Sensitivity studies on the high-pressure melt ejection model in MELCOR are presented in Sections 5 and 6, on user-input parameters controlling the initial debris source and the subsequent debris interaction, respectively; sensitivity studies on other MELCOR models affecting direct containment heating are given in Section 7. Results from a scaling study using the 1:40-scale ANL tests are presented in Section 8. Section 9 contains the results of our time step and machine dependency sensitivity studies. Comparison with results obtained by CONTAIN is done in Section 10. Section 11 summarizes the code and modelling problems identified during these assessment analyses. The conclusions of this MELCOR assessment study are presented in Section 12. A brief description of the MELCOR FDI/HPME/DCH model is included in Appendix A, and a listing of the input used for the Surtsey IET-1 reference calculation is given in Appendix B.

2 Facility and Test Description

2.1 1:10 Linear Scale Surtsey DCH Test Facility

The Surtsey Test facility at Sandia is used to perform scaled experiments that simulate high-pressure melt ejection (HPME) in a nuclear power plant, investigating the phenomena associated with direct containment heating (DCH). In these tests, high-temperature, chemically reactive melt is ejected by high-pressure steam into a 1:10 linear scale model of a reactor cavity. Debris is entrained by the steam blowdown into the Surtsey vessel where specific phenomena, such as the effect of subcompartment structures, water in the cavity, and hydrogen generation and combustion, can be studied.

Figure 2.1.1 gives a composite view of the Surtsey vessel, the HPME delivery system, and the instrument penetration ports at six levels in the Surtsey vessel. A more detailed view of the HPME delivery system and of the cavity and instrument chute for these IET experiments is presented in Figure 2.1.2. (The circled numbers in these and following figures correspond to channel numbers in the data acquisition system. That experimental data identification is not used in this report; therefore, those circled numbers are not identified or discussed further.)

In the Surtsey IET tests [10-17], 1:10 linear scale models of the Zion reactor pressure vessel (RPV), cavity, in-core instrument tunnel, and subcompartment structures were used. The RPV was modelled with a melt generator that consisted of a steel pressure barrier, a cast MgO crucible, and a thin steel liner. The melt-generator/crucible had a hemispherical bottom head containing a graphite limiter plate with a 4cm exit hole to simulate the ablated hole in the RPV bottom head that would be formed by ejection of an instrument guide tube and subsequent hole ablation in a severe accident.

The cavity used was a 1:10 linear scale model of the Zion reactor cavity. The inclined portion of the instrument tunnel entered the bottom head of Surtsey at a 26° incline from vertical, as it does in Zion. A false concrete floor was constructed in the Surtsey vessel similar to the floor of the Zion basement so that the inclined portion of the instrument tunnel was ~2.7 times the correct scaled length of the Zion instrument tunnel exit. (This floor was constructed in Surtsey to match the configuration of the ANL facility, described in the next subsection.)

The subcompartment structures, shown in cross-section in Figure 2.1.3 and illustrated schematically in Figure 2.1.4, included 1:10 linear scale models of the crane wall, four steam generators, four reactor coolant pumps (RCPs), the opening in the floor of the seal table room for the instrument guide tubes, the seal table room, the biological shield, the refueling canal, the radial beams and the gratings at the RCP deck, and the operating deck. The steam generators, RCPs and gratings were made of steel, and the other structures were constructed of reinforced concrete. All of the structures were painted with an epoxy-base paint.

In the majority of the IET experiments, the steam accumulator tank was pressurized with superheated steam. After the pressurization sequence, the iron-oxide/aluminum/-

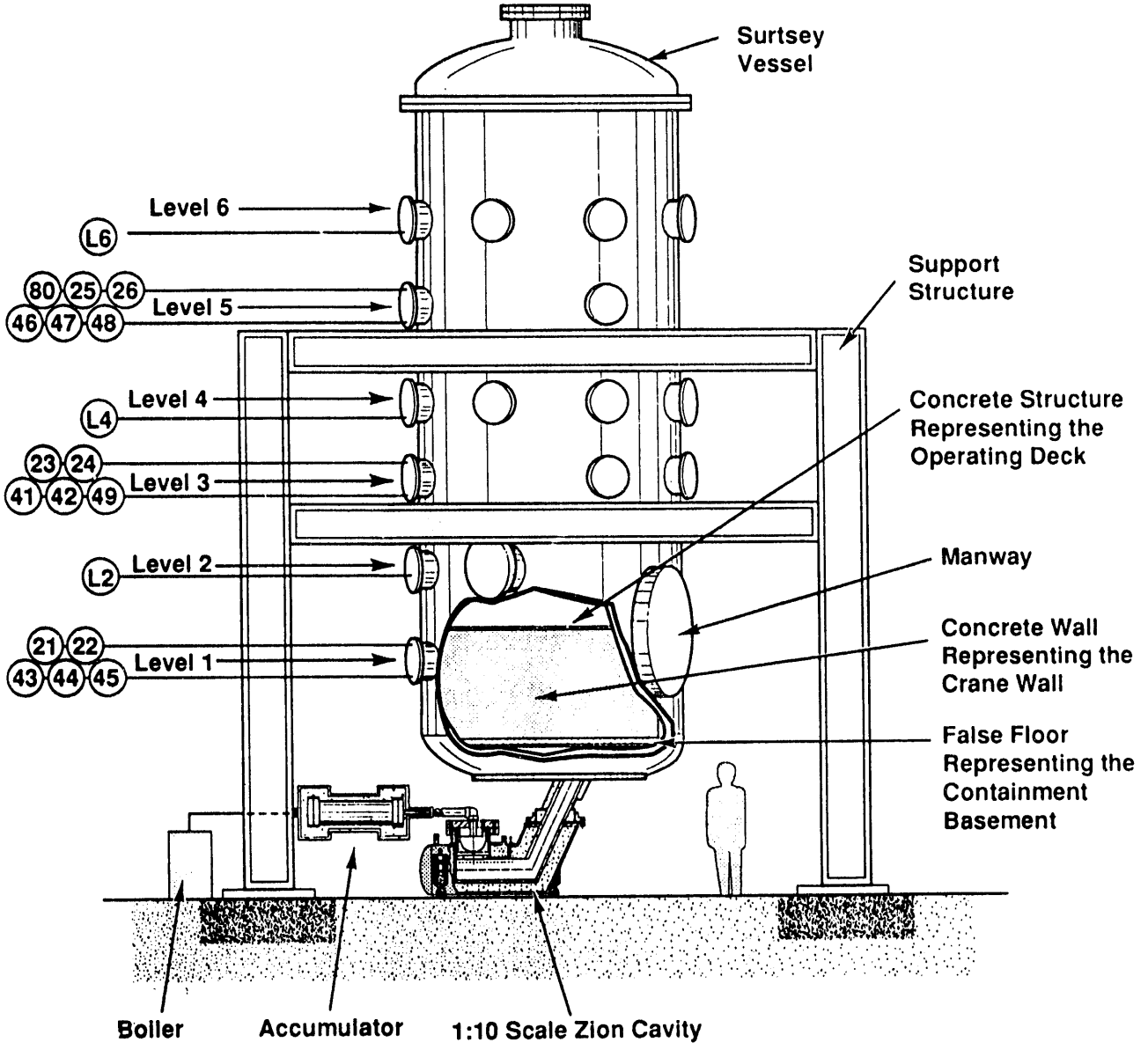

Note: All pressure transducers have individual penetrations.

Figure 2.1.1. Surtsey Vessel, HPME Ejection System and Instrumentation Ports Used in the SNL/IET Experiments (from [10])

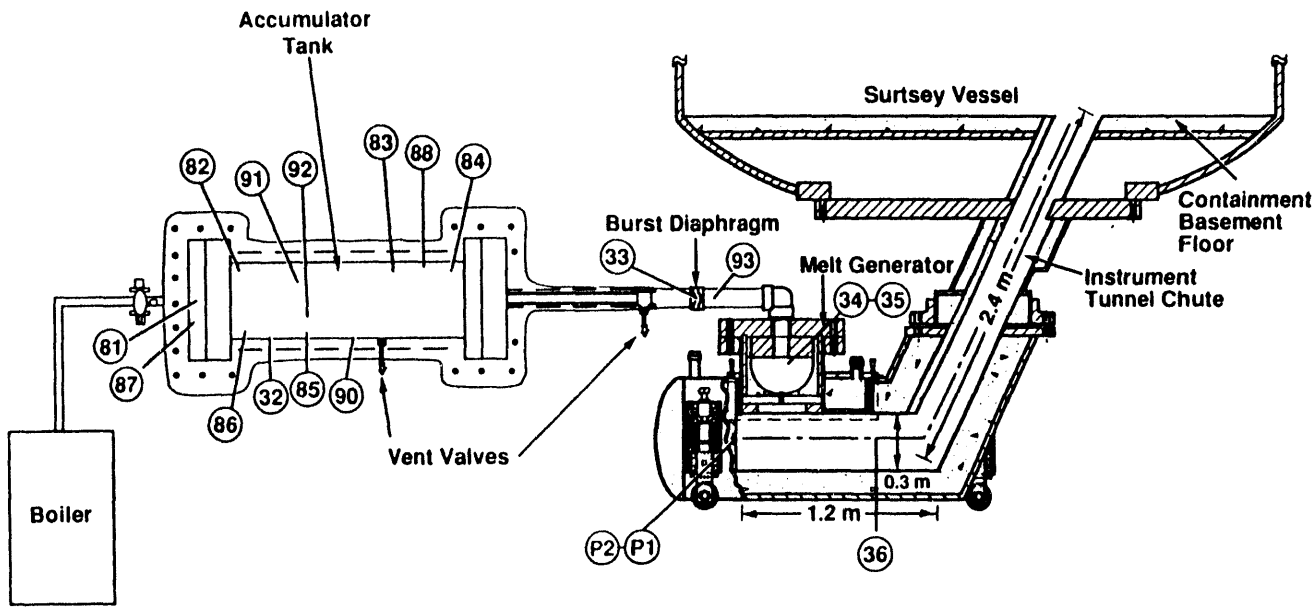

Figure 2.1.2. HPME Ejection System (High-Pressure Steam Boiler, Steam Accumulator, Melt Generator), Cavity and Instrument Chute Used in the SNL IET Experiments (from [10])

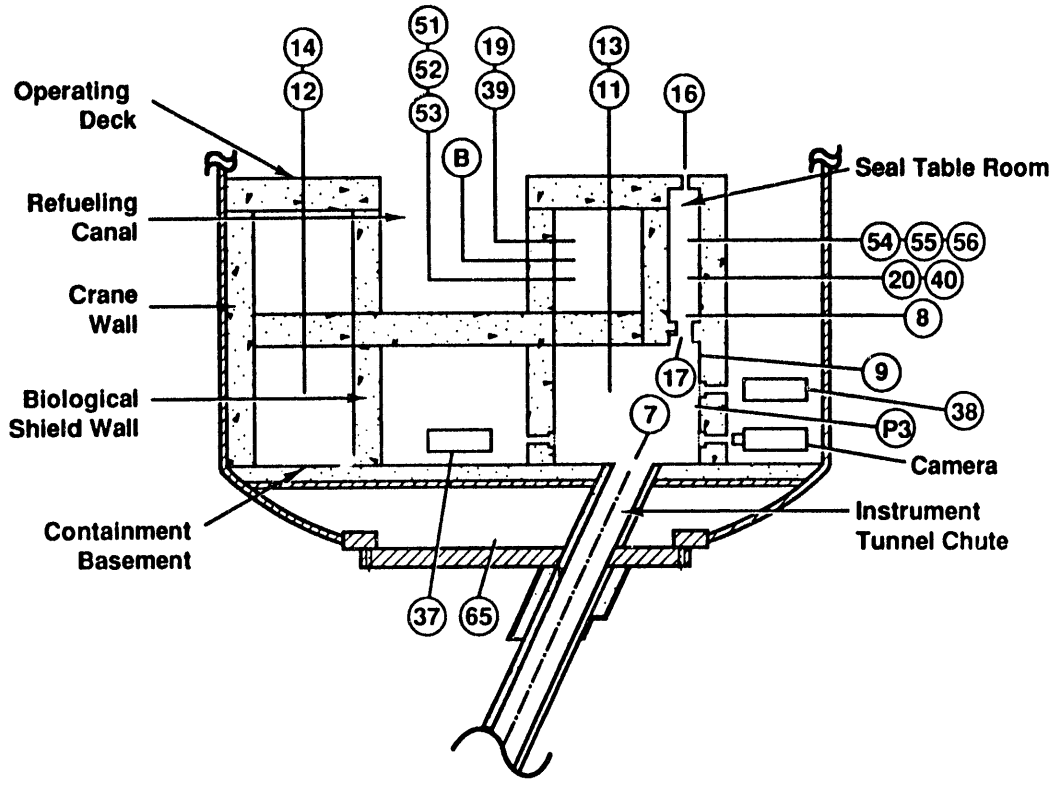

Figure 2.1.3. Cross-Sectional View of Subcompartments in Surtsey Vessel Used in the SNL/IET Experiments (from [10])

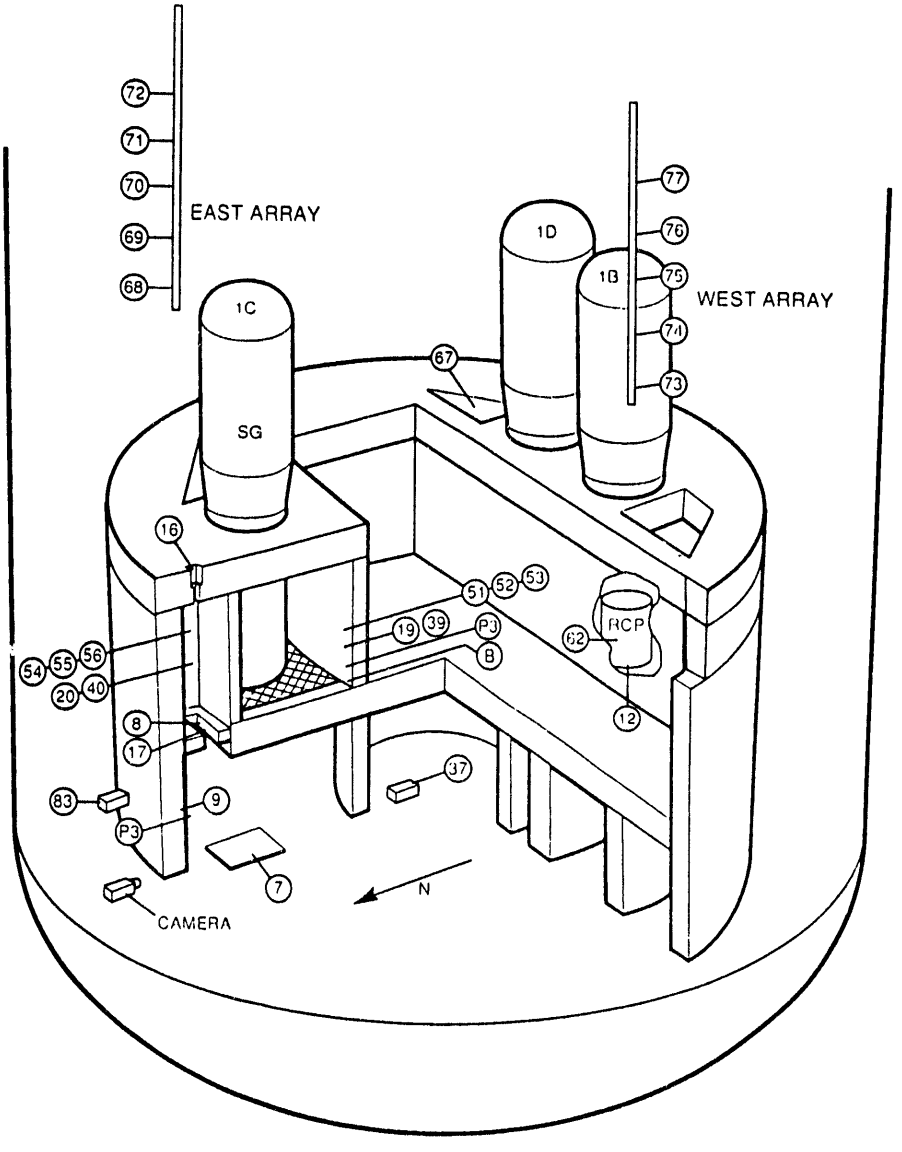

Figure 2.1.4. Isometric View of Subcompartments in Surtsey Vessel Used in the SNL/IET Experiments (from [10])

chromium thermite mixture was ignited remotely. After the thermite was ignited, the pressure in the crucible rapidly increased, verifying that the thermite reaction had started and signalling the operator to fail the burst diaphragm separating the steam accumulator tank and the molten thermite in the melt generator, bringing superheated steam into contact with the molten thermite. Zero time for the HPME experiments was set at the time at which the melt in the crucible failed a fusible brass plug at the bottom of the crucible and was expelled by high-pressure steam into the cavity.

A series of experiments were done investigating the effects of high pressure melt ejection on direct containment heating:

1. Test SNL/IET-1 was the baseline test, while test SNL/IET-1R was a replicate test investigating experiment reproducability [10].

2. Test(s) SNL/IET-2A, SNL/IET-2B and SNL/IET-2C [11] were a set of separate-effects experiments performed to measure the temperature of molten thermite as it exited the melt generator.

3. Test SNL/IET-3 replicated test SNL/IET-1 except the vessel contained a mixture of air and nitrogen [12]; no steam explosion occurred in SNL/IET-3 as it had in SNL/IET-1, but instead there was a vigorous hydrogen burn.

4. Test SNL/IET-4 [13] replicated test SNL/IET-3 except the Surtsey vessel contained slightly more pre-existing oxygen and water was placed on the basement floor inside the crane wall.

5. Test SNL/IET-5 conditions were similar to those in SNL/IET-4, except the vessel atmosphere was classically inert [14], with CO_2 used to suppress hydrogen combustion,

6. Test SNL/IET-6 initial conditions [15] were similar to those in SNL/IET-3, except the vessel atmosphere contained pre-existing hydrogen to represent partial oxidation of the zirconium in the core.

7. Test SNL/IET-7 initial conditions were similar to those in SNL/IET-4, except the vessel atmosphere contained pre-existing hydrogen to represent partial oxidation of the zirconium in the core [16].

8. In SNL/IET-8 [17], the molten thermite flowed under gravity through the hole in the melt generator into the reactor cavity, which was half filled with water; in SNL/IET-8B, the molten thermite was ejected by high-pressure steam (as in most of the earlier IET tests) into the reactor cavity, which was again half filled with water.

Initial conditions for the SNL/IET tests are given in Tables 2.1.1 and 2.1.2; Table 2.1.1 gives initial conditions common to all the Surtsey experiments, while Table 2.1.2 gives initial conditions for those parameters whose values were varied in the Surtsey tests.

Table 2.1.1. Common Initial Conditions for the SNL/IET Experiments

Thermite Total (kg)	4.30
Surtsey Vessel Volume (m^3)	
Subcompartments	4.65
Upper Dome	85.15
Total	89.8

Table 2.1.2. Individual Experiment Initial Conditions for the SNL/IET Experiments

Parameter	IET-1	IET-1R	IET-3	IET-4	IET-5	IET-6	IET-7	IET-8	IET-8B
Hole Diameter (cm)									
Initial	3.5	3.5	3.5	3.5	3.5	3.5	3.5	3.5	3.5
Final	4.04	4.02	4.53	4.22	4.31	3.91	4.08	3.5	4.1
Steam Accumulator									
Pressure (MPa)	7.1	6.3	6.1	6.7	6.0	6.3	5.9	-	6.25
Temperature (K)	600	585	585	555	584	571	599	-	554
Mass (gm-moles)	440	477	456	582	457	505	416.4	-	538
Water Mass (kg)									
Cavity	3.48	3.48	3.48	3.48	3.48	3.48	3.48	62	62
Basement	0	0	0	71.1	71.1	0	71.1	71.1	71.1
Vessel Atmosphere									
Pressure (MPa)	0.20	0.20	0.19	0.20	0.20	0.198	0.21	0.20	0.203
Temperature (K)	295	295	279	286	303	308	302.7	304.1	298
Composition (mole %)									
N_2	99.90	99.78	90.60	90.00	16.90	87.10	85.95	85.32	85.80
O_2	0.03	0.19	9.00	9.59	4.35	9.79	9.57	9.85	9.79
H_2	0	0.02	0	0	2.76	2.59	3.97	4.33	3.91
CO_2	0.01	0	0.02	0.02	75.80	0	0.03	0.03	0.03
other	0.06	0.01	0.38	0.39	0.13	0.52	0.48	0.47	0.47

The most significant variables measured in the Surtsey IET tests were the overall increase in pressure and temperature in the Surtsey vessel, the cavity local pressure, the amount of hydrogen generated by the reaction of metallic debris with steam driving gas and with water in the cavity, the debris temperatures as it exited the instrument tunnel and as it struck the crane wall, debris velocities based on breakwires in seal table room openings, and the mass of debris recovered from the Surtsey vessel. In some of the later tests, cameras were used to determine if the subcompartment structures filled immediately with aerosols, and to obtain information about the debris flow regime and velocity; also in some of the later tests, post-test sieve analysis was done on debris recovered from the Surtsey vessel outside the subcompartment structures to determine particle size distribution.

Table 2.1.3 gives a debris recovery summary for the Surtsey IET experiments. The total molten mass available for dispersal into the vessel was usually ~20% greater than the initial thermite charge due to melting of the inner wall of the crucible, vaporization of the fusible brass plug, ablation of concrete in the cavity and structures, and oxidation of metallic debris.

Table 2.1.4 summarizes the comparative results of the IET tests for overall vessel pressurization and for hydrogen generation and combustion. The total amount of hydrogen generated by steam/metal reactions was calculated by subtracting the measured amount of pretest hydrogen from the sum of the measured amount of posttest hydrogen plus the estimated amount of hydrogen burned; the hydrogen combustion given was based on the assumption that all oxygen depletion was due to reaction with hydrogen and was calculated using the stoichiometric chemical reaction for the formation of water:

$$n_{burn}(H_2) = 2[n_0(O_2) - n_f(O_2)]$$

$$n_{prod}(H_2) = n_{burn}(H_2) + n_f(H_2) - n_0(H_2)$$

where the n's are the number of moles and the subscripts 0 and f refer to initial and final values, respectively. Final gas concentrations were measured from grab bottle samples mostly taken 30min after the HPME transient in all tests, at levels 2,4 and 6 in the Surtsey vessel; in some experiments, gas grab samples were also available 0-2s after the start of the HPME transient (in the cavity), 2-5s after the start of the HPME transient (inside the subcompartment structures) and at 2min after the HPME transient (at the same three levels in the vessel). There was little difference in the gas grab samples taken in the vessel at 2 and 30min, but there were large differences in gas composition in the cavity and inside the subcompartment structures during the HPME transient, as would be expected.

There is a significant increase in hydrogen combustion from tests SNL/IET-3 and SNL/IET-4 (186 and 236 gm-moles, respectively), which had no pre-existing hydrogen, to tests SNL/IET-6 and SNL/IET-7 (335 and 321 gm-moles, respectively), with no pre-existing hydrogen. In both tests with pre-existing hydrogen, more hydrogen burned than

Table 2.1.3. Debris Masses Recovered for the SNL/IET Experiments

	IET-1	IET-1R	IET-3	IET-4	IET-5	IET-6	IET-7	IET-8	IET-8B
Initial Thermite (kg)	43.0	43.0	43.0	43.0	43.0	43.0	43.0	43.0	43.0
Recovered Mass (kg)									
Crucible	4.54	4.63	4.50	4.76	2.60	2.27	6.74	0.23	2.56
Cavity/Chute	7.06	13.19	16.80	9.54	20.07	8.47	13.31	42.31	5.55
Subcompartment	38.03	32.41	31.30	32.67	31.22	36.60	33.99	5.81	26.99
Dome	4.98	3.80	3.00	8.04	1.89	5.87	2.71	2.76	15.87
Total	54.61	54.03	55.60	55.02	55.79	53.21	56.75	51.11	50.97

Table 2.1.4. Results Summary for the SNL/IET Experiments

	IET-1	IET-1R	IET-3	IET-4	IET-5	IET-6	IET-7	IET-8	IET-8B
HPME ΔP_{MAX} (kPa)									
Dome	98	110	246	262	103	279	271	87	243
H_2 (gm-moles)									
Pretest	~0	~0	~0	~0	202	180	284	307	288
Produced	223	252	223	297	313	308	271	107	247
Burned	1	12	186	236	50	335	321	114	202

was produced by oxidation during HPME, indicating some of the pre-existing hydrogen was burned. However, there is not a corresponding significant increase in peak vessel pressures measured. Therefore, the pre-existing hydrogen must have recombined on a time scale much longer than the HPME time scale not to have contributed to the peak pressure increase.

2.2 1:40 Linear Scale COREXIT/CWTI DCH Test Facility

Counterpart IET tests are being performed at Sandia in the Surtsey facility (1:10 scale) and at ANL in the Corium Ex-Vessel Interaction (COREXIT) facility (1:40 scale), in an experimental program to investigate the effects of scale on DCH phenomena.

A schematic of the experiment apparatus [18-24] is given in Figure 2.2.1. Major components of the facility include an explosion-resistant containment cell, an expansion vessel and a high-pressure steam boiler. A concrete cavity model is contained within an outer pipe body, as shown in Figure 2.2.2. Bolted on top of the pipe body is a saddle piece, referred to as the top cap, which contains the melt generator and injecter (MGI). The cavity keyway is elongated by a transition chute which connects the cavity to the bottom of the expansion vessel. The elongation is required in order to allow room for the melt generator to fit underneath the expansion vessel; the keyway is thus elongated by 2.7 times its correctly scaled length.

The model used for the Zion subcompartment structures is shown in Figure 2.2.3, and is a scaled-down version of the subcompartments model used in the SNL/IET tests. Prominent features which are modelled include the seal table room, refueling canal, biological shield wall, reactor coolant pumps, steam generators, floor grating and operating deck floor. The walls and floors were constructed from concrete and mortar, and the structures painted with epoxy paint. This model was built up from the lower flange of the expansion vessel. The perimeter of the model is defined by a circular concrete wall which simulates the crane wall in the plant.

Test operations were begun by preheating the accumulator, the MGI and all piping associated with the test delivery system, until predetermined temperatures were obtained. If called for by the test, water was added to the cavity. The expansion vessel, steam generator and accumulator were brought to test-specified pressures. Each test was begun by starting the data acquisition system and starting a timer which applied power to an igniter assembly which started the thermite reaction. At a specified time after applying power to the igniter, the isolation steam valve was actuated followed by the steam valve which introduces steam into the MGI. At some time after the steam introduction, the thermite reaction reached and failed the brass plug in the melt generator, which started the high-pressure melt ejection.

A series of experiments were done investigating the effects of high pressure melt ejection on direct containment heating:

1. Test ANL/IET-1 was the baseline test, while test ANL/IET-1R and ANL/IET-1RR were replicate tests investigating experiment reproducability [18, 19]. This

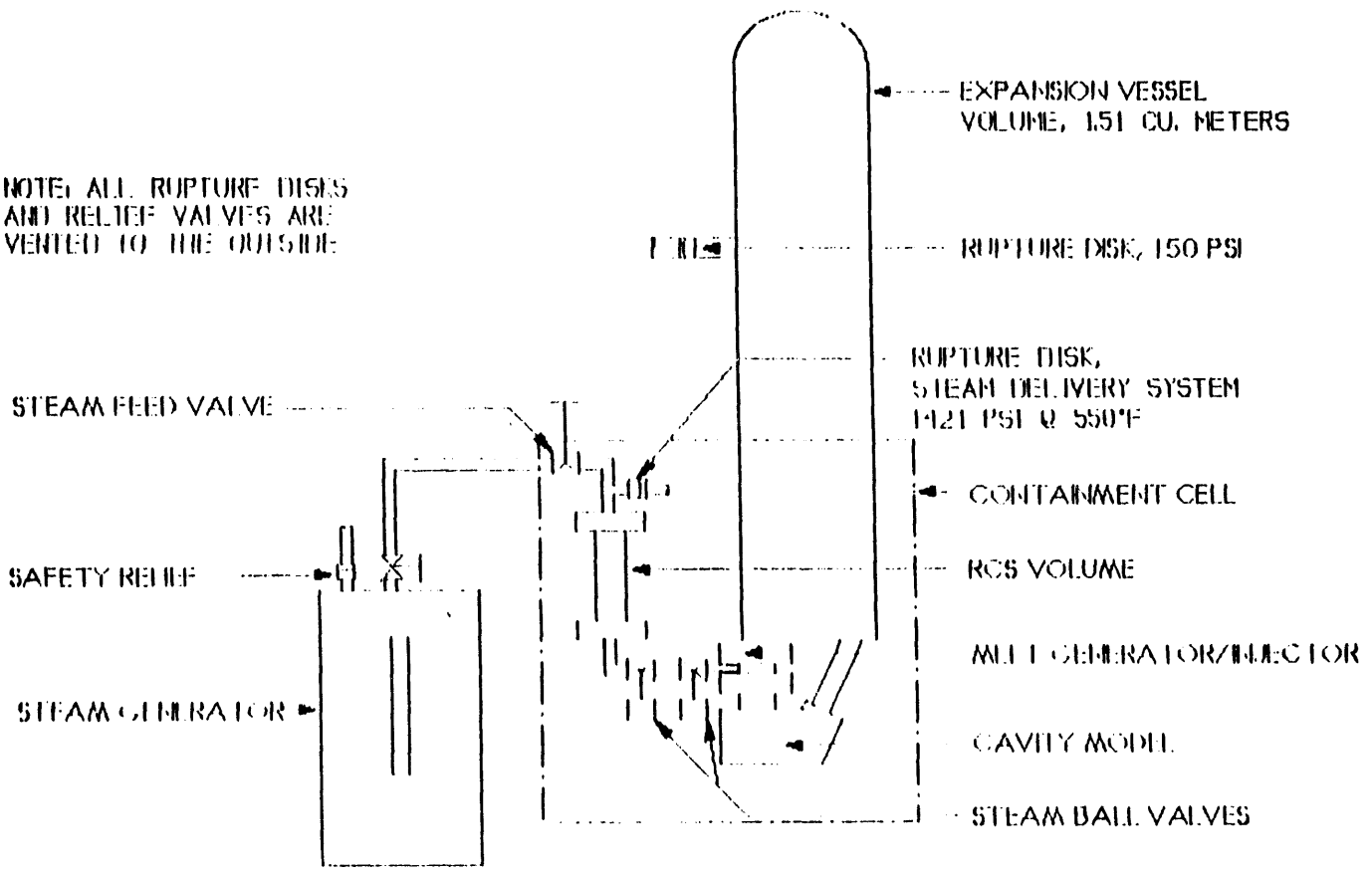

Figure 2.2.1. COREXIT Facility Used in the ANL/IET Experiments (from [19])

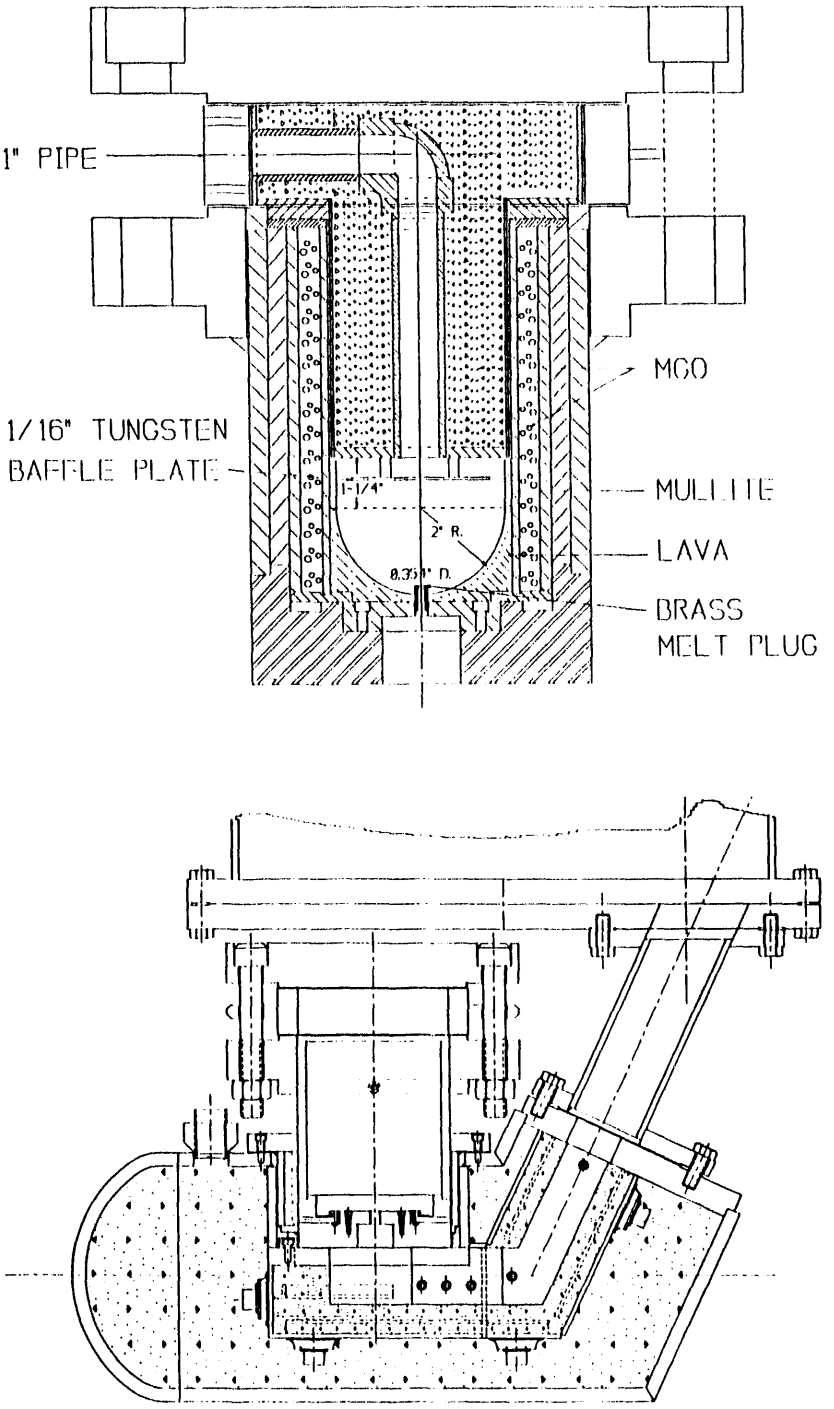

Figure 2.2.2. HPME System, Cavity and Instrument Chute Used in the ANL/IET Experiments (from [19])

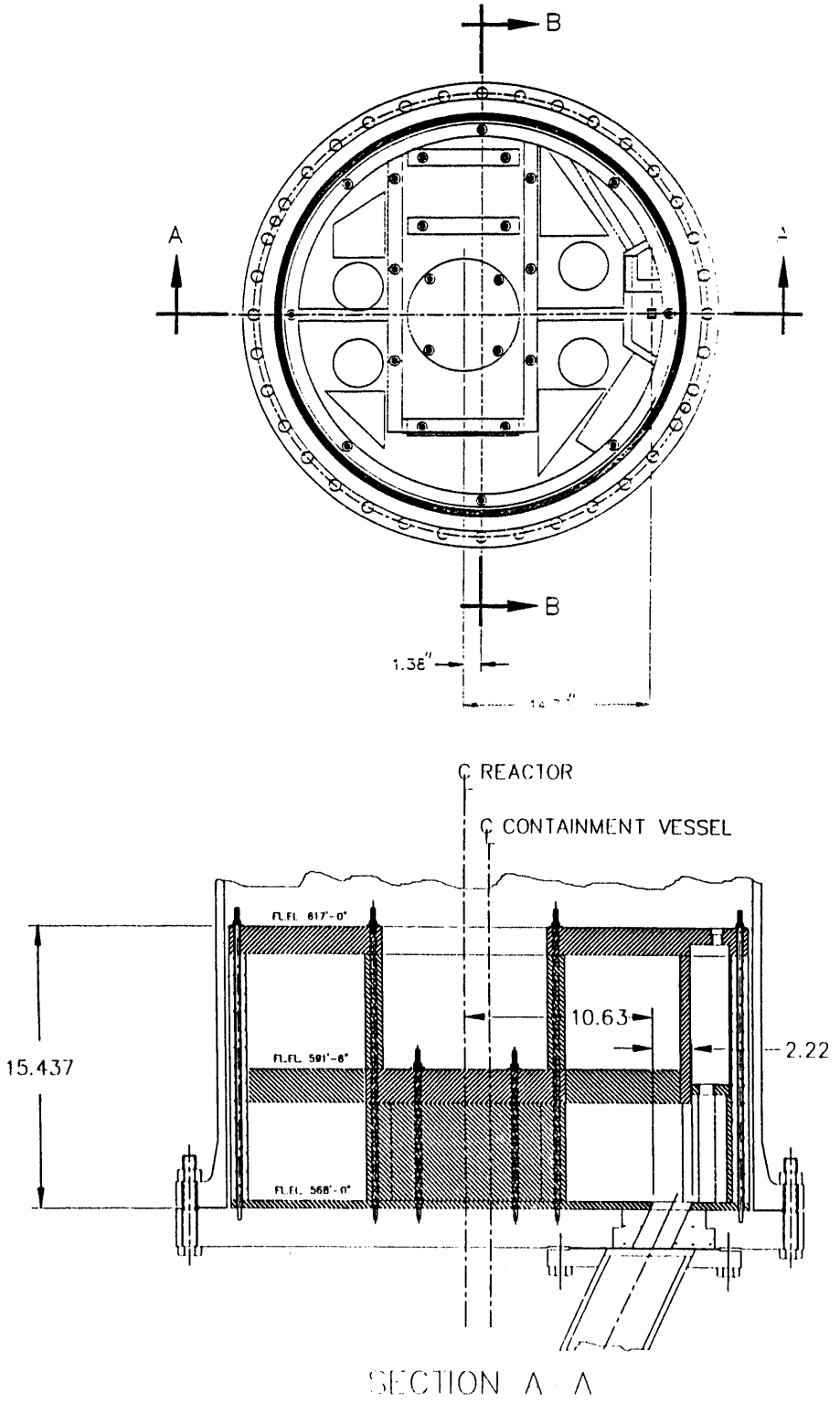

Figure 2.2.3. Cross-Sectional Views of Subcompartments in ANL Vessel Used in the ANL/IET Experiments (from [19])

was designed to be a counterpart test to SNL/IET-1 and SNL/IET-1R (discussed in the previous subsection). In particular, the difficulties with late application of steam and consequent elongation of RCS blowdown time were removed in test ANL/IET-1RR.

2. Test ANL/IET-2 [20] was a repeat of ANL/IET-1 with a higher driving pressure.

3. Test ANL/IET-3 nominally repeated the same initial conditions of ANL/IET-1, ANL/IET-1R and ANL/IET-1RR, with the exception of the containment atmosphere, which contained an equal mixture of air and nitrogen [21].

4. Test ANL/IET-6 [22] nominally repeated the initial conditions of ANL/IET-3, except the containment atmosphere contained pre-existing hydrogen and a smaller thermite charge was used.

5. Test ANL/IET-7 nominally repeated the same initial conditions of ANL/IET-3, with the exception that the containment pressure was reduced by one-half [23] and a smaller thermite charge was used (as in ANL/IET-6).

6. Test ANL/IET-8 [24] nominally repeated the same initial conditions of ANL/IET-3 with a different containment atmosphere gas composition, and a smaller thermite charge (as in ANL/IET-6).

Initial conditions for the ANL/IET tests are given in Tables 2.2.1 and 2.2.2; Table 2.2.1 gives initial conditions common to all the ANL experiments, while Table 2.2.2 gives initial conditions for those parameters whose values were varied in the ANL tests.

The most significant variables measured in the ANL/IET tests were the overall increase in pressure and temperature in the ANL vessel, the cavity local pressure, the amount of hydrogen generated by the reaction of metallic debris with steam driving gas and with water in the cavity, the debris temperatures as it exited the instrument tunnel and as it struck the crane wall, and the mass of debris recovered from the ANL vessel.

Table 2.2.3 gives a debris recovery summary for the ANL/IET experiments. (The total molten mass available for dispersal into the vessel was usually ~20% greater than the initial thermite charge due to melting of the inner wall of the crucible, vaporization of the fusible brass plug, ablation of concrete in the cavity and structures, and oxidation of metallic debris.) Table 2.2.4 summarizes the comparative results of the IET tests for overall vessel pressurization and for hydrogen generation and combustion.

Table 2.2.1. Common Initial Conditions for the ANL/IET Experiments

ANL Vessel Volume (m^3)	
Subcompartments	0.077
Upper Dome	1.43
Total	1.51

Table 2.2.2. Individual Experiment Initial Conditions for the ANL/IET Experiments

Parameter	IET-1	IET-1R	IET-1RR	IET-3	IET-6	IET-7	IET-8
Thermite Composition (gm)							
FeO	558.0	558.0	558.0	558.0	485.2	485.2	485.2
Cr	88.6	88.6	88.6	88.6	77.0	77.0	77.0
Al	173.4	173.4	173.4	173.4	150.8	150.8	150.8
Total	820.0	820.0	820.0	820.0	713.0	713.0	713.0
Hole Diameter (cm)							
Initial	0.9	0.9	1.1	1.1	1.1	1.1	1.1
Final	0.9	0.9	1.3	1.1	1.1	1.1	1.1
Steam Accumulator							
Pressure (MPa)	6.0	6.2	6.7	5.7	6.6	6.1	6.5
Temperature (K)	600	600	600	600	600	600	600
Mass (gm-moles)	7.44	8.55	9.84	8.43	9.65	8.88	9.36
Water Mass (gm)							
Cavity	55.0	55.0	55.0	55.0	55.0	55.0	55.0
Vessel Atmosphere							
Pressure (MPa)	0.20	0.20	0.20	0.20	0.20	0.10	0.20
Temperature (K)	318	318	318	318	318	318	477
Composition (mole %)							
N_2	99.4	99.9	99.9	88.8	87.5	87.5	37.9
O_2	0.5	0.0026	0.12	10.8	9.9	9.9	7.7
H_2	<0.01	<0.01	<0.01	<0.01	2.0	4.0	3.9
CO_2	0.0048	0.004	0.011	0.011	0.013	0.013	–
H_2O	–	–	–	–	–	–	50.0
other	<0.01	<0.006	<0.005	<0.02	<0.01	0.47	0.5

Table 2.2.3. Debris Masses Recovered for the ANL/IET Experiments

	IET-1	IET-1R	IET-1RR	IET-3	IET-6	IET-7	IET-8
Initial Thermite (gm)	820.0	820.0	820.0	820.0	713.0	713.0	713.0
Recovered Mass (gm)							
MGI	87.4	4.0	43.3	67.3	30.3	4.0	11.8
Cavity/Chute	541.6	197.1	260.8	232.2	262.7	153.7	179.3
Seal Table Room	–	–	148.9	163.1	167.9	113.6	158.7
Remaining Subcompartments	339.0	551.1	358.2	428.2	339.6	448.9	405.3
Total in Subcompartments	339.0	551.1	507.1	591.3	507.5	562.5	564.0
Outside Structures	66.7	87.7	114.6	37.8	81.3	26.2	22.6†
Total	1034.7	839.9	925.8	928.6	881.8	746.48	804.5

†An unknown amount of debris was lost during the vacuuming procedure.

Table 2.2.4. Results Summary for the ANL/IET Experiments

	IET-1	IET-1R	IET-1RR	IET-3	IET-6	IET-7	IET-8
HPME ΔP_{MAX} (kPa)							
Cavity	420	920	550	200	480	430	290
Dome	105	170	150	190	250	166	133
H_2 (gm-moles)							
Pretest	~0	~0	~0	~0	2.28	~0	3.1
Produced	1.51	4.00	4.00	4.65	4.89	5.1	5.6
Burned	~0	~0	~0	3.50	4.22	3.66	1.0

3 MELCOR Computer Model

(This section presupposes some familiarity with the MELCOR FDI/HPME/DCH model, its terminology and modelling assumptions, and its input requirements. A brief description of the model, excerpted from [26], is included in Appendix A for the convenience of interested readers.)

Note that most individual parameters in our MELCOR input models were not separately adjusted in each of our MELCOR SNL/IET and ANL/IET experiment analyses to best match data for each individual experiment. Instead, the basic control-volume/flow-path/heat-structure model was kept the same for all SNL/IET experiments analyzed, and a single set of debris source, distribution and interaction time parameters was used for all the SNL/IET experiments analyzed. Similarly, the basic CVH/FL/HS input model and the debris source, distribution and interaction time parameters was used for all the ANL/IET calculations were the same. The only test-specific changes made were to set the initial pressures, temperatures, gas composition, and liquid pool heights to match individual experiment initial conditions.

3.1 1:10-Scale Surtsey Test Facility MELCOR Model

The MELCOR input model used for the SNL IET experiment calculations is shown in Figure 3.1.1. Five control volumes, five flow paths, and twelve heat structures were used in the reference MELCOR model. (A copy of the input used for the Surtsey IET-1 reference calculation is given in the appendix, for documentation.)

Two control volumes represent the (horizontal) cavity and (inclined) chute, respectively. The Surtsey vessel was subdivided into two control volumes, one for the subcompartments and another for the upper dome. The final control volume modelled the steam source. Five flow paths were provided for straight flow through the system, and for recirculation from the upper dome to the subcompartment volume. Volumes and heights were generally taken from the test data reports [10-17], while some of the flow path parameters were taken from the CONTAIN input decks [27], because there was not enough information in the published test reports to fully define the required input (such as flow area, opening heights, elevations, loss coefficients).

The control-volume nodalization was set to approximate the level of detail provided in the post-test debris recovery distribution data provided in the test data reports [10-17]; we judged that a finer subdivision in the subcompartments was not warranted because the MELCOR DCH model requires the final debris distribution to be input on a per-volume basis, and there were no data available on a finer scale for either input or comparison. The "recirculation" flow path was provided to allow for the fact that in the actual facility a number of openings exist between the various subcompartments and the vessel dome, with the potential of inflow in some openings and outflow in others. The area of that recirculation flow path was set to 10% of the area of the straight-through flow path from

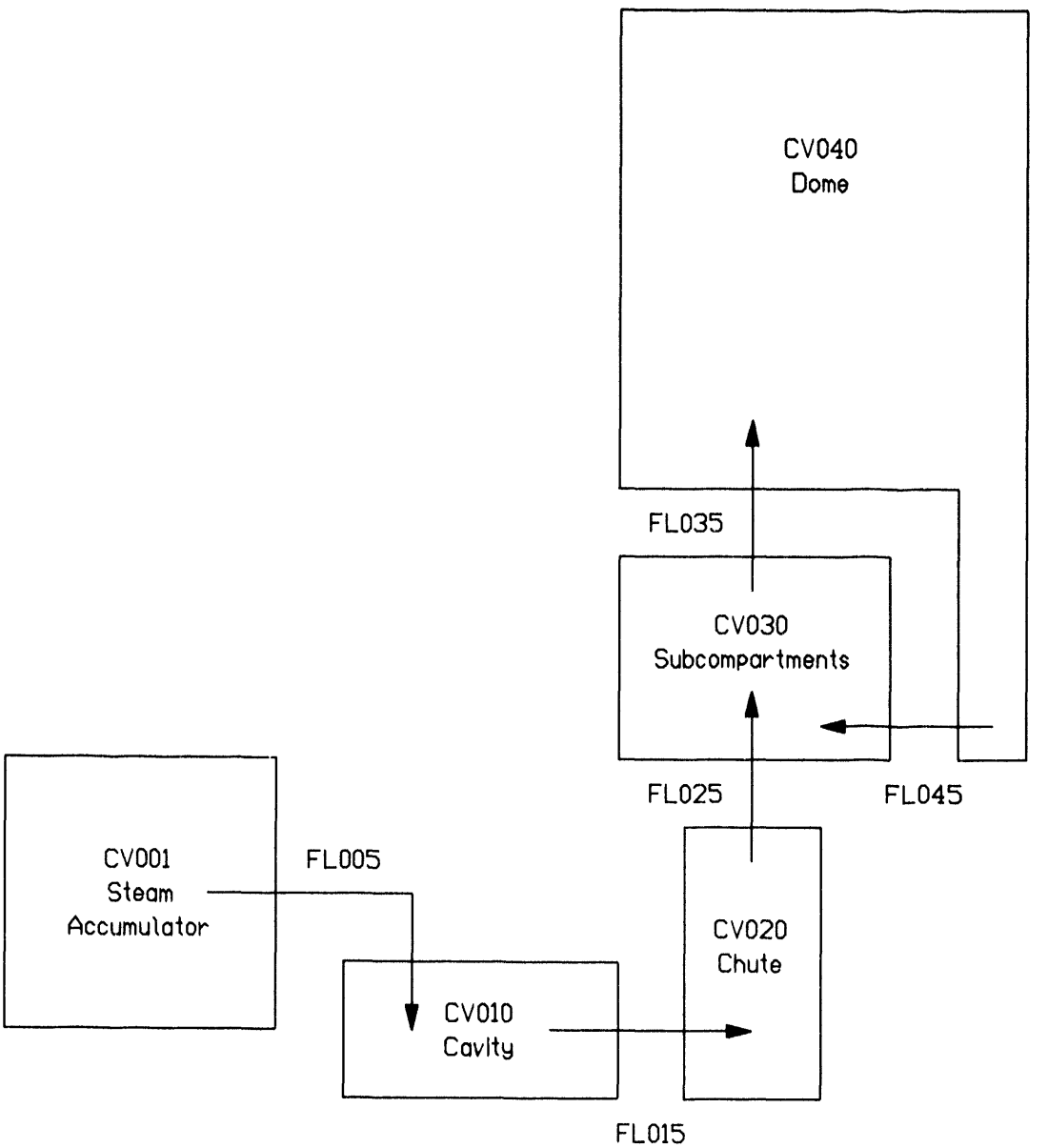

Figure 3.1.1. Reference MELCOR Model for SNL/IET Experiment Analyses

the subcompartments to the dome. (Sensitivity studies were done with that recirculation flow path area increased and decreased, with results summarized in Section 7.3.)

A valve with a time-dependent area was used in the flow path from the steam accumulator to the cavity to control the rate of steam injection, with the opening rate adjusted to provide a valve opening at a constant rate between 0 and 1s. Although different final hole diameters were identified in the test reports for the opening from the melt generator to the cavity, the input was kept the same for all the SNL/IET experiments analyzed for the valve and associated time-dependent area used in the flow path from the steam accumulator to the cavity to control the rate of steam injection. In the experiments the thermite reaction products and the steam were injected through the same opening, with some indication in the data of occasional plugging and flow interruption. In the MELCOR model the debris is inserted separately, directly to its ultimate destination; thus MELCOR does not model any debris blockage or obstruction possibly affecting the steam injection rate. We simply adjusted the opening rate to match the observed steam accumulator depressurization rates in the various tests reasonably well (as discussed in more detail in Section 5.1).

The post-reaction thermite debris was added directly through tabular function input using the FDI HPME "stand-alone" mode, rather than input *via* COR package or TP (Transfer Process) package input. The FDI input for debris amount, temperature and distribution were kept the same in our MELCOR input for all tests analyzed, although there were differences identified in the test reports in debris distribution. The difficulty here was that, while the original amount of thermite mass was very carefully kept constant in all experiments, both the amount retained in the melt generator and the excess debris collected post-test (from melting of the inner wall of the crucible, vaporization of the fusible brass plug, ablation of concrete in the cavity and structures, and oxidation of metallic debris) introduce significant uncertainty into the debris source. We chose to use reasonable, representative values for the debris mass and distribution for the Surtsey IET experiments, and address the variation in both total mass and distribution through sensitivity studies.

The input parameters for the debris source used in the MELCOR input are given in Table 3.1.1. The debris amount was kept constant at 43kg for all the SNL/IET experiments analyzed, neglecting both the small excess in and the small variations in total amount of debris collected (summarized in Table 2.1.3). The debris temperature was set to 2300K temperature. The final collected debris distributions given in the test data reports (and in Table 2.1.3) was used to estimate a single, average distribution of debris into the various control volumes. The MELCOR FDI/HPME model input allows the user to specify debris distribution both into control volume atmospheres and directly onto heat structures (as well as directly into a CORCON cavity, not included in these calculations). All of the debris in our IET assessment analyses was placed initially into control volume atmospheres and then allowed to settle out; no debris was specified to be deposited immediately directly onto heat structures. A tabular function was used to specify the melt injection as a function of time and was adjusted to try to match the rate of pressure and temperature increase in the vessel. (Sensitivity studies varying the

debris total amount, temperature, distribution and injection timing within a reasonable range of data uncertainty are presented in Sections 5.3, 5.4, 5.5, and 5.2.)

A single set of characteristic interaction times was specified for all the seven of the 1:10-scale tests analyzed (SNL/IET-1 through SNL/IET-7). The values used in our reference SNL/IET analyses are given in Table 3.1.2. The characteristic times for settling (τ_{set}) of debris in the control volume atmospheres onto floor heat structures were based upon free-fall times for the various volume heights, and are therefore proportional to volume heights and constant in the various tests; there could be some test-to-test variations in turbulent flow circulation patterns, thermal buoyancy effects, *etc.*, but these were assumed negligible. The characteristic oxidation and heat transfer times were assumed to depend primarily on parameters such as average airborne or deposited particle concentrations, which in a given geometry should be approximately constant for identical melt debris and blowdown steam sources such as used in the tests analyzed. (Section 6 summarizes sensitivity studies done varying these characteristic interaction time input parameters individually over wide ranges of values.)

The characteristic times for oxidation and heat transfer (τ_{ox} and τ_{ht}, respectively) of debris in the control volume atmospheres, as well as a characteristic time for oxidation of debris deposited on heat structures (τ_{hs-ox}), in Table 3.1.2 were selected after numerous iterations as giving reasonable agreement with a subset of test data (in particular, vessel pressure, subcompartment temperature and hydrogen production and combustion) in the SNL/IET experiments simulated.

Note that there is no reason to assume that the debris source and interaction input parameter set given in Tables 3.1.1 and 3.1.2 is unique (*i.e.*, the only set to provide reasonable agreement with the selected test data); it is also not guaranteed that the iterative procedure followed results in an input parameter set that would yield the best agreement with data, or agreement with data for the "correct" reasons (*i.e.*, representing the actual behavior). For example, freezing some of the parameter values early in this iterative process undoubtedly affected the values assumed for other parameters. Further, experiment ambiguities may have led to incorrect modelling assumptions which would also affect the values chosen for various parameters. In particular, the choice of a very short time constant for airborne debris oxidation (0.025s in the reference analyses) was driven by trying to match the reported hydrogen production and combustion data; sensitivity study results in Section 6.1 show very little difference in calculated pressures or temperatures for 0.01s $\leq \tau_{ox} \leq$ 0.1s, and the hydrogen production and combustion later derived from a molar balance assuming only steam/metal reactions (as in the test data analysis) is in better agreement with test data for the longer characteristic oxidation times tried ($\tau_{ox} \sim$ 0.1s).

In the majority of our IET analysis calculations, the burn package was activated, but burn was suppressed in all control volumes except the vessel dome. The minimum (CO_2 + H_2O) mole fraction limit for inerting volumes was left unchanged from the default value of 0.55 (which was sufficient to prevent hydrogen combustion in SNL/IET-5, as observed in that experiment). The minimum hydrogen mole fraction in the ignition criterion in the absence of igniters was set to 0.0, and the combustion completeness was also set to

Table 3.1.1. MELCOR FDI/HPME Debris Input Parameters Used for the SNL/IET Experiments

Debris Composition (kg)	
Al_2O_3	16.056
Fe	21.699
Cr	4.649
Al	0.596
Total	43.00
Debris Temperature (K)	2300
Debris Distribution (%)	
Cavity	15
Chute	10
Subcompartment	65
Dome	10
Debris Injection Timing (Cumulative Fraction)	
by t=0s	0
by t=0.1s	0.05
by t=0.2s	0.1
by t=0.3s	0.15
by t=0.4s	0.2
by t=0.5s	0.3
by t=0.6s	0.5
by t=0.7s	0.8
by t=0.8s	0.9
by t=0.9s	0.95
by t=1.0s	1.0

Table 3.1.2. Characteristic Interaction Times Used in Reference MELCOR Model for SNL IET Experiment Analyses

Interaction Time	Value (s)
Airborne Debris:	
Oxidation	0.025
Heat Transfer	0.40
Settling	
Cavity	0.15
Chute	0.35
Subcompartment	0.25
Dome	0.60
Deposited Debris:	
Oxidation	600.0

0.0. This combination of input prevented the burning of any pre-existing hydrogen, but allowed burning of any additional hydrogen generated during the HPME. This is because a combustion completeness equal to 0.0 does not mean no combustion; instead, specifying a combustion completeness of 0 causes the code logic to try to maintain the mole fractions after the burn equal to the mole fractions before, so that new hydrogen introduced during a time step, either by oxidation or by advection, will be burned but pre-existing hydrogen will remain present and generally unreacted. This particular combination of input was found to produce reasonable agreement with test data in all cases. (The results of sensitivity studies using other possible input settings are described in Section 7.1.)

Note that the combustion completeness did not have to be reset to 0 in the input, because in these problems the LeChatelier formula Y is simply the hydrogen mole fraction x_{H_2} (because $x_{CO} = 0.0$) and, with the hydrogen mole fraction ignition limit reset to 0.0, the LeChatelier formula at the beginning of the burn (Y_{MAX}) is also 0.0, and the default correlation used in MELCOR gives combustion completeness CC=0.0 for $Y_{MAX} \leq 0.03746$. Therefore, with a hydrogen mole fraction ignition limit of 0.0, the combustion completeness correlation used in MELCOR automatically gives a combustion completeness value of 0.

The heat structure input was generally taken from CONTAIN input [27], because there was not enough information in the published test reports to fully define the required input (such as heat structure surface areas, thicknesses, elevations, *etc.*). The cavity, chute, subcompartments and dome control volumes were each defined to have corresponding floor, wall and roof heat structures, for a total of twelve heat structures. These structures were specified to use "external" heat transfer coefficient correlations on

the inside surface, with the volume length/height input as the characteristic length, while on their outside surface the heat structures were specified to be adiabatic. The nodes were very closely spaced on the inner surface and moved progressively farther apart in the depths of the structures, to better resolve the steep temperature gradients expected near the surface. Radiation heat transfer using the gray gas model was enabled with an emissivity of 0.8. All heat structures used MELCOR's steady-state temperature-gradient self-initialization option.

Most of our calculations were run with control volume flow areas reduced by factors of $\geq$10 from their default values, to enhance convective heat transfer from the control volume atmospheres to the heat structure surfaces. (The control volume flow areas are used only to obtain volume velocities for use in the calculation of convective heat transfer coefficients; changing control volume flow areas does not affect flow path calculations at all.) The convective heat transfer was enhanced for two reasons:

First, our preliminary calculations showed that the flow through the system in these calculations was primarily that associated with the steam blowdown only, flowing from the steam accumulator through the cavity and chute volumes to the subcompartments and then to the dome. The MELCOR FDI/HPME/DCH model does not model transport of debris between and through volumes but instead deposits the debris directly at its ultimate destination, using the same time-dependent deposition in all volumes regardless of their distance from the debris source. Thus, instead of debris being transported into an "upstream" volume (*e.g.*, the cavity or the subcompartments) with the blowdown steam and the resultant additional heating adding to the driving force pushing flow further "downstream" (*e.g.*, from the cavity to the chute or the subcompartments to the dome), the MELCOR logic does not represent this additional flow driving force and in contrast has debris appearing "upstream" and heating the atmosphere in upstream volumes, if anything contributing a retarding force to the expected flow. This results in lower velocities, and is more benign than the transient HPME blowdown actually occurring in the experiments, with transport of hot debris together with the steam blowdown.

Decreasing volume flow areas results in increased volume velocities more characteristic of the turbulent conditions that might be expected during HPME, and the associated turbulent forced convection heat transfer to structures. For the subcompartment control volume, in particular, it also reflects the fact that there is not a single, large, open subcompartment volume in the Surtsey facility but instead a collection of subcompartments, each with smaller volume and internal flow area and with smaller-area openings connecting the subcompartments to each other and to the dome. Thus, a (default) volume flow area of $\geq$4.5m^2 obtained using the subcompartment volume of 4.65m^3 and a height of $\geq$1m may not be indicative of the actual velocities in the subcompartments.

In addition, the MELCOR FDI/HPME/DCH model does not account for any radiation directly from airborne debris to surrounding structures (or from deposited debris directly to atmosphere). There is little or no calculated atmosphere-structure radiation heat transfer early in these transients (except in IET-5), because MELCOR only considers radiation heat transfer for steam and/or CO_2 in atmospheres. In IET-5, some atmosphere-structure radiation heat transfer is calculated because of the large amount

of CO_2 used to inert the system; however, in most of the experiment simulations there is very little steam present early in the transient, because any blowdown steam is consumed in debris oxidation soon after arrival, and very little CO_2 present at all. The lack of steam and/or CO_2 in the atmosphere would if anything enhance radiation heat transfer from airborne debris to structures because there would be little absorption in the intervening atmosphere. Hand calculations indicate that this could be a significant heat transfer mechanism, early in the transient. Because there is no way in MELCOR to model this effect, too much energy may be deposited in the atmosphere by the airborne debris; because there is no convenient way to enhance atmosphere-structure radiation heat transfer in general, we relied on increasing convective heat transfer instead to help remove that energy.

For these reasons, most of our calculations were run with control volume flow areas reduced by factors of $\geq$10 from their default values, to obtain volume velocities more characteristic of the turbulent conditions that might be expected during HPME, and the associated turbulent forced convection heat transfer to structures, and to partially account for the lack of any radiation from airborne debris to structures. The results of a sensitivity study showing the effect of increasing volume velocities and hence convective heat transfer coefficients and overall heat transfer to structures are given in Section 7.2.

Our reference MELCOR IET experiment analyses were run with the coefficient for heat transfer from deposited debris to structure surface reduced to 1w/m^2-K. This was originally done to avoid temperature iteration convergence problems, and was not changed when the temperature solution algorithm was improved and made more robust (as discussed in Section 11). To see what effect this had on our analyses, a set of calculations were run with that heat transfer coefficient progressively increased to 10w/m^2-K, 100w/m^2-K, and 1000w/m^2-K (the default value), with results described in Section 6.5.

The user-specified maximum time step in the reference calculations was 1s. The code then ran at an internally-determined time step during the high-pressure melt ejection, as discussed in Section 4, and at the user-specified maximum time step later in the transient period analyzed. Results of a time-step study on the SNL/IET reference calculations are given in Section 9.2. The majority of these IET DCH MELCOR calculations were run on a SUN Sparc2 workstation; results of a machine-dependency study for the SNL/IET reference calculations are given in Section 9.1.

3.2 1:40-Scale COREXIT Test Facility MELCOR Model

The MELCOR input deck for the ANL 1:40-scale test analyses was very similar to that for the Surtsey 1:10-scale facility and tests, shown in Figure 3.1.1. Control volume volumes and heights, and the blowdown orifice flow area, were taken from the test data reports [18-21] whenever possible. Otherwise, the input values used for the SNL/IET analyses were simply adjusted as appropriate by the difference in scale factor between the two facilities (*i.e.*, 1/4 for heights or lengths, 1/16 for flow areas or surface areas). The opening time for the steam blowdown valve and for melt injection was scaled by

1/4 from the SNL/IET input used, based upon examination of the experimental results. The debris amount and distribution were taken from the test data reports, as were the initial steam and atmosphere conditions. Again, as in our Surtsey IET analyses, most individual parameters in our MELCOR input model were not separately adjusted in each of our MELCOR ANL/IET experiment analyses to best match data for each experiment considered. As in our Surtsey IET analyses, the initial pressures, temperatures, gas composition, and liquid pool heights were set to match individual experiment initial conditions (summarized in Table 2.2.2); however, for the ANL/IET analyses it was also necessary to adjust the total debris mass, which changed from one value in the earlier tests (820gm) to a smaller value (713gm) in the later tests.

Our MELCOR assessment analyses for these 1:40-scale ANL/IET experiments were done in several steps, concentrating on the scaling of the phenomena. First, the ANL facility geometry and test conditions were modelled (and/or scaled) as just discussed, with no change in the characteristic interaction times input to the MELCOR FDI HPME model, with results given in Section 8.2. However, there is no reason to expect to match the ANL/IET data only scaling the facility geometry and test conditions – it seems intuitively obvious that the characteristic interaction time for airborne debris settling should be scaled as the height of the volume; it is not intuitively obvious whether the characteristic interaction times for oxidation of airborne or deposited debris, or for heat transfer from airborne debris to atmosphere, should be scaled or not. Therefore, we scaled the various characteristic interaction times also, individually and in combination, in more sets of calculations, with results given in Section 8.3. Finally, the other non-standard MELCOR input used for the 1:10-scale SNL/IET experiment analyses (*i.e.*, hydrogen combustion parameters, volume flow areas and velocities used to determine heat transfer correlations, and recirculation from the dome to the subcompartments) were varied and the impact on calculated results evaluated in Sections 8.4 through 8.6.

4 Reference Calculation Results

This section presents MELCOR assessment analysis results for the 1:10 linear scale SNL/IET experiments performed in the Surtsey vessel at Sandia. Results for analyses of the 1:40 linear scale ANL/IET experiments done at Argonne are presented in Section 8, as a scaling sensitivity study.

Figure 4.1 shows the masses of Al and of Fe and Cr that were oxidized during the transient, together with the masses of oxygen and steam that reacted with the debris. The default assumption in the MELCOR FDI/HPME/DCH model is sequential oxidation. Thus, Zr (not present in this case) would be oxidized first, followed by Al and then by steel; because the Fe and Cr injected are treated as components of injected "steel" with a user-specified composition, they are assumed to oxidize at the same rate. Similarly, the MELCOR FDI/HPME/DCH model assumes steam oxidation in a volume only if there is insufficient oxygen available to support the prescribed oxidation rate; oxygen is therefore consumed first whenever available. This hierarchical oxidation model is reflected in the results which show almost all of the Al injected was calculated to be oxidized but only about 45-70% of the injected Fe and Cr was oxidized. Almost all of the debris oxidation occurs in $\leq$1s, while the debris is being injected into the system, although there is a small additional amount of oxidation later, between $\sim$1s and $\sim$1.5s, in the SNL/IET-1 and SNL/IET-1R calculations. The plots in the figure show that, in the the SNL/IET-1 and SNL/IET-1R calculations, all the available oxygen was depleted within $\leq$0.5s, leaving some debris unoxidized until the arrival of sufficient blowdown steam. (Recall that the MELCOR FDI/HPME/DCH model assumes debris immediately transported to its final destination, while the accumulator steam blowdown was modelled as a transient process.)

Masses involved in the calculated FDI/HPME/DCH reactions are summarized in Table 4.1. (The molar balances are not exact because of the limited number of significant digits used and because of using round number for molecular weights, for convenience.) These numbers reflect the MELCOR calculation only; there is no experimental data available on how much of the debris collected post-test was oxidized and, as discussed in Section 2.1, the experimenters assumed in their data analysis that debris reacted only with steam, not with free oxygen. (Recall that this is the opposite of the MELCOR assumption that oxidation of metals with free oxygen occurs preferentially to oxidation with steam.)

Total amounts of hydrogen generated and burned in these SNL/IET tests are given in Figures 4.2 and 4.3, respectively. (Note the different time scales on these two figures.) Almost all of the hydrogen generated during debris/steam reactions is generated in t$\leq$1s, when the debris is being injected into the system; there is a small additional amount of hydrogen generated later (between $\sim$1s and $\sim$1.5s) in the SNL/IET-1 and SNL/IET-1R calculations. No significant amounts of additional hydrogen are generated at later times in these reference calculations. In contrast, about 0.3kg (150gm-moles) of hydrogen are burned within the first second or two, and another 0.03-0.06kg (15-30gm-moles) are burned between $\sim$1.5s and $\sim$3.5s. MELCOR calculates HPME/DCH to last

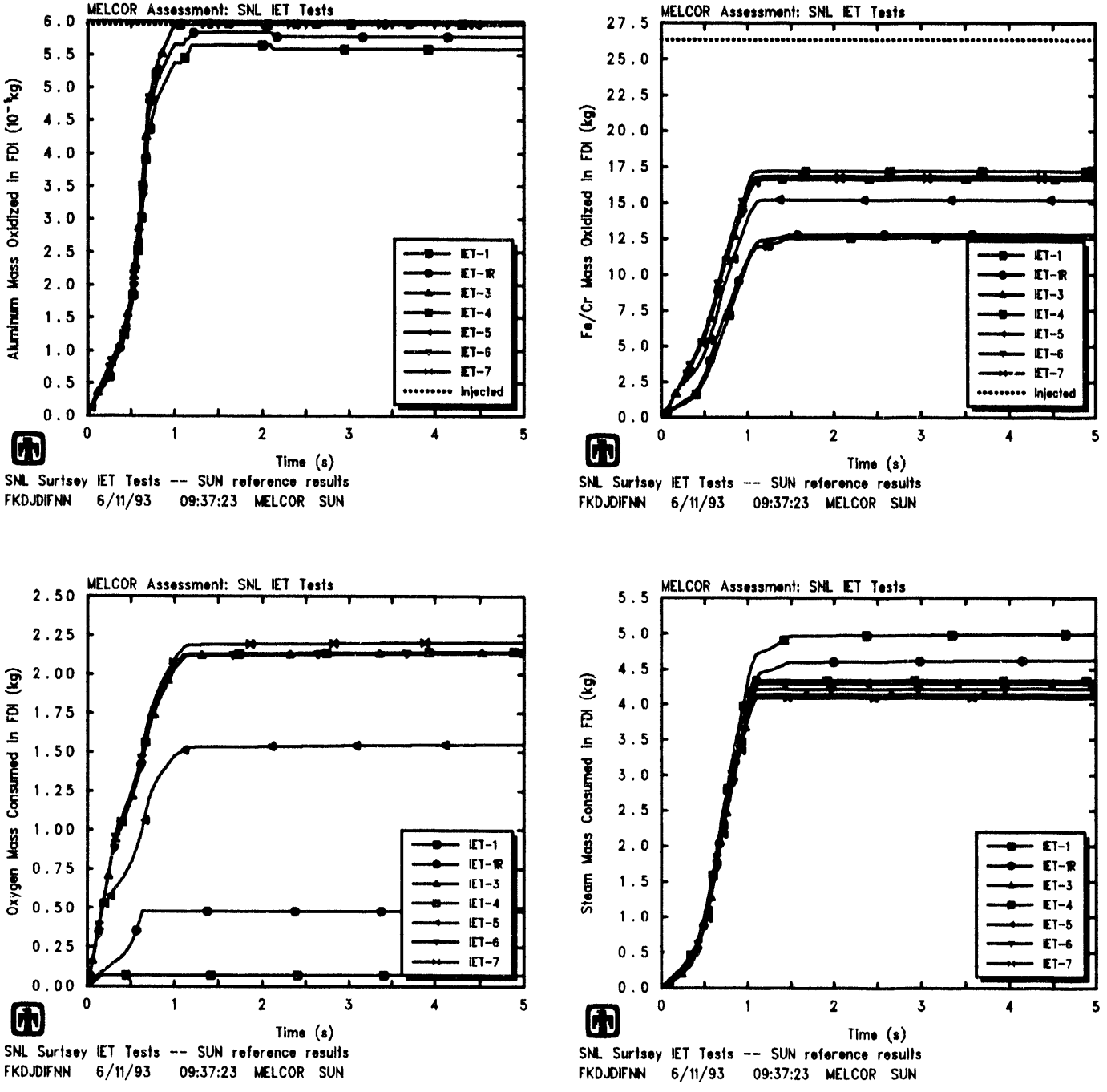

Figure 4.1. Aluminum (upper left) and Fe/Cr (upper right) Masses Oxidized, and Oxygen (lower left) and Steam (lower right) Masses Reacted for SNL/IET Experiments – Reference Calculation

$\leq$4s, based upon default criteria in the code for airborne debris temperature, mass and density. However, another $\sim$0.04kg (20gm-moles) are calculated to be burned later in the SNL/IET-3 and SNL/IET-6 analyses and another $\leq$0.1kg (50gm-moles) are calculated to be burned later in the SNL/IET-4 and SNL/IET-7 analyses, as some hydrogen is advected from the subcompartments to the vessel dome where it is assumed to burn. There is thus significant late-time hydrogen burn in our MELCOR calculations for those test simulations where the vessel atmosphere was not inert. (Sections 7.3 and 9.2 will show that both the early-time and the late-time hydrogen burn is quite sensitive to the recirculation flow between the subcompartments and the vessel dome, while the late-time hydrogen burn is quite sensitive to the time step used.)

The overall hydrogen behavior calculated in these IET experiment analyses is summarized in Table 4.2. The values given include the amount of hydrogen pre-existing in the vessel, the amount produced by HPME steam/metal reactions, the amount burned and the final amount.

It is difficult to quantitatively compare the measured and calculated hydrogen production and combustion because of the basic assumption made by the experimenters that all oxygen depletion was due to reaction with hydrogen. Thus, as discussed in Section 2.1, the experimenters assumed in their data analysis that debris reacted only with steam, not with free oxygen, which is the opposite of the MELCOR assumption that oxidation of metals with free oxygen occurs preferentially to oxidation with steam. Figure 4.1 and Table 4.1 show that MELCOR did predict significant interaction of free oxygen with debris in those tests where oxygen was present (*i.e.*, SNL/IET-3 through SNL/IET-7).

Table 4.3 summarizes the overall hydrogen behavior measured and calculated in these IET experiments and analyses. For the test data, the total amount of hydrogen generated by steam/metal reactions was obtained by subtracting the measured amount of pretest hydrogen from the sum of the measured amount of posttest hydrogen plus the estimated amount of hydrogen burned; the hydrogen combustion given was based on the assumption that all oxygen depletion was due to reaction with hydrogen, as described in Section 2.1. The MELCOR values given include both the actual amounts of hydrogen produced by HPME steam/metal reactions and burned, and the amounts of hydrogen produced and burned that would be calculated using the initial and final oxygen and hydrogen moles from the MELCOR analyses, using the same formulae as in the experiment data analysis. (However, note that the experimental results come from analyzing gas grab bottle samples taken from the Surtsey vessel at 30min, while the MELCOR results are taken from output at 20s.)

The two sets of MELCOR values differ by twice the number of moles of O_2 consumed by direct metal/oxygen reactions. There is little difference found in the hydrogen production evaluated using the experimental procedure and actually calculated by MELCOR in the tests with little or no free oxygen present (*i.e.*, SNL/IET-1 and SNL/IET-1RR); however, note that, for these two tests and for SNL/IET-5, assuming all oxygen depletion was due to combustion reaction with hydrogen does result in a small mass of hydrogen calculated to be burned, quite similar to the experimental results given. The actual moles of hydrogen produced and burned in these MELCOR analyses appear gener-

Table 4.1. Calculated HPME/DCH Mass Results Summary for the SNL/IET Experiments – Reference Calculation

	MELCOR (gm-moles)				
	Oxidized		Reacted		Produced
	Al	Fe/Cr	Oxygen	Steam	H_2
IET-1	20.9	227.7	2.2	284.2	286.2
IET-1R	21.6	231.3	15.0	263.8	265.7
IET-3	22.1	301.1	69.2	230.2	231.8
IET-4	22.1	311.3	69.2	241.1	242.8
IET-5	22.1	275.0	51.3	238.7	240.3
IET-6	22.1	304.8	69.0	234.4	236.0
IET-7	22.1	302.6	71.3	227.6	229.2

Table 4.2. Calculated Hydrogen Results Summary for the SNL/IET Experiments Reference Calculation

Experiment	MELCOR Hydrogen Balance (gm-moles)			
	Pre-existing	Produced	Burned	End-of-calculation
IET-1	0	286	0	286
IET-1R	0	266	0	266
IET-3	0	232	188	44
IET-4	0	243	209	34
IET-5	204	240	0	444
IET-6	183	236	218	201
IET-7	288	229	223	294

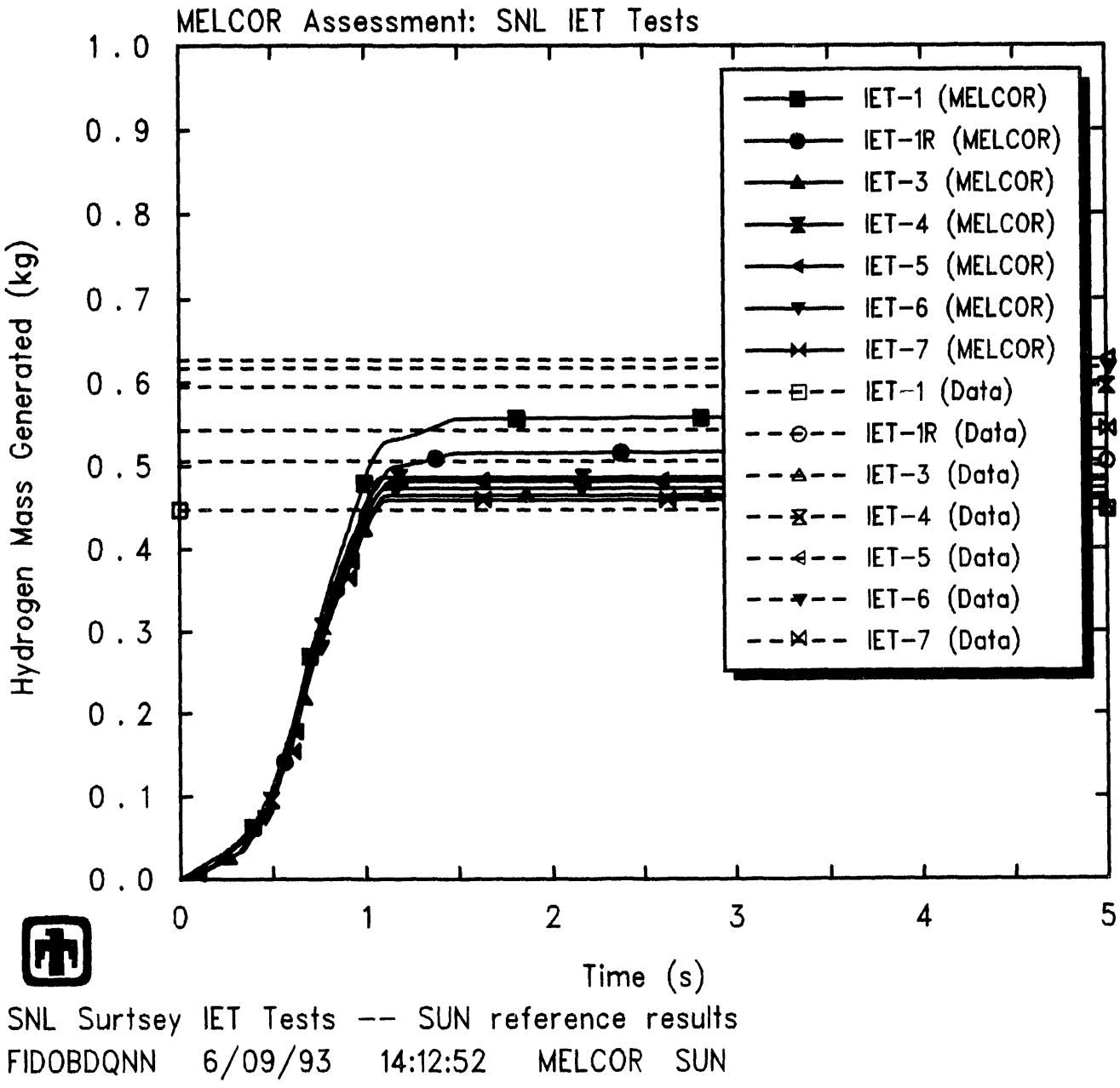

Figure 4.2. Hydrogen Production for SNL/IET Experiments Reference Calculation

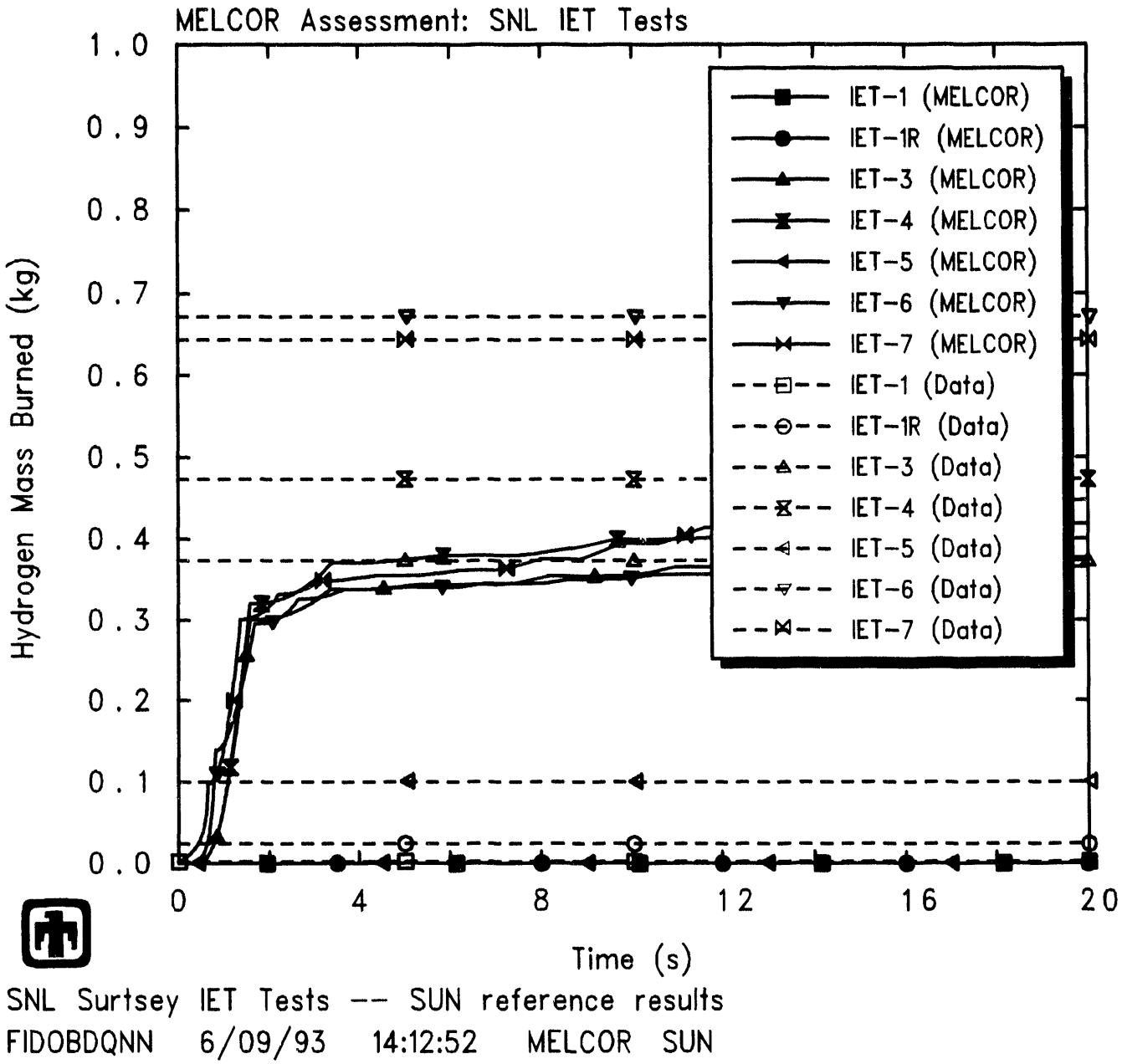

Figure 4.3. Hydrogen Combustion for SNL/IET Experiments – Reference Calculation

ally less than measured values, especially in the experiments with hydrogen combustion, while the hydrogen production and combustion calculated using the experimental procedure on the MELCOR results are generally greater than measured. Also, the actual amount of hydrogen calculated to be produced by MELCOR is lower in the tests with oxygen initially present (SNL/IET-3 through SNL/IET-7) than in the experiments with no significant oxygen initially present (SNL/IET-1 and SNL/IET-1R), while deriving the amounts of hydrogen produced and burned assuming only steam/metal reactions yields greater hydrogen production in SNL/IET-3 through SNL/IET-7 than in SNL/IET-1 and SNL/IET-1R, reproducing the trend seen in the tabulated experimental data.

Overall, the "correct" answers are likely to lie somewhere between the two limiting assumptions. It is unlikely that there is no oxidation of metal with free oxygen at all (as assumed in the experimental analysis protocol). However, MELCOR would be expected to exaggerate the relative degree to which metal oxidizes with free oxygen *vs* with steam, because of the hierarchical assumptions in the MELCOR FDI/HPME/DCH model and because, in the experiment, the debris transport probably lags the steam/hydrogen mixture flow, so that not much of the debris gets to see much oxygen, while in the MELCOR model the debris is immediately transported to its ultimate distribution (as discussed in more detail in Sections 3.1 and 5.2) within 1s while the steam blowdown is modelled "normally" as a transient process taking several seconds.

(The quantification of hydrogen production and combustion in the SNL/IET experiments assuming that all oxygen depletion was due to reaction with hydrogen had an unforeseen effect on our MELCOR analyses. In particular, the choice of a very short time constant for airborne debris oxidation (0.025s in the reference analyses) was driven by trying to explicitly match the reported hydrogen production and combustion data; sensitivity study results show very little difference in calculated pressures or temperatures for $0.01\text{s} \leq \tau_{ox} \leq 0.1\text{s}$, because the oxidation rate is essentially limited by availability of steam and/or oxygen at the shorter characteristic interaction times, and the hydrogen production and combustion results later derived from a molar balance assuming only steam/metal reactions (as in the test data analysis) is in better agreement with test data for calculations using longer characteristic airborne-debris oxidation times ($\tau_{ox} \geq 0.1\text{s}$), which seems a more reasonable value based on physical grounds.)

Figures 4.4 and 4.5 depict the hydrogen and oxygen mole fractions, respectively, in the subcompartments and dome. The test data comes from gas grab bottle samples taken in the Surtsey vessel at 2 and 30min, and a data point from a grab bottle sample taken at 2-7s in the subcompartments is included. Note that the data is included primarily to show late-time response and should not be interpreted as showing constant conditions throughout the test period; the single data point available in the subcompartments at 2-7s indicates substantial atmosphere composition variations occurred early in the transient. The calculations show a rapid transient during the first few seconds, during HPME, and then generally show a gradual approach to the final, post-test data.

Figure 4.6 compares Surtsey vessel pressures measured in the SNL/IET experiments to pressures calculated in our final, reference MELCOR analyses. (The pressures measured at three levels in the Surtsey vessel with three different pressure transducers were

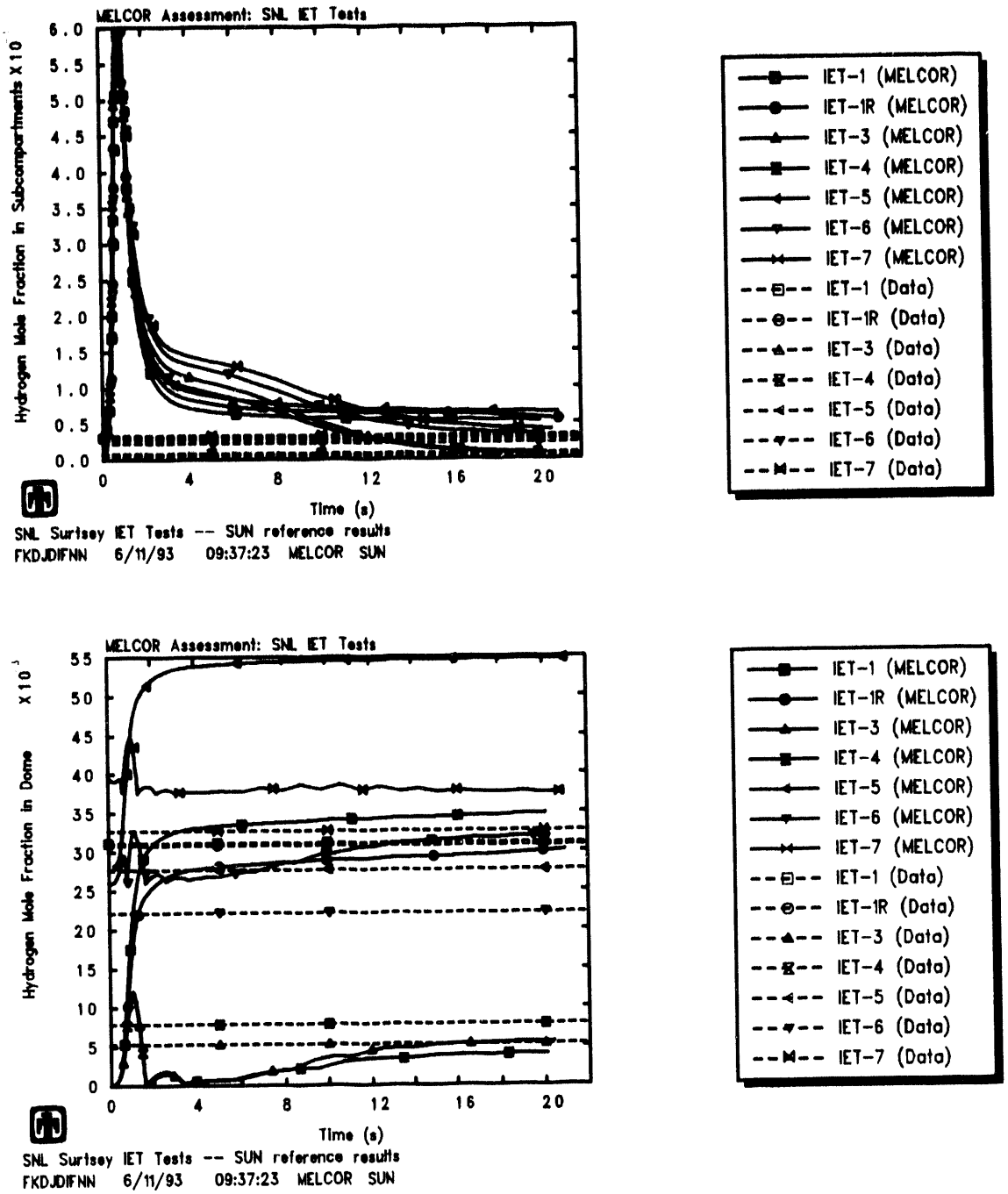

Figure 4.4. Hydrogen Mole Fractions in the Subcompartments (top) and Dome (bottom) for SNL/IET Experiments Reference Calculation

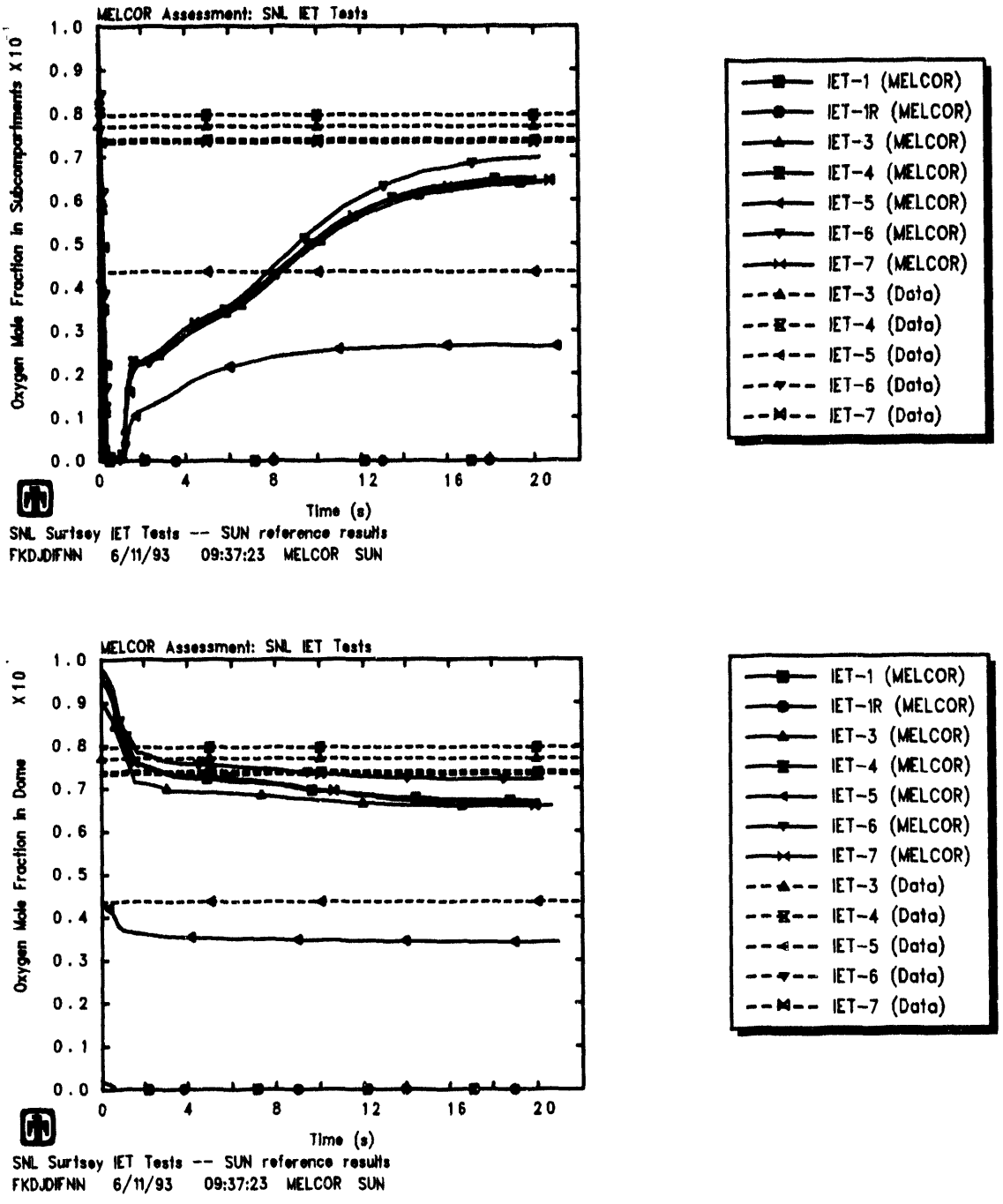

Figure 4.5. Oxygen Mole Fractions in the Subcompartments (top) and Dome (bottom) for SNL/IET Experiments - Reference Calculation

virtually identical; the pressures calculated in the subcompartments control volume and the upper-dome control volume were also virtually identical.) The pressure signature observed falls into two major subdivisions, caused by the effect of hydrogen combustion. In tests SNL/IET-1 and SNL/IET-1R, the vessel was inerted with nitrogen and the hydrogen produced by steam reaction with metallic debris during blowdown could not burn; in SNL/IET-5, the vessel was "classically inerted" with carbon dioxide and again very little hydrogen combustion occurred. When the hydrogen (pre-existing or HPME-generated) was allowed to burn with oxygen in the vessel atmosphere, pressure increases rose from ~100kPa to 240-280kPa, a significant contribution to containment pressurization. The lack of substantially higher peak pressures in tests with pre-existing hydrogen indicates that combustion of pre-existing hydrogen did not occur on the same time scale as the HPME.

Table 4.4 compares the measured and calculated peak pressures for the tests analyzed, and also indicates how much of the predicted pressurization was due to the steam blowdown, HPME reactions and hydrogen combustion, respectively. (The individual pressurization contributions are obtained from sensitivity studies with either no melt injection or no hydrogen burn included in the MELCOR input model; the sensitivity studies with no hydrogen burn included are presented in Section 7.1.)

Qualitatively, the MELCOR results in Figure 4.6 correctly reproduce the subdivision of the pressure response into two major families, caused by the effect of hydrogen combustion, as seen in the test data. (Recall that the MELCOR input model was adjusted to approximate the observed hydrogen combustion behavior in these DCH experiments, as discussed in Sections 3.1 and 7.1.) Quantitatively, the MELCOR results in Figure 4.6 and in Table 4.4 also correctly reproduce a peak pressure rise of ~100kPa due to HPME and ~150kPa due to hydrogen combustion, with little pressurization (10-20kPa) from the steam blowdown.

Measured and calculated temperatures in the subcompartments are compared in Figures 4.7 and 4.8, for the three tests with little or no hydrogen burn and for the four tests in which hydrogen combustion occurred, respectively. Thermocouple results are shown for any data available, including one or more of the following: the temperature inside the subcompartment structures, temperatures inside the seal room, the temperatures in the triangular vent spaces above the pump models, and temperatures measured by thermocouples suspended ~10cm under the reactor coolant pump mockups. The single data trace for the temperature inside the subcompartment structures usually corresponds to three aspirated thermocouples in a thermocouple assembly yielding nearly identical temperature *vs* time curves. When multiple measurements are available, they show significant local temperature gradients present. The MELCOR results are generally judged to be in reasonably good agreement with the test data. Note that, although little or no hydrogen combustion occurred in SNL/IET-1, SNL/IET-1R and SNL/IET 5 while significant hydrogen combustion occurred in SNL/IET-3, SNL/IET-4, SNL/IET-6 and SNL/IET-7, the peak gas temperatures in the subcompartment structures measured in all these tests were almost identical; this indicates that the primary mechanism for heating the subcompartment atmosphere was probably debris/gas heat transfer and not

Table 4.3. Hydrogen Results for the SNL/IET Experiments – Reference Calculation

Experiment	Hydrogen (gm-moles)					
	Produced			Burned		
	Data†	MELCOR¶	MELCOR‡	Data†	MELCOR¶	MELCOR‡
IET-1	233	286	266	3	0	4
IET-1R	248	266	267	11	0	28
IET-3	227	232	352	190	188	313
IET-4	303	243	361	240	209	332
IET-5	319	240	313	53	0	91
IET-6	319	236	354	345	218	307
IET-7	274	229	351	323	223	350

†from gas grab bottle samples at 30min
¶actual end-of-calculation values at 20s
‡calculated from initial and final oxygen and hydrogen moles assuming only steam/metal reactions

Table 4.4. Peak Pressures for the SNL/IET Experiments – Reference Calculation

Experiment	ΔP_{MAX} (kPa)				
		Total	Blowdown	HPME	H_2 Burn
	Data	MELCOR	only	only	only
IET-1	98	84	18	66	0
IET-1R	103	102	21	81	0
IET-3	246	276	18	102	156
IET-4	262	285	24	96	155
IET-5	103	93	17	76	0
IET-6	279	266	16	105	145
IET-7	271	264	28	89	147
IET-8A	87				
IET-8B	243				

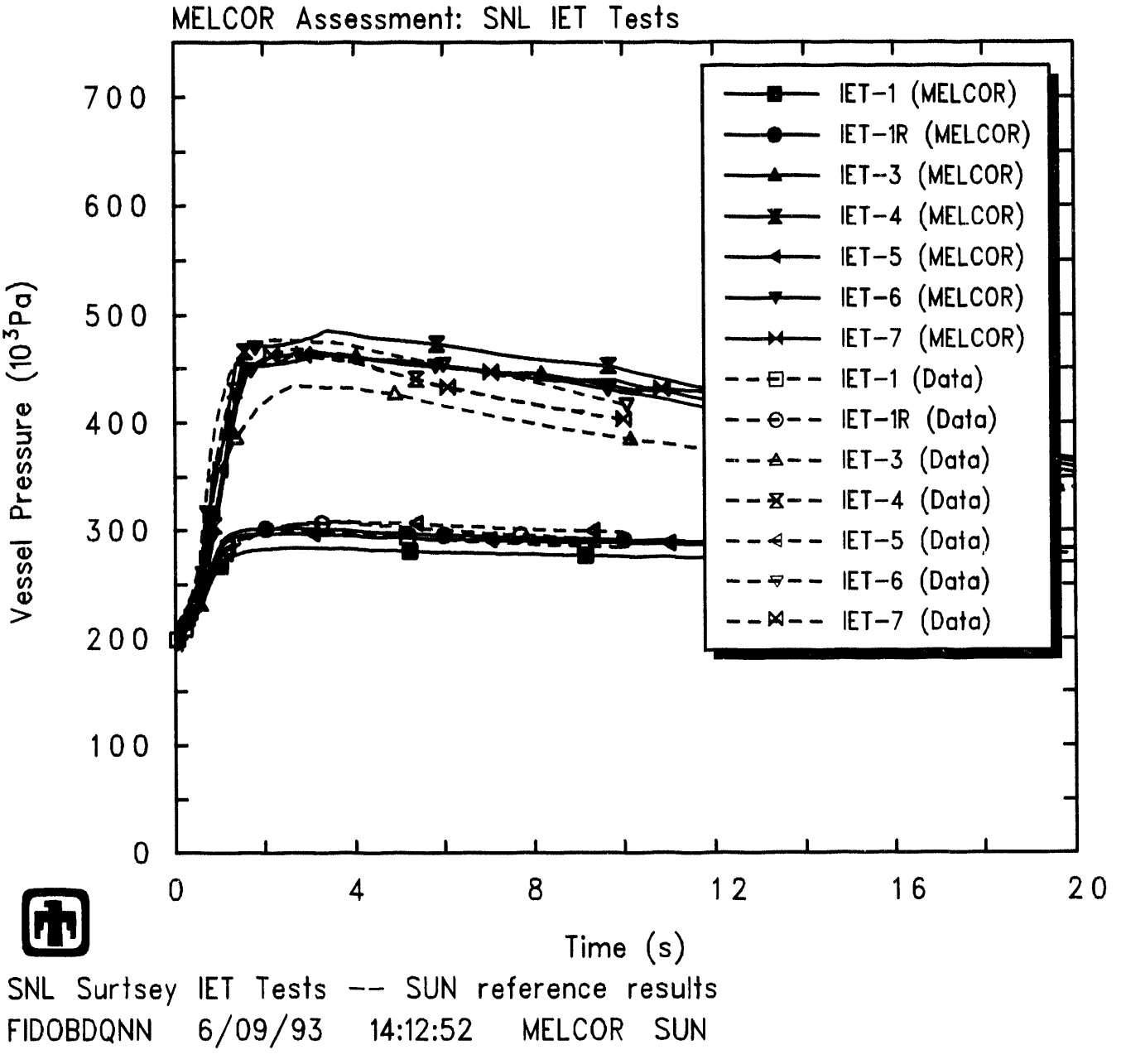

Figure 4.6. Vessel Pressures for SNL/IET Experiments – Reference Calculation

hydrogen combustion. To reproduce this behavior, in the MELCOR input we specified hydrogen combustion to be suppressed in all control volumes except the vessel dome.

Figures 4.9 and 4.10 present observed and predicted temperatures in the upper dome, above the operating deck, for two tests with little or no hydrogen burn and for four tests in which hydrogen combustion occurred, respectively. (No test data was available for test SNL/IET-1R.) Thermocouple results are given for three levels in the dome, with the levels identified in Figure 2.1.1); measured temperatures typically decreased with increasing elevation. When available, additional thermocouple results also are included for arrays in the dome, which measured temperatures from about level 3 to halfway between level 5 and 6; those arrays are shown in Figure 2.1.4). The MELCOR vessel dome atmosphere temperature results are generally in good agreement with the test data, given the localized response of the thermocouples. The significantly higher vessel temperatures observed in the tests with substantial hydrogen combustion (SNL/IET-3, SNL/IET-4, SNL/IET-6 and SNL/IET-7, in Figure 4.10) than in the tests with little or no hydrogen combustion (SNL/IET-1, SNL/IET-1R and SNL/IET-5, in Figure 4.9) are also found in the MELCOR calculations. This result is expected, because the vessel dome average temperature response is closely coupled to the vessel pressure behavior, and thus the reasonably good agreement between measurement and calculation for vessel pressures in FigureP-base is reflected in similar good agreement in observed and predicted average vessel temperatures.

No comparisons are given for the local cavity pressure. Because the MELCOR DCH model does not model transport of debris into and through the cavity, but instead immediately places the debris at its ultimate destination, the predicted cavity and chute pressures are basically the same as the subcompartments and upper vessel pressures. There is no capability to model transient debris-coolant interactions in the cavity.

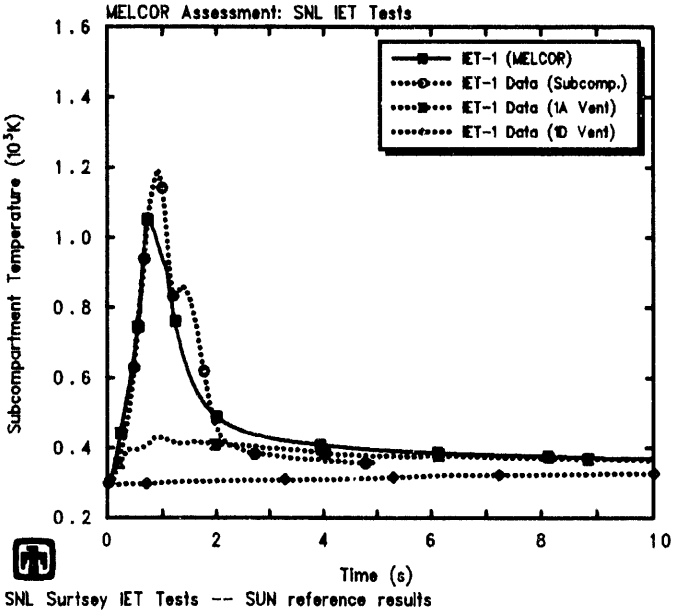

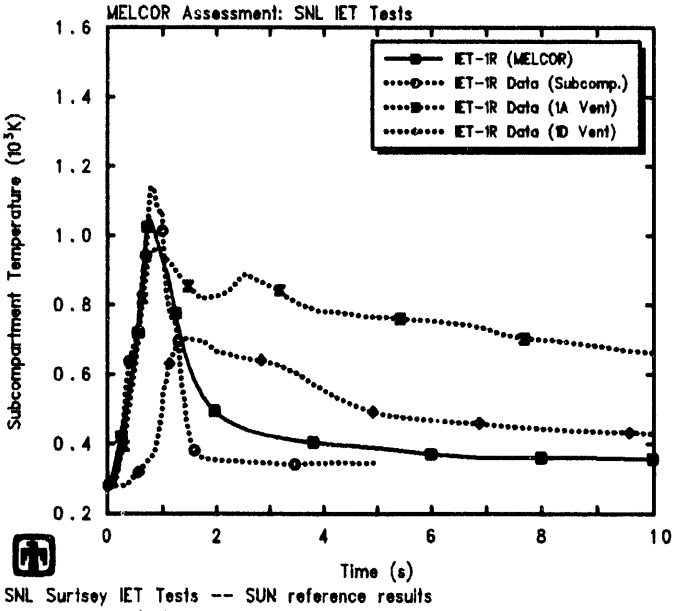

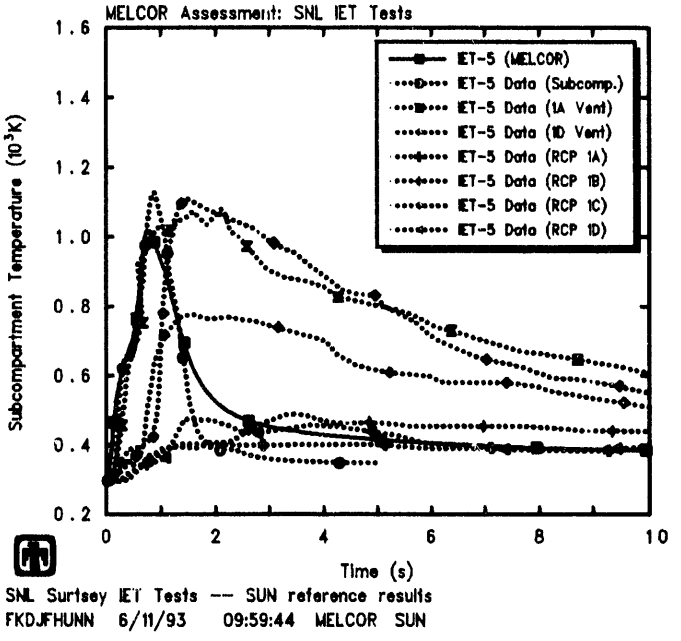

Figure 4.7. Subcompartment Temperatures for Experiments SNL/IET-1 (upper left), SNL/IET-1R (lower left) and SNL/IET-5 (middle right) Reference Calculation

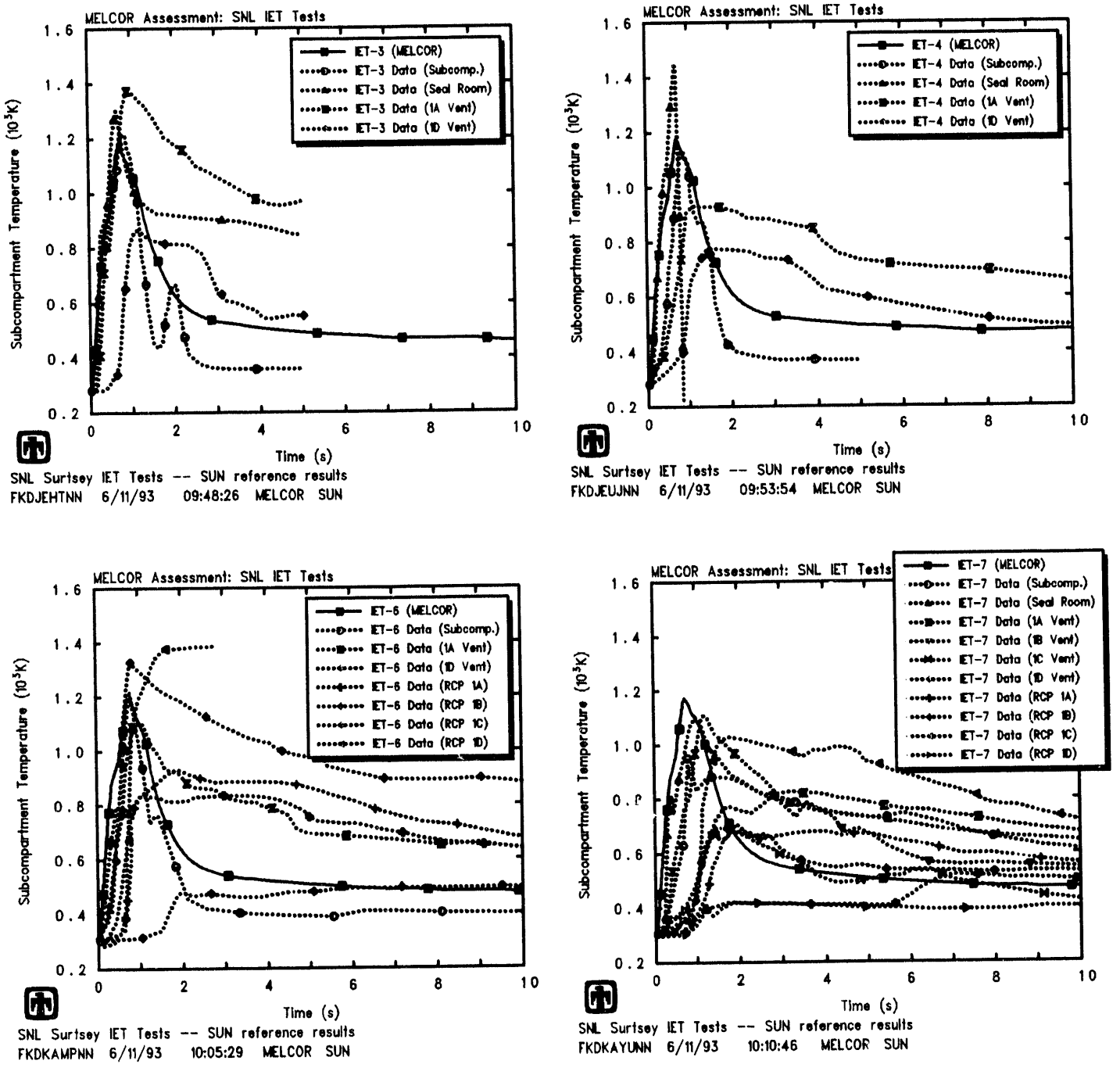

Figure 4.8. Subcompartment Temperatures for Experiments SNL/IET-3 (upper left), SNL/IET-4 (upper right), SNL/IET-6 (lower left) and SNL/IET-7 (lower right) — Reference Calculation

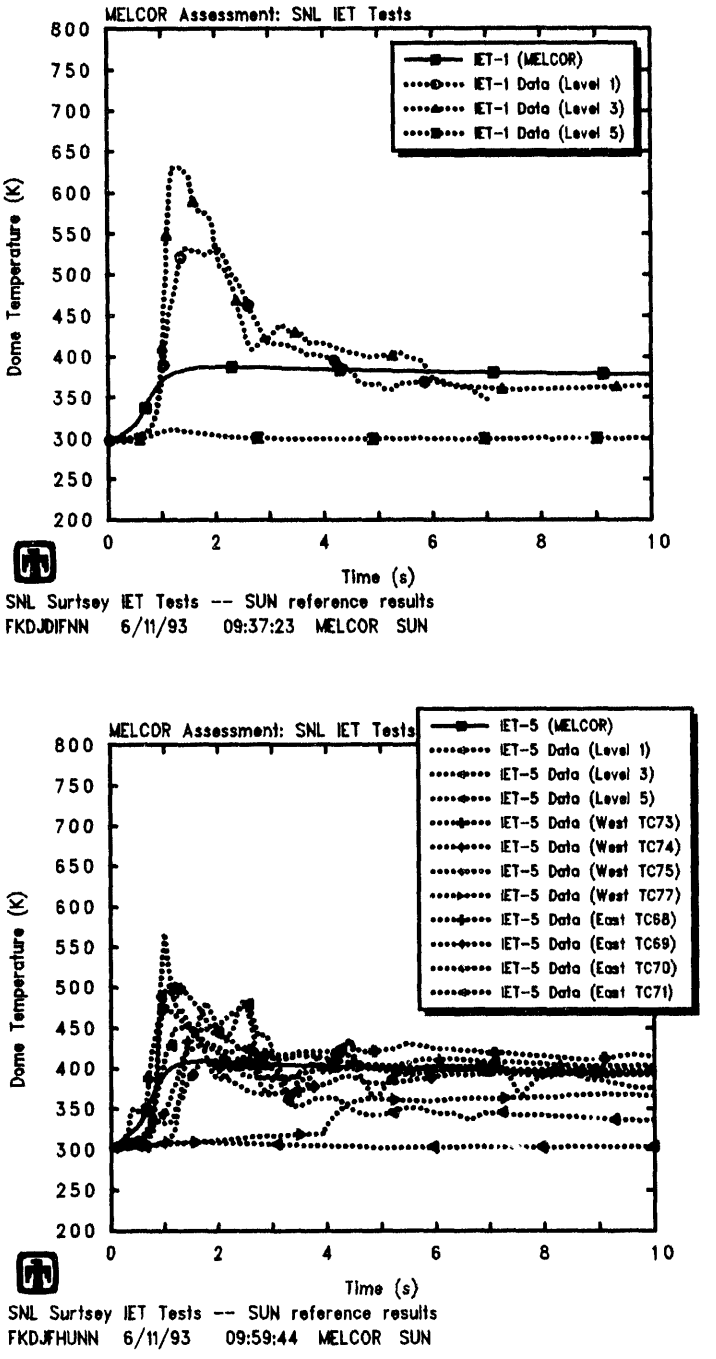

Figure 4.9. Dome Temperatures for Experiments SNL/IET-1 (top) and SNL/IET-5 (bottom) - Reference Calculation

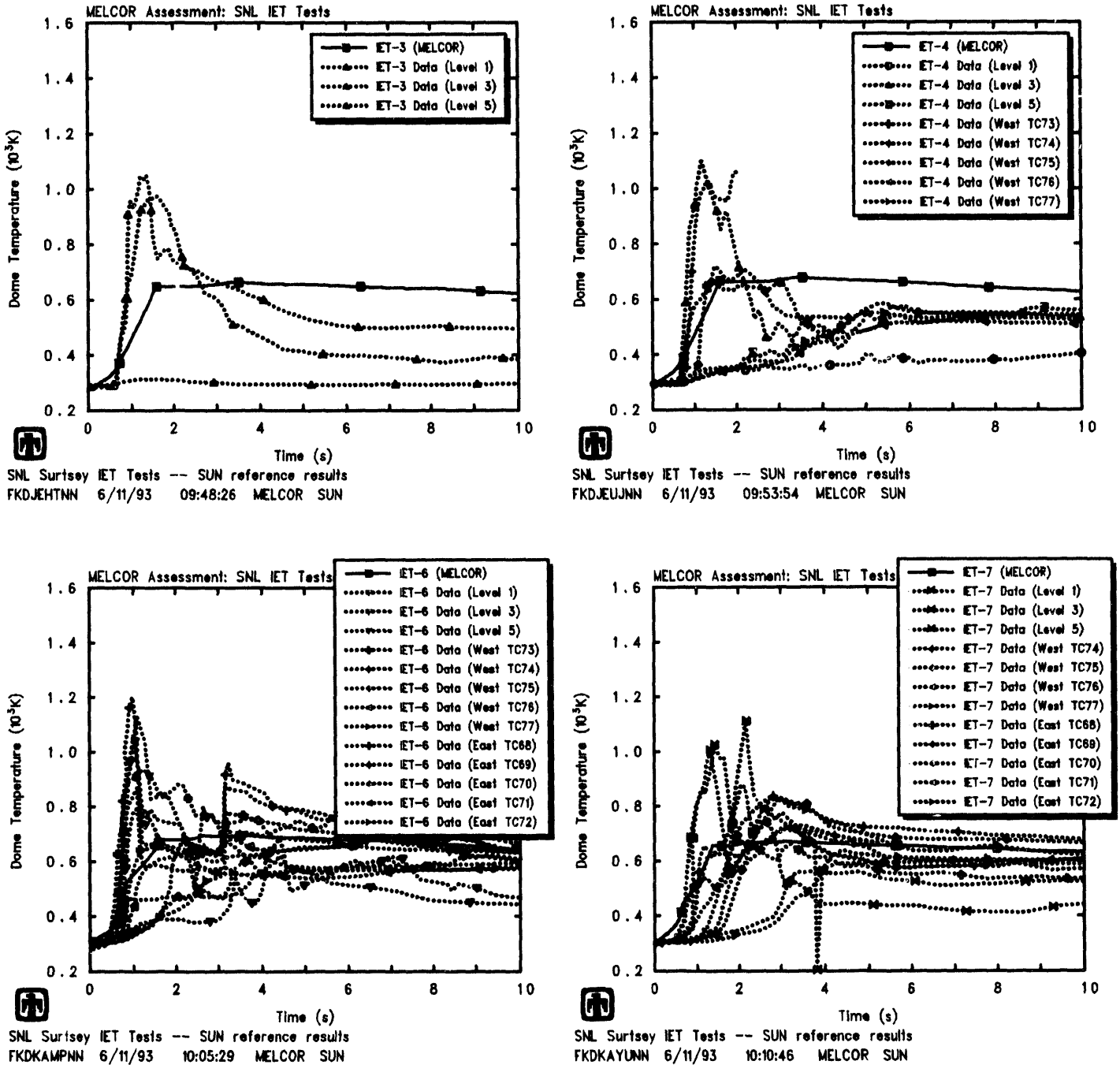

Figure 4.10. Dome Temperatures for Experiments SNL/IET-3 (upper left), SNL/IET-4 (upper right), SNL/IET-6 (lower left) and SNL/IET-7 (lower right) – Reference Calculation

5 Experiment Uncertainty Studies

There are experimental uncertainties in both the exact values to be used for some MELCOR input values and in the modelling approach taken to represent other test conditions. As described in this section, a set of sensitivity studies has been done varying those parameters to determine how the results could be affected by such experiment uncertainties.

5.1 Steam Blowdown

As described in Section 3.1, a valve with a time-dependent area was used in the flow path from the steam accumulator to the cavity to control the rate of steam injection, with the opening rate adjusted to match the observed steam accumulator depressurization rates reasonably well. Although different final hole diameters were identified in the test reports for the opening from the melt generator to the cavity (as given in Table 2.1.2), the input was kept the same for the valve and associated time-dependent area used in the flow path from the steam accumulator to the cavity to control the rate of steam injection. In the experiments the thermite reaction products and the steam were injected through the same opening, with some indication in the data of occasional plugging and flow interruption. In the MELCOR model the debris is inserted separately, directly to its ultimate destination; thus MELCOR does not model any debris blockage or obstruction possibly affecting the steam injection rate.

The valve opening rate was selected to match the observed steam accumulator depressurization rates in the various tests reasonably well. Calculations were done using valve opening times of 0.5s, 1s, 2s and 4s, with the time-dependent area increasing linearly in all cases. Figure 5.1.1 shows predicted pressures in the steam delivery volume during the blowdown process for all tests analyzed, using the different valve opening times, together with experimental data for comparison. The calculated blowdown is obviously too rapid with the valve opening over 0.5s, and too slow with the valve opening over 4s. The steam accumulator depressurization predicted with a valve opening time of 2s appears in slightly better agreement with test data than the results using a valve opening time of 1s, and the 2s opening time was used in the rest of our Surtsey HET assessment analyses.

The corresponding predicted vessel pressures are presented in Figure 5.1.2, with test data included for reference. The effect of varying the steam blowdown timing is reflected in a small change in the peak vessel pressure, with slightly higher pressures predicted for the more rapid steam blowdown, in the tests with hydrogen burn occurring; little or no effect is visible for the cases with no hydrogen burn.

The lack of any visible effect of varying the steam blowdown timing for the cases with no hydrogen burn is due to the small contribution made by the steam blowdown to the overall vessel response, as shown in Section 4. The slight rise in vessel pressure seen with the more rapid steam blowdown in the cases with hydrogen burn is due to more steam being available early in the HPME reaction so that more hydrogen is generated

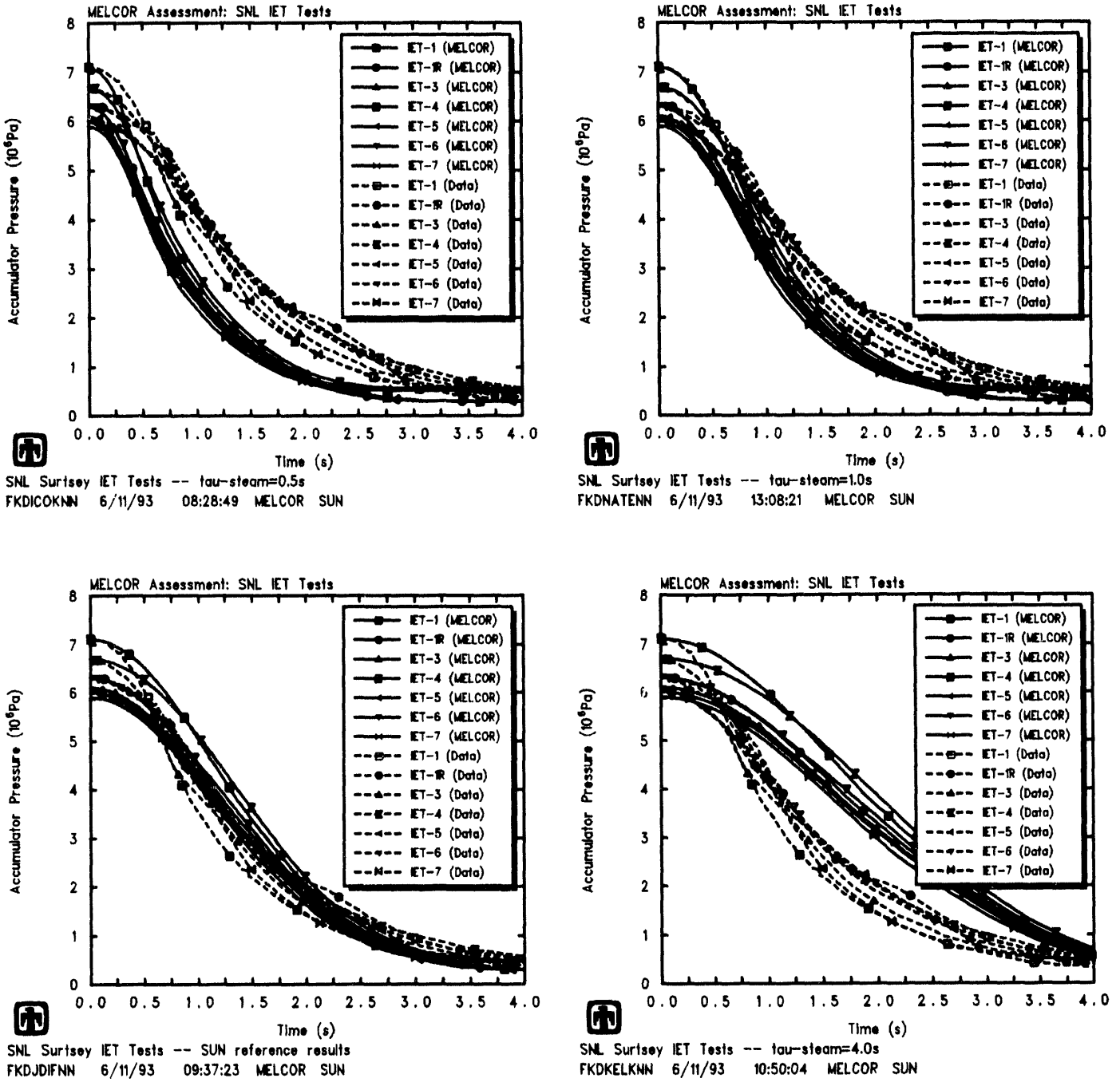

Figure 5.1.1. Steam Accumulator Pressures for SNL/IET Experiments Using Valve Opening Times of 0.5s (upper left), 1s (upper right), 2s (lower left) and 4s (lower right) Steam Blowdown Sensitivity Study

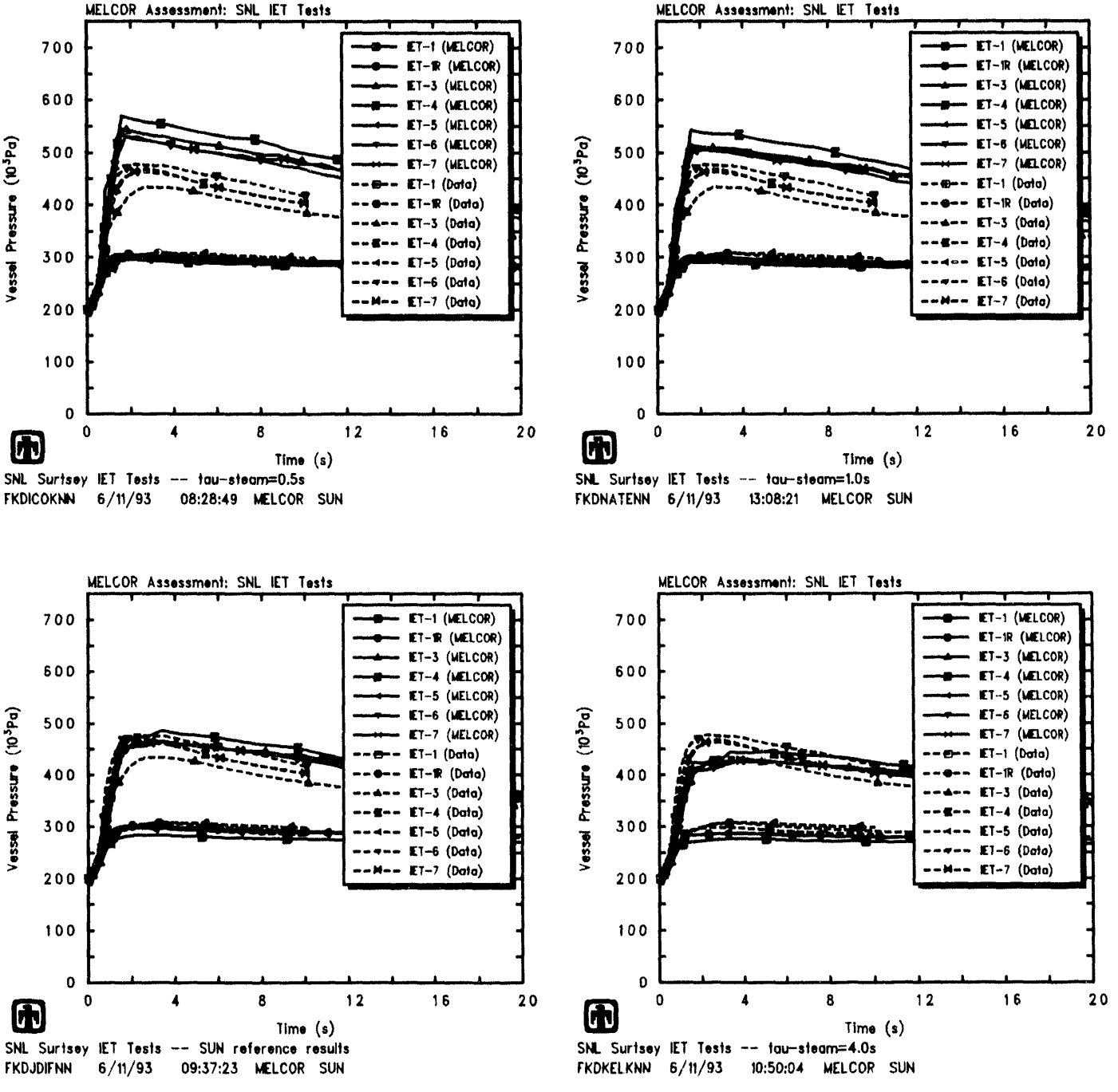

Figure 5.1.2. Vessel Pressures for SNL/IET Experiments Using Valve Opening Times of 0.5s (upper left), 1s (upper right), 2s (lower left) and 4s (lower right) Steam Blowdown Sensitivity Study

in steam-debris interactions; the subsequent burning of the greater amount of hydrogen generated then produces the increase in vessel pressure. Tables 5.1.1 and 5.1.2 illustrate this by comparing the amounts of hydrogen generated and burned, respectively, in these various cases. Test data estimates of the amounts of hydrogen produced and burned are included for reference.

5.2 Melt Injection Timing

The MELCOR DCH model does not model transient transport of debris into and through the system, but instead immediately places the debris at its ultimate destination. MELCOR uses a single function for the time-dependence of the melt injection in all control volumes and heat structures; in reality, the melt reaches the subcompartments later than the cavity, and the dome later than the subcompartments.

Melt injection could begin at t=0, since that is defined as the time that the brass plug at the bottom of the crucible failed and was expelled by high-pressure steam into the cavity. Cavity pressure data indicates a pressure spike from fuel-coolant interaction (FCI) as molten brass, steel and thermite enters the cavity between 0 and ~0.3s, followed by debris entrainment from the cavity into the subcompartments between about 0.4s and 0.8s. High-speed cameras showed debris particles ejected from the subcompartment structures toward the upper dome of the Surtsey vessel, with aerosols visible at ~0.1s and hydrogen jet burning visible at about 0.2-0.4s; at about 1s, molten particles were seen to fall, implying that debris injection and entrainment was over.

The time-dependence of the melt addition in the MELCOR input was adjusted to match the rate of pressure and temperature increase in the vessel. Melt injection was always assumed to start at time=0, but the time period over which melt injection was specified to occur was varied from 0.1s though 0.5s and 1s to 2.5s in these sensitivity study analyses; in each case, the injection rate was assumed constant within the time period.

Resulting predicted vessel pressures are shown in Figure 5.2.1, together with the test data. The effect of lengthening the melt injection timing is reflected in a progressive delay in the peak vessel pressure and a corresponding increase in the magnitude of the peak pressure. As in the steam blowdown timing study results, the change is more pronounced in the tests with hydrogen burn occurring, with little or no effect visible for the cases with no hydrogen burn. The calculated pressurization is obviously too low and too early with a melt injection period of 0.1s, and too high and too late with a melt injection period of 2.5s. The best agreement for vessel pressure is found using melt injection periods of 0.5-1.0s.

Tables 5.2.1 and 5.2.2 compare the amounts of hydrogen generated and burned, respectively, in these various cases. The amount of hydrogen produced is a very strong function of the melt injection period assumed, as is the amount of hydrogen burned. The hydrogen production calculated assuming a melt injection period of 1s is in best agreement with data. (The hydrogen combustion predicted appears too low in all cases,

Table 5.1.1. Hydrogen Generation for the SNL/IET Experiments – Steam Blowdown Sensitivity Study

Experiment	Hydrogen Produced (gm-moles)				
	Data†	MELCOR ‡ τ_{VLV} =			
		0.5s	1s	2s	4s
IET-1	233	438/409	369/343	286/266	224/207
IET-1R	248	407/401	341/338	266/267	210/212
IET-3	227	335/443	298/409	232/352	181/308
IET-4	303	350/458	314/428	243/361	181/319
IET-5	319	365/425	310/374	240/313	188/267
IET-6	319	339/445	305/414	236/354	183/309
IET-7	274	327/438	294/405	229/351	178/305

†from gas grab bottle samples at 30min
‡(actual values at 20s)/ (assuming only steam/metal reactions)

Table 5.1.2. Hydrogen Combustion for the SNL/IET Experiments – Steam Blowdown Sensitivity Study

Experiment	Hydrogen Burned (gm-moles)				
	Data†	MELCOR ‡ τ_{VLV} =			
		0.5s	1s	2s	4s
IET-1	3	0/4	0/4	0/4	0/4
IET-1R	11	0/28	0/28	0/28	0/28
IET-3	190	272/387	242/359	188/313	147/278
IET-4	240	300/414	272/390	209/332	164/296
IET-5	53	0/88	0/88	0/91	0/94
IET-6	345	257/373	234/351	182/307	140/272
IET-7	323	321/437	286/404	223/350	173/304

†from gas grab bottle samples at 30min
‡(actual values at 20s)/ (assuming only steam/metal reactions)

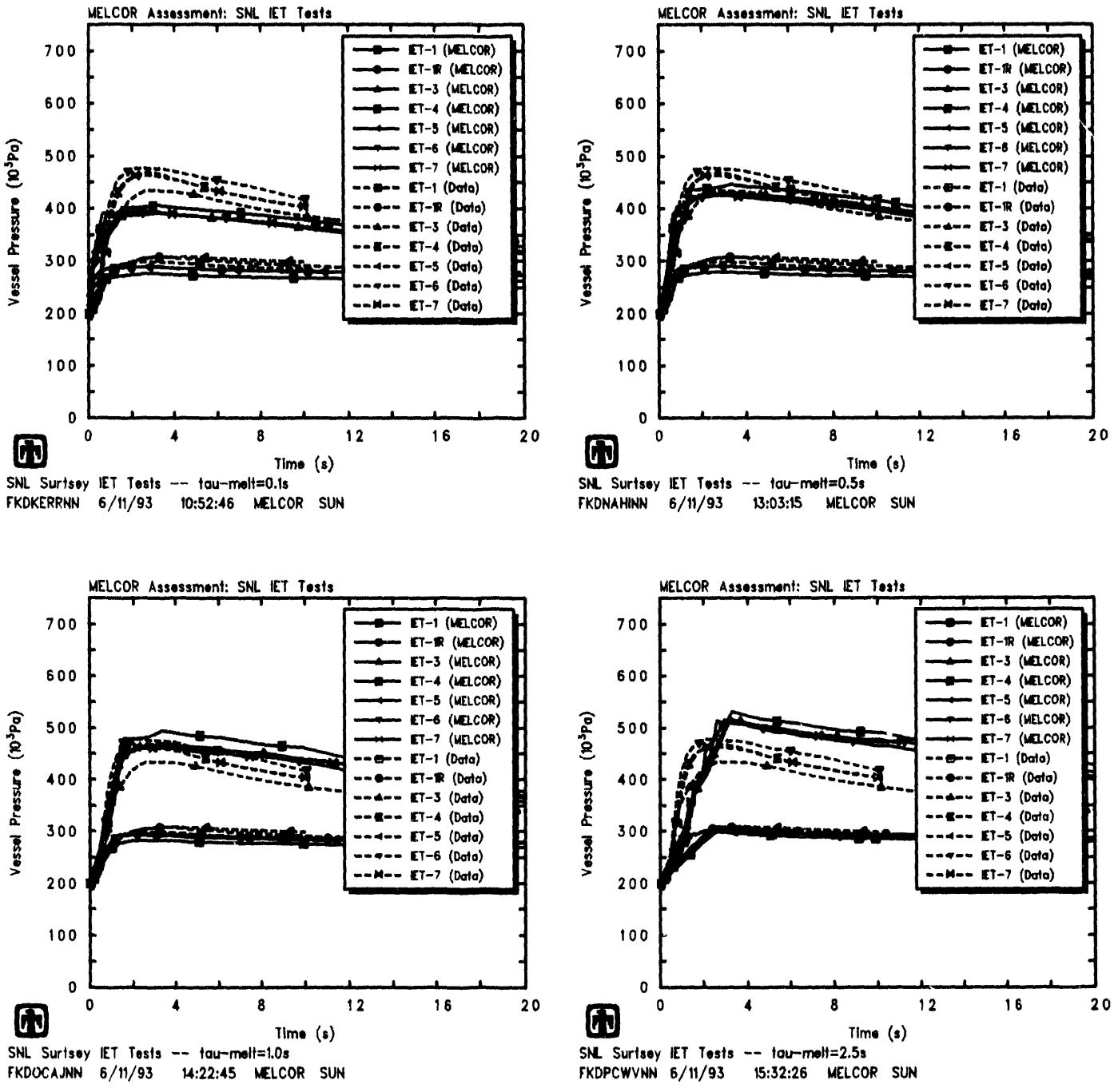

Figure 5.2.1. Vessel Pressures for SNL/IET Experiments Using Melt Injection Times of 0.1s (upper left), 0.5s (upper right), 1s (lower left) and 2.5s (lower right) Melt Injection Timing Sensitivity Study

as a fraction of the amount of hydrogen generated, but recall that we are comparing calculated values at 20s with experiment estimates based upon gas grab bottle samples taken at 30min; also recall that the test data indicates some late-time hydrogen burn must have occurred, and the analyses also show a gradual increase in the amount of hydrogen burned during the later time periods.)

The timing assumed for the melt injection also has a very strong effect on the subcompartment temperatures predicted, as illustrated in Figure 5.2.2. The calculated subcompartment temperatures rise during the assumed injection period, and begin dropping rapidly after melt injection stops, resulting in a strong peak at the end of the injection period. The calculated subcompartment temperature rise is obviously too early with a melt injection period of 0.1s and also with a period of 0.5s, and much too late with a melt injection period of 2.5s. The best agreement is found using a melt injection period of 1s, but the different inflections in the test data curves and in the MELCOR results suggest that the melt injection may not have occurred at a constant rate during the injection period.

Based upon the results for the vessel pressure, hydrogen generation and subcompartment temperatures, the remainder of our analyses were run with a melt injection period of 1s, with most of the injection occurring during the second half of that period. (The actual values used were given in Table 3.1.1.) This $\leq$1s melt injection period is in reasonable agreement with test observations, especially given that the MELCOR DCH model does not account for any localized timing delays due to debris transport to different locations.

5.3 Melt Injection Amount

Table 2.1.3 gave a debris recovery summary for the Surtsey HET experiments. The total debris mass recovered from the vessel was usually greater than the initial thermite charge due to melting of the inner wall of the crucible, vaporization of the fusible brass plug, ablation of concrete in the cavity and structures, and oxidation of metallic debris. Despite the careful duplication of the initial 43kg thermite charge in the Surtsey HET experiments, the different amounts of debris collected from the melt generator and from the vessel result in some uncertainty in the actual amount and composition of melt injected into the vessel, as indicated in Table 5.3.1.

The majority of our MELCOR analyses simply specified the original 43kg thermite charge mass, neglecting both the retention of any debris in the melt generator and the addition of any debris due to melting of the inner wall of the crucible, vaporization of the fusible brass plug, ablation of concrete in the cavity and structures, and oxidation of metallic debris. (The same assumption was made in the CONTAIN analyses [27].) To help determine the effect of the injection mass source uncertainty, calculations were done in which the total melt mass injected was reduced to 80% and 90%, and increased to 110%, of the basecase 43kg melt source. The fractional amounts of Al_2O_3, Fe and Cr in the debris, the debris temperature and fractional distribution, and the fraction injected *vs* time were unchanged.

Table 5.2.1. Hydrogen Generation for the SNL/IET Experiments - Melt Injection Timing Sensitivity Study

Experiment	Hydrogen Produced (gm-moles)				
	Data†	MELCOR ‡			
		τ_{Debris}=			
		0.1s	0.5s	1s	2.5s
IET-1	233	144/129	207/189	293/271	458/418
IET-1R	248	134/142	192/197	271/270	439/418
IET-3	227	146/269	157/310	239/374	352/474
IET-4	303	99/278	162/319	251/390	346/474
IET-5	319	108/208	167/258	244/322	390/447
IET-6	319	97/269	160/313	239/374	351/472
IET-7	274	96/267	154/306	231/365	350/470

‡end-of-calculation values at 20s
‡(actual values at 20s)/ (assuming only steam/metal reactions)

Table 5.2.2. Hydrogen Combustion for the SNL/IET Experiments - Melt Injection Timing Sensitivity Study

Experiment	Hydrogen Burned (gm-moles)				
	Data†	MELCOR ‡			
		τ_{Debris}=			
		0.1s	0.5s	1s	2.5s
IET-1	3	0/4	0/4	0/4	0/4
IET-1R	11	0/26	0/26	0/26	0/26
IET-3	190	87/262	135/290	191/331	255/391
IET-4	240	93/273	145/305	214/358	272/413
IET-5	53	0/109	0/103	0/97	0/95
IET-6	345	82/257	129/286	184/325	246/385
IET-7	323	94/267	150/305	225/365	333/466

‡end-of-calculation values at 20s
‡(actual values at 20s)/ (assuming only steam/metal reactions)

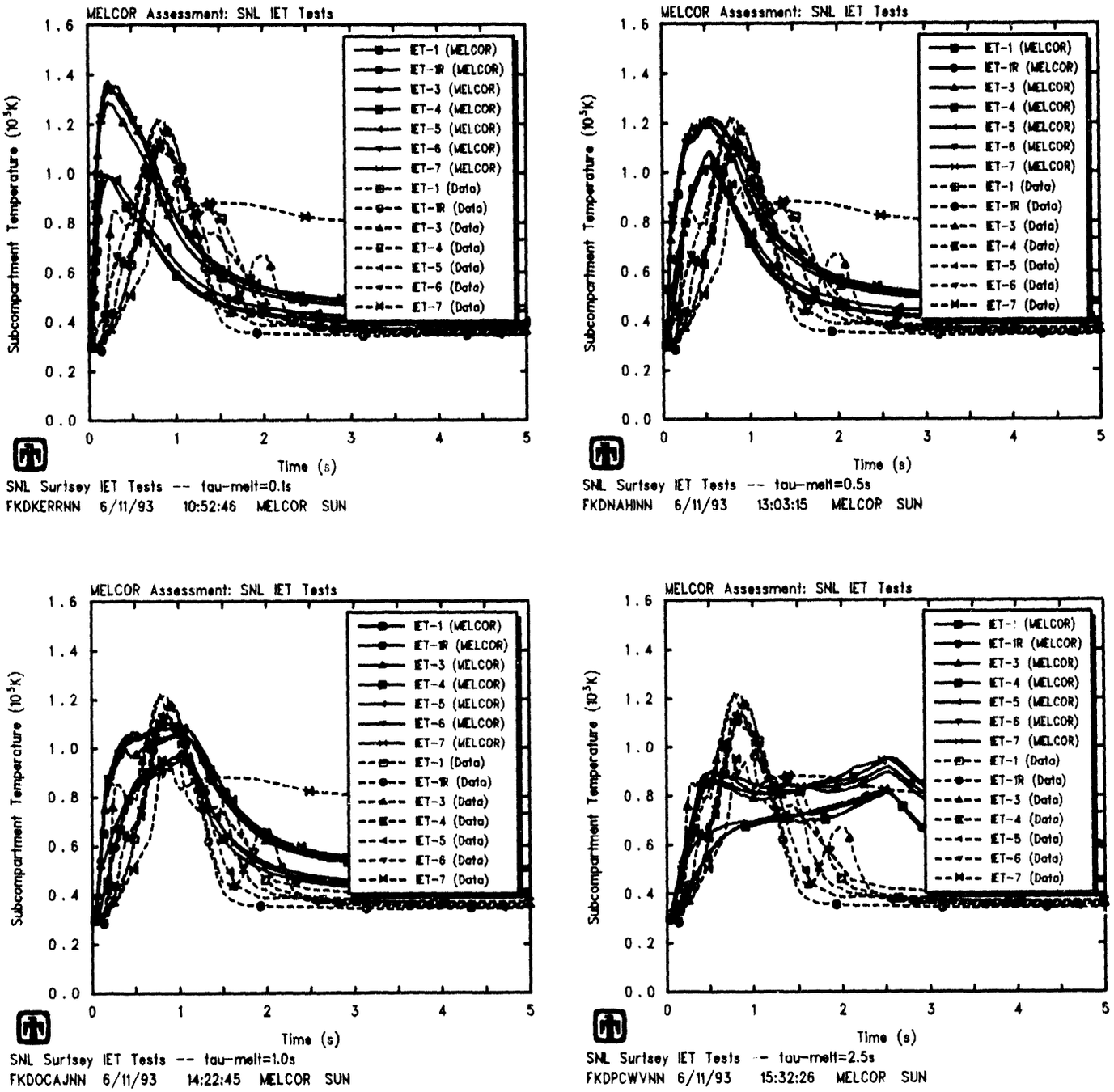

Figure 5.2.2. Subcompartment Temperatures for SNL/IET Experiments Using Melt Injection Times of 0.1s (upper left), 0.5s (upper right), 1s (lower left) and 2.5s (lower right) Melt Injection Timing Sensitivity Study

Table 5.3.1. Debris Masses for the SNL/IET Experiments – Melt Injection Amount Sensitivity Study

	IET-1	IET-1R	IET-3	IET-4	IET-5	IET-6	IET-7
% Excess Mass Recovered (Total)†	27	26	29	40	30	24	32
% Excess Mass Recovered (excluding Crucible)‡	9.6	9.4	8.8	19	5.1	4.5	13
% Initial Charge Recovered from Crucible¶	10.6	10.8	10.5	22.7	6.0	5.3	15.7
% Initial Charge Injected into System§	89	89	90	77	94	95	84
% Total Collected Recovered from Crucibleß	8.3	8.6	8.1	16.3	4.7	4.3	11.9
% Total Collected Injected into System£	92	91	92	84	95	96	88

†(Total mass recovered - 43kg) / 43kg
‡[Total mass recovered from (cavity/chute+subcompartments+dome) - 43kg] / 43kg
¶(Mass recovered from crucible) / 43kg
§[Mass recovered from (cavity/chute+subcompartments+dome)] / 43kg
ß(Mass recovered from crucible) / (Total mass recovered)
£[Mass recovered from (cavity/chute+subcompartments+dome)] / (Total mass recovered)

Figure 5.3.1 shows pressures in the vessel predicted using various melt amounts, together with experimental data for comparison. As would be expected, the vessel pressurization increases as more melt mass is injected during the HPME. Also, as seen in many of our other sensitivity study analyses, the effect is larger for those tests with hydrogen burn occurring than in the cases with no hydrogen burn.

Tables 5.3.2 and 5.3.3 present the amounts of hydrogen generated and burned, respectively, in these various cases. Test data estimates of the amounts of hydrogen produced and burned are included for reference. There is a small increase in both hydrogen production and combustion with increasing melt injection amount.

Figure 5.3.2 gives subcompartment temperatures calculated using various melt amounts, together with experimental data. As seen in the hydrogen production and combustion, there is a small increase in subcompartment temperature with increasing melt injection amount.

5.4 Melt Injection Temperature

Test data indicated a debris temperature of 2300K, which was the value used in our MELCOR reference analyses whose results were given in Section 4. As a sensitivity study, calculations were run with the debris temperature set to 2000K, 2300K, 2500K and 3000K. Values in the 2300K-2500K range were considered most likely in the experiments; 2000K and 3000K were selected as bounding values based upon zircaloy melting at ~2100-2200K and on UO_2 melting at 3113K.

Vessel pressures predicted varying the debris temperature are presented in Figure 5.4.1, together with test data. The effect of increasing the melt temperature is to increase the vessel pressures calculated. Tables 5.4.1 and 5.4.2 summarize the amounts of hydrogen generated and burned, respectively, with very little dependence on melt temperature visible.

This debris temperature variation has the strongest effect on the subcompartment temperatures predicted, as indicated in Figure 5.4.2. The calculated subcompartment temperatures increase with increasing debris temperature, with a 1000K increase in debris temperature producing a ~500K increase in subcompartment peak temperatures.

5.5 Melt Injection Distribution

As noted at the start of Section 5.2, the MELCOR DCH model does not model transient transport of debris into and through the system, but instead immediately places the debris at its ultimate destination. The debris fractions placed in each control volume and on each heat structure are controlled solely by user input. In these IET analyses, the debris injected was all placed in various control volume atmospheres and then allowed to settle out onto floor heat structures; no debris was specified to be deposited directly onto any heat structures.

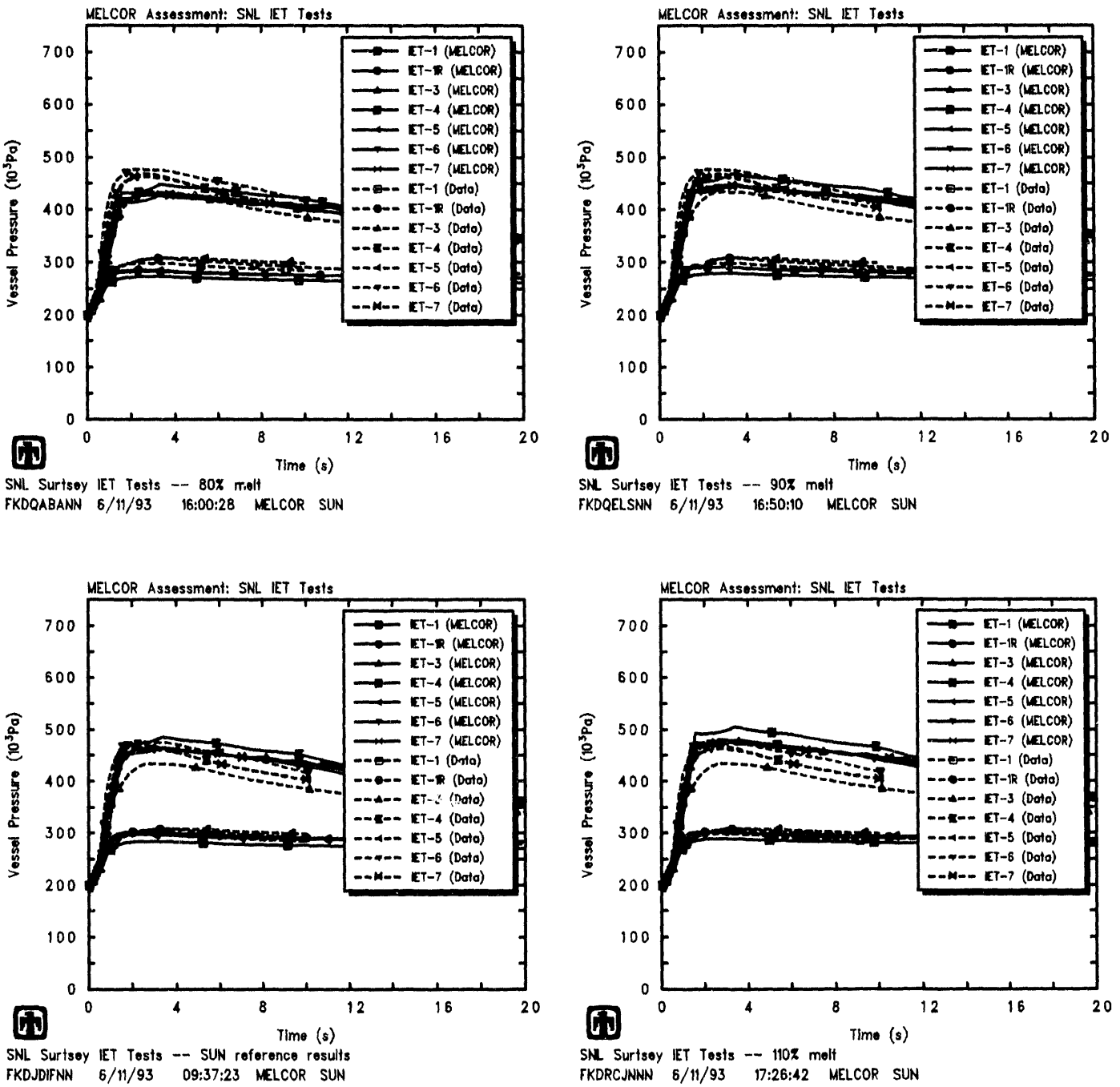

Figure 5.3.1. Vessel Pressures for SNL/IET Experiments Using Melt Masses of 80% (upper left), 90% (upper right), 100% (lower left) and 110% (lower right) the Initial Charge – Melt Injection Amount Sensitivity Study

Table 5.3.2. Hydrogen Generation for the SNL/IET Experiments – Melt Injection Amount Sensitivity Study

Experiment	Hydrogen Produced (gm-moles)				
	Data†	MELCOR ‡ (% Initial Charge)			
		80	90	100	110
IET-1	233	249/231	268/248	286/266	301/278
IET-1R	248	227/231	248/250	266/267	281/280
IET-3	227	199/303	215/326	232/352	245/371
IET-4	303	211/312	229/340	243/361	262/389
IET-5	319	208/269	225/292	240/313	255/334
IET-6	319	201/307	216/329	236/354	249/376
IET-7	274	194/300	212/325	229/351	242/369

†from gas grab bottle samples at 30min
‡(actual values at 20s)/ (assuming only steam/metal reactions)

Table 5.3.3. Hydrogen Combustion for the SNL/IET Experiments – Melt Injection Amount Sensitivity Study

Experiment	Hydrogen Burned (gm-moles)				
	Data†	MELCOR ‡ (% Initial Charge)			
		80	90	100	110
IET-1	3	0/4	0/4	0/4	0/4
IET-1R	11	0/28	0/28	0/28	0/28
IET-3	190	161/268	173/289	188/313	197/328
IET-4	240	181/286	197/311	209/332	225/357
IET-5	53	0/77	0/84	0/91	0/99
IET-6	345	156/267	168/287	182/307	192/326
IET-7	323	189/300	206/323	223/350	236/368

†from gas grab bottle samples at 30min
‡(actual values at 20s)/ (assuming only steam/metal reactions)

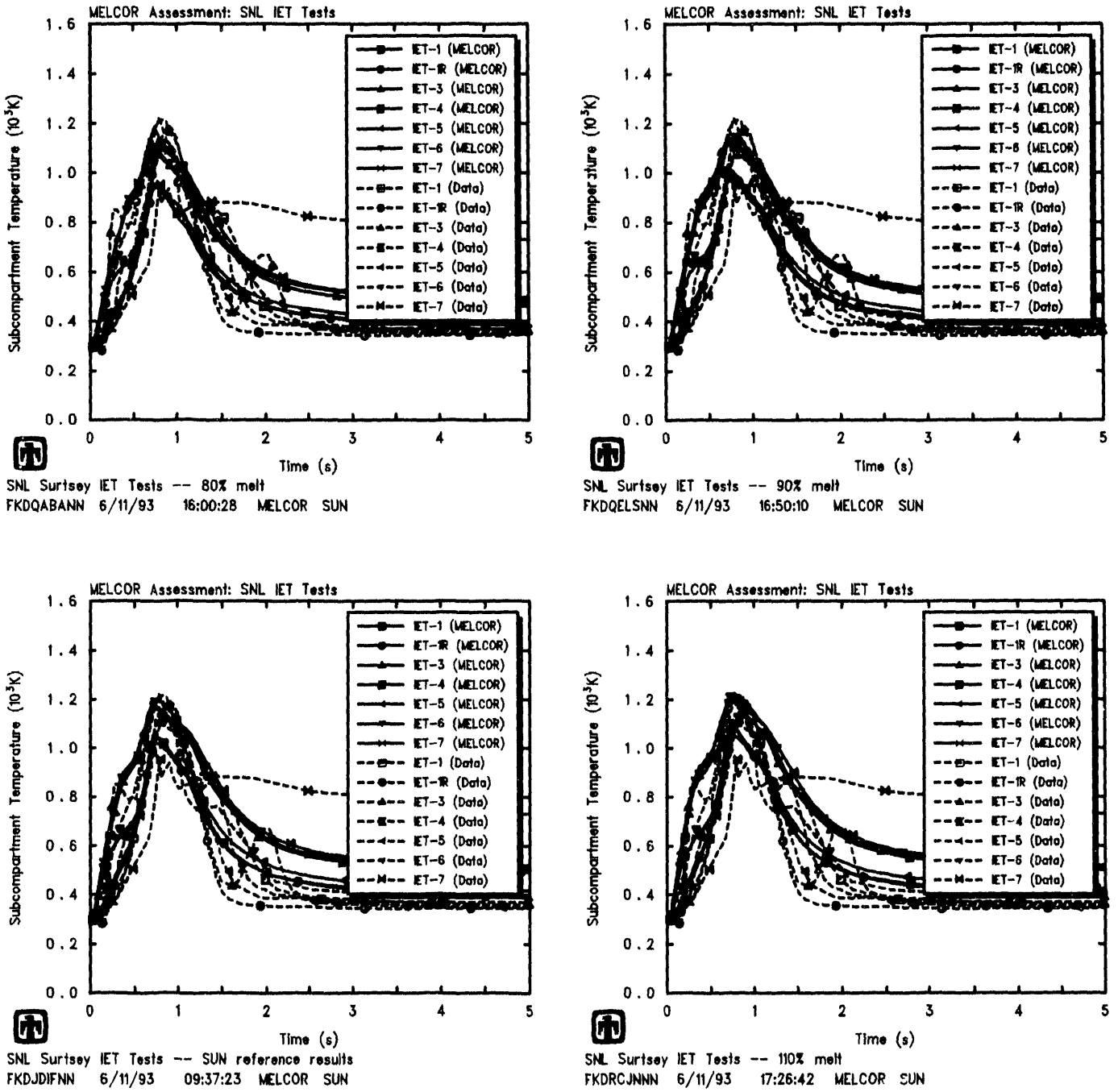

Figure 5.3.2. Subcompartment Temperatures for SNL/IET Experiments Using Melt Masses of 80% (upper left), 90% (upper right), 100% (lower left) and 110% (lower right) the Initial Charge Melt Injection Amount Sensitivity Study

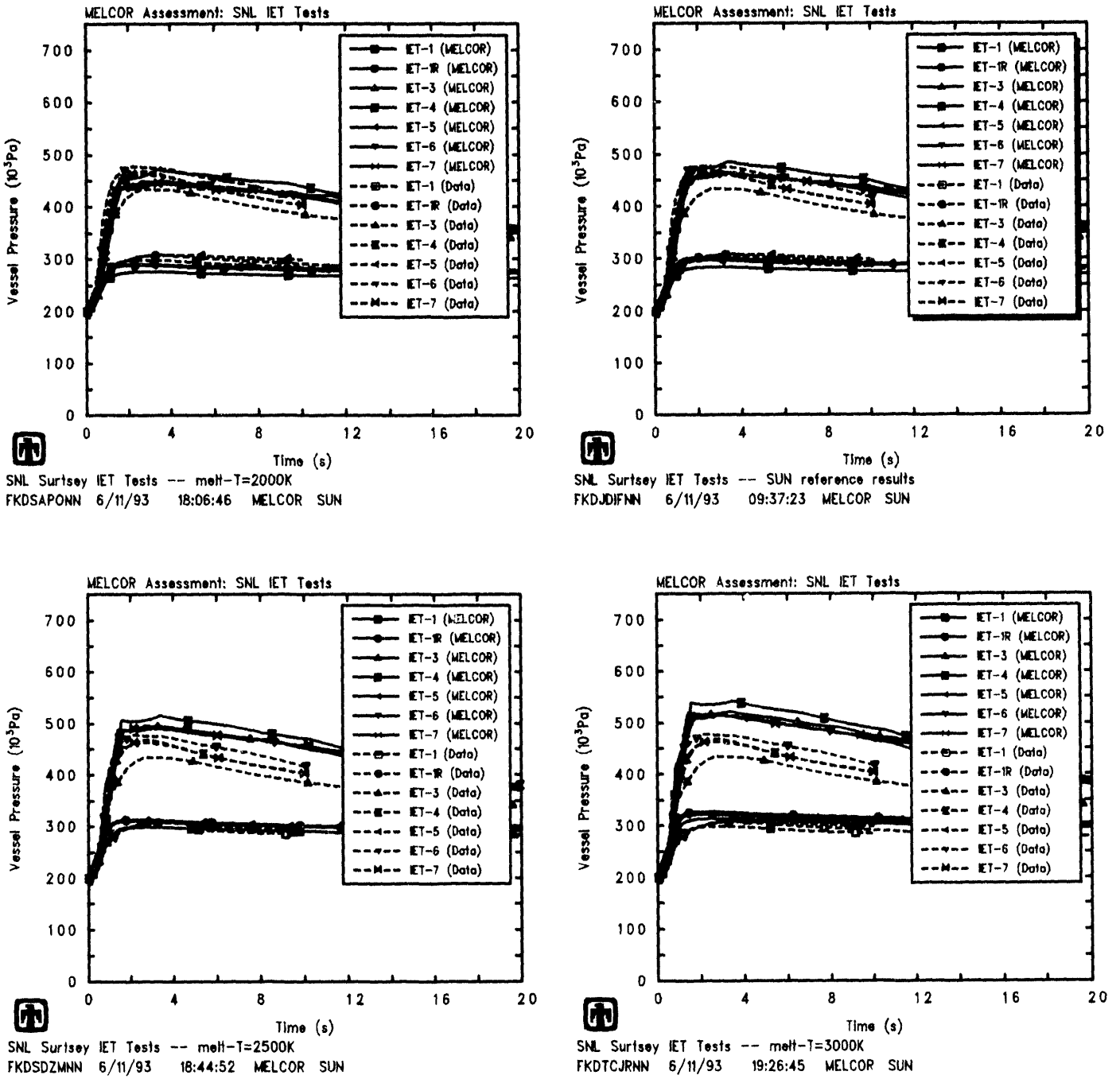

Figure 5.4.1. Vessel Pressures for SNL/IET Experiments Using Melt Temperatures of 2000K (upper left), 2300K (upper right), 2500K (lower left) and 3000K (lower right) Melt Temperature Sensitivity Study

Table 5.4.1. Hydrogen Generation for the SNL/IET Experiments – Melt Temperature Sensitivity Study

Experiment	Hydrogen Produced (gm-moles)				
	Data†	MELCOR ‡ T_{Debris}=			
		2000K	2300K	2500K	3000K
IET-1	233	276/255	286/266	301/281	313/293
IET-1R	248	254/253	266/267	280/286	295/298
IET-3	227	221/341	232/352	248/364	261/374
IET-4	303	238/355	243/361	260/374	275/387
IET-5	319	228/301	240/313	257/330	269/343
IET-6	319	230/348	236/354	253/367	256/370
IET-7	274	218/338	229/351	248/363	256/370

†from gas grab bottle samples at 30min
‡(actual values at 20s)/ (assuming only steam/metal reactions)

Table 5.4.2. Hydrogen Combustion for the SNL/IET Experiments – Melt Temperature Sensitivity Study

Experiment	Hydrogen Burned (gm-moles)				
	Data†	MELCOR ‡ T_{Debris}=			
		2000K	2300K	2500K	3000K
IET-1	3	0/4	0/4	0/4	0/4
IET-1R	11	0/28	0/28	0/28	0/28
IET-3	190	176/301	188/313	204/325	218/336
IET-4	240	201/323	209/332	227/345	243/359
IET-5	53	0/92	0/91	0/92	0/92
IET-6	345	174/299	182/307	199/319	207/327
IET-7	323	212/337	223/350	240/360	248/366

†from gas grab bottle samples at 30min
‡(actual values at 20s)/ (assuming only steam/metal reactions)

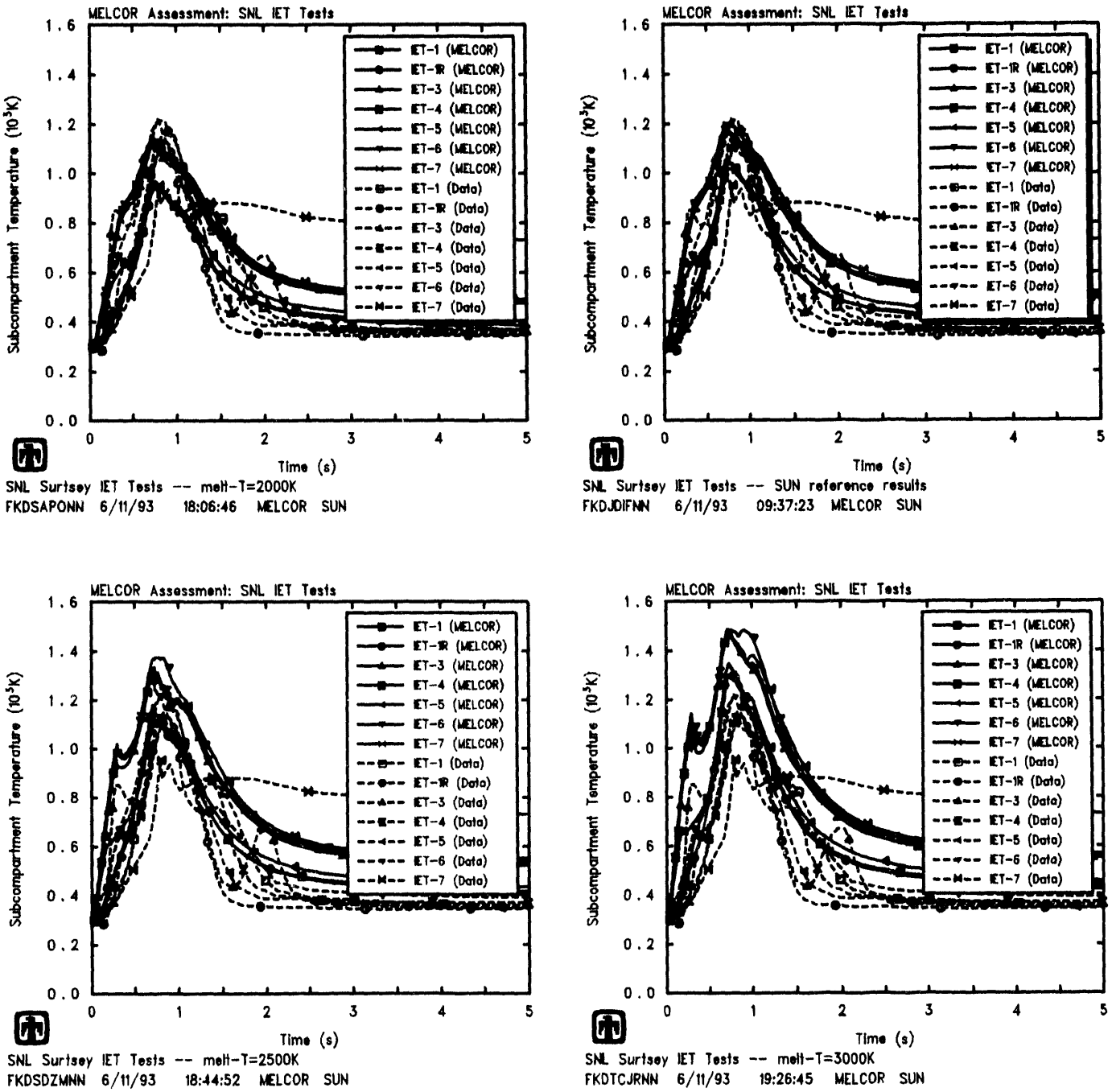

Figure 5.4.2. Subcompartment Temperatures for SNL/IET Experiments Using Melt Temperatures of 2000K (upper left), 2300K (upper right), 2500K (lower left) and 3000K (lower right) Melt Temperature Sensitivity Study

Table 5.5.1. Debris Masses for the SNL/IET Experiments – Debris Distribution Sensitivity Study

	IET-1	IET-1R	IET-3	IET-4	IET-5	IET-6	IET-7
Distribution (%)							
Cavity/Chute	14	27	33	17	38	17	27
Subcompartments	76	66	61	59	59	72	68
Dome	10	7	6	14	0	0	5

There is no guidance from the experiments on how much debris stuck to walls immediately rather than circulating and falling through the atmosphere before settling. The experimental debris distribution is based upon post-test collection of debris from the vessel and does not distinguish between debris deposited immediately or later. We assumed it was not likely that a large fraction of the debris immediately adhered permanently to a structure surface, given the highly turbulent conditions visible in the video records.

Table 2.1.3 presented a debris recovery summary for the Surtsey IET experiments. Table 5.5.1 gives melt distribution patterns derived from that test data. Although there were small differences in the test data debris distributions, the FDI input debris distribution was kept the same in our MELCOR input for all tests analyzed (with 15% and 10% of the debris input to the cavity and chute, respectively, 65% to the subcompartments and 10% to the dome).

However, in most plant analyses, there will be no equivalent data set providing guidance on HPME melt distribution. To evaluate the effect of the debris distribution assumed on the overall DCH behavior calculated, calculations were done in which the experimental debris distribution for each test was used, and in which 65% of the debris was placed either in the cavity and chute (with 25% in the subcompartments and 10% in the dome) or in the dome (with 25% in the cavity and chute and 10% in the subcompartments).

Figure 5.5.1 shows pressures in the vessel predicted using the various melt distributions, together with experimental data. There is very little difference seen in using a single basecase debris distribution or in using more experiment-specific distributions; this is not surprising because the variations are generally quite small. The major difference is seen for the calculation with most (65%) of the debris specified to go to the dome (with 25% in the cavity and chute and 10% in the subcompartments). The higher pressures calculated in that case are due to the deposition of a majority of the debris into a volume with a longer characteristic settling time (proportional to the volume height) which allows more time for oxidation and especially for heat transfer from airborne debris to the atmosphere; other effects may also be involved to some extent, *e.g.* a proportionally greater atmospheric heat capacity and less atmosphere-to-structure heat loss. The characteristic

settling times in the cavity, chute and subcompartments are roughly similar, and there is therefore no big difference found in atmosphere heating and vessel pressurization whether most of the debris is assumed to go to the cavity/chute or to the subcompartments.

Tables 5.5.2 and 5.5.3 present the amounts of hydrogen generated and burned, respectively, in these various cases. Test data estimates of the amounts of hydrogen produced and burned are included for reference. Again, there is very little difference seen in using a single basecase debris distribution or in using more experiment-specific distributions; this is not surprising because the variations are generally quite small. There is somewhat more hydrogen produced when more of the debris is assumed to go to the cavity and chute; these regions are closer to the blowdown steam accumulator source, and oxidation is therefore less likely to be limited by steam availability in this case. For the same reason, less hydrogen is predicted to be produced in IET-1 and IET-1R when most of the debris is assumed to go to the dome; the dome is further downstream from the blowdown steam accumulator source, and oxidation is therefore more limited by steam availability in this region for these two tests. In the remainder of the experiment simulations assuming most of the debris going to the dome, much less hydrogen production is calculated because most of the debris is being oxidized by the relatively large amount of free oxygen available in the dome which, unlike steam oxidation, produces no hydrogen as a reaction product. (Note that, in the MELCOR FDI HPME model, a hierarchy is assumed with debris oxidation consuming free oxygen before steam.)

Figure 5.5.2 gives subcompartment temperatures calculated using various melt amounts, together with experimental data. As found in the pressure and hydrogen production and combustion comparisons, there is very little difference seen in using a single basecase debris distribution or in using more experiment-specific distributions, because the test-to-test debris-distribution variations are generally quite small. The calculated subcompartment temperatures are significantly lower when the majority of the debris is assumed to go to either the dome or to the cavity/chute; as would be expected, the predicted temperatures in the dome and/or in the cavity and chute increase if more debris is assumed to go to the corresponding volume.

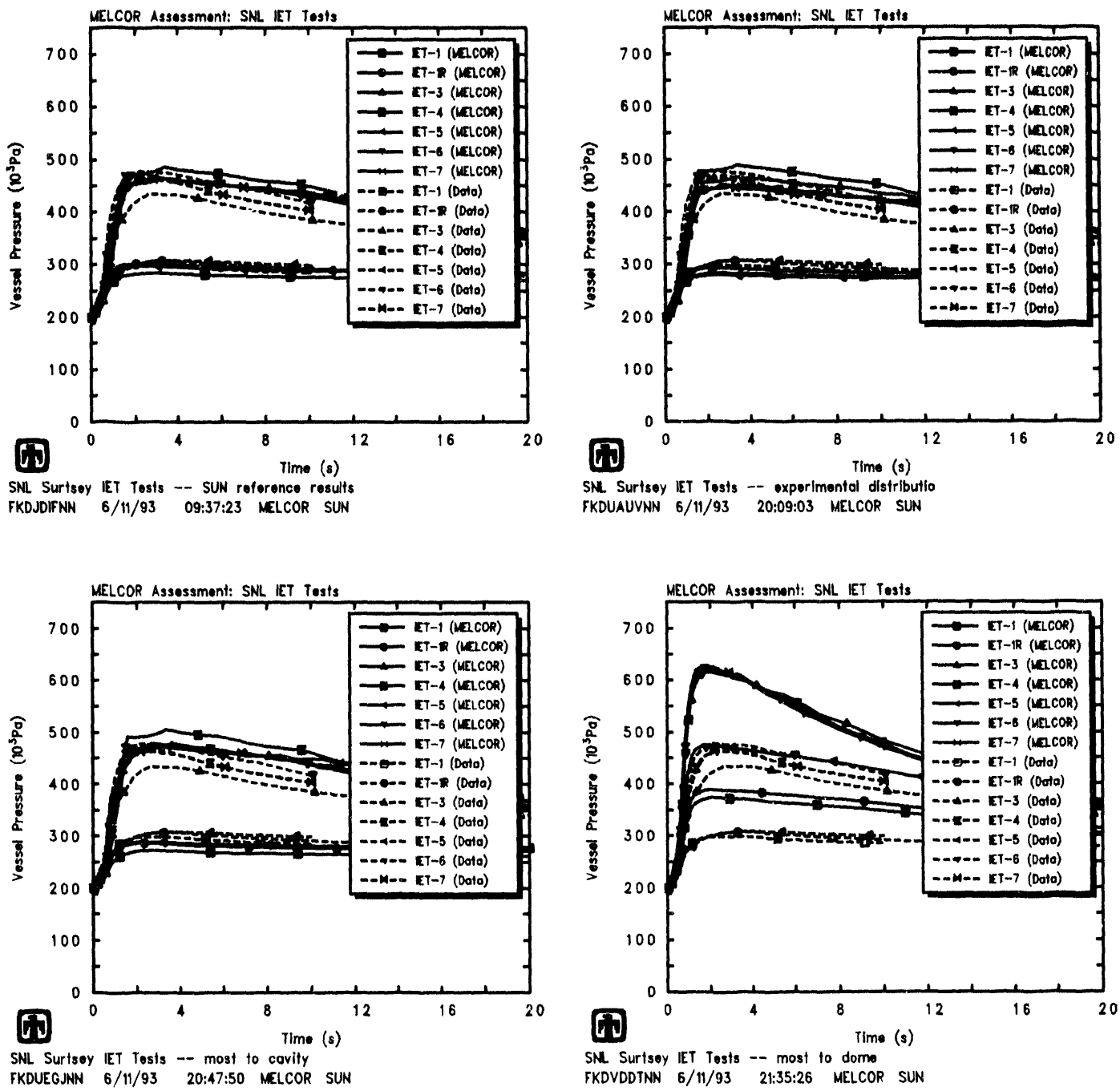

Figure 5.5.1. Vessel Pressures for SNL/IET Experiments Using Basecase Melt Distribution (upper left), Experimental Melt Distribution (upper right), Melt Mostly into Cavity (lower left) and Melt Mostly into Dome (lower right) Melt Distribution Sensitivity Study

Table 5.5.2. Hydrogen Generation for the SNL/IET Experiments - Melt Distribution Sensitivity Study

Experiment	Hydrogen Produced (gm-moles)				
	Data†	MELCOR ‡			
		Basecase Distribution	Experimental Distribution	Mostly into Cavity	Mostly into Dome
IET-1	233	286/266	251/232	332/307	245/233
IET-1R	248	266/267	272/272	315/311	226/239
IET-3	227	232/352	266/354	279/378	122/497
IET-4	303	243/361	220/367	295/396	122/496
IET-5	319	240/313	273/321	288/348	144/490
IET-6	319	236/354	214/336	285/385	122/496
IET-7	274	229/351	232/330	274/374	122/494

†from gas grab bottle samples at 30min
‡(actual values at 20s)/ (assuming only steam/metal reactions)

Table 5.5.3. Hydrogen Combustion for the SNL/IET Experiments - Melt Distribution Sensitivity Study

Experiment	Hydrogen Burned (gm-moles)				
	Data†	MELCOR ‡			
		Basecase Distribution	Experimental Distribution	Mostly into Cavity	Mostly into Dome
IET-1	3	0/4	0/4	0/4	0/4
IET-1R	11	0/28	0/28	0/28	0/28
IET-3	190	188/313	220/313	220/328	82/460
IET-4	240	209/332	186/338	251/358	95/471
IET-5	53	0/91	0/66	0/85	0/357
IET-6	345	182/307	164/293	216/325	78/456
IET-7	323	223/350	226/328	265/371	120/494

†from gas grab bottle samples at 30min
‡(actual values at 20s)/ (assuming only steam/metal reactions)

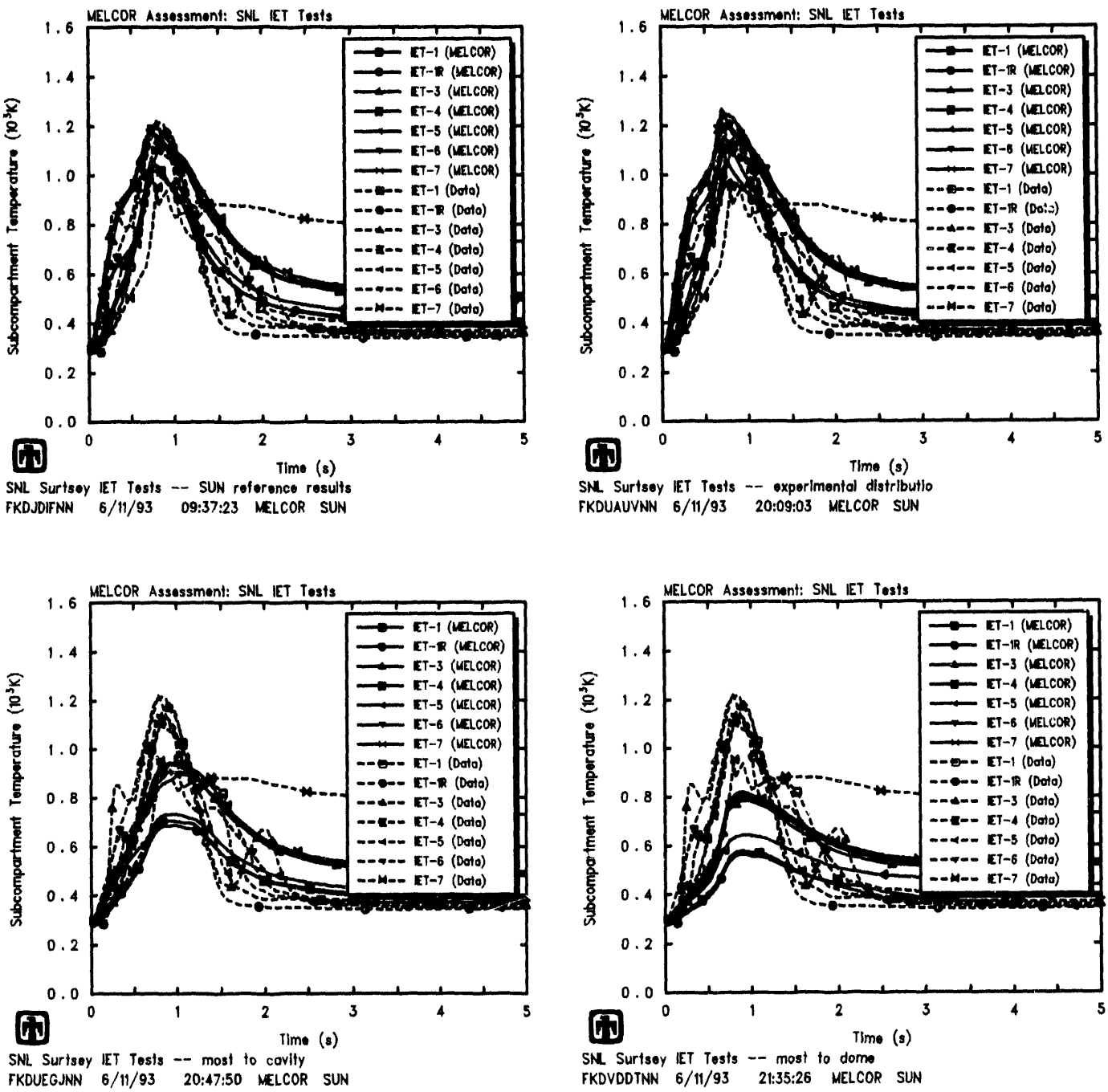

Figure 5.5.2. Subcompartment Temperatures for SNL/IET Experiments Using Basecase Melt Distribution (upper left), Experimental Melt Distribution (upper right), Melt Mostly into Cavity (lower left) and Melt Mostly into Dome (lower right) – Melt Distribution Sensitivity Study

6 DCH Modelling Studies

There are a number of user-input parameters in the high-pressure melt ejection model in MELCOR. These parameters define both the initial debris source and the subsequent debris interaction. The effects of varying the assumed debris source (injection timing, temperature and distribution) were evaluated in the previous section, as part of the experimental-condition uncertainty study. In this section, the effects of varying the characteristic debris interaction times are investigated.

The processes modelled include oxidation of the metallic debris components in both steam and oxygen, surface deposition of the airborne debris by trapping or settling, and heat transfer to the atmosphere and to deposition surfaces; first-order rate equations with user-specified time constants for oxidation, heat transfer and settling are used to determine the rate of each process.

6.1 Airborne Debris Oxidation Characteristic Time

The reference analyses discussed in Section 4 used a user-input characteristic time of 0.025s for oxidation of debris suspended in control volume atmospheres. (Oxidation of settled debris is controlled by a separate characteristic time, as discussed in Section 6.4.) A sensitivity study was done in which this airborne debris characteristic oxidation time was reduced to 0.005s and 0.01s, and increased to 0.05s, 0.1s and 0.5s; these values were selected to cover a large range of magnitude. All other parameters were left unchanged.

Resulting predicted vessel pressures for four of these six characteristic times are shown in Figure 6.1.1 (together with the test data). Tables 6.1.1 and 6.1.2 compare the amounts of hydrogen generated and burned, respectively, in all six cases considered.

The major trend visible in these results is that, with a very long characteristic airborne debris oxidation time, the overall pressurization, and both the hydrogen production and combustion, are all obviously underpredicted; the underprediction is worst in those cases where significant hydrogen combustion occurs, because using a long characteristic oxidation time ($\geq$ the characteristic settling time) results in substantially less hydrogen produced and consequently less pressurization due to combustion of that hydrogen.

Using shorter characteristic airborne debris oxidation times ($\leq$0.1s) gives generally similar results because in all these cases the oxidation is generally limited by the availability of oxygen and/or steam. The amount of pre-existing oxygen varies from test to test, as does the amount and timing of the steam injected with the melt debris. The occasional small, non-monotonic changes seen in pressurization and hydrogen production and combustion for the shortest oxidation characteristic time values for some of the tests (for example, calculated hydrogen production for IET-4 going up from 243gm-moles with τ_{ox}=0.025s to 244gm-moles with τ_{ox}=0.01s but then dropping to 240gm-moles with τ_{ox}=0.005s) are the result of interactions between different initial oxygen inventories, different steam flows and different oxidation rates causing localized steam-starvation and/or oxygen-starvation to occur at slightly different times in the different control volumes.

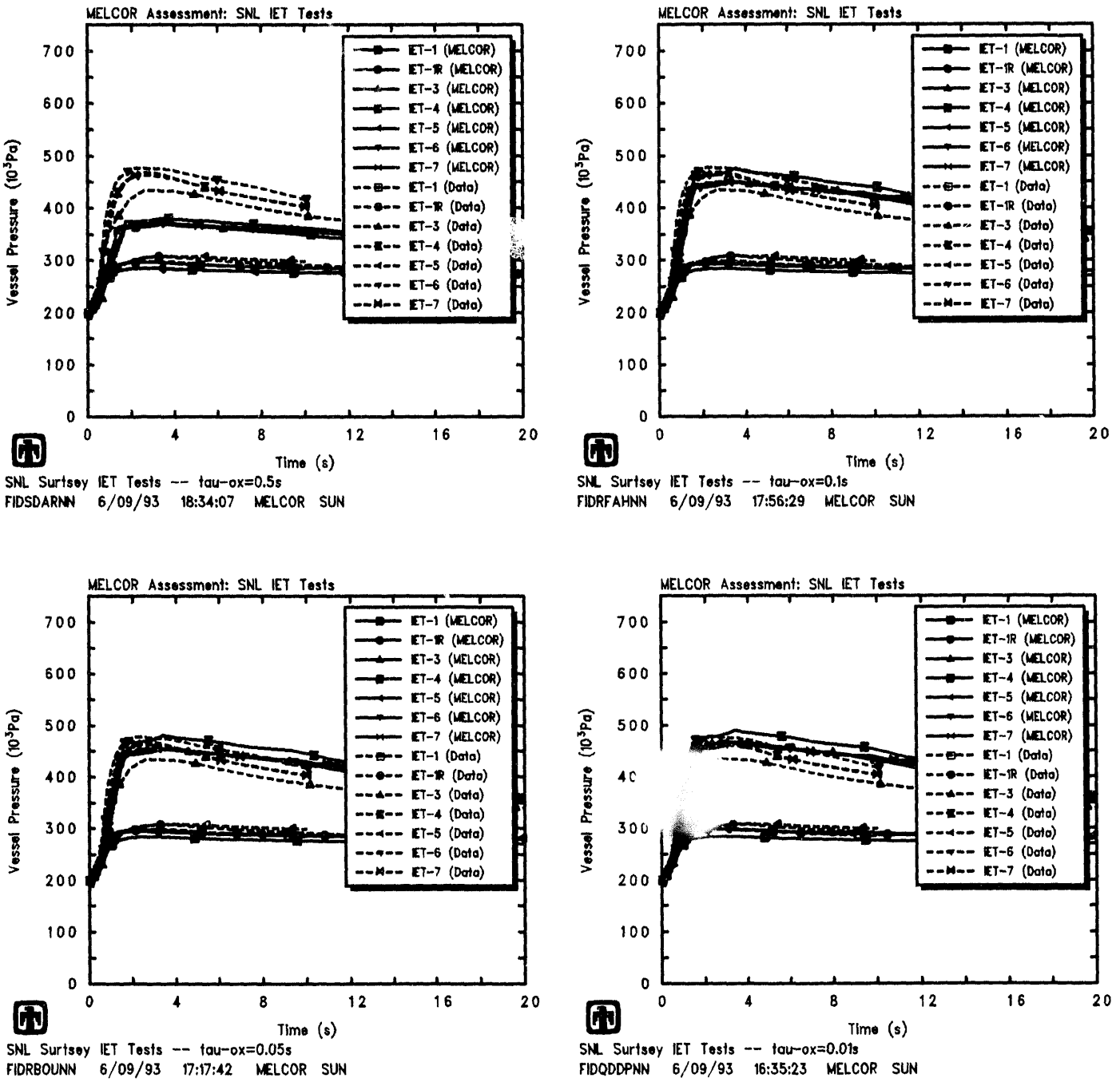

Figure 6.1.1. Vessel Pressures for SNL/IET Experiments Using Airborne Debris Characteristic Oxidation Times of 0.5s (upper left), 0.1s (upper right), 0.05s (lower left) and 0.01s (lower right) – Airborne Debris Oxidation Characteristic Time Sensitivity Study

Table 6.1.1. Hydrogen Generation for the SNL/IET Experiments - Airborne Debris Oxidation Characteristic Time Sensitivity Study

Experiment	Data†	Hydrogen Produced (gm-moles) MELCOR‡ $\tau_{ox}=$					
		0.005s	0.01s	0.025s	0.05s	0.1s	0.5s
IET-1	233	271/251	280/261	286/266	286/266	281/261	200/181
IET-1R	248	252/254	260/262	266/267	261/262	260/260	175/181
IET-3	227	229/351	232/352	232/352	229/338	222/324	110/193
IET-4	303	240/362	244/365	243/361	243/352	230/334	108/192
IET-5	319	237/313	238/314	240/313	237/305	232/297	131/183
IET-6	319	228/350	234/356	236/354	233/341	224/325	109/192
IET-7	274	221/345	228/350	229/351	223/337	216/320	107/190

†from gas grab bottle samples at 30min
‡(actual values at 20s)/ (assuming only steam/metal reactions)

Table 6.1.2. Hydrogen Combustion for the SNL/IET Experiments - Airborne Debris Oxidation Characteristic Time Sensitivity Study

Experiment	Data†	Hydrogen Burned (gm-moles) MELCOR‡ $\tau_{ox}=$					
		0.005s	0.01s	0.025s	0.05s	0.1s	0.5s
IET-1	3	0/4	0/4	0/4	0/4	0/4	0/4
IET-1R	11	0/28	0/28	0/28	0/28	0/28	0/28
IET-3	190	185/311	187/312	188/313	183/298	180/286	95/181
IET-4	240	208/333	211/335	209/332	208/322	199/308	96/183
IET-5	53	0/95	0/95	0/91	0/87	0/82	0/63
IET-6	345	177/305	183/311	182/307	178/293	173/280	84/173
IET-7	323	216/344	222/349	223/350	217/335	209/318	100/189

†from gas grab bottle samples at 30min
‡(actual values at 20s)/ (assuming only steam/metal reactions)

The characteristic airborne debris oxidation times assumed have very little overall effect on the subcompartment temperatures predicted, as illustrated in Figure 6.1.2, because most of the oxygen initially in the subcompartments is depleted by the time the calculated subcompartment temperature peaks at ~1s and the chemical energy released by metal-steam reaction is relatively small. Note, however, that there is a small increase in subcompartment temperatures visible early in the HPME transient ($t \leq 0.5$s) with decreasing characteristic airborne debris oxidation times, when metal-oxygen reaction is calculated to occur.

6.2 Airborne Debris Heat Transfer Characteristic Time

The reference analyses discussed in Section 4 used a user-input characteristic time of 0.40s for heat transfer between airborne debris and the adjacent control volume atmospheres. (The heat transfer between settled debris and the heat structure surface it settles onto is controlled by a separate heat transfer coefficient, controllable through sensitivity coefficient input.) In a sensitivity study, this airborne debris characteristic heat transfer time was reduced to 0.05s, 0.1s and 0.25s, and increased to 0.5s and 1s. All other parameters were left unchanged.

Figure 6.2.1 shows pressures in the vessel predicted using several airborne debris characteristic heat transfer times, together with experimental data for comparison. As would be expected, the vessel pressurization increases as the airborne debris characteristic heat transfer time is shortened.

Tables 6.2.1 and 6.2.2 present the amounts of hydrogen generated and burned, respectively, using the various values of airborne debris characteristic heat transfer times. (Test data estimates of the amounts of hydrogen produced and burned are included for reference.) There appears to be a trend of decreasing hydrogen production and combustion with increasing airborne debris characteristic heat transfer time. Again, the occasional small non-monotonic changes seen in calculated results for some of the tests (for example, calculated hydrogen production for IET-1 increasing with smaller characteristic heat-transfer times to 286gm-moles with τ_{ht}=0.4s then dropping to 284gm-moles with τ_{ht}=0.25s but then increasing again to 312gm-moles with τ_{ht}=0.1s) are the result of interactions between different initial oxygen inventories, different steam flows and different interaction rates causing localized steam-starvation and/or oxygen-starvation conditions to occur at slightly different times in different control volumes.

Figure 6.2.2 gives subcompartment temperatures calculated using several airborne debris characteristic heat transfer times, together with experimental data. As would be expected, this variable (together with predicted temperatures in the other control volumes) is affected most by varying the airborne debris characteristic heat transfer time; the control volume atmosphere temperatures increase as the airborne debris characteristic heat transfer time is shortened.

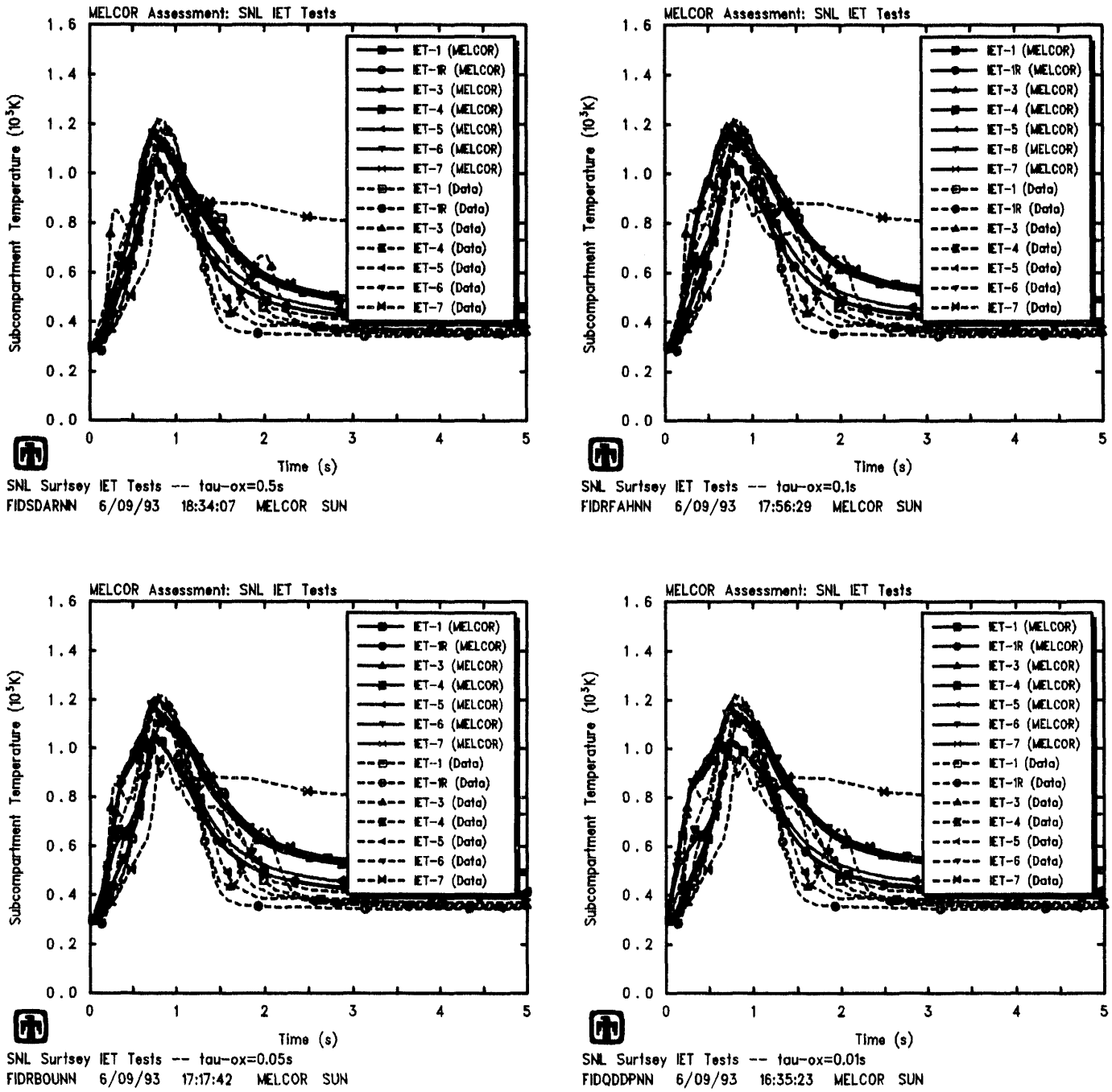

Figure 6.1.2. Subcompartment Temperatures for SNL/IET Experiments Using Airborne Debris Oxidation Characteristic Times of 0.5s (upper left), 0.1s (upper right), 0.05s (lower left) and 0.01s (lower right) – Airborne Debris Oxidation Characteristic Time Sensitivity Study

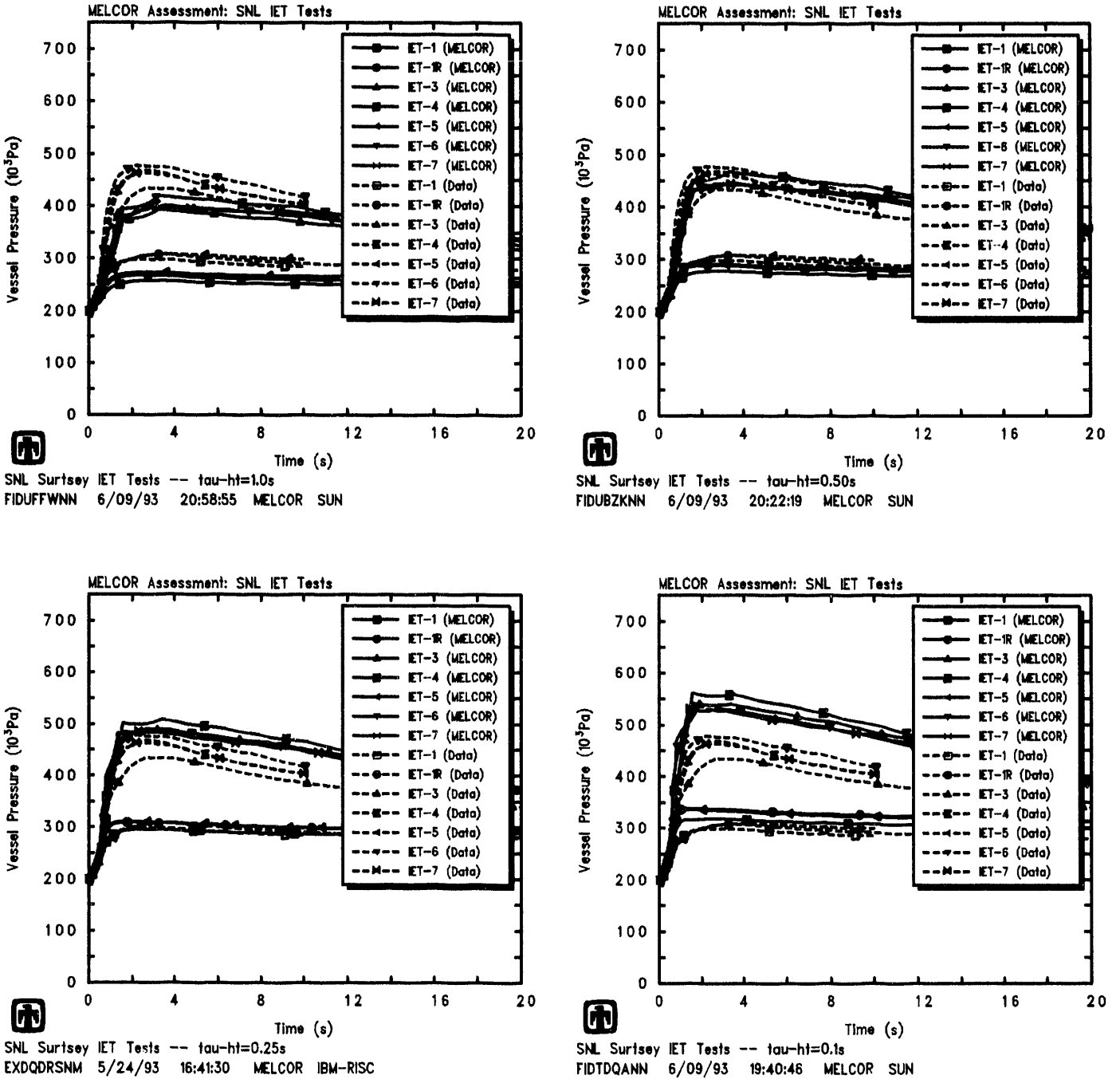

Figure 6.2.1. Vessel Pressures for SNL/IET Experiments Using Airborne Debris Characteristic Heat Transfer Times of 1s (upper left), 0.5s (upper right), 0.25s (lower left) and 0.1s (lower right) – Airborne Debris Heat Transfer Characteristic Time Sensitivity Study

Table 6.2.1. Hydrogen Generation for the SNL/IET Experiments – Airborne Debris Heat Transfer Characteristic Time Sensitivity Study

Experiment	Hydrogen Produced (gm-moles)						
	Data†	MELCOR‡					
		τ_{ht}=					
		0.05s	0.1s	0.25s	0.4s	0.5s	1s
IET-1	233	316/296	312/292	284/264	286/266	273/252	234/214
IET-1R	248	302/307	299/303	275/280	266/267	252/253	214/214
IET-3	227	254/380	262/385	241/360	232/352	217/341	182/311
IET-4	303	265/393	279/400	248/368	243/361	234/353	195/321
IET-5	319	274/351	279/354	252/325	240/313	226/300	189/261
IET-6	319	256/382	268/385	249/367	236/354	220/342	186/311
IET-7	274	250/374	258/378	232/353	229/351	216/337	179/305

†from gas grab bottle samples at 30min
‡(actual values at 20s)/ (assuming only steam/metal reactions)

Table 6.2.2. Hydrogen Combustion for the SNL/IET Experiments – Airborne Debris Heat Transfer Characteristic Time Sensitivity Study

Experiment	Hydrogen Burned (gm-moles)						
	Data†	MELCOR‡					
		τ_{ht}=					
		0.05s	0.1s	0.25s	0.4s	0.5s	1s
IET-1	3	0/4	0/4	0/4	0/4	0/4	0/4
IET-1R	11	0/28	0/28	0/28	0/28	0/28	0/28
IET-3	190	220/351	227/354	199/322	188/313	174/303	139/273
IET-4	240	241/372	251/376	217/340	209/332	198/322	162/292
IET-5	53	0/95	0/94	0/92	0/91	0/92	0/92
IET-6	345	216/347	218/342	195/319	182/307	167/295	135/268
IET-7	323	242/370	250/374	226/351	223/350	211/337	175/307

†from gas grab bottle samples at 30min
‡(actual values at 20s)/ (assuming only steam/metal reactions)

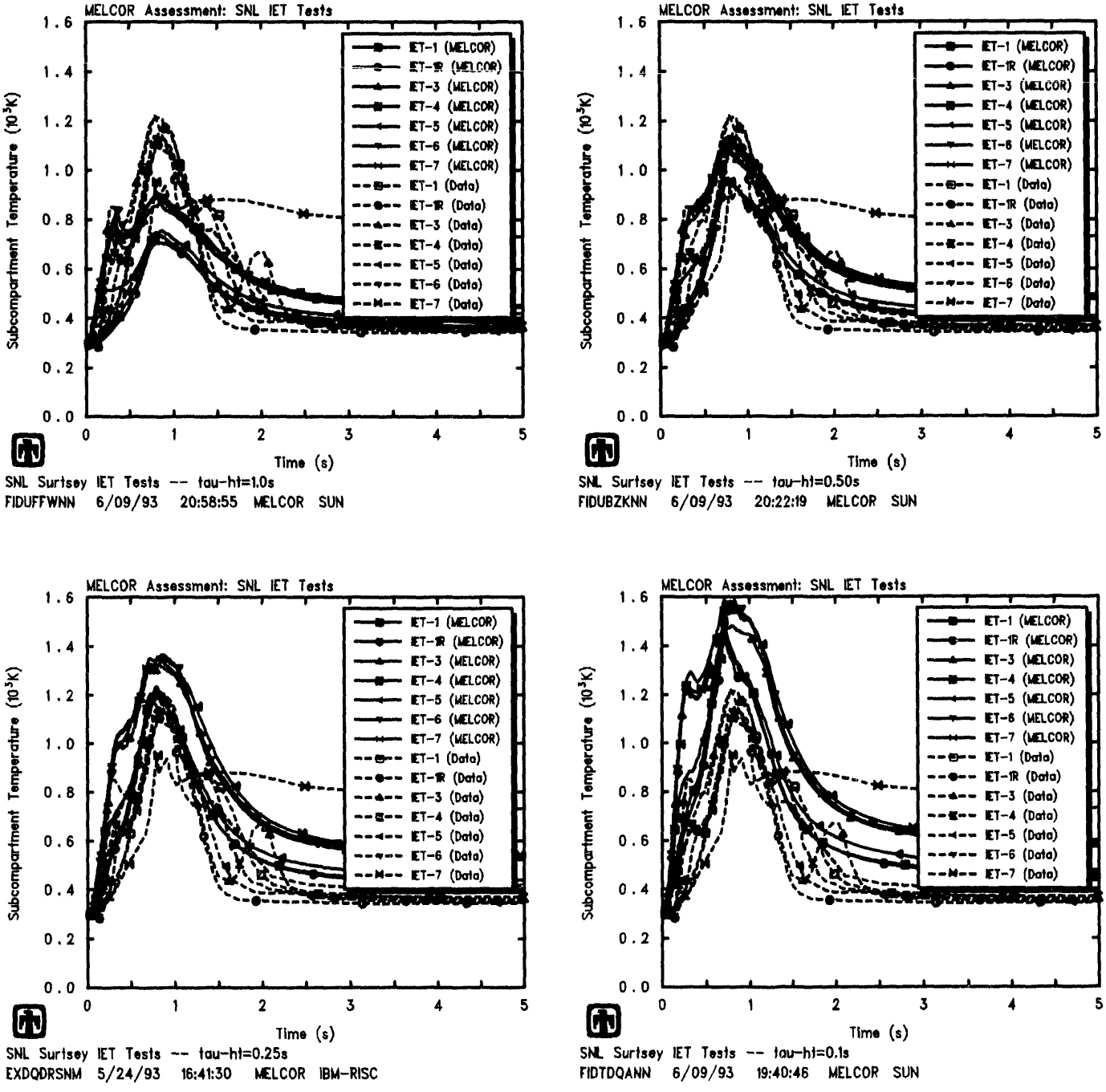

Figure 6.2.2. Subcompartment Temperatures for SNL/IET Experiments Using Airborne Debris Characteristic Heat Transfer Times of 1s (upper left), 0.5s (upper right), 0.25s (lower left) and 0.1s (lower right) - Airborne Debris Heat Transfer Characteristic Time Sensitivity Study

6.3 Airborne Debris Settling Characteristic Time

The reference analyses discussed in Section 4 used a range of user-input characteristic times for settling of airborne debris from control volume atmospheres onto associated "floor" heat structure surfaces, with the characteristic settling times generally proportional to the control volume height (0.15s in the cavity, 0.35s in the chute, 0.25s in the subcompartments and 0.60s in the upper dome). In a sensitivity study, this airborne debris characteristic settling time was set to several fixed values (0.05s, 0.1s, 0.25s, 0.5s and 1s) and set the same in all control volumes. All other parameters were left unchanged.

Vessel pressures predicted using various values of characteristic settling times are presented in Figure 6.3.1, together with test data. The effect of increasing the airborne debris characteristic settling time is to increase the vessel pressures calculated, as would be expected because it increases the available time for both oxidation and heat transfer to occur.

Tables 6.3.1 and 6.3.2 summarize the amounts of hydrogen generated and burned, respectively, with the amount of hydrogen both produced and burned generally increasing with increasing airborne debris characteristic settling times.

Increasing the airborne debris characteristic settling times has the same effect on the subcompartment temperatures predicted as on the overall pressurization and both hydrogen production and combustion, as indicated in Figure 6.3.2. The calculated subcompartment temperatures increase with increasing airborne debris characteristic settling time, due to the longer periods available for heat transfer between airborne debris and atmosphere to occur in the subcompartments. The difference between cases with and without significant hydrogen combustion also increases with increasing airborne debris characteristic settling time, because using a long characteristic settling time results in substantially more hydrogen produced, and consequently more overall pressurization and heatup due to combustion of hydrogen produced in or convected into the dome.

6.4 Deposited Debris Oxidation Characteristic Time

The reference analyses discussed in Section 4 used a user-input characteristic time of 600s for oxidation of debris settled onto structures. (Oxidation of airborne debris is controlled by a separate characteristic time, as discussed in Section 6.1.) A sensitivity study was done in which this deposited-debris characteristic oxidation time was reduced to 10s and 60s, and increased to 1800s, to cover a wide range of magnitudes. All other parameters were left unchanged.

Figure 6.4.1 shows pressures in the vessel predicted using these various deposited debris characteristic oxidation times, together with experimental data. There is generally little effect on either the peak or the long-term pressurization as the deposited debris characteristic oxidation time is varied.

Tables 6.4.1 and 6.4.2 present the amounts of hydrogen generated and burned, respectively, in these various cases. Test data estimates of the amounts of hydrogen produced

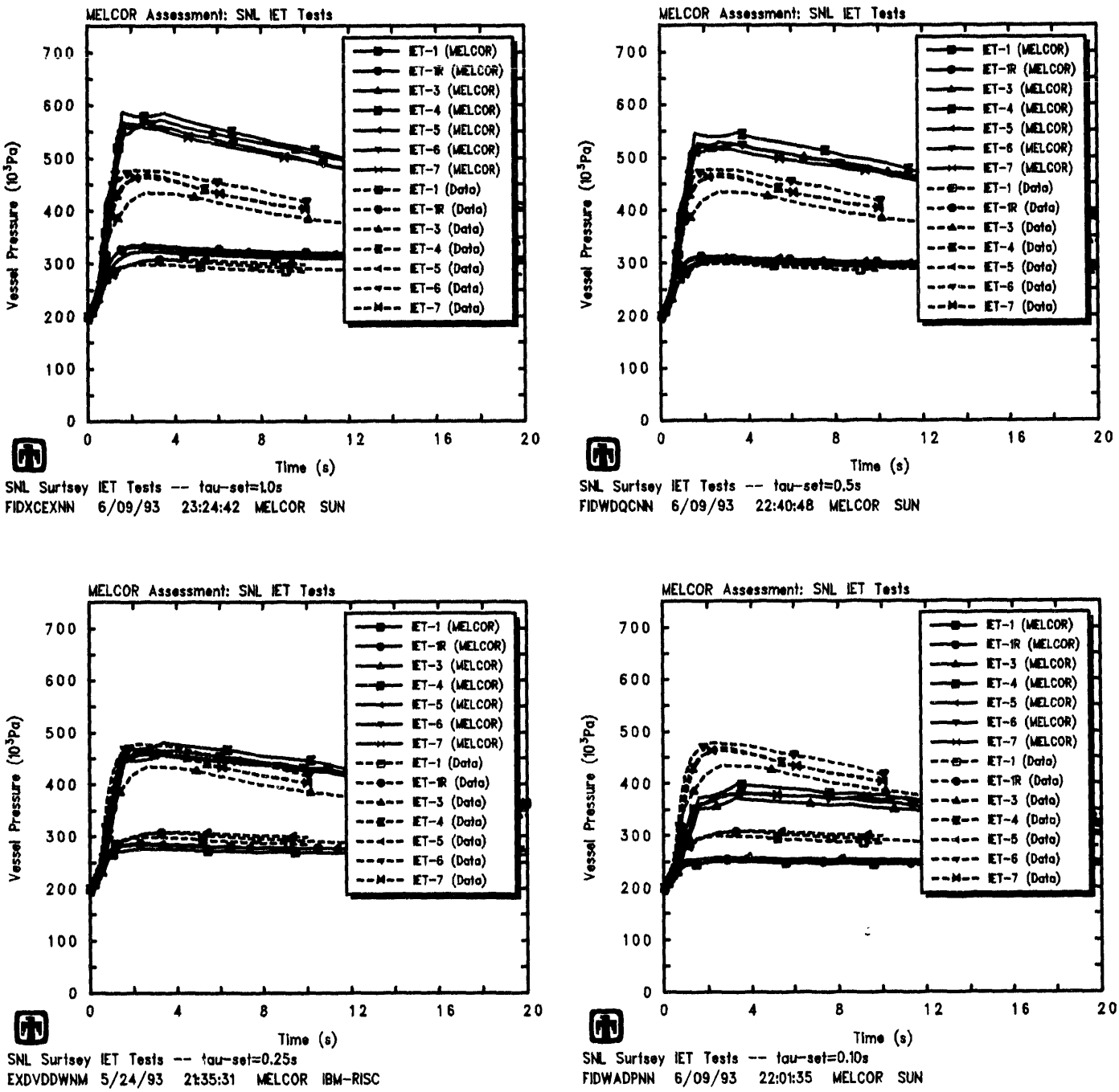

Figure 6.3.1. Vessel Pressures for SNL/IET Experiments Using Airborne Debris Characteristic Settling Times of 1s (upper left), 0.5s (upper right), 0.25s (lower left) and 0.1s (lower right) - Airborne Debris Settling Characteristic Time Sensitivity Study

Table 6.3.1. Hydrogen Generation for the SNL/IET Experiments - Airborne Debris Settling Characteristic Time Sensitivity Study

Experiment	Hydrogen Produced (gm-moles)					
	Data†	MELCOR‡				
				$\tau_{set}=$		
		0.05s	0.1s	0.25s	0.5s	1s
IET-1	233	177/161	221/203	295/275	346/325	390/368
IET-1R	248	163/171	206/210	294/295	328/331	370/371
IET-3	227	139/245	183/293	242/357	288/405	316/435
IET-4	303	151/255	194/306	256/373	305/421	330/449
IET-5	319	146/206	189/256	257/328	294/369	337/413
IET-6	319	144/245	187/300	240/374	293/411	319/437
IET-7	274	138/242	181/293	244/361	281/401	305/429

†from gas grab bottle samples at 30min
‡(actual values at 20s)/ (assuming only steam/metal reactions)

Table 6.3.2. Hydrogen Combustion for the SNL/IET Experiments - Airborne Debris Settling Characteristic Time Sensitivity Study

Experiment	Hydrogen Burned (gm-moles)					
	Data†	MELCOR‡				
				$\tau_{set}=$		
		0.05s	0.1s	0.25s	0.5s	1s
IET-1	3	0/4	0/4	0/4	0/4	0/4
IET-1R	11	0/28	0/28	0/28	0/28	0/28
IET-3	190	104/216	138/254	199/320	248/370	279/403
IET-4	240	118/228	162/278	223/343	274/393	303/425
IET-5	53	0/74	0/82	0/88	0/94	0/97
IET-6	345	100/208	139/258	205/323	246/370	267/391
IET-7	323	136/245	176/294	237/360	274/398	298/427

†from gas grab bottle samples at 30min
‡(actual values at 20s)/ (assuming only steam/metal reactions)

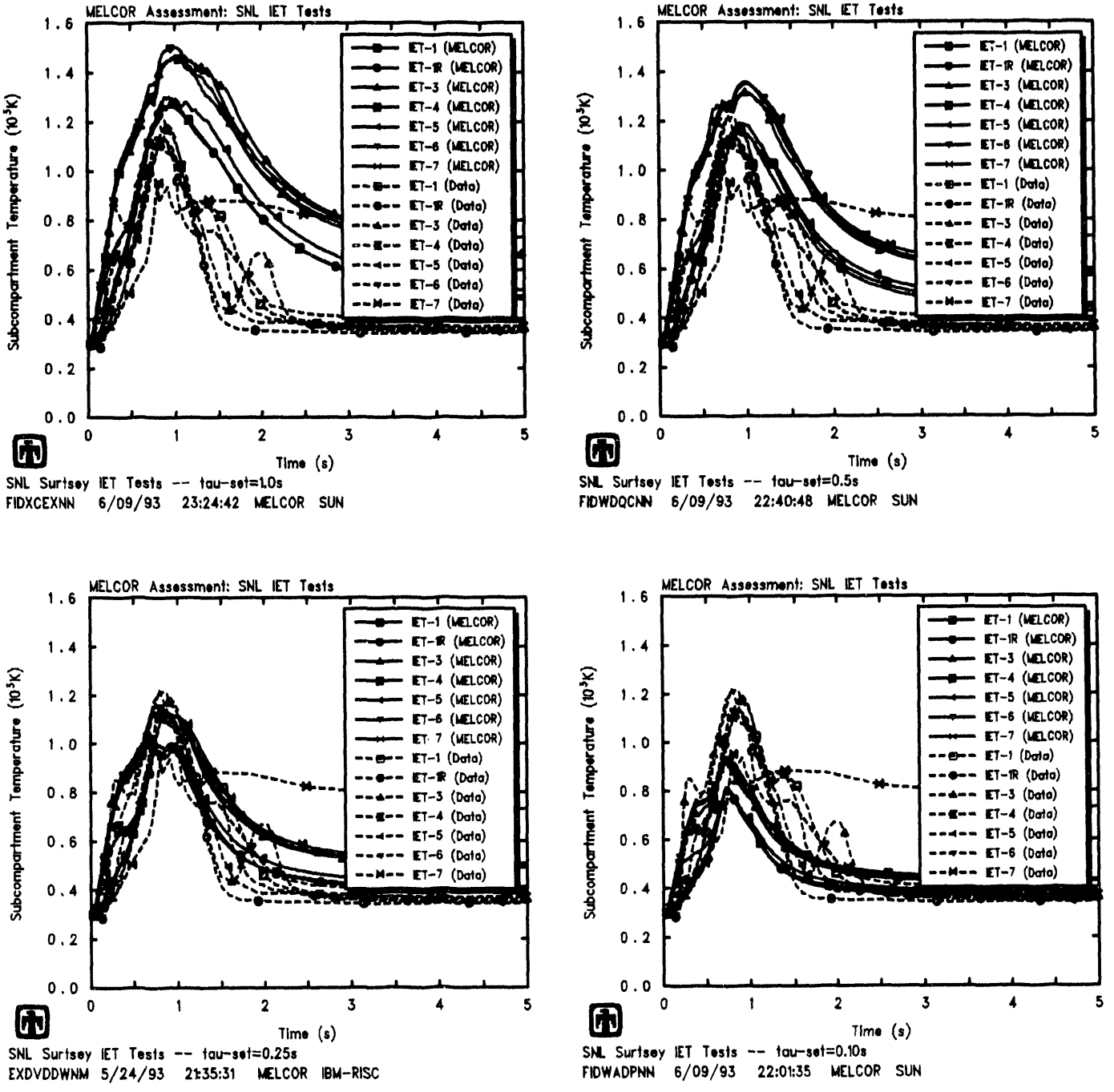

Figure 6.3.2. Subcompartment Temperatures for SNL/IET Experiments Using Airborne Debris Characteristic Settling Times of 1s (upper left), 0.5s (upper right), 0.25s (lower left) and 0.1s (lower right) Airborne Debris Settling Heat Transfer Characteristic Time Sensitivity Study

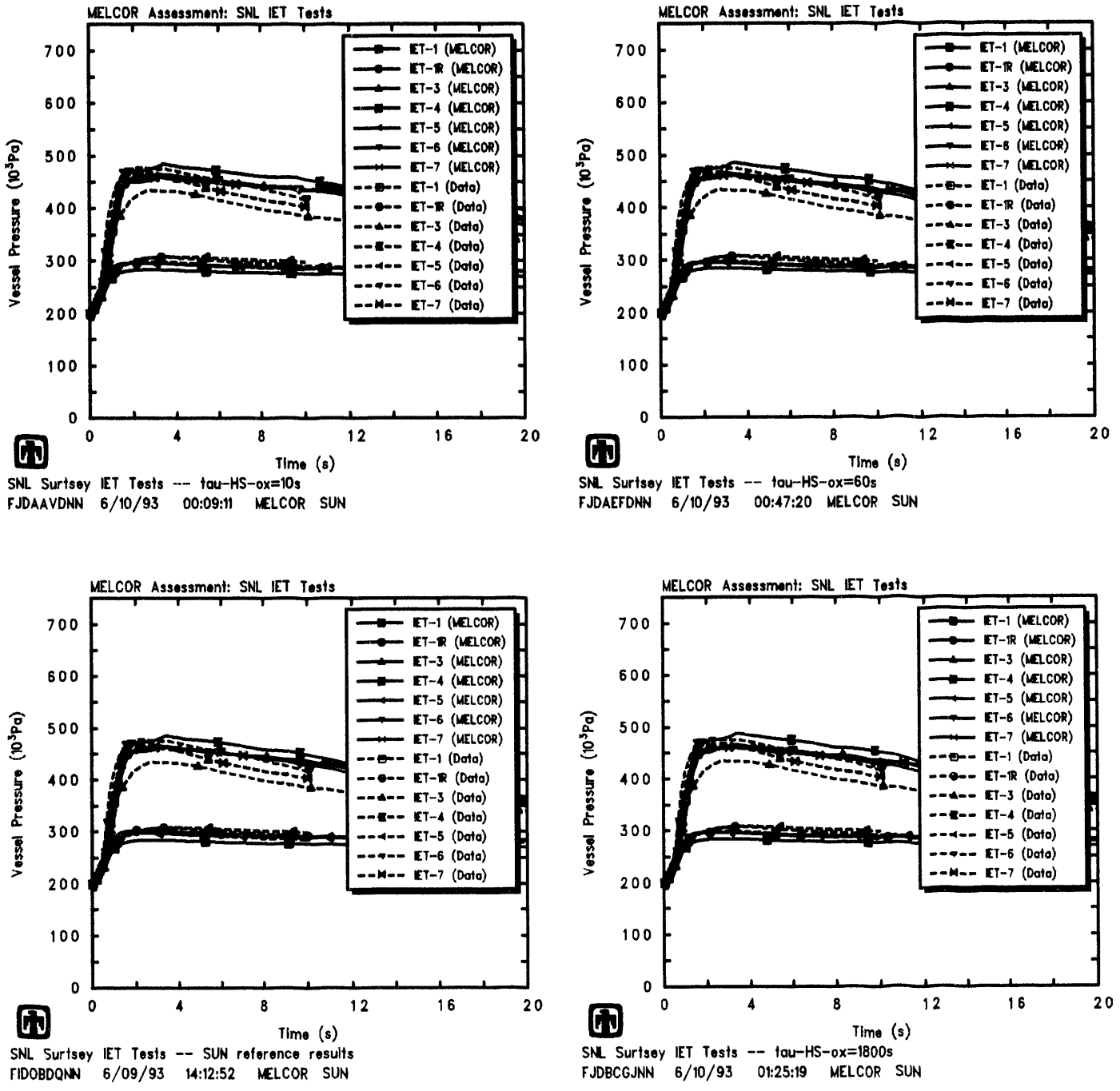

Figure 6.4.1. Vessel Pressures for SNL/IET Experiments Using Deposited Debris Characteristic Oxidation Times of 10s (upper left), 60s (upper right), 600s (lower left) and 1800s (lower right) – Deposited Debris Oxidation Characteristic Time Sensitivity Study

and burned are included for reference. The total amount of hydrogen generated increases as the characteristic oxidation time for deposited debris is decreased, as would be expected, because more hydrogen accumulates late in the transient as the debris settled and/or deposited onto structures continues to oxidize. There is little effect seen on the amount of hydrogen burned, however, because the hydrogen combustion primarily occurs early in the transient, on a time scale of a few seconds or less.

Figure 6.4.2 gives subcompartment temperatures calculated using various deposited debris characteristic oxidation times, together with experimental data. As with the vessel pressure shown in Figure 6.4.1, there is generally little effect on either the peak or the long-term temperature response as the deposited debris characteristic oxidation time is varied.

6.5 Deposited Debris Heat Transfer Coefficient

As noted in Section 3.1, the basecase MELCOR IET experiment analyses were run with the coefficient for heat transfer from deposited debris to structure surface reduced to 1w/m^2-K. This was originally done to avoid temperature iteration convergence problems, and was not changed when the temperature solution algorithm was improved and made more robust (as discussed in Section 11). To see what effect this had on our analyses, a set of calculations were run with that heat transfer coefficient progressively increased to 10w/m^2-K, 100w/m^2-K, and 1000w/m^2-K (the default value).

Figure 6.5.1 shows pressures in the vessel predicted using the different debris-to-structure heat transfer coefficients, together with experimental data. There is little difference visible, especially in the early-time peak pressures, with the major difference being slightly higher late-time pressures for larger debris-to-structure heat transfer coefficients.

Tables 6.5.1 and 6.5.2 present the amounts of hydrogen generated and burned, respectively, in these various cases. Test data estimates of the amounts of hydrogen produced and burned are included for reference. Again, there is very little difference apparent, especially for heat transfer coefficient values in the 1-100w/m^2-K range, with a slight increase seen in both hydrogen production and (as a consequence) hydrogen combustion for the default value of 1000w/m^2-K.

Figure 6.5.2 gives subcompartment temperatures calculated using various debris-to-structure heat transfer coefficients, together with experimental data. As found for the pressure comparison presented in Figure 6.5.1, there is little difference visible, especially in the early-time peak temperatures, with the major difference being slightly higher late-time temperatures for larger debris-to-structure heat transfer coefficients.

Table 6.4.1. Hydrogen Generation for the SNL/IET Experiments – Deposited Debris Oxidation Characteristic Time Sensitivity Study

Experiment	Hydrogen Produced (gm-moles)				
	Data†	MELCOR‡			
		τ_{HS-ox}=			
		10s	60s	600s	1800s
IET-1	233	472/403	354/301	286/266	281/264
IET-1R	248	436/386	332/294	266/267	261/265
IET-3	227	288/479	235/388	232/352	235/351
IET-4	303	288/481	249/396	243/361	246/361
IET-5	319	365/423	250/334	240/313	240/310
IET-6	319	284/479	241/389	236/354	235/350
IET-7	274	283/474	233/385	229/351	225/344

†from gas grab bottle samples at 30min
‡(actual values at 20s)/ (assuming only steam/metal reactions)

Table 6.4.2. Hydrogen Combustion for the SNL/IET Experiments – Deposited Debris Oxidation Characteristic Time Sensitivity Study

Experiment	Hydrogen Burned (gm-moles)				
	Data†	MELCOR‡			
		τ_{HS-ox}=			
		10s	60s	600s	1800s
IET-1	3	0/4	0/4	0/4	0/4
IET-1R	11	0/28	0/28	0/28	0/28
IET-3	190	199/411	188/348	188/313	190/311
IET-4	240	223/434	210/366	209/332	211/330
IET-5	53	0/130	0/112	0/91	0/89
IET-6	345	191/407	182/341	182/307	180/301
IET-7	323	263/476	225/385	223/350	220/343

†from gas grab bottle samples at 30min
‡(actual values at 20s)/ (assuming only steam/metal reactions)

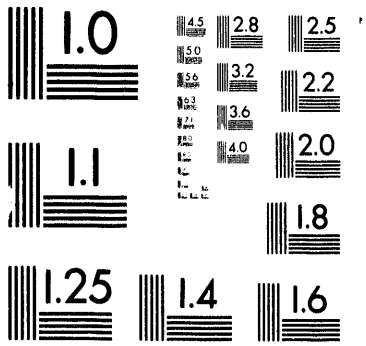
1.0
1.1
1.25
1.4
1.6
1.8
2.0
2.2
2.5
2.8
3.2
3.6
4.0
4.5
5.0
5.6
6.3

2 of 3

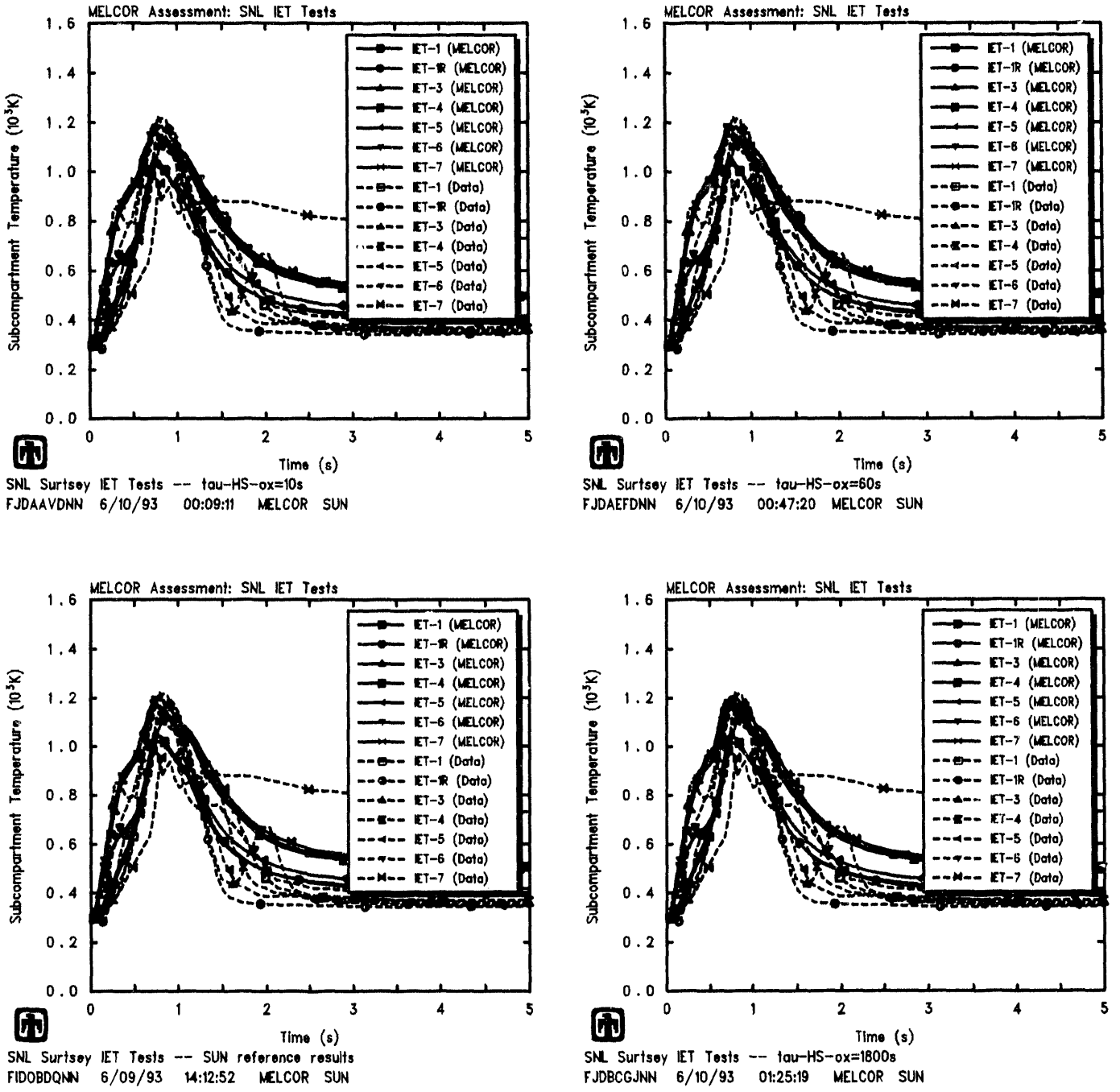

Figure 6.4.2. Subcompartment Temperatures for SNL/IET Experiments Using Deposited Debris Characteristic Oxidation Times of 10s (upper left), 60s (upper right), 600s (lower left) and 1800s (lower right) Deposited Debris Oxidation Characteristic Time Sensitivity Study

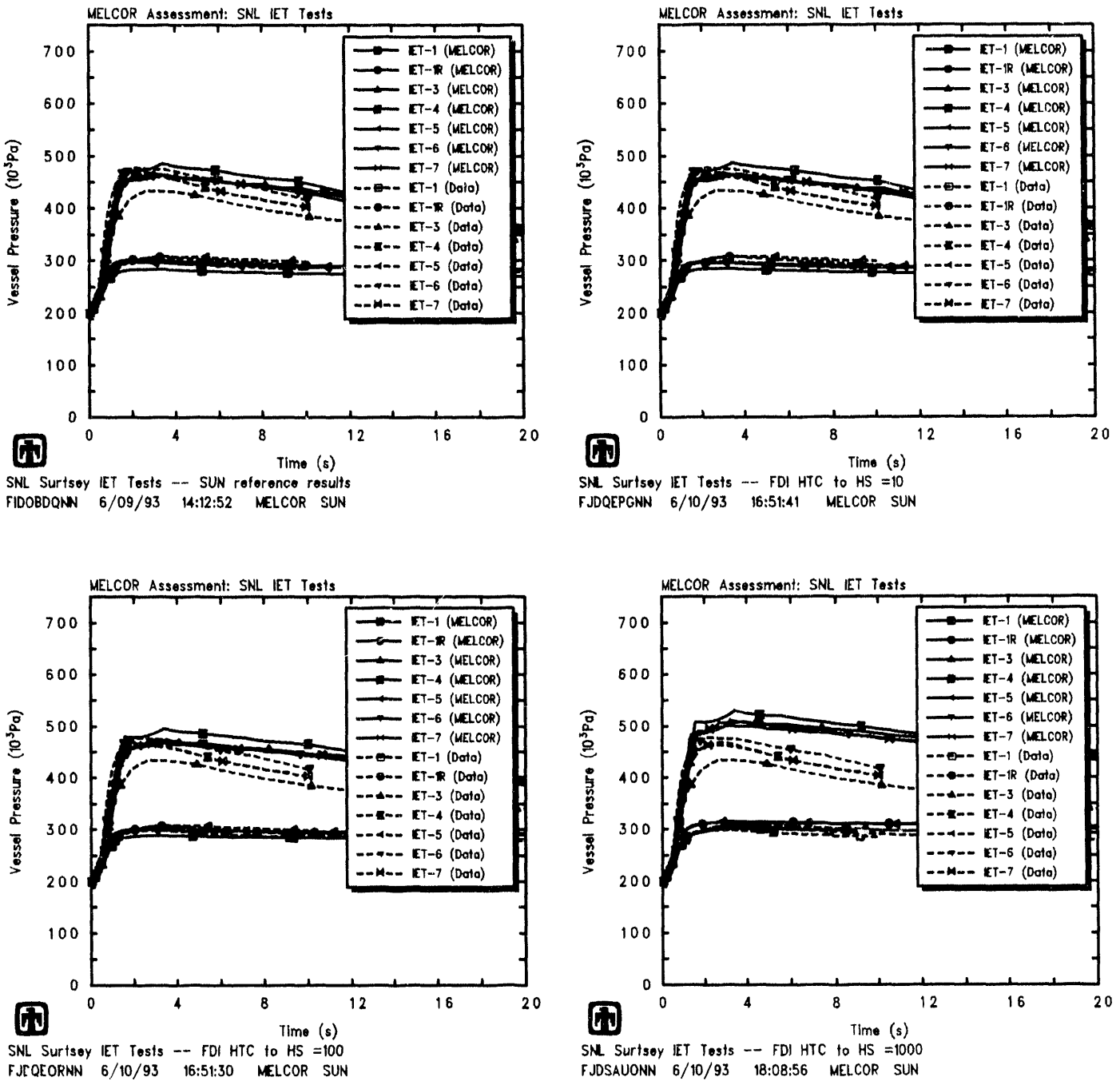

Figure 6.5.1. Vessel Pressures for SNL/IET Experiments Using Deposited Debris Heat Transfer Coefficient of 1w/m^2-K (upper left), 10w/m^2-K (upper right), 100w/m^2-K (lower left) and 1000w/m^2-K (lower right) Deposited Debris Heat Transfer Coefficient Sensitivity Study

Table 6.5.1. Hydrogen Generation for the SNL/IET Experiments - Deposited Debris Heat Transfer Coefficient Sensitivity Study

Experiment	Hydrogen Produced (gm-moles)				
	Data†	MELCOR‡ HTC_{FDI-HS}=			
		1w/m^2-K	10w/m^2-K	100w/m^2-K	1000w/m^2-K
IET-1	233	286/266	284/264	287/273	307/294
IET-1R	248	266/267	266/266	266/270	286/296
IET-3	227	232/352	231/350	234/351	252/347
IET-4	303	243/361	247/364	248/361	264/353
IET-5	319	240/313	242/313	243/319	260/337
IET-6	319	236/354	237/355	239/353	256/348
IET-7	274	229/351	230/350	230/347	246/342

†from gas grab bottle samples at 30min
‡(actual values at 20s)/ (assuming only steam/metal reactions)

Table 6.5.2. Hydrogen Combustion for the SNL/IET Experiments - Deposited Debris Heat Transfer Coefficient Sensitivity Study

Experiment	Hydrogen Burned (gm-moles)				
	Data†	MELCOR‡ HTC_{FDI-HS}=			
		1w/m^2-K	10w/m^2-K	100w/m^2-K	1000w/m^2-K
IET-1	3	0/4	0/4	0/4	0/4
IET-1R	11	0/28	0/28	0/28	0/28
IET-3	190	188/313	186/310	193/315	220/327
IET-4	240	209/332	211/333	215/333	235/339
IET-5	53	0/91	0/90	0/89	0/88
IET-6	345	182/307	182/307	187/307	211/317
IET-7	323	223/350	224/349	222/344	231/339

†from gas grab bottle samples at 30min
‡(actual values at 20s)/ (assuming only steam/metal reactions)

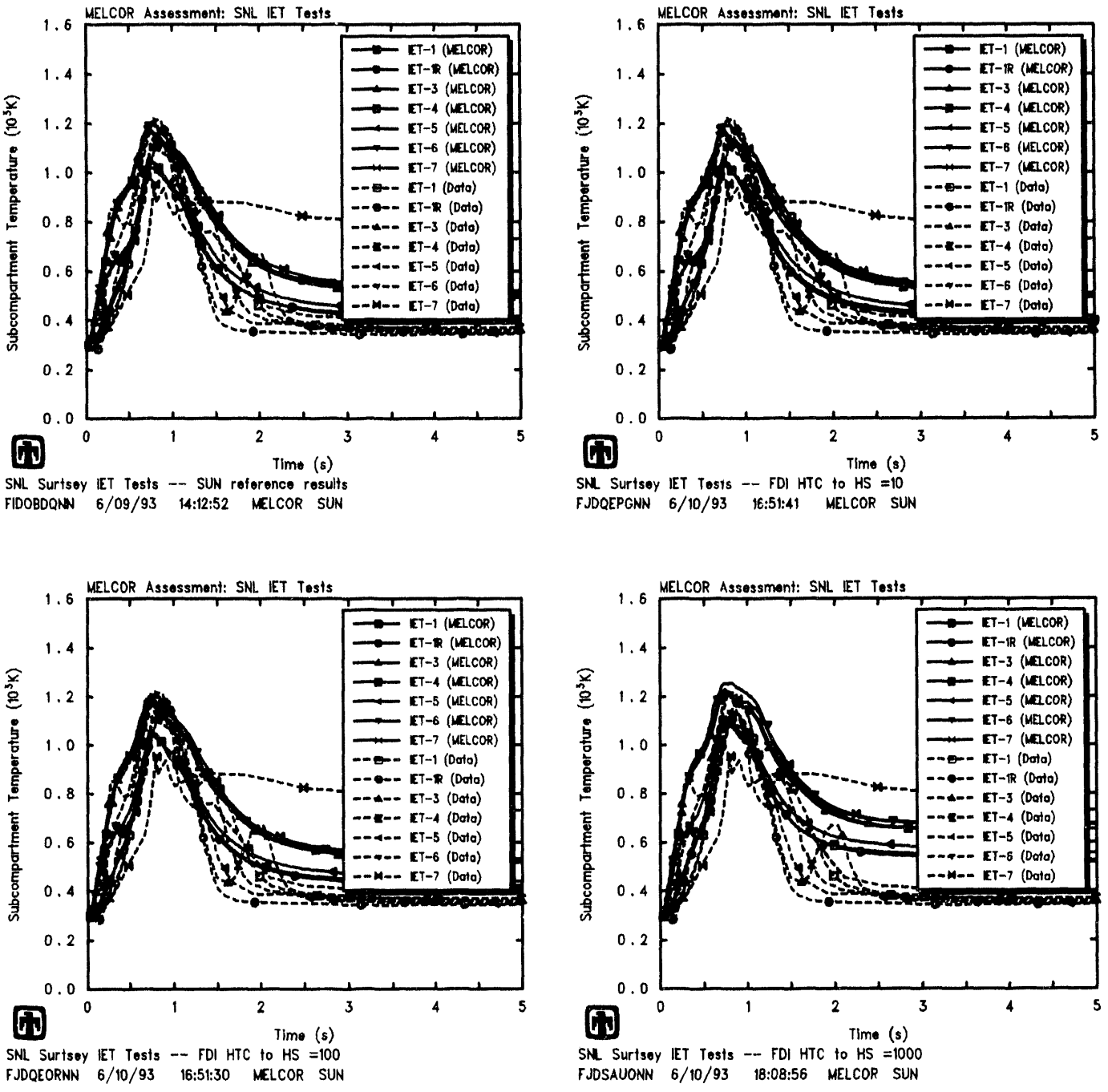

Figure 6.5.2. Subcompartment Temperatures for SNL/IET Experiments Using Deposited Debris Heat Transfer Coefficient of 1w/m^2-K (upper left), 10w/m^2-K (upper right), 100w/m^2-K (lower left) and 1000w/m^2-K (lower right) Deposited Debris Heat Transfer Coefficient Sensitivity Study

7 Other Modelling Studies

In addition to the sensitivity studies on user-input parameters controlling the initial debris source and the subsequent debris interaction, respectively, in the new MELCOR high-pressure melt ejection model in MELCOR, presented in Sections 5 and 6, several other non-default input modelling changes involving other MELCOR code packages were required in our IET assessment analyses, as already discussed in Section 3.1. This section presents the studies whose results demonstrate the need for those non-default input modelling changes.

7.1 Hydrogen Combustion

As described in Section 3.1, in the majority of our IET analysis calculations, the burn package was activated. However, burns were suppressed in all control volumes except the vessel dome; this was based upon the experimental observation that a jet of hydrogen produced by steam blowdown and debris oxidation burned as it vented from the subcompartments to the upper dome. The default ignition criterion in the absence of igniters was set to a hydrogen mole fraction of 0.0, but the combustion completeness was also set to 0.0; this prevents the burning of any pre-existing hydrogen, but allows burning of any additional hydrogen generated during the HPME. This was based upon the experimental observation that the pre-existing hydrogen that burned did not burn on a time scale that had a significant impact on the peak pressure [15, 16]. This particular combination of input was found to produce reasonable agreement with test data in all cases.

To evaluate this input selection, sensitivity studies using other possible input settings were done. Sets of calculations were done with the burn package inactivated; with the burn package active but all default input used; with the default hydrogen-mole-fraction ignition criterion in the absence of igniters and the combustion completeness both set to 0.0, but burn allowed in all control volumes; and with the default hydrogen-mole-fraction ignition criterion in the absence of igniters set to 0.0 but the combustion completeness either calculated from the default correlation or set to 1.0 (with burn suppressed in all control volumes except the vessel dome).

The predicted vessel pressures are presented in Figure 7.1.1 for some of the hydrogen combustion studies. Tables 7.1.1 and 7.1.2 compare the amounts of hydrogen generated and burned, respectively, in all these various cases. Subcompartment temperatures corresponding to the pressures shown in Figure 7.1.1 are given in Figure 7.1.2. (Experimental data are included for reference.)

The calculations done with the burn package inactivated and with the burn package active but all default input used produced identical results; no hydrogen combustion occurred even with the burn package activated because the hydrogen and oxygen mole fraction concentrations precluded ignition.

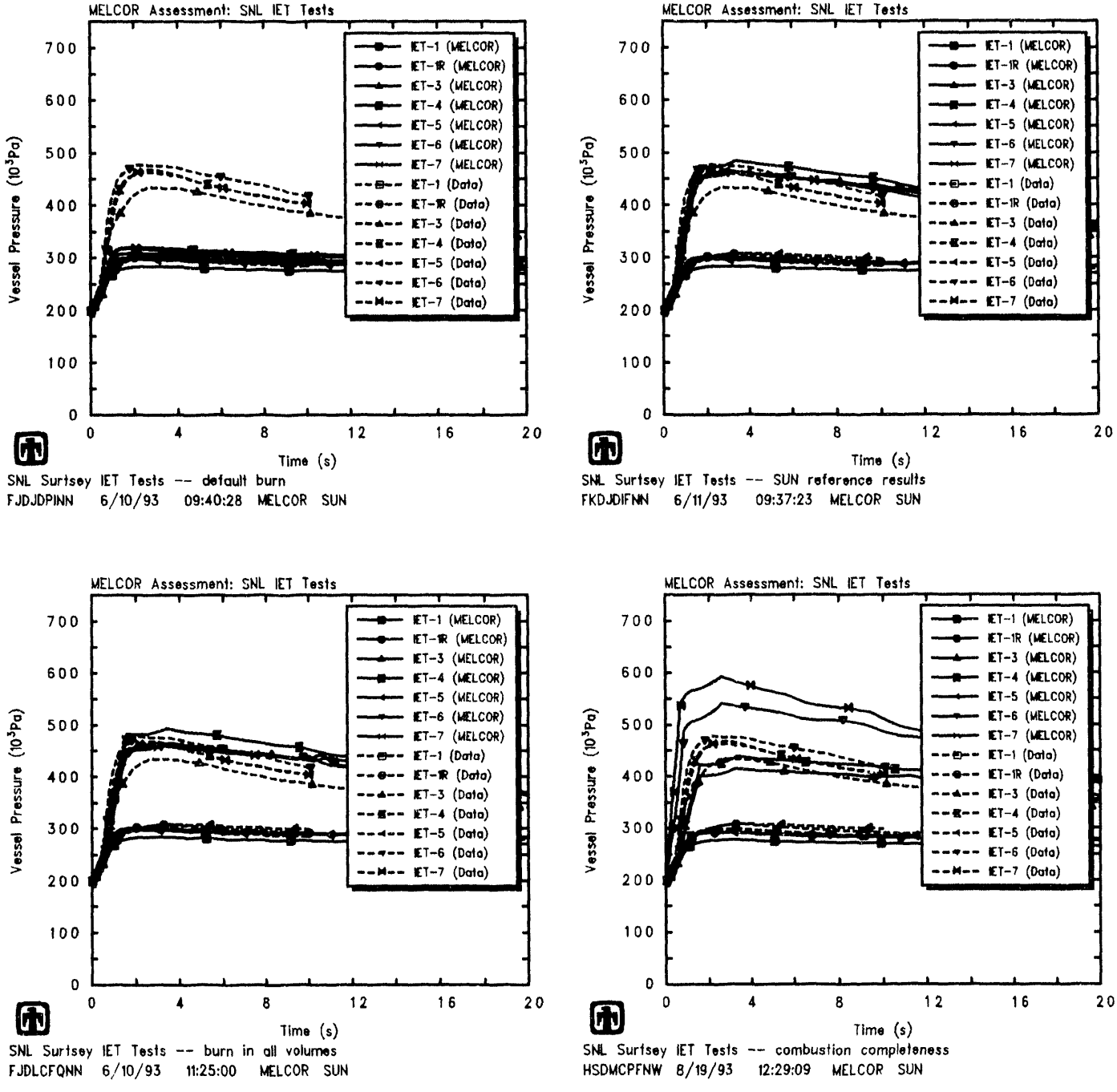

Figure 7.1.1. Vessel Pressures for SNL/IET Experiments with Default Burn Parameters (upper left), Basecase with Burn in the Dome Only with Zero Ignition Limit and Combustion Completeness of 0 (upper right), with Burn in all Volumes with Zero Ignition Limit and Combustion Completeness of 0 (lower left) and with Burn in the Dome Only with Zero Ignition Limit but Combustion Completeness of 1 (lower right) Hydrogen Combustion Sensitivity Study

Table 7.1.1. Hydrogen Generation for the SNL/IET Experiments – Hydrogen Combustion Sensitivity Study

Experiment	Hydrogen Produced (gm-moles)						
	Data†	MELCOR‡					
		no-burn	def-burn	burn in dome only with CC=0	burn in dome only with default CC	burn in all vol with CC=0	burn in dome only with CC=1
IET-1	233	286/266	286/266	286/266	286/266	286/266	218/199
IET-1R	248	266/267	266/267	266/267	266/267	266/267	200/203
IET-3	227	233/342	233/342	232/352	232/352	242/350	162/291
IET-4	303	247/351	247/351	243/361	243/361	256/370	177/307
IET-5	319	240/313	240/313	240/313	240/313	240/313	172/249
IET-6	319	238/344	238/344	236/354	236/354	240/351	170/300
IET-7	274	230/336	230/336	229/351	229/351	230/348	167/295

†from gas grab bottle samples at 30min

‡(actual values at 20s)/ (assuming only steam/metal reactions

Table 7.1.2. Hydrogen Combustion for the SNL/IET Experiments – Hydrogen Combustion Sensitivity Study

Experiment	Hydrogen Burned (gm-moles)						
	Data†	MELCOR‡					
		no-burn	def-burn	burn in dome only with CC=0	burn in dome only with default CC	burn in all vol with CC=0	burn in dome only with CC=1
IET-1	3	0/4	0/4	0/4	0/4	0/4	0/4
IET-1R	11	0/28	0/28	0/28	0/28	0/28	0/28
IET-3	190	0/126	0/126	188/313	188/313	208/321	158/291
IET-4	240	0/123	0/123	209/332	209/332	232/350	174/307
IET-5	53	0/91	0/91	0/91	0/91	0/91	0/92
IET-6	345	0/126	0/126	182/307	182/307	215/328	350/471
IET-7	323	0/125	0/125	223/350	229/350	239/357	452/567

†from gas grab bottle samples at 30min

‡(actual values at 20s)/ (assuming only steam/metal reactions

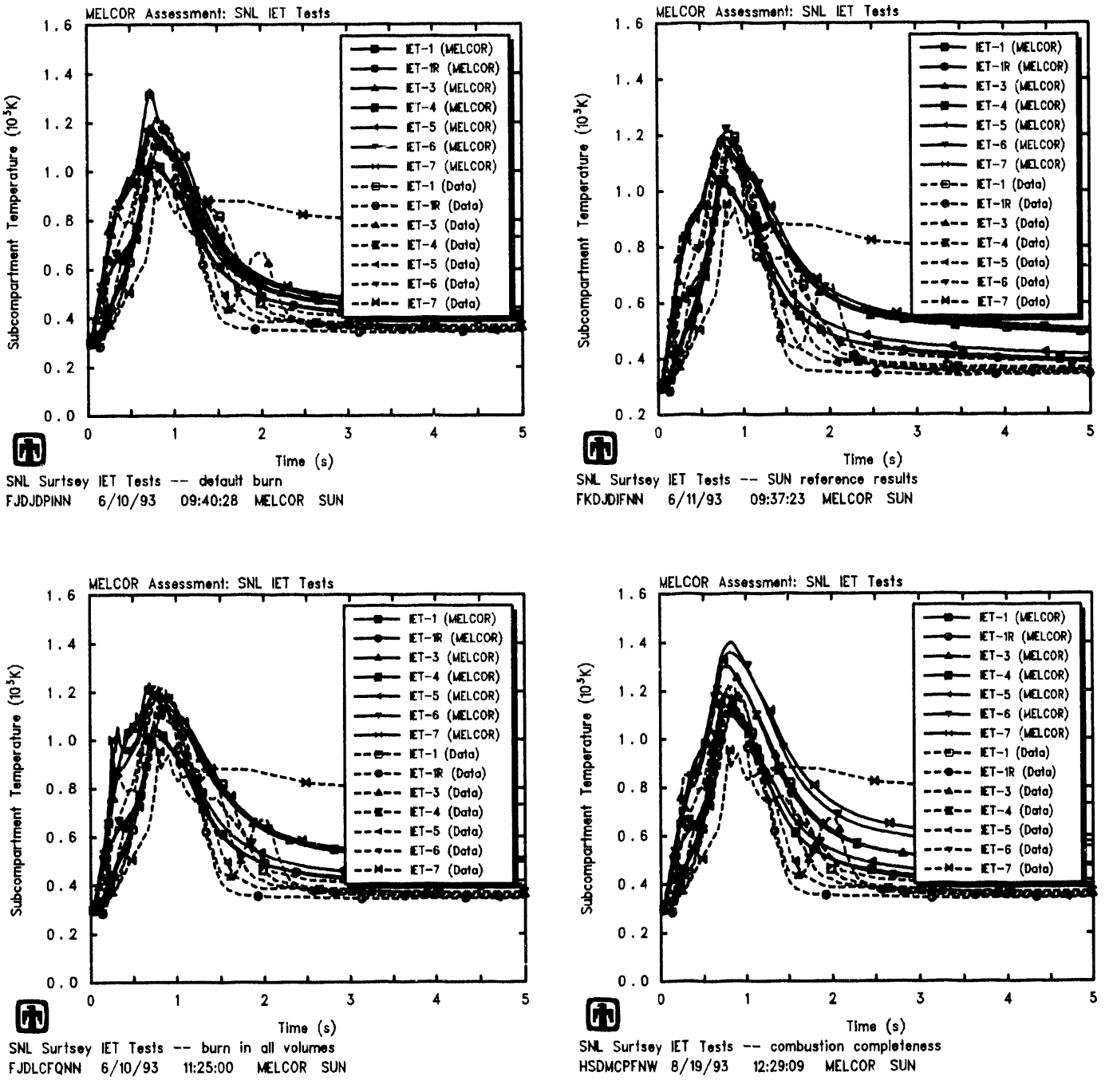

Figure 7.1.2. Subcompartment Temperatures for SNL/IET Experiments with Default Burn Parameters (upper left), Basecase with Burn in the Dome Only with Zero Ignition Limit and Combustion Completeness of 0 (upper right), with Burn in all Volumes with Zero Ignition Limit and Combustion Completeness of 0 (lower left) and with Burn in the Dome Only with Zero Ignition Limit but Combustion Completeness of 1 (lower right) Hydrogen Combustion Sensitivity Study

The hydrogen combustion behavior predicted using default burn package input is clearly qualitatively different than observed in these experiments. It was obvious from the test results that the hydrogen mole fraction ignition criterion had to be reset to ~0, at least during the DCH period. It appeared from the SNL/IET-5 test results that the steam and CO_2 mole fraction limits for inerting volumes did not need to be changed, and there was no clear indication from the test data whether the oxygen mole fraction ignition criterion had to be altered (so it wasn't).

The results obtained with the combustion completeness set to 0 and with the default combustion completeness correlation used were identical. This is because in these problems the LeChatelier formula is simply the hydrogen mole fraction (because $x_{CO} = 0.0$) and, with the hydrogen mole fraction ignition limit reset to 0.0, the LeChatelier formula at the beginning of the burn (Y_{MAX}) is also 0.0, and the default correlation used in MELCOR gives combustion completeness CC=0.0 for $Y_{MAX} \leq 0.03746$. Note that a combustion completeness equal to 0.0 does not mean no combustion; instead, it tries to maintain the mole fractions after the burn to be equal to the mole fractions before, so that new hydrogen introduced during a time step, either by oxidation or by advection, will be burned but pre-existing hydrogen will remain present and generally unreacted. This agrees much better with experimental data than the results obtained using a combustion completeness of 1.0, which produces much higher vessel pressurization and hydrogen combustion in the tests with pre-existing hydrogen than observed in the experiments.

7.2 Heat Transfer to Structures

As discussed in Section 3.1, most of our calculations were run with control volume flow areas reduced by factors of $\geq$10 from their default values, to enhance convective heat transfer from the control volume atmospheres to the heat structure surfaces. (Recall that the control volume flow area is used only to calculate the velocities used in convective heat transfer correlations, and thus decreasing the volume flow area is a simple and direct way of multiplying volume flow velocities; these studies did not change flow path areas or velocities.) This was done for two reasons:

First, the flow through the system in these calculations was primarily that associated with the steam blowdown only, flowing from the steam accumulator through the cavity and chute volumes to the subcompartments and then to the dome. The MELCOR FDI/HPME/DCH model does not model transport of debris between and through volumes but instead deposits the debris directly at its ultimate destination, using the same time-dependent deposition in all volumes regardless of their distance from the debris source. In reality, the melt reaches the subcompartments later than the cavity, and the dome later than the subcompartments. Thus, instead of debris being transported into an "upstream" volume (*e.g.*, the cavity or the subcompartments) with the blowdown steam and the resultant additional heating adding to the driving force pushing flow further "downstream" (*e.g.*, from the cavity to the chute or the subcompartments to the dome), the MELCOR logic does not represent this additional flow driving force and in contrast has debris appearing "upstream" and heating the atmosphere in upstream volumes, if

anything contributing a retarding force to the expected flow. Thus the only flows generated in these MELCOR analyses were those associated with the steam accumulator blowdown, a relatively benign event compared to high-pressure melt ejection with hot debris mixed with the blowdown steam (as can be seen from the relative contributions to vessel pressurization given in Table 4.4).

Decreasing volume flow areas results in increased volume velocities more characteristic of the turbulent conditions that might be expected during HPME, and the associated turbulent forced convection heat transfer to structures. For the subcompartment control volume, in particular, it also reflects the fact that there is not a single, large, open subcompartment volume in the Surtsey facility but instead a collection of subcompartments, each with smaller volume and internal flow area and with smaller-area openings connecting the subcompartments to each other and to the dome. Thus, a (default) volume flow area of $\geq 4.5 m^2$ obtained using the subcompartment volume of $4.65 m^3$ and a height of $\geq 1 m$ may not be indicative of the actual velocities in the subcompartments.

In addition, the MELCOR FDI/HPME/DCH model does not account for any radiation directly from airborne debris to surrounding structures (or from deposited debris directly to atmosphere). There is little or no calculated atmosphere-structure radiation heat transfer early in these transients (except in IET-5), because MELCOR only considers radiation heat transfer for steam and/or CO_2 in atmospheres. In IET-5, some atmosphere-structure radiation heat transfer is calculated because of the large amount of CO_2 used to inert the system; however, in most of the experiment simulations there is very little steam present early in the transient, because any blowdown steam is consumed in debris oxidation soon after arrival, and very little CO_2 present at all. The lack of steam and/or CO_2 in the atmosphere would if anything enhance radiation heat transfer from airborne debris to structures because there would be little absorption in the intervening atmosphere. Because there is no way in MELCOR to model this effect, too much energy may be deposited in the atmosphere by the airborne debris; because there is no convenient way to enhance atmosphere-structure radiation heat transfer in general, we relied on increasing convective heat transfer instead to help remove that energy.

Figure 7.2.1 presents the heat transfer coefficients calculated for the subcompartment wall structure inner surface by MELCOR, with no adjustment to volume flow areas or to overall heat transfer; this heat transfer coefficient sums both the convective and radiative terms. During the first second, the heat transfer coefficient is in the $\sim$5-25w/m^2-K range (except for IET-5) and (except for IET-5) is due primarily to convective heat transfer. The larger heat transfer coefficients in IET-5 and after $\sim$1s for the other test simulations (when steam is no longer being consumed in debris oxidation and a significant steam mole fraction appears) are due to the addition of a radiation term equivalent to $\leq 50 w/m^2$-K, which then drops in magnitude as the atmosphere temperature drops.

The radiation heat transfer coefficient for an emissivity of 0.8 and a wall temperature of 300K was estimated [34] to be $\sim 65 w/m^2$-K for an atmosphere temperature of 1000K and $\sim 425 w/m^2$-K for an atmosphere at 2000K, in reasonable agreement with the MELCOR value given the effect of gas components other than steam and CO_2 present. However, spread sheet calculations [34] suggest that forced convection heat transfer co-

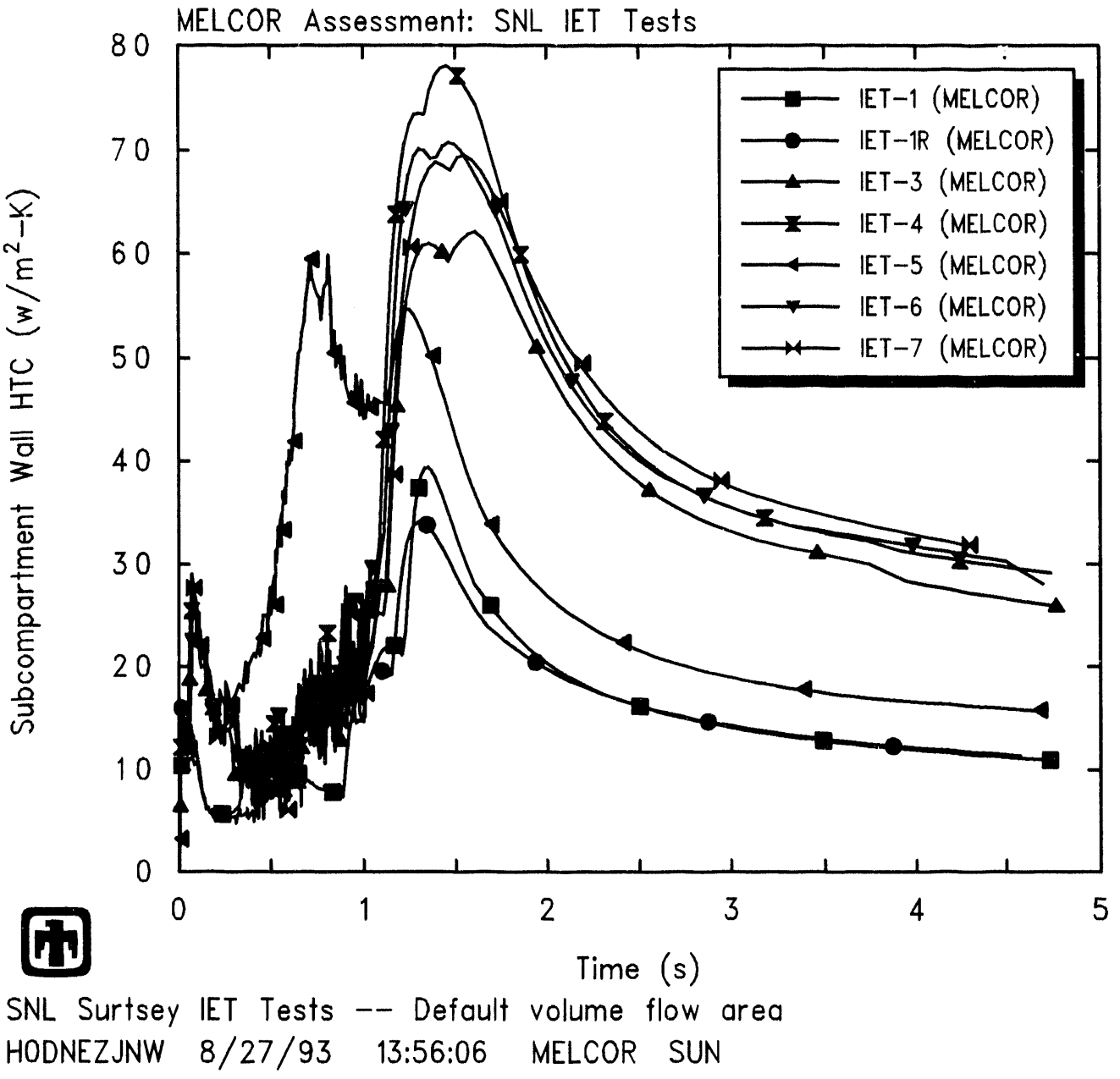

Figure 7.2.1. Subcompartment Atmosphere-to-Structure Heat Transfer Coefficients for SNL/IET Experiments Using Default Volume Flow Areas/Velocities -- Convective Heat Transfer Sensitivity Study

efficients should be in the ~50-125w/m^2-K range for conditions characteristic of the subcompartments in the SNL/IET experiments near the time of peak temperature and pressure. This is significantly higher than the convective heat transfer coefficients calculated in MELCOR with no volume flow area or characteristic velocity adjustment. (Similarly, the convective heat transfer coefficient given by MELCOR for the cavity and chute is in the 20-250w/m^2-K range, while spread sheet calculations [34] suggest that forced convection heat transfer coefficients should be in the ~6000-1500w/m^2-K range for conditions characteristic of the cavity in the SNL/IET experiments near the time of peak temperature and pressure.)

Other hand calculations [35] showed that the effective heat transfer coefficient for direct radiation from airborne debris in the subcompartments to the structure walls (an effect not modelled by MELCOR) could be of the order $0.2/R_d$, where R_d is the debris particle radius. This assumes a debris temperature of 2300K, a wall temperature of 300K, and an emissivity of 1, and also assumes that the airborne debris particles occupy negligible volume so that the radiation view factor from the airborne debris to the walls is ~1. Posttest sieve analysis of debris recovered from outside the subcompartment structures in SNL/IET-6 [15] shows diameters ranging from 0.05mm to 10mm; for 10mm-diameter debris particles, the effective heat transfer coefficient for radiation to structures would be ~20w/m^2-K, while for 0.1mm-diameter debris particles, the effective heat transfer coefficient for radiation to structures would be ~2,000w/m^2-K. This could therefore be a significant heat transfer mechanism, early in the transient. Because there is no way in MELCOR to model this effect, too much energy may be deposited in the atmosphere by the airborne debris; because there is no convenient way to enhance atmosphere-structure radiation heat transfer in general, we relied on increasing convective heat transfer instead to help remove that energy.

To evaluate the effect of heat transfer to the structures, a set of sensitivity calculations were done with the default volume flow areas and with the volume flow areas progressively reduced by factors of 10, 100 and 1000. Figure 7.2.2 presents the resulting atmosphere-to-structure heat transfer coefficients for the subcompartments. Note that, while decreasing the volume flow area by a given factor increases the volume velocity by that same factor, the heat transfer coefficient does not change by the same factor, both because changing the velocity can change the heat transfer mode and hence the correlation used and because most of the correlations depend on the velocity to a power ($v^{0.8}$ for turbulent forced convection, $v^{0.5}$ for laminar forced convection and $v^{0.33}$ or $v^{0.25}$ for natural convection). Thus, increasing default volume areas by 10 increased subcompartment atmosphere-to-structure convective heat transfer coefficients by $\leq$10 but increasing default volume areas by 100 only increased convective heat transfer coefficients by ~50 and increasing increasing default volume areas by 1000 only increased convective heat transfer coefficients by ~250.

Resulting predicted vessel pressures with the default volume flow areas and with the volume flow areas progressively reduced by factors of 10, 100 and 1000 are shown in Figure 7.2.3, together with the test data. The effect of increasing volume velocities and therefore increasing overall heat transfer to structures is to reduce the overall vessel

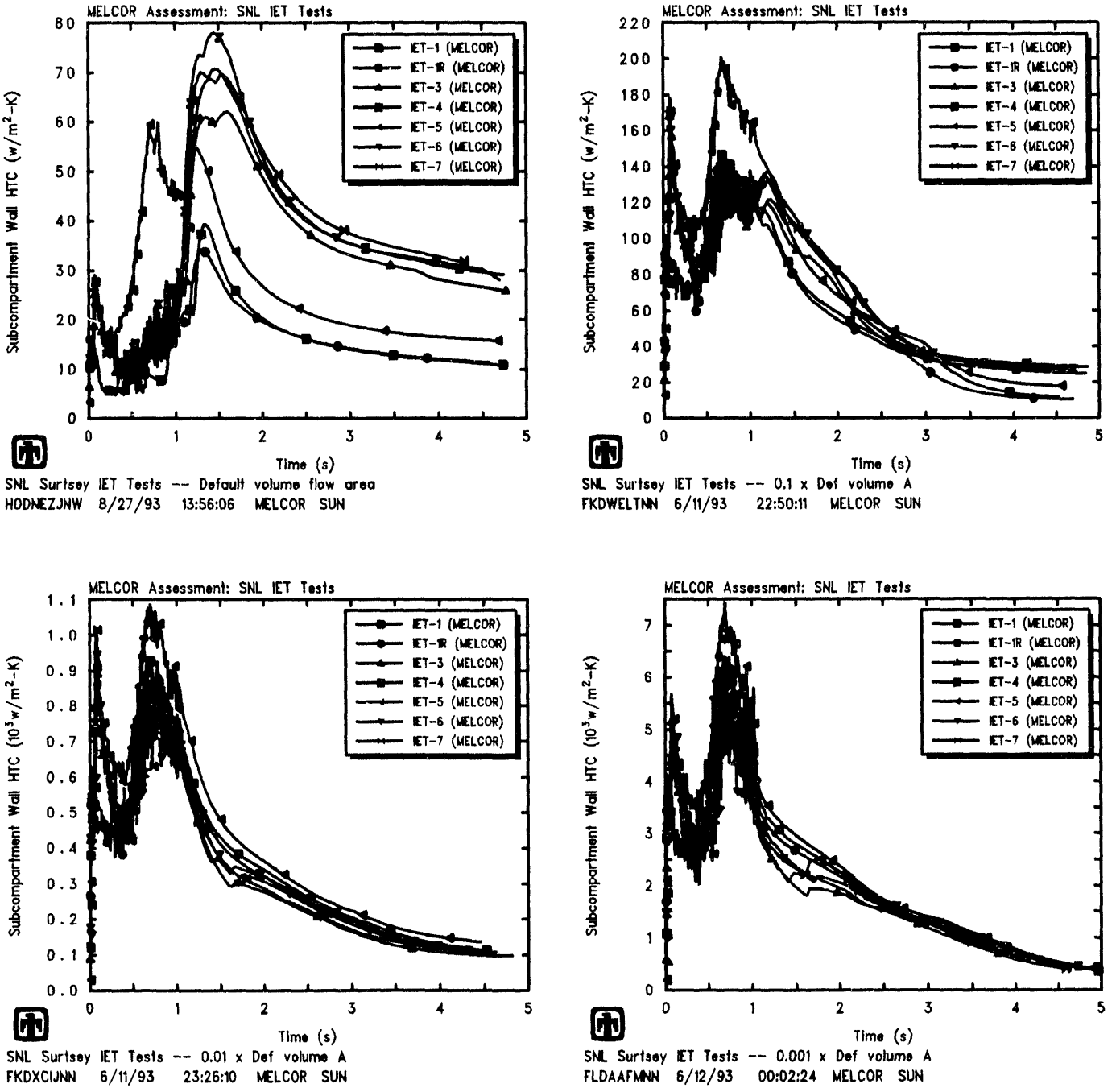

Figure 7.2.2. Subcompartment Atmosphere-to-Structure Heat Transfer Coefficients for SNL/IET Experiments Using Default Volume Flow Areas/Velocities (upper left), 0.1 × Volume Flow Areas (upper right), 0.01 × Volume Flow Areas (lower left) and 0.001 × Volume Flow Areas (lower right) – Convective Heat Transfer Sensitivity Study

pressurization calculated.

Tables 7.2.1 and 7.2.2 compare the amounts of hydrogen generated and burned, respectively, in these various cases. While the trend is not as strong as that seen in the vessel pressure responses, slightly more hydrogen generation is calculated as the heat transfer to structures is increased in most cases; the hydrogen combustion varies as the hydrogen production, so increasing production tends to increase combustion also.

The volume areas and velocities have a very strong effect on the temperatures predicted, as illustrated in Figure 7.2.4 for the subcompartments. The calculated temperatures are much higher than measured using the default volume flow areas and velocities or using volume flow areas and velocities decreased and increased by an order of magnitude, respectively; increasing the volume velocities (reducing the default volume flow areas) by 1000 produces significantly lower temperatures than measured in the subcompartments. These changes in atmosphere temperatures are a direct result of changing heat transfer from atmosphere to structures, as would be expected.

7.3 Recirculation Flow

The input model in our MELCOR analyses provided flow paths for straight-through flow from the steam accumulator to the cavity and chute through the (lumped-together) subcompartments to the vessel dome, and also for recirculation from the upper dome to the subcompartments. That "recirculation" flow path was provided to allow for the fact that in the actual facility a number of openings exist between the various subcompartments and the vessel dome, with the potential of inflow in some openings and outflow in others. The are*a of that recirculation flow path was set to 10% of the area of the straight-through flow path from the subcompartments to the dome. Sensitivity studies were done with that recirculation flow path area increased and decreased by a factor of 10 (*i.e.*, set equal to the area of the straight-through flow path from the subcompartments to the dome, and set to 1% of the area of the straight-through flow path from the subcompartments to the dome), and also simply set to zero.

Figure 7.3.1 shows pressures in the vessel predicted using various recirculation flow path areas (including a zero-area case), together with test data. There are visible qualitative and quantitative differences in predicted vessel pressurization both for less and for more recirculation flow than assumed in our basecase, reference analyses.

The vessel pressurization calculated is slightly lower as the recirculation flow is reduced to zero. The direct containment heating in these experiments is primarily driven by debris oxidation in the subcompartments. Because the oxidation rate in the subcompartments is steam- and oxygen-limited, varying the recirculation flow varies the amount of oxygen swept into the subcompartments from the large reservoir in the dome, and thus affects the oxidation rate. In addition, varying the recirculation flow affects the rates at which the rapidly-heated subcompartment atmosphere is mixed with the much cooler, much larger atmosphere in the dome.

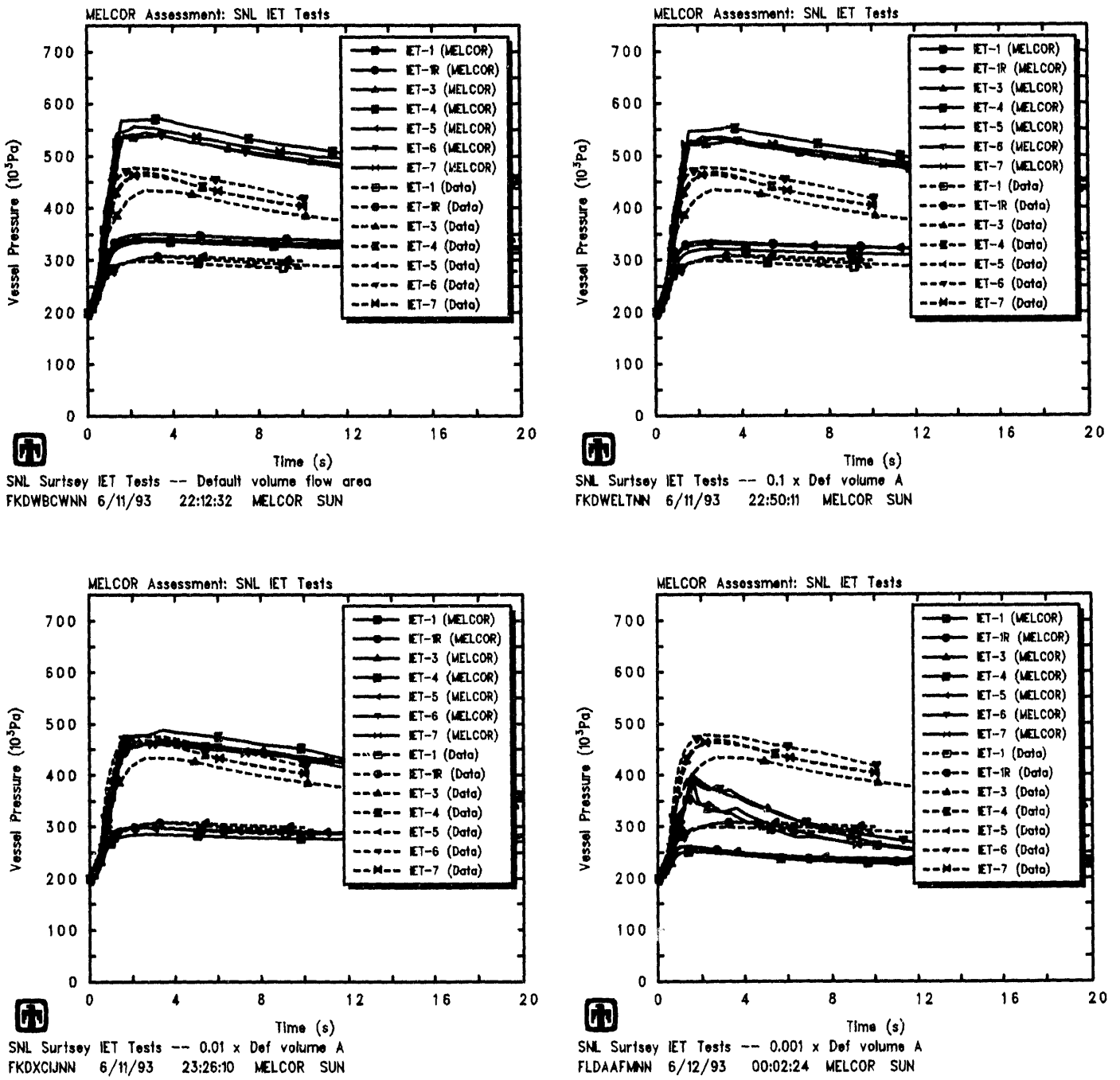

Figure 7.2.3. Vessel Pressures for SNL/IET Experiments Using Default Volume Flow Areas/Velocities (upper left), 0.1 × Volume Flow Areas (upper right), 0.01 × Volume Flow Areas (lower left) and 0.001 × Volume Flow Areas (lower right) Convective Heat Transfer Sensitivity Study

Table 7.2.1. Hydrogen Generation for the SNL/IET Experiments - Convective Heat Transfer Sensitivity Study

Experiment	Hydrogen Produced (gm-moles)				
	Data†	MELCOR‡ A_{VOL}=			
		Def	0.1×Def	0.01×Def	0.001×Def
IET-1	233	285/269	284/268	285/263	287/273
IET-1R	248	263/271	265/273	264/261	268/278
IET-3	227	229/340	231/344	229/349	233/331
IET-4	303	241/354	247/359	242/361	247/347
IET-5	319	236/313	239/313	240/314	241/321
IET-6	319	232/356	232/344	234/352	235/333
IET-7	274	224/342	225/337	225/343	231/336

†from gas grab bottle samples at 30min
‡(actual values at 20s)/ (assuming only steam/metal reactions)

Table 7.2.2. Hydrogen Combustion for the SNL/IET Experiments - Convective Heat Transfer Sensitivity Study

Experiment	Hydrogen Burned (gm-moles)				
	Data†	MELCOR‡ A_{VOL}=			
		Def	0.1×Def	0.01×Def	0.001×Def
IET-1	3	0/4	0/4	0/4	0/4
IET-1R	11	0/28	0/28	0/28	0/28
IET-3	190	205/320	203/321	189/314	203/309
IET-4	240	223/339	225/341	210/333	227/332
IET-5	53	0/93	0/92	0/92	0/91
IET-6	345	199/318	197/314	181/305	191/296
IET-7	323	227/349	226/344	219/343	226/335

†from gas grab bottle samples at 30min
‡(actual values at 20s)/ (assuming only steam/metal reactions)

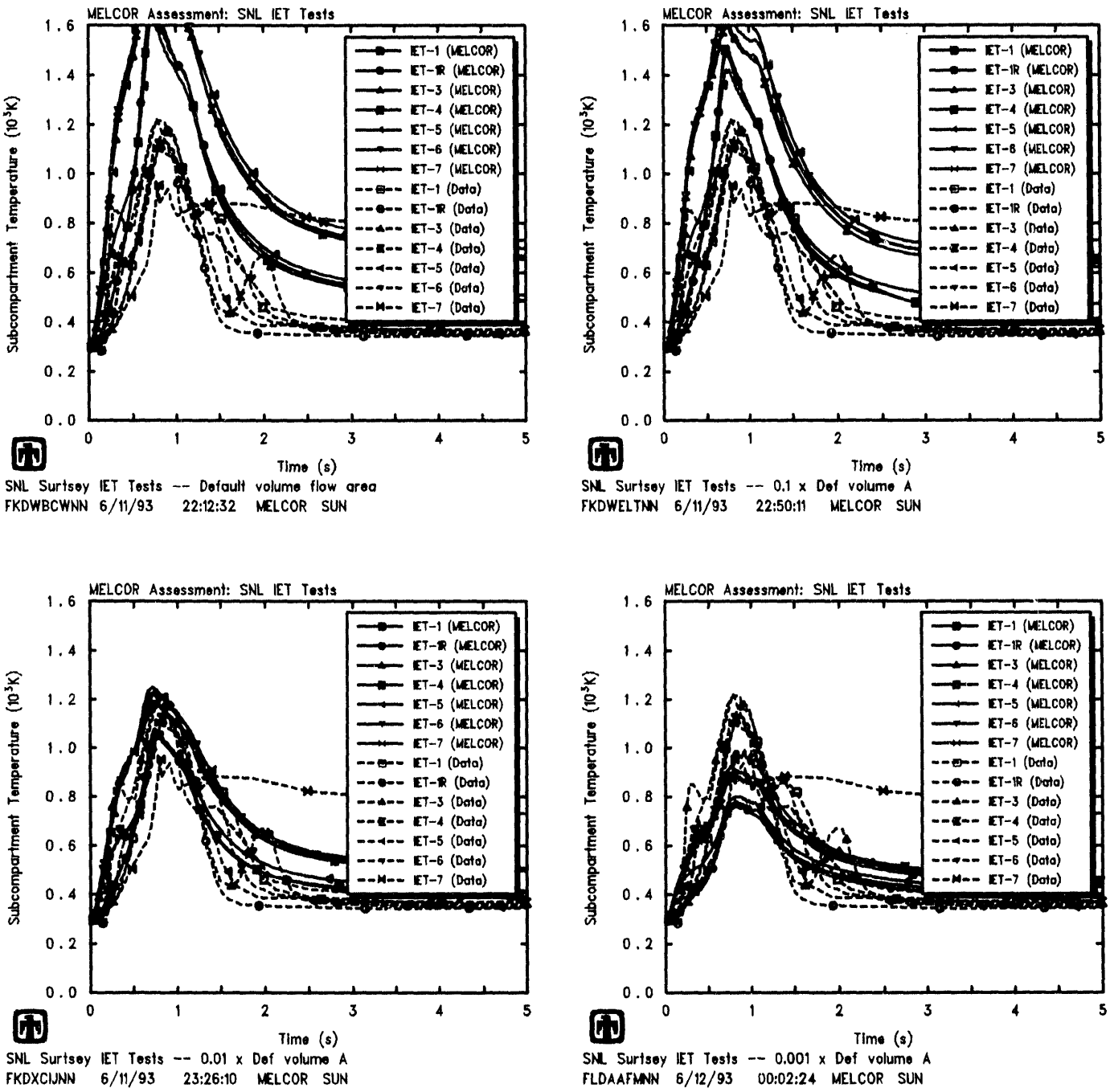

Figure 7.2.4. Subcompartment Temperatures for SNL/IET Experiments Using Default Volume Flow Areas/Velocities (upper left), 0.1 × Volume Flow Areas (upper right), 0.01 × Volume Flow Areas (lower left) and 0.001 × Volume Flow Areas (lower right) Convective Heat Transfer Sensitivity Study

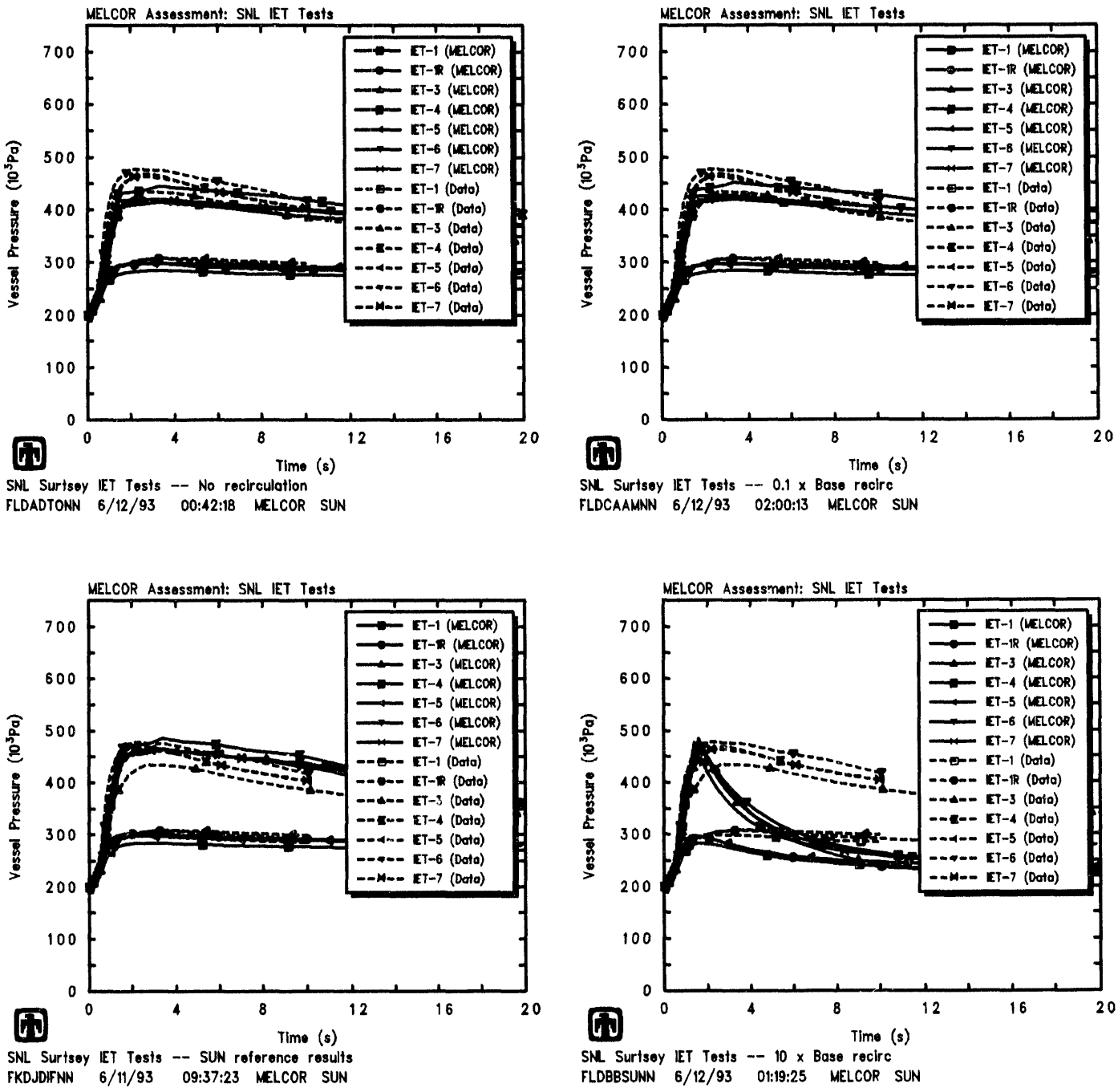

Figure 7.3.1. Vessel Pressures for SNL/IET Experiments for No Recirculation (upper left), 0.1 × Basecase (upper right), Basecase (lower left) and 10 × Basecase (lower right) – Recirculation Flow Sensitivity Study

Increasing the recirculation flow does not appear to affect the peak vessel pressure very much, but there is a much more rapid depressurization after $\leq$2s for the large recirculation flow, qualitatively unlike both the test data and the reference analysis results. The rapid depressurization occurs because varying the recirculation flow affects the volume velocities used to calculate heat transfer coefficients. Figure 7.3.2 compares the flows rates into ("straight-through") and out of ("recirculation") the dome and the dome inside surface heat transfer coefficients calculated for the reference analyses and for the sensitivity study increasing the recirculation flow area. The flows are nearly stagnant in the reference analyses after about 2s, while significant flows persist in the sensitivity study increasing the recirculation flow area throughout most of the transient period considered; the heat transfer coefficients in the reference analyses drop by about an order of magnitude after about 2s, to $\leq$25w/m^2-K, while the dome inside surface heat transfer coefficients calculated for the sensitivity study increasing the recirculation flow area remain $\geq$100w/m^2-K throughout most of the transient period considered. Thus the vessel atmosphere loses substantially more energy to the walls more quickly after the first few seconds of the HPME transient in the sensitivity study calculation increasing the recirculation flow area.

Tables 7.3.1 and 7.3.2 present the amounts of hydrogen generated and burned, respectively, in these various cases. Test data estimates of the amounts of hydrogen produced and burned are included for reference. While there is no systematic variation in hydrogen production as the recirculation flow area is increased, there is a significant difference in the amount of hydrogen combustion calculated for the two sets of calculations with little or no recirculation, compared to the hydrogen combustion calculated in the two sets of calculations with basecase or more recirculation; this is because increased recirculation flow draws more hydrogen from the subcompartments where it was generated to the dome where oxygen is available for reaction and where combustion is permitted to occur.

Figure 7.3.3 gives subcompartment temperatures calculated using various recirculation flow areas and flow rates, together with experimental data. While there is not much change in the magnitude of the peak subcompartment temperatures being calculated, there is a much broader temperature peak in the cases with little or no recirculation flow assumed, probably due to reduced mixing of the hotter subcompartment atmosphere with the cooler dome atmosphere.

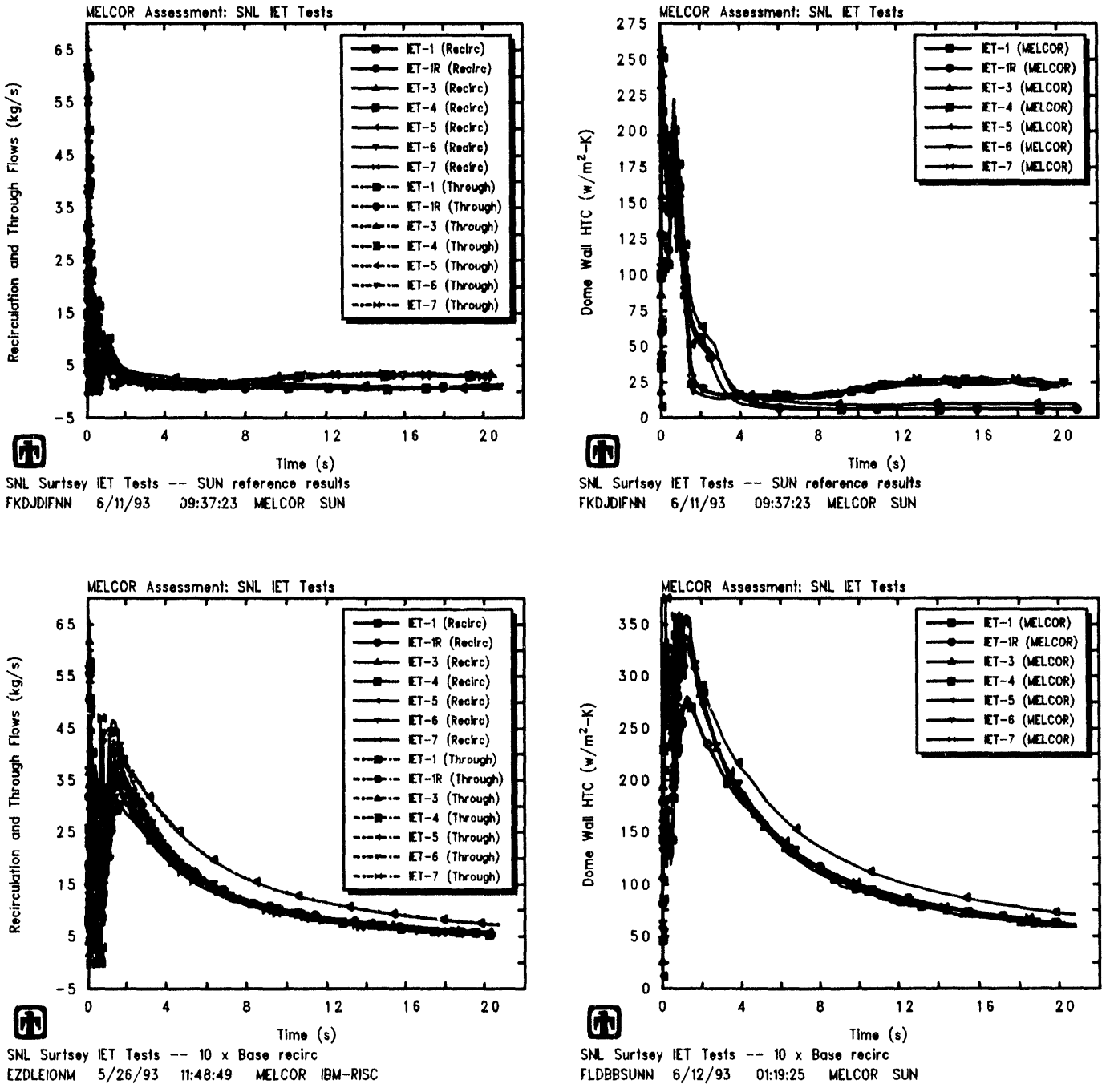

Figure 7.3.2. Flows into and out of the Vessel Dome (left) and Dome Inside Surface Heat Transfer Coefficients for SNL/IET Experiments for Basecase (top) and 10 × Basecase (bottom) Recirculation Flow Sensitivity Study

Table 7.3.1. Hydrogen Generation for the SNL/IET Experiments - Recirculation Flow Sensitivity Study

Experiment	Hydrogen Produced (gm-moles)				
	Data†	MELCOR‡ (× Basecase)			
		0 (none)	0.1	1	10
IET-1	233	282/200	282/208	286/266	288/277
IET-1R	248	263/189	262/197	266/267	267/281
IET-3	227	242/170	240/182	232/352	210/386
IET-4	303	253/180	254/195	243/361	220/396
IET-5	319	246/210	244/226	240/313	235/344
IET-6	319	244/166	243/179	236/354	208/395
IET-7	274	236/156	237/223	229/351	207/395

†from gas grab bottle samples at 30min
‡(actual values at 20s)/ (assuming only steam/metal reactions)

Table 7.3.2. Hydrogen Combustion for the SNL/IET Experiments - Recirculation Flow Sensitivity Study

Experiment	Hydrogen Burned (gm-moles)				
	Data†	MELCOR‡ (× Basecase)			
		0 (none)	0.1	1	10
IET-1	3	0/4	0/4	0/4	0/4
IET-1R	11	0/28	0/28	0/28	0/28
IET-3	190	113/170	119/182	188/313	208/384
IET-4	240	129/179	137/194	209/332	218/394
IET-5	53	0/56	0/61	0/91	0/122
IET-6	345	110/159	117/171	218/307	202/388
IET-7	323	111/164	118/175	223/350	209/396

†from gas grab bottle samples at 30min
‡(actual values at 20s)/ (assuming only steam/metal reactions)

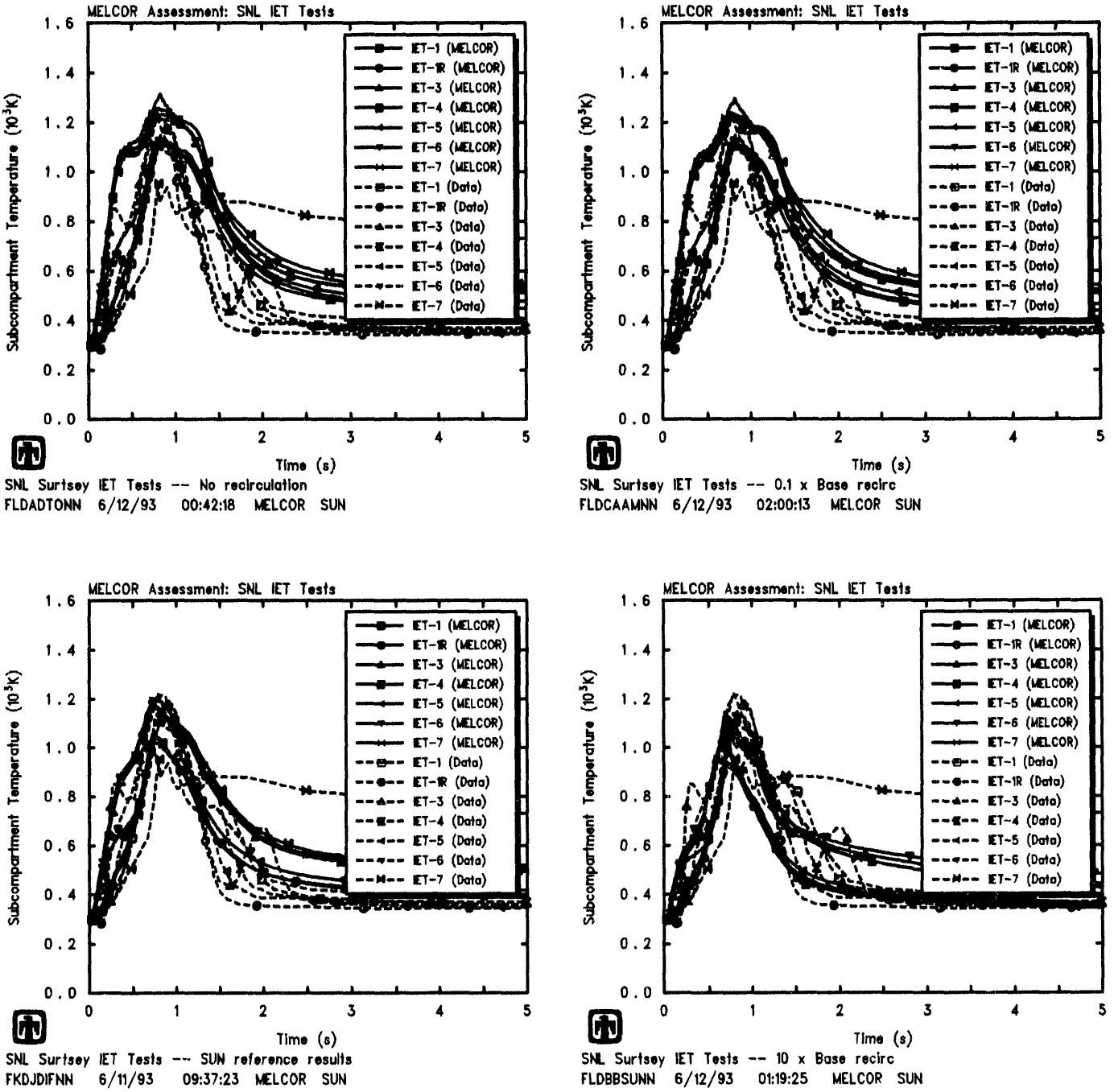

Figure 7.3.3. Subcompartment Temperatures for SNL/IET Experiments for No Recirculation (upper left), 0.1 × Basecase (upper right), Basecase (lower left) and 10 × Basecase (lower right) Recirculation Flow Sensitivity Study

8 Scaling Sensitivity Study

Several counterpart tests to the SNL/IET direct containment heating experiments done at Sandia in the 1:10 linear scale Surtsey facility were performed at ANL in the 1:40 linear scale COREXIT facility, in an experimental program to investigate the effects of scale on DCH phenomena. The ANL facility and test program is described in Section 2.2. Tests ANL/IET-1RR, ANL/IET-3 and ANL/IET-6 were counterpart tests to the SNL/IET-1, SNL/IET-1R, SNL/IET-3 and SNL/IET-6 Surtsey experiments. (We did not consider the early counterpart tests, ANL/IET-1 and ANL/IET-1R, because of problems in the experimental procedure affecting steam/debris blowdown timing.)

Our analysis of the ANL/IET experiments was complicated by several factors. As discussed briefly in Section 3.2, there was not enough facility information and drawings available in the ANL letter reports [18-24] to develop a MELCOR input model for the COREXIT facility IET configuration; we often had to simply assume the Surtsey input model numbers scaled directly to the ANL test facility. Also, some of the copies we had of the letter reports describing the tests and results [18-24] were incomplete, with both figures and pages of text occasionally missing, and those letter reports generally contained very little analysis of the test results. For example, while there was some discussion about the overscaled melt mass being used in ANL/IET-1RR and ANL/IET-3 to compensate for expected melt retention in the melt generator/crucible, we found no discussion on why the smaller melt mass was used for ANL/IET-6 and on what effect this change would have on comparison of results. Further, we have found little or no documented analysis comparing the counterpart test behavior at the two different facilities and scales, identifying and discussing similarities and differences, although we would have expected this to be an important and high-priority result of the test program.

We did find a limited discussion of the scaling and reproducibility of the SNL/IET-1 and SNL/IET-1R test set done in the Surtsey vessel and the ANL/IET-1R and ANL/IET-1RR test set done at Argonne [36]. However, that scaling analysis seemed overly complicated, with different time and pressure scale factors used for each individual experiment (rather than for each experiment set), and did not address the issue of hydrogen-combustion scaling in the other counterpart tests (IET-3 and IET-6) at all. We therefore performed our own, limited review of the facility data scalability in order to complete this required part of this MELCOR assessment task.

8.1 Facility and Data Scaling Background Discussion

Table 8.1.1 compares some of the facility parameters and the degree to which scaling was preserved. The numbers in the SNL and ANL facility columns come either from the published data reports [10-24] or in a few cases from [36]. The scaling comparison done in this table is only between the two facilities; the degree to which either facility correctly scaled actual plant conditions is not considered here. Only large discrepancies in scaling are noted; we considered differences $\leq$5-10% negligible. (Note that the 1:10-scale and

1:40-scale descriptors usually used for these facilities are approximate. An exact scaling factor of 3.922 was used in the comparisons in this table.)

This comparison identifies several scaling concerns:

1. The melt mass in the earlier ANL tests (ANL/IET-1RR and ANL/IET-3) was significantly overscaled.

2. The blowdown steam source was significantly overscaled in volume and, for similar steam pressures and temperatures, therefore significantly overscaled in mass and energy.

3. Although the downstream volumes into which the steam was blowing down were correctly scaled, the ANL vessel aspect ratio ($\sim$5) was significantly greater than the Surtsey vessel aspect ratio ($\sim$ 3).

Figure 8.1.1 shows the steam accumulator blowdown measured for four of the SNL tests (SNL/IET-1, SNL/IET-1R, SNL/IET-3 and SNL/IET-6), together with the steam accumulator blowdown measured for three of the ANL counterpart tests (ANL/IET-1RR, ANL/IET-3 and ANL/IET-6); we did not consider either the ANL/IET-1 or ANL/IET-1R experiments as successful counterpart tests. In this figure, the times for the 1:10-scale Surtsey tests have been multiplied by 1/4 to correspond to the 1:40-scale ANL tests, a factor equivalent to assuming that velocities were kept constant in the two facilities. The crossplot results indicate that this simple scaling works quite well (at least as well as the more complicated scaling used in [36]), with test-to-test variations in each facility at least as large as facility-to-facility variations.

The corresponding measured vessel pressures (with the times in the SNL test results scaled by the same 1/4 multiplier) are presented in Figure 8.1.2. While the results qualitatively scale, with greater pressurization in cases with hydrogen combustion, there are a number of quantitative discrepancies. The first thing to note in both Figure 8.1.2 and in comparing peak vessel pressures given in Tables 2.1.4 and 2.2.4 is that the maximum pressure rise due to DCH in the smaller-scale ANL facility is significantly ($\sim$50%) greater than the maximum pressurization due to DCH observed in the tests done in Surtsey. This is probably partially due to the relatively larger steam blowdown source and melt mass in ANL/IET-1RR compared to SNL/IET-1 and SNL/IET-1R, but the difference is so large that it also indicates that DCH energy-transfer efficiency was greater at the smaller scale. The second thing to note is that the pressurization due to hydrogen combustion is significantly less in the smaller-scale ANL facility than observed in the tests done in Surtsey, especially given the greater pressurization due to DCH. The third thing to note is that there is a much greater difference between the early-time peak vessel pressurization in the ANL 1:40-scale tests with and without pre-existing hydrogen than in the counterpart SNL 1:10-scale tests, especially given the $\sim$15% decrease in melt mass from ANL/IET-3 to ANL/IET-6.

Tables 8.1.2 and 8.1.3 summarize the hydrogen production and combustion data from these counterpart tests (with the SNL test results scaled by a $1/4^3$ multiplier). Again,

Table 8.1.1. Facility Scaling for the SNL and ANL IET Experiments

Parameter Parameter	SNL (1:10 scale)	ANL (1:40 scale)	Discrepancy in Scaling §
Thermite (kg)	43.0	0.820†	+15%
Thermite (kg)	43.0	0.713‡	-
Steam Accumulator Volume (m^3)	0.30	0.006	+20%
Cavity/Chute Volume (m^3)	0.245	0.004	-
Cavity/Chute Length (m)	2.4	0.61	-
Cavity Water (kg)	3.48	0.055	-
Subcompartment Volume (m^3)	4.65	0.077	-
Subcompartment Height (m)	1.52	0.39	-
Dome Volume (m^3)	85.15	1.43	-
Vessel Total Volume (m^3)	89.8	1.51	-
Vessel Height (m)	9.9	3.4	+35%
Vessel Diameter (m)	3.38	0.76	-12%
Vessel Area (m^2)	9.0	0.454	-23%

§"+" if ANL facility/test overscale
†for IET-1RR and IET-3
‡for IET-6

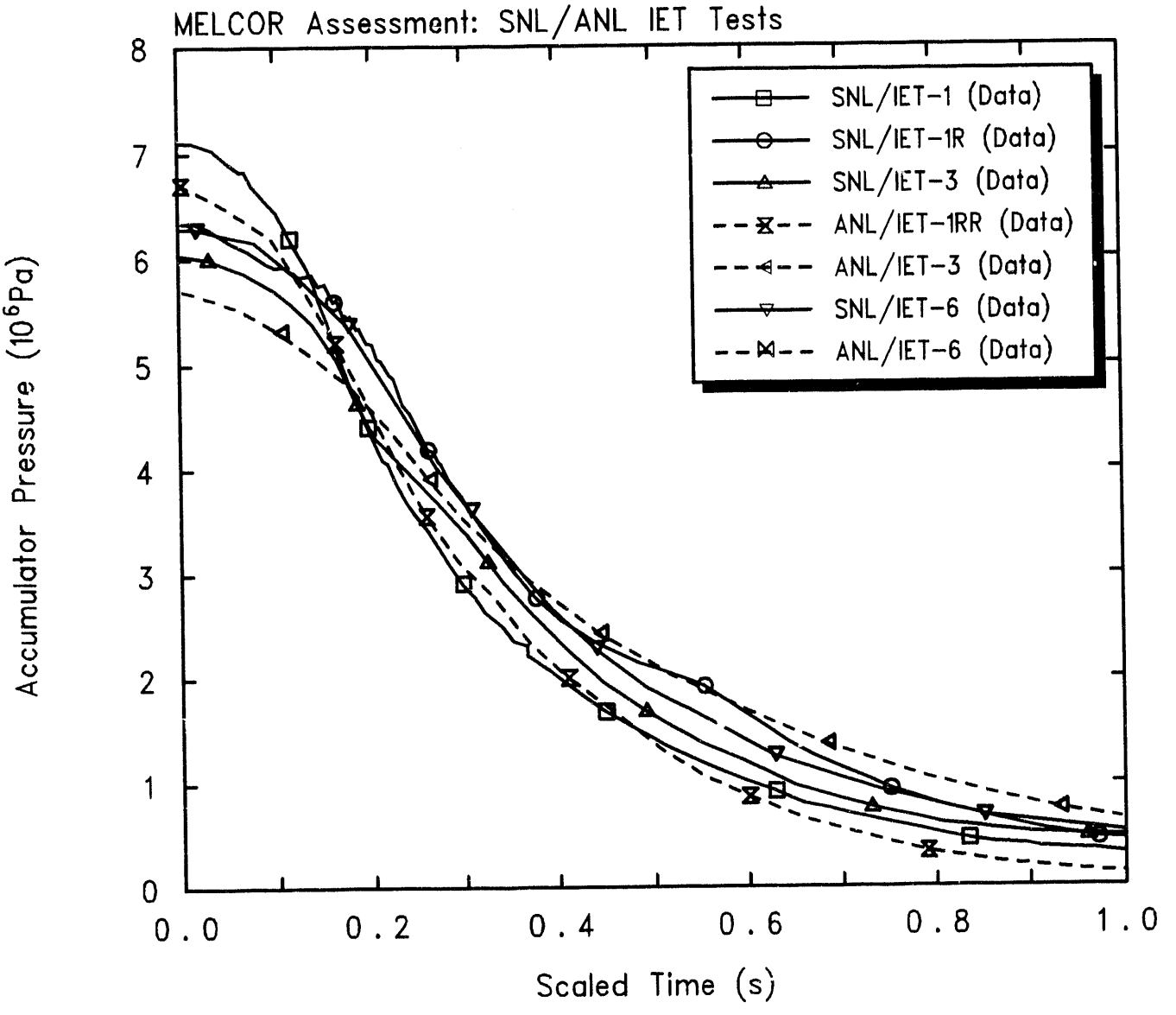

Figure 8.1.1. Scaled, Measured Steam Accumulator Pressures for SNL and ANL Counterpart IET Experiments - Scaling Study

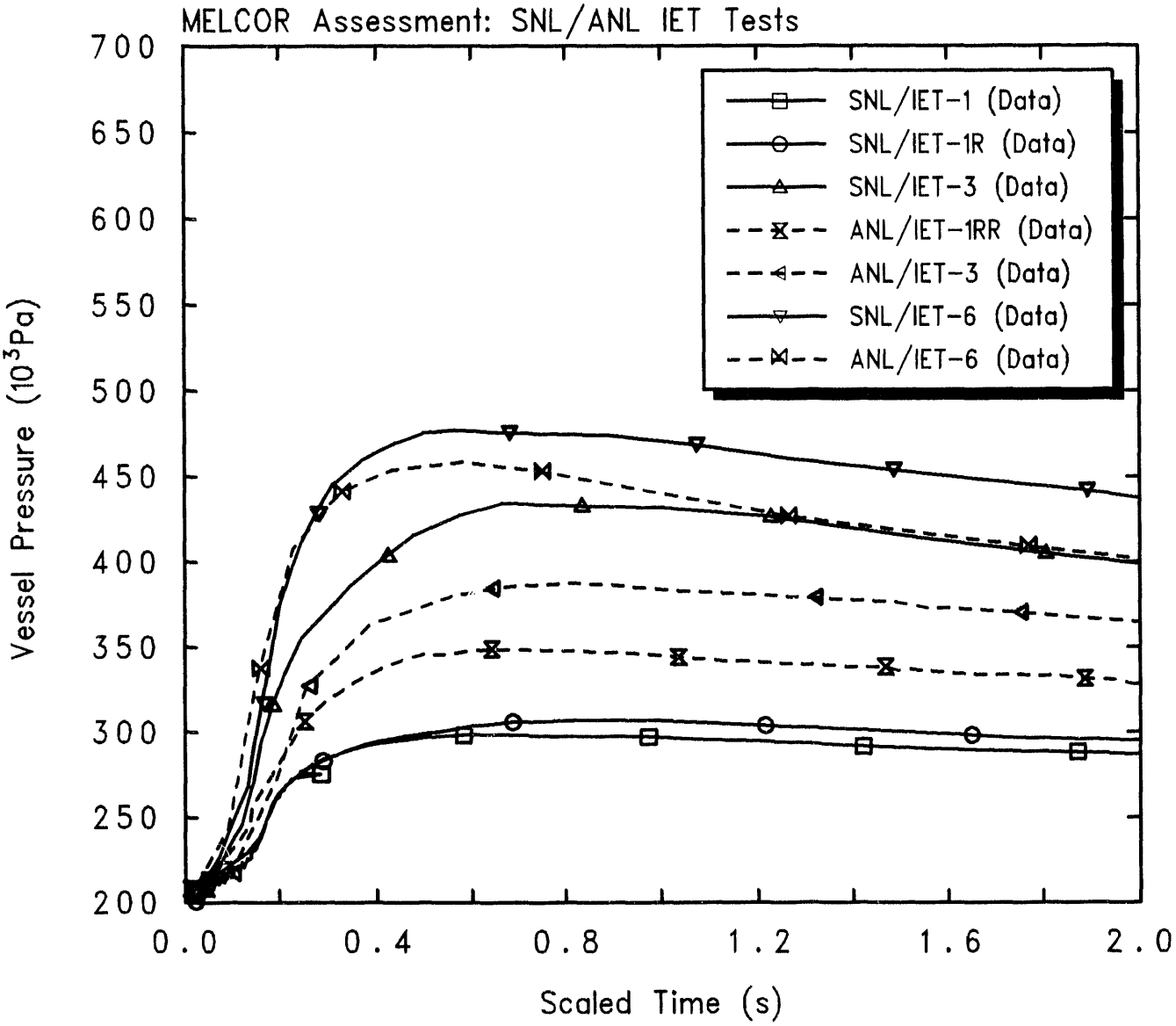

Figure 8.1.2. Scaled, Measured Vessel Pressures for SNL and ANL Counterpart IET Experiments - Scaling Study

while the results qualitatively scale, with more hydrogen production and combustion in the case with pre-existing hydrogen, there are a number of quantitative discrepancies. In particular, the hydrogen production in both ANL/IET-1RR and in ANL/IET-6 is 5% less than the corresponding scaled SNL/IET hydrogen production, but the hydrogen production in ANL/IET-3 is ~25% more than the corresponding scaled SNL/IET-3 hydrogen production. The small number of data points and the lack of a clear trend make it impossible to decide how much of the difference is due to scaling effects and how much simply to experimental uncertainties and test-to-test variations. Qualitatively, the data from the smaller-scale ANL facility shows slightly less variation in the amount of hydrogen produced in the various tests, and always has less hydrogen burned than produced (although there are very few data points), while the SNL data shows some pre-existing hydrogen must have burned in IET-6.

The hydrogen data somewhat contradict the vessel pressurization data given in Figure 8.1.2, because there was relatively more difference in pressurization between ANL/IET-3 and ANL/IET-6 than between SNL/IET-3 and SNL/IET-6, but with significantly less difference in both hydrogen production and combustion; this suggests the existence of differences in time scales for oxidation, combustion and heat transfer at the different size scales.

Our MELCOR assessment analyses for these 1:40-scale ANL/IET experiments were done in several steps, concentrating on the scaling of the phenomena. First, the ANL facility geometry and test conditions were modelled (and/or scaled) as discussed in Section 3.2, with no change in the characteristic interaction times input to the MELCOR FDI HPME model. Those characteristic interaction times were then scaled also, in another set of calculations. Finally, the other non-standard MELCOR input used for the Surtsey 1:10-scale SNL/IET experiment analyses (*i.e.*, hydrogen combustion parameters, volume flow areas and velocities used to determine heat transfer correlations, and recirculation from the dome to the subcompartments) were varied and the impact on calculated results evaluated.

8.2 Scaling Facility Geometry and Test Conditions

In the first set of calculations done, the ANL facility geometry and test conditions were modelled (and/or scaled) as discussed in Section 3.2, with no change in the characteristic interaction times input to the MELCOR FDI HPME model. Volumes and heights, and the blowdown flow area, were taken from the test data reports whenever possible; otherwise, the input values used for the SNL/IET analyses were simply adjusted as appropriate by the difference in scale factor between the two facilities. The debris amount and distribution were taken from the test data reports, as well as the initial steam and atmosphere conditions; the times in the steam blowdown valve opening and the debris injection timing were both scaled by 1/4 from the values used for our SNL/IET reference analyses.

Resulting predicted vessel pressures for the smaller-scale ANL tests are shown in Figure 8.2.1, together with the test data. The corresponding calculated results and

Table 8.1.2. Scaled, Measured Hydrogen Generation for SNL and ANL Counterpart IET Experiments – Scaling Study

Experiment	Hydrogen Produced (gm-moles)		
	SNL Data	ANL Data	SNL Data (Scaled to ANL)
IET-1	233		3.7
IET-1R	248		4.2
IET-1RR		4.0	
IET-3	227	4.65	3.7
IET-6	319	4.89	5.1

Table 8.1.3. Scaled, Measured Hydrogen Combustion for SNL and ANL Counterpart IET Experiments – Scaling Study

Experiment	Hydrogen Burned (gm-moles)		
	SNL Data	ANL Data	SNL Data (Scaled to ANL)
IET-1,1RR	3		0.04
IET-1R	11		0.2
IET-1RR		–	
IET-3	190	3.50	3.1
IET-6	345	4.22	5.6

test data for the larger-scale counterpart SNL experiments are also included for comparison, both with the time scaled by 1/4. The peak pressurization predicted in this case for ANL/IET-1RR is very similar (~100kPa) to that predicted for SNL/IET-1 and SNL/IET-1R, significantly less than the ~150kPa measured, and the rise time is relatively slower in the ANL/IET-1RR simulation than in the SNL/IET-1 and SNL/IET-1R calculations, while the data shows the same time dependence with this time scaling. In contrast, the peak pressurization predicted scaling only geometry for ANL/IET-3 and ANL/IET-6 is significantly higher (~300kPa) both than that measured (200-250kPa) and than that predicted and measured for SNL/IET-3 and SNL/IET-6 (~250kPa); however, the calculated pressure rise times again are relatively slower in the ANL/IET-3 and ANL/IET-6 simulations than in the corresponding SNL/IET calculations or the test data.

8.3 Scaling Characteristic Interaction Times

There is no reason to expect to match the ANL 1:40-scale test results only by scaling the Surtsey facility geometry and using the ANL test conditions. It seems intuitively obvious that the characteristic interaction time for airborne debris settling should be scaled as the height of the volume. Therefore, a set of ANL/IET calculations were done with the characteristic settling times for airborne debris reduced by 1/4 in each volume. However, it is not intuitively obvious whether the characteristic interaction times for oxidation of airborne or deposited debris, or for heat transfer from airborne debris to atmosphere, should be scaled or not. In more sets of calculations, we scaled the various characteristic interaction times also by 1/4, both individually and in combination, in addition to scaling the characteristic settling times.

Figure 8.3.1 gives predicted vessel pressures for the smaller-scale ANL tests, calculated using settling characteristic times reduced by the length scale factor, together with the test data and the corresponding time-scaled calculated results and test data for the larger-scale counterpart SNL experiments for comparison. The peak pressurization predicted in this case for all three ANL/IET experiment simulations is significantly less than either test data or the SNL/IET calculated results, and (as in the case shown in Figure 8.2.1) the calculated pressure rise times again are relatively slower in all three ANL/IET simulations than in the corresponding SNL/IET calculations or the test data.

These results indicate that the other characteristic interaction times (for oxidation of airborne or deposited debris, and for heat transfer from airborne debris to atmosphere) probably should be scaled also, because these results indicate that more rapid oxidation energy release and transfer to atmosphere is required to match the ANL test data. Further calculations were done with the airborne-debris oxidation and heat transfer characteristic times individually scaled by 1/4 (with the settling characteristic time also scaled), and with all the characteristic times scaled.

Vessel pressures for the smaller-scale ANL tests predicted using both oxidation and settling characteristic times reduced by the length scale factor, are depicted in Figure 8.3.2, again with the test data and the corresponding time-scaled calculated results

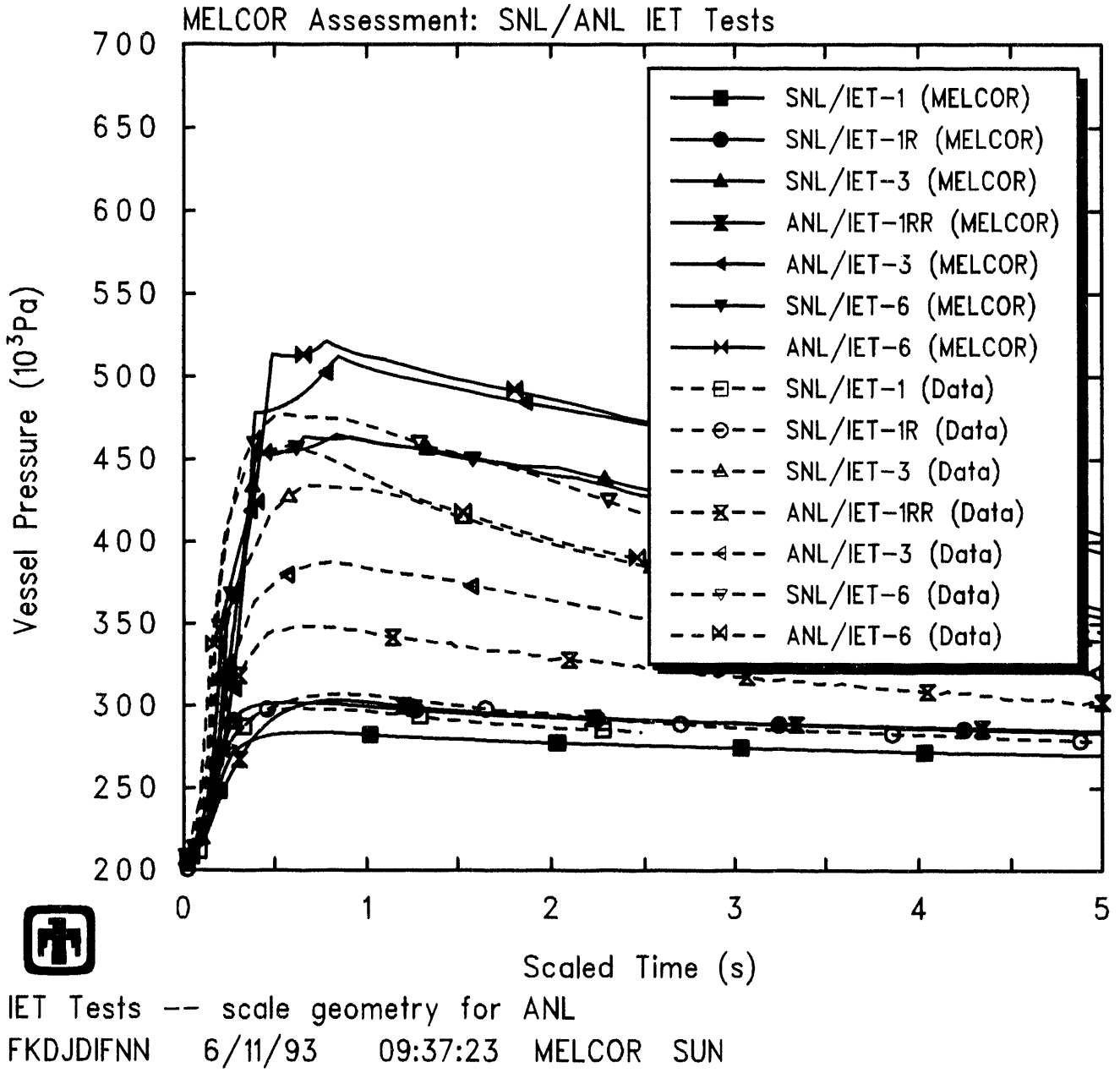

Figure 8.2.1. Scaled Vessel Pressures for SNL and ANL Counterpart IET Experiments – Scaling Facility Geometry and Test Conditions

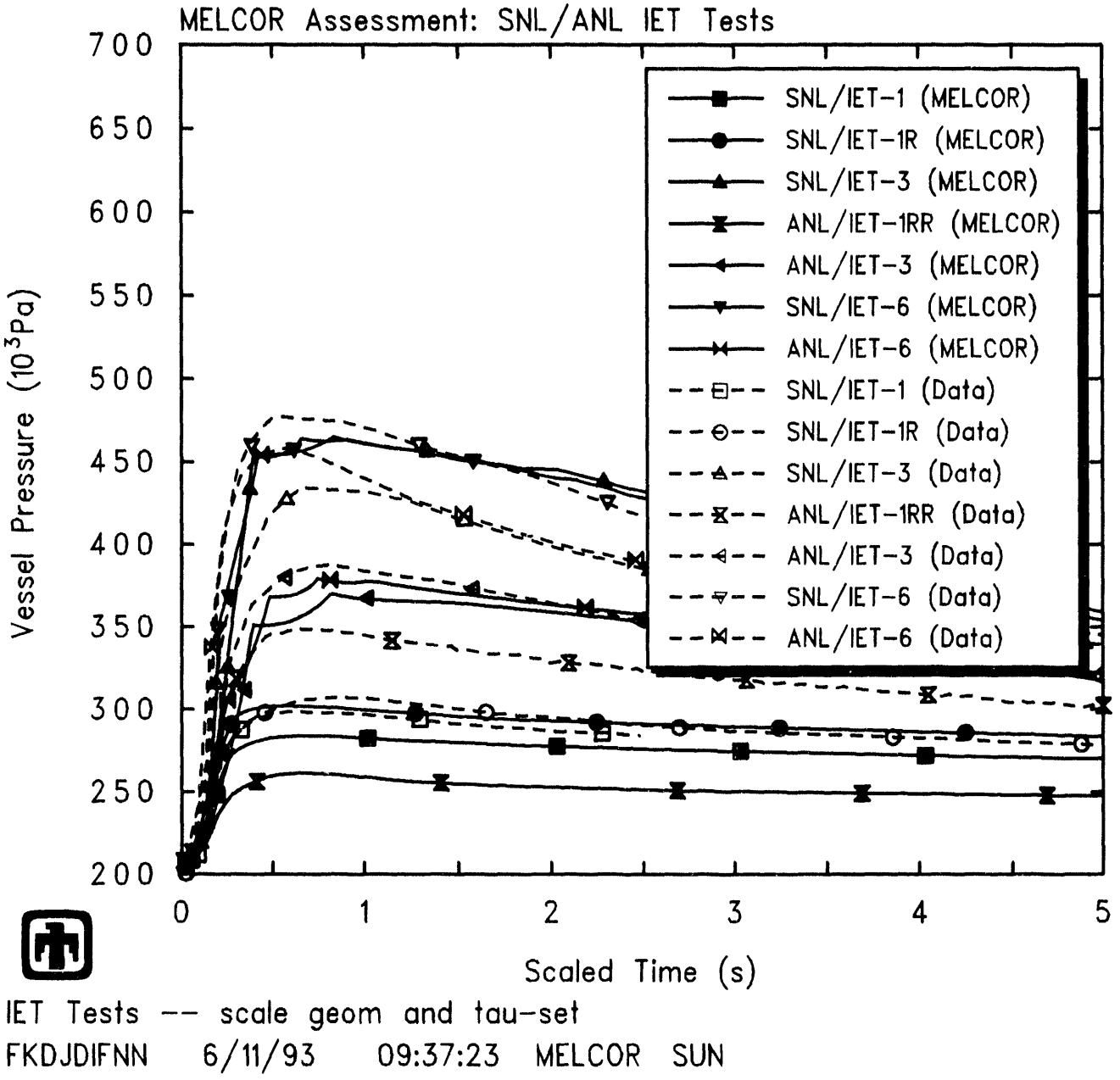

Figure 8.3.1. Scaled Vessel Pressures for SNL and ANL Counterpart IET Experiments – Scaling Airborne-Debris Settling Characteristic Interaction Times

and test data for the larger-scale counterpart SNL experiments for comparison. There is no change in peak pressurization predicted in this case for ANL/IET-1RR and only a small increase in peak pressurization predicted for ANL/IET-3 and ANl/IET-6, compared to the results obtained using only a scaled settling characteristic time (Figure 8.3.1).

Figure 8.3.3 gives predicted vessel pressures for the smaller-scale ANL tests, calculated using both airborne-debris heat transfer and settling characteristic times reduced by the length scale factor, with the test data and the corresponding time-scaled calculated results and test data for the larger-scale counterpart SNL experiments included for comparison. The peak pressurization predicted in this case for all three ANL/IET experiment simulations is significantly higher than for the cases illustrated in Figure 8.3.1, and is in good agreement with the peak pressurization calculated for the counterpart SNL tests; the rise time in this case for all three ANL/IET experiment simulations also is in very good agreement with corresponding results calculated for the counterpart SNL tests. Because of the differences in the experimental behavior discussed in Section 8.1, although the results for the ANL/IET experiment simulations now agree quite well with the scaled SNL/IET results, the predicted peak pressure for ANL/IET-1RR (~100kPa) is still significantly less than that measured (~150kPa), while the predicted peak pressure for ANL/IET-3 (~250kPa) is significantly higher than that measured (~200kPa).

Vessel pressures for the smaller-scale ANL tests predicted using all characteristic times (for airborne- and deposited-debris oxidation, and airborne-debris settling and heat transfer to atmosphere) reduced by the length scale factor are shown in Figure 8.3.4, again with the test data and the corresponding time-scaled calculated results and test data for the larger-scale counterpart SNL experiments for comparison. There is no change in peak pressurization predicted in this case for ANL/IET-1RR and only a small increase in peak pressurization predicted for ANL/IET-3 and ANl/IET-6, compared to the results obtained using only scaled heat transfer and settling characteristic times (Figure 8.3.3), very similar to the small difference found between results obtained using only scaled settling characteristic times (Figure 8.3.1) and using scaled oxidation and settling characteristic times (Figure 8.3.2), verifying that the vessel pressurization results are much more sensitive to the settling and heat transfer characteristic interaction times than to either the airborne- or deposited-debris oxidation characteristic interaction times.

Tables 8.3.1 and 8.3.2 compare the amounts of hydrogen generated and burned, respectively, in the ANL small-scale test simulations for all the scaling cases considered so far. There are a number of disagreements between calculation and data, both qualitative and quantitative, in all cases. The small number of data points and the uncertainty associated with the methods of estimating hydrogen production and combustion from late-time gas grab bottle samples, however, preclude any definitive judgements on the significance of the differences seen.

The test data shows more hydrogen production in ANL/IET-3 than in ANL/IET-1RR, and more hydrogen production in ANL/IET-6 than in ANL/IET-3; the calculations consistently show more hydrogen production in ANL/IET-1RR than in ANL/IET-3 or ANL/IET-6. The same trend can be found in the MELCOR simulations of the larger-scale SNL tests: the test data indicate more hydrogen production in SNL/IET-4 through

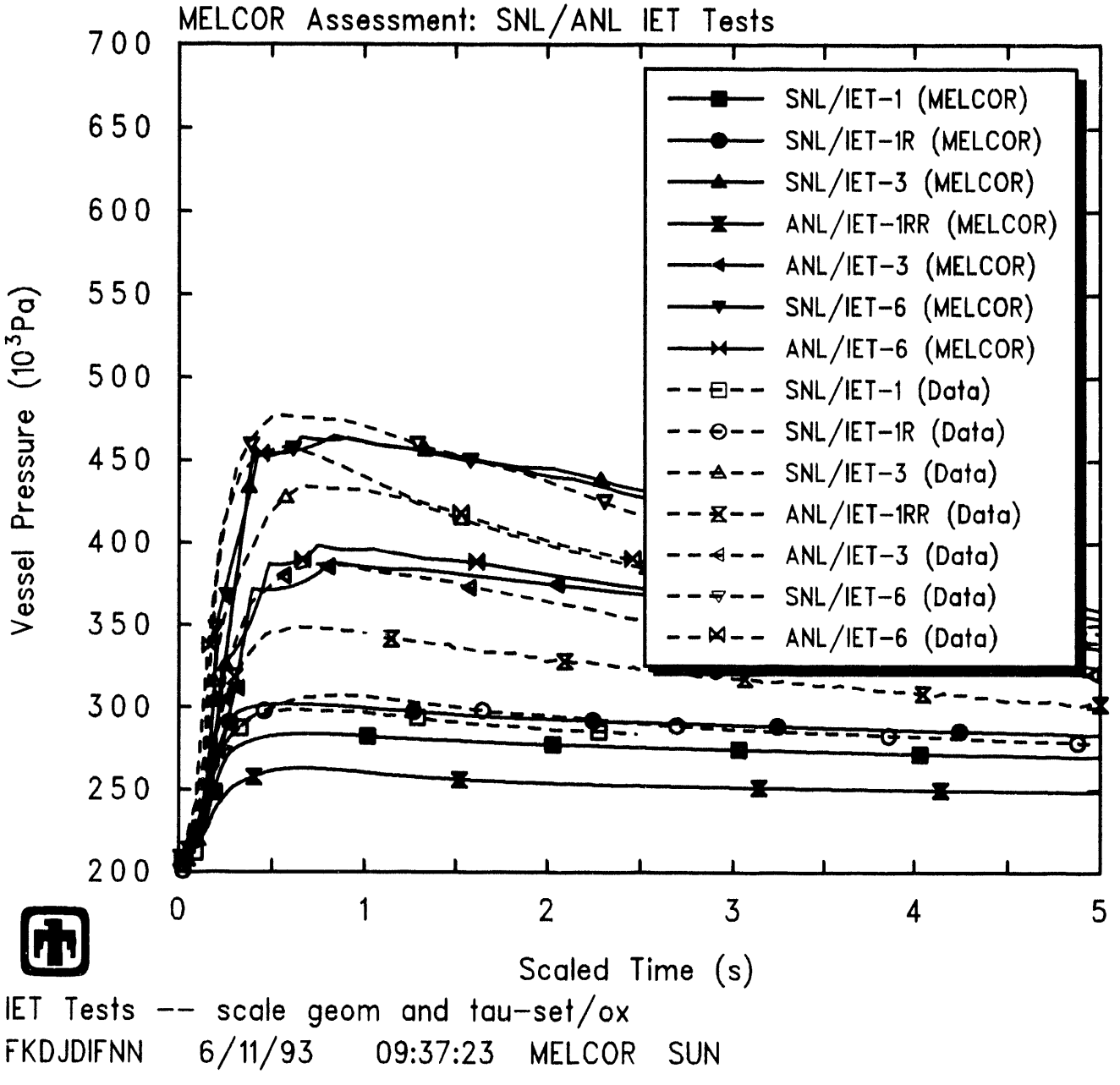

Figure 8.3.2. Scaled Vessel Pressures for SNL and ANL Counterpart IET Experiments – Scaling Airborne-Debris Oxidation and Settling Characteristic Interaction Times

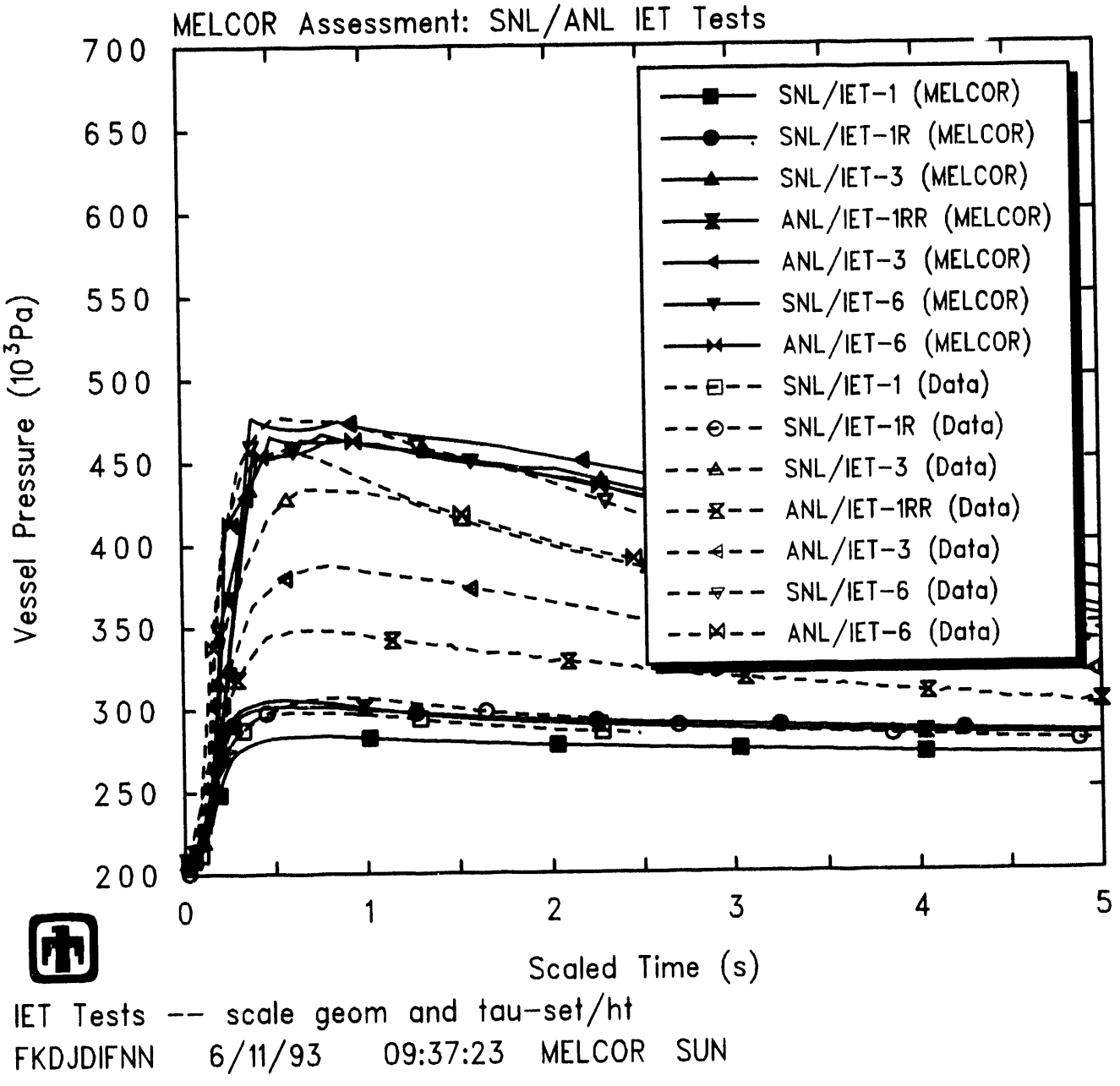

Figure 8.3.3. Scaled Vessel Pressures for SNL and ANL Counterpart IET Experiments - Scaling Airborne-Debris Heat Transfer and Settling Characteristic Interaction Times

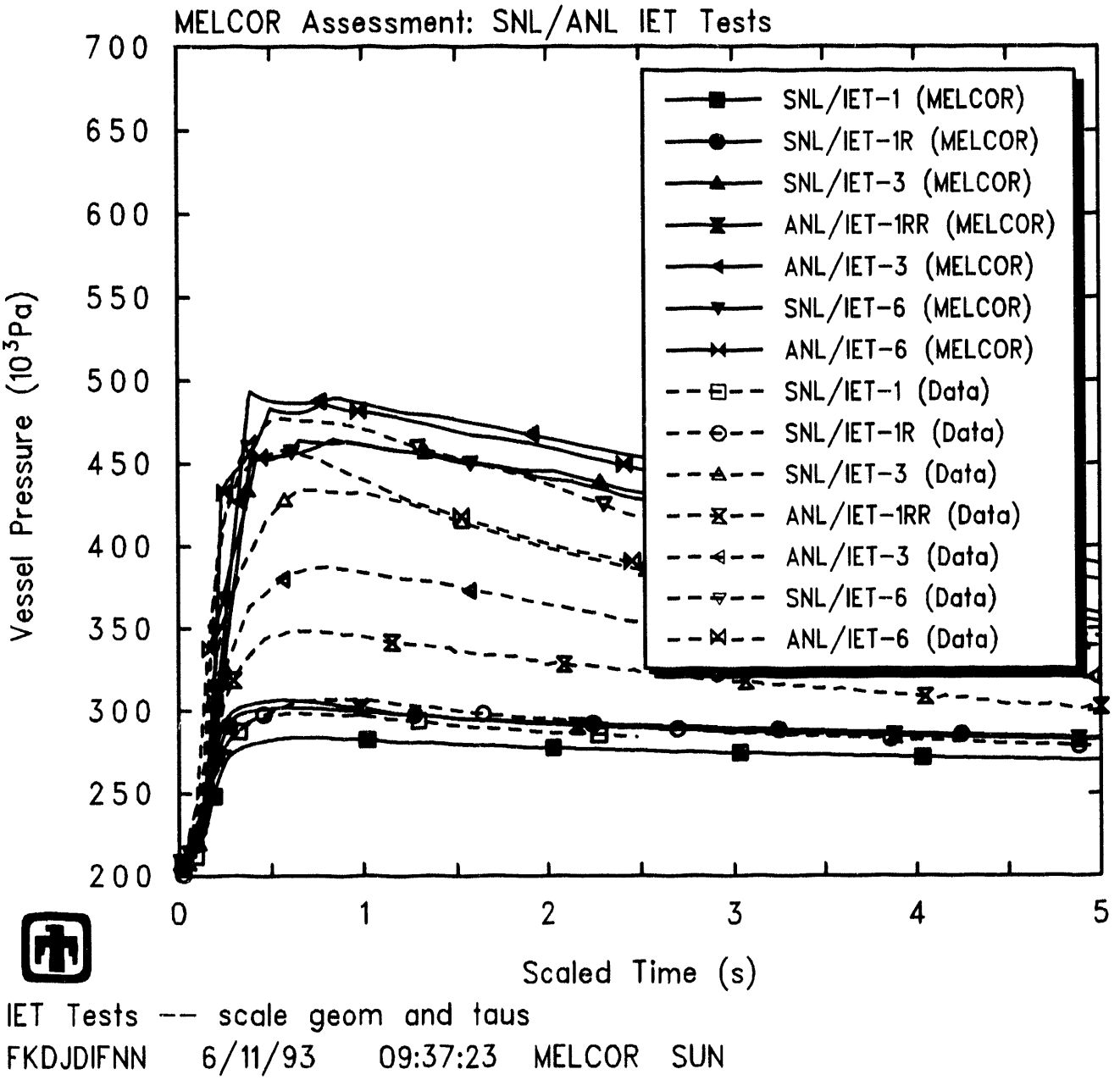

Figure 8.3.4. Scaled Vessel Pressures for SNL and ANL Counterpart IET Experiments Scaling All Characteristic Interaction Times

Table 8.3.1. Hydrogen Generation for the ANL/IET Experiments – Scaling Facility Geometry and Test Conditions, and Characteristic Interaction Times

Experiment	Hydrogen Produced (gm-moles)					
	Data†	MELCOR‡				
			scaled geom and			
			τ_{SET}	τ_{SET}/τ_{OX}	τ_{SET}/τ_{HT}	all τs
IET-1RR	4.0	6.43/6.30	4.59/4.52	4.57/4.51	6.00/5.88	6.55/6.33
IET-3	4.65	5.63/7.53	3.35/5.05	3.49/5.69	4.81/6.24	5.00/7.04
IET-6	4.89	5.39/7.16	3.30/5.08	3.55/5.59	4.47/6.01	5.01/6.90

†from gas grab bottle samples at 30min
‡(actual values at 20s)/ (assuming only steam/metal reactions)

Table 8.3.2. Hydrogen Combustion for the ANL/IET Experiments – Scaling Facility Geometry and Test Conditions, and Characteristic Interaction Times

Experiment	Hydrogen Burned (gm-moles)					
	Data†	MELCOR‡				
			scaled geom and			
			τ_{SET}	τ_{SET}/τ_{OX}	τ_{SET}/τ_{HT}	all τs
IET-1RR		0/0.26	0/0.26	0/0.26	0/0.26	0/0.26
IET-3	3.50	4.50/6.52	2.14/3.96	2.32/4.63	3.72/5.26	3.84/6.02
IET-6	4.22	4.39/6.24	2.09/3.97	2.30/4.43	3.33/4.96	3.61/5.63

†from gas grab bottle samples at 30min
‡(actual values at 20s)/ (assuming only steam/metal reactions)

SNL/IET-7 than in SNL/IET-1 and SNL/IET-1R, while the calculations consistently show more hydrogen production in SNL/IET-1 and SNL/IET-1R than in the later tests. (The difference is not simply due to hydrogen combustion differences, because the comparisons for SNL/IET-3 and SNL/IET-5 do not fit such a simple trend.) Also, the test data show more hydrogen burned in ANL/IET-6 than in ANL/IET-3, while the calculations consistently show the opposite, although the difference is quite small, and could be due to slow, late-time combustion of hydrogen; similar comparisons for the larger-scale SNL tests and analyses show a similar trend comparing SNL/IET-3 and SNL/IET-6, but not when comparing SNL/IET-4 and SNL/IET-7 (also a pair without and with pre-existing hydrogen, but with the addition of basement condensate water). Scaling cases which predicted peak vessel pressures in reasonable agreement with test data predicted more hydrogen production than measured, especially for ANL/IET-1RR, while scaling cases that predicted peak vessel pressures significantly lower than observed data predicted about the right amount of hydrogen production.

Note that these results tend to confirm the experimental observation that DCH energy-transfer efficiency is greater at smaller scale (because we include the effects of the relatively larger steam blowdown source and melt mass in ANL/IET-1RR compared to SNL/IET-1 and SNL/IET-1R), and that there is less pressurization due to hydrogen combustion at smaller scale.

8.4 Varying Hydrogen Combustion Parameters

As described in Sections 3.1 and 7.1, in the majority of our SNL/IET analysis calculations, the burn package was activated. However, burns were suppressed in all control volumes except the vessel dome; this was based upon the experimental observation that a jet of hydrogen produced by steam blowdown and debris oxidation burned as it vented from the subcompartments to the upper dome. The default ignition criterion in the absence of igniters was set to a hydrogen mole fraction of 0.0, but the combustion completeness was also set to 0.0; this prevents the burning of any pre-existing hydrogen, but allows burning of any additional hydrogen generated during the HPME. This was based upon the experimental observation that the pre-existing hydrogen that burned did not burn on a time scale that had a significant impact on the peak pressure. This particular combination of input was found to produce reasonable agreement with test data in all the 1:10-scale SNL/IET experiments analyzed, as discussed in Section 7.1 which presented results of sensitivity studies using other possible burn-package input settings.

The results of both our own, limited review of the facility and data scalability (Section 8.1) and of our ANL test simulations scaling facility geometry (Section 8.2) and characteristic interaction times (Section 8.3) indicate that the pressurization due to hydrogen combustion is significantly less in the smaller-scale ANL facility than in the larger-scale SNL tests (especially given the apparent greater pressurization due to DCH at smaller scale), and that there appears to be a greater effect of pre-existing hydrogen in the ANL 1:40-scale tests than in the counterpart SNL 1:10-scale tests.

There are several possible contributors to the different hydrogen combustion behavior at smaller scales. It is harder to keep hydrogen jets burning at smaller scales because the "same" combustion energy release rate needs to heat up non-burning diluent gas entrained into the jet more quickly at smaller scales, because of more rapid mixing and dilution. Also, in this particular case, the different aspect ratios in the two facilities ($\sim$5 for the ANL vessel and $\sim$3 for the SNL vessel) may provide relatively less oxygen in the immediate neighborhood of the jet in the taller, thinner ANL vessel.

There is no input mechanism to model these factors in the burn package in MELCOR. Sensitivity studies were done in which the hydrogen mole fraction limit for ignition was increased from 0.0 to 0.01, 0.02, 0.03, 0.04 and 0.05 in the ANL experiment analyses (with the default value in the absence and presence of igniters being 0.10 and 0.07, respectively).

Vessel pressures for the smaller-scale ANL tests predicted using some of these higher hydrogen-mole-fraction ignition criteria are shown in Figure 8.4.1, again with the test data and the time-scaled calculated results and test data for the larger-scale counterpart SNL experiments for comparison. (In these calculations, the characteristic interaction times also were scaled by the length factor, so these results should be compared to those presented in Figure 8.3.4 using a 0.0 hydrogen mole fraction ignition limit to evaluate the effects of using different hydrogen ignition limits and therefore different amounts of hydrogen combustion.) The results indicate that, as expected, reducing the amount of hydrogen combustion does reduce the vessel pressurization predicted in ANL/IET-3 and ANL/IET-6. Note that different degrees of reduction are required to match the experimental data for ANL/IET-3 and ANL/IET-6.

Tables 8.4.1 and 8.4.2 compare the amounts of hydrogen generated and burned, respectively, in the ANL small-scale test simulations for all the hydrogen-combustion ignition-limit variations considered so far. As expected, changing the hydrogen mole fraction combustion ignition limit has no effect on hydrogen production through oxidation of debris, but the hydrogen combustion predicted drops off as the hydrogen mole fraction combustion ignition limit is increased. Note that values which give good agreement on peak vessel pressurization seem to give too little hydrogen burn, but this may be due to gradual, late-time hydrogen combustion in the experiment, which is not modelled in these analyses.

No additional work was done attempting to increase the late-time burn and/or the burn of pre-existing hydrogen.

8.5 Varying Convective Heat Transfer

In our first set of calculations done for the smaller-scale ANL tests, the facility geometry (if not explicitly specified in the test data reports) was simply adjusted as appropriate by the difference in scale factor between the two facilities (*i.e.*, 1/4 for heights or lengths, 1/16 for flow areas or surface areas). The volume flow areas, which had been reduced to obtain volume velocities more characteristic of the turbulent conditions that might

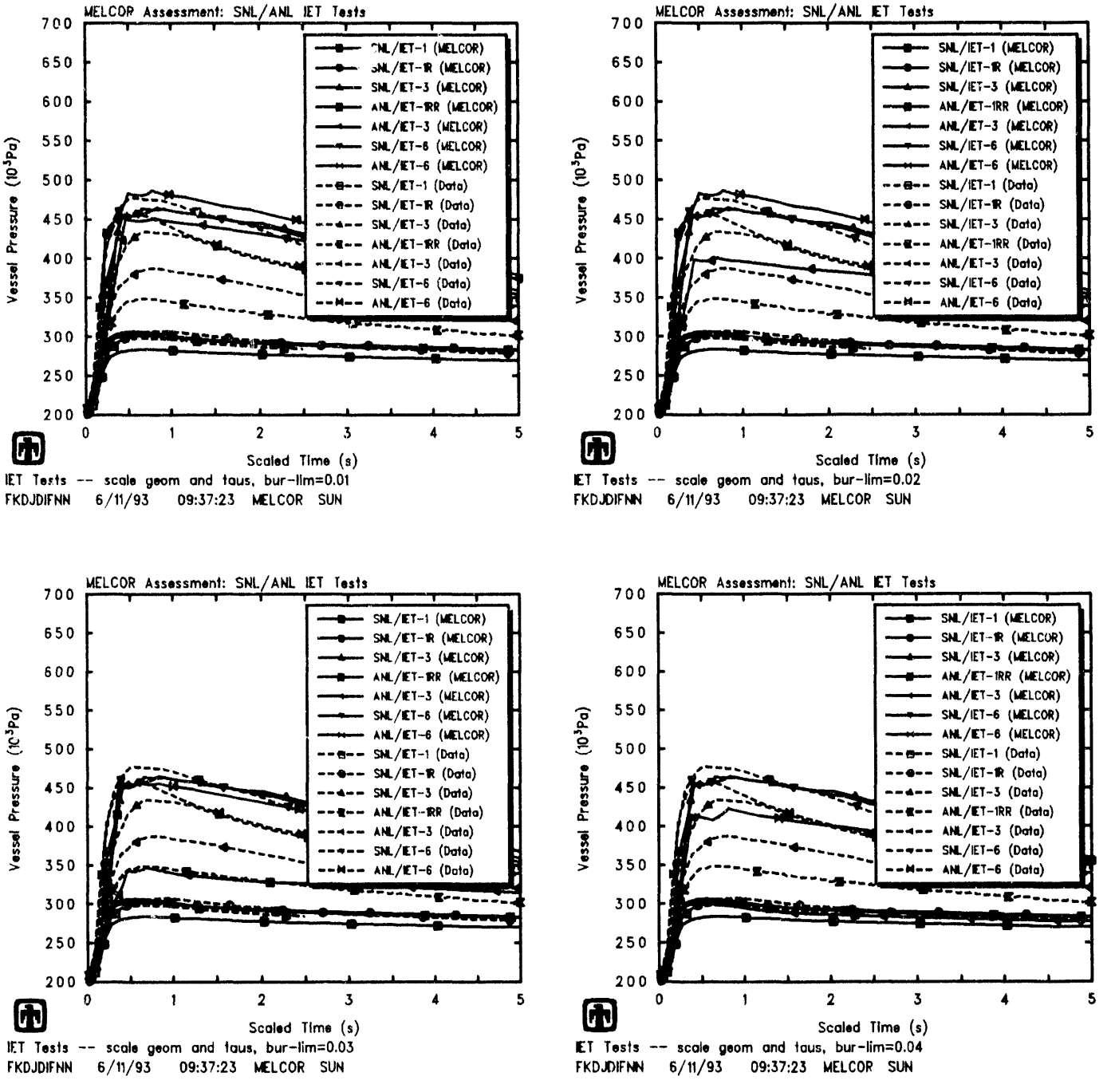

Figure 8.4.1. Scaled Vessel Pressures for SNL and ANL Counterpart IET Experiments Using Hydrogen Mole Fraction Ignition Limits of 0.01 (upper left), 0.02 (upper right), 0.03 (lower left) and 0.04 (lower right) for the ANL Experiment Simulations Varying Hydrogen Combustion Parameters

Table 8.4.1. Hydrogen Generation for the ANL/IET Experiments – Varying Hydrogen Combustion Parameters

Experiment	Hydrogen Produced (gm-moles)						
	Data†	MELCOR‡ ignition x_{H_2}=					
		0.0	0.01	0.02	0.03	0.04	0.05
IET-1RR	4.0	6.55/6.33	6.55/6.33	6.55/6.33	6.55/6.33	6.55/6.33	6.55/6.33
IET-3	4.65	5.00/7.09	5.00/7.09	5.00/7.09	5.00/7.09	5.00/7.09	5.00/7.09
IET-6	4.89	5.01/6.95	5.01/6.95	5.01/6.95	5.01/6.95	5.01/6.95	5.01/6.95

†from gas grab bottle samples at 30min
‡(actual values at 20s)/ (assuming only steam/metal reactions)

Table 8.4.2. Hydrogen Combustion for the ANL/IET Experiments – Varying Hydrogen Combustion Parameters

Experiment	Hydrogen Produced (gm-moles)						
	Data†	MELCOR‡ ignition x_{H_2}=					
		0.0	0.01	0.02	0.03	0.04	0.05
IET-1RR	–	0/0.26	0/0.26	0/0.26	0/0.26	0/0.26	0/0.26
IET-3	3.50	3.84/6.02	2.92/5.12	1.95/4.25	0.85/3.21	0/2.39	0/2.39
IET-6	4.22	3.61/5.63	3.61/5.63	3.61/5.63	2.78/4.87	2.01/4.12	1.98/4.10

†from gas grab bottle samples at 30min
‡(actual values at 20s)/ (assuming only steam/metal reactions)

be expected during HPME, and the associated turbulent heat transfer to structures (as discussed in Sections 3.1 and 7.2), also were scaled by 1/16 from the input values used for the 1:10-scale SNL test analyses.

The results for the ANL/IET-1RR test simulations using those area-scaled volume flow areas (given in Sections 8.2 and 8.4) had too little vessel pressurization calculated due to direct containment heating, one possible contributor to which could be too much heat transfer to structures. A set of calculations was done assuming the convective turbulent heat transfer coefficient scaled with length (*i.e.*, with boundary layer thickness) rather than with area, so that the user-input volume flow areas for the 1:40-scale ANL experiment simulations were scaled by 1/4 from the input values used for the 1:10-scale SNL test analyses.

Figure 8.5.1 gives predicted vessel pressures for the smaller-scale ANL tests, calculated using volume flow areas scaled by the 1/4 length factor rather than by the 1/16 area factor, together with the test data and the corresponding time-scaled calculated results and test data for the larger-scale counterpart SNL experiments for comparison. (In these calculations, the characteristic interaction times also were scaled by the length factor, so these results should be compared to those presented in Figure 8.3.4 to evaluate the effects of using different volume flow areas, velocities and convective heat transfer coefficients.) The peak pressurization predicted in this case for all three ANL/IET experiment simulations is significantly greater than either test data or the SNL/IET calculated results. These results, which together with those in Figure 8.3.4 bound the ANL/IET-1RR data, suggest that some of the "missing" extra pressurization due to DCH at small scale (*i.e.*, in ANL/IET-1RR) may be due to differences in heat transfer to structures at smaller and at larger scale.

8.6 Varying Recirculation Flow

The input model in our 1:10-scale SNL/IET test analyses provided flow paths for straight flowthrough from the steam accumulator to the cavity and chute through the (lumped-together) subcompartments to the vessel dome, and also for recirculation from the upper dome to the subcompartments. The area of the recirculation flow path was set to 10% of the area of the straight-through flow path from the subcompartments to the dome, based upon the results of sensitivity studies (as discussed in Sections 3.1 and 7.3). In our first set of calculations done for the smaller-scale ANL tests, the corresponding recirculation flow path area (as all other flow path areas except the steam blowdown valve area) was simply adjusted by the difference in scale factor between the two facilities, *i.e.*, 1/16 for flow areas. There is no reason to believe that the recirculation pattern is identical in the two facilities, especially given the difference in aspect ratio in the two facilities ($\sim$5 for the ANL vessel and $\sim$3 for the SNL vessel). Therefore, sensitivity studies were done for the ANL test simulations with that recirculation flow path area increased and decreased by a factor of 10.

Vessel pressures for the smaller-scale ANL tests predicted assuming both reduced and increased recirculation flows are depicted in Figure 8.6.1, again with the test data

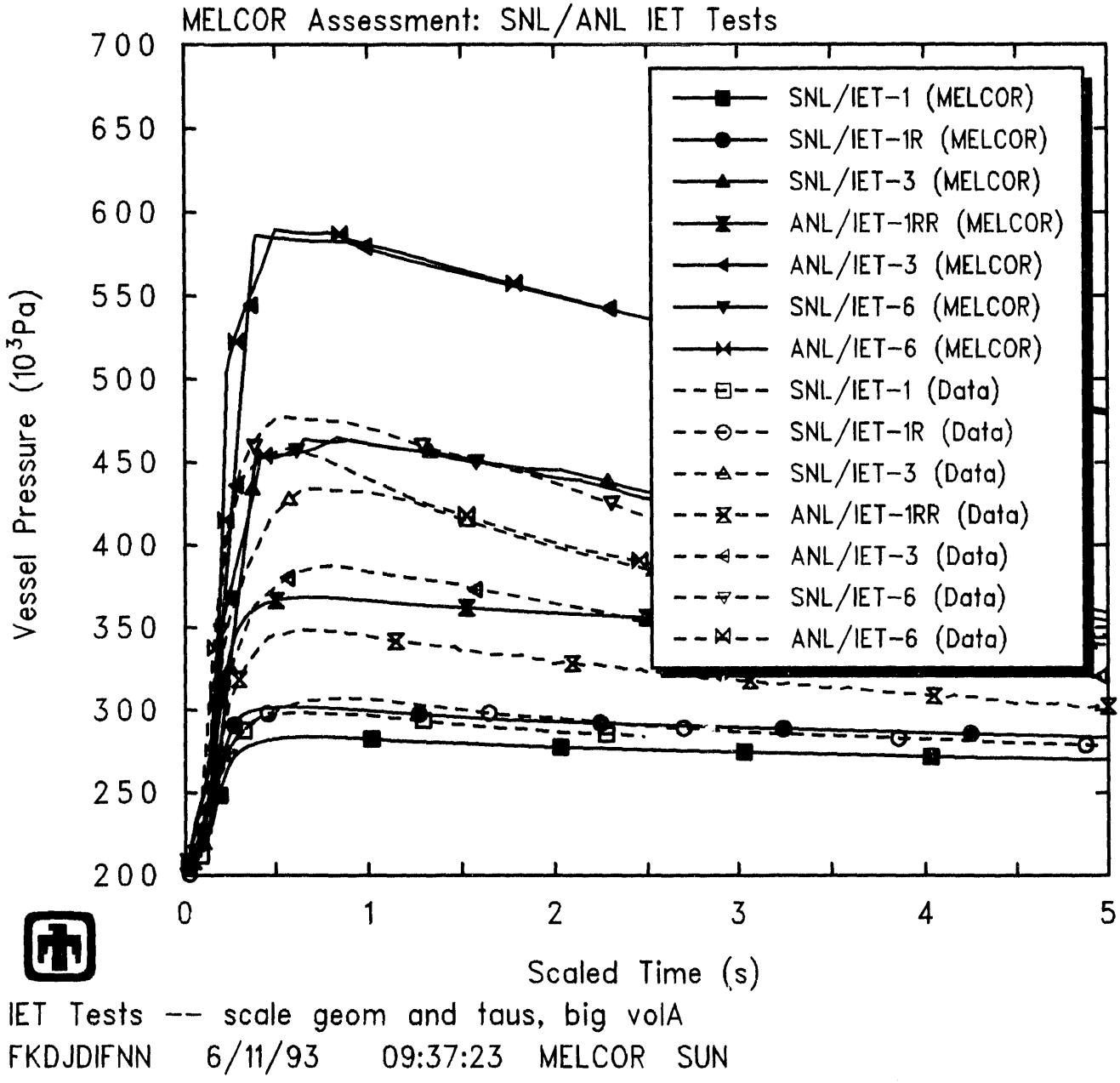

Figure 8.5.1. Scaled Vessel Pressures for SNL and ANL Counterpart IET Experiments – Varying Convective Heat Transfer

and the corresponding time-scaled calculated results and test data for the larger-scale counterpart SNL experiments for comparison. (In these calculations, the characteristic interaction times also were scaled by the length factor, so these results should be compared to those presented in Figure 8.3.4 to evaluate the effects of assuming different recirculation flow areas.) There is little change in peak pressurization predicted in this case for all three ANL/IET experiment simulations, but there is a substantial change in the subsequent dropoff rate, with more rapid depressurization calculated with more recirculation assumed. While a recirculation flow area equal to the original flow area from the subcompartments to the dome is obviously too big, the pressure dropoff rate in the ANL data clearly would be matched better by assuming a recirculation flow area greater than the 10% assumed in the SNL experiment analyses.

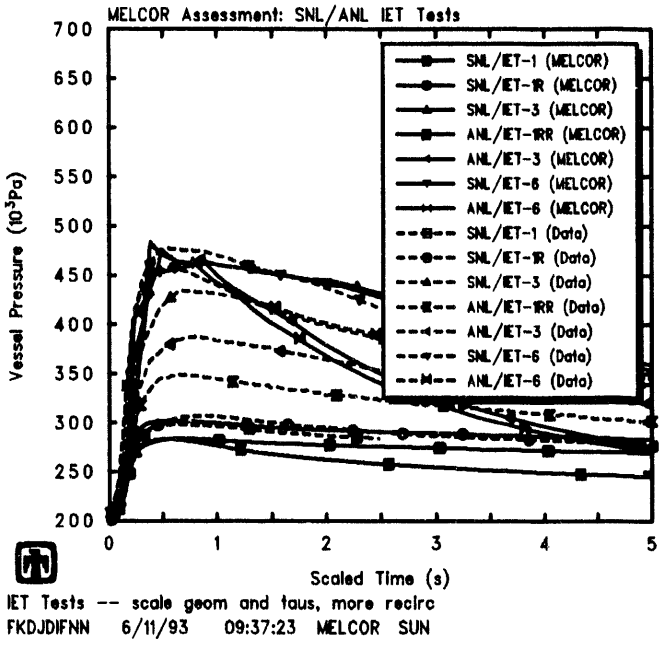

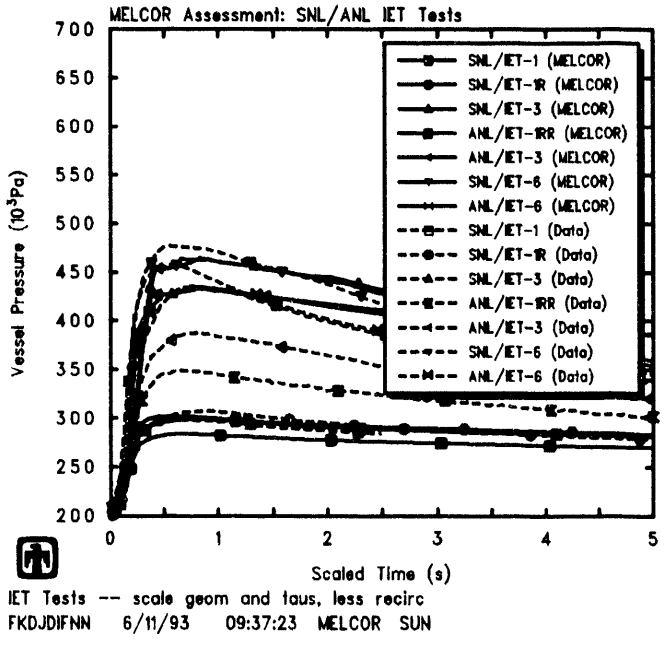

Figure 8.6.1. Scaled Vessel Pressures for SNL and ANL Counterpart IET Experiments – Increasing (top) and Reducing (bottom) Recirculation Flow

9 Time Step Effects and Machine Dependency

There has been a lot of discussion recently on numeric effects seen in various MELCOR calculations [37], producing either differences in results for the same input on different machines or differences in results when the time step used is varied. Several calculations have been done to identify whether any such effects existed in our DCH IET assessment analyses.

9.1 Machine Dependencies

The calculations discussed in detail in Section 4, and the majority of our sensitivity study analyses, were run on a SUN Sparc2 workstation. The Surtsey SNL/IET reference calculations were rerun, using the same code version (1.8NN), on an IBM RISC-6000 Model 550 workstation, on an HP 755 workstation, on a CRAY Y-MP8/864, and on a 50MHz 486 PC.

The predicted vessel pressures for the SUN, IBM and HP workstation, and Cray and PC, calculation sets are presented in Figures 9.1.1 and 9.1.2 for the tests without and with hydrogen combustion, respectively. Tables 9.1.1 and 9.1.2 compare the amounts of hydrogen generated and burned, respectively, in these equivalent calculations performed on the various platforms. (Experimental data are included for reference.)

There is generally excellent agreement among results generated on these various hardware platforms. The biggest difference seen is in the vessel pressurization predicted for SNL/IET-1R on the SUN Sparc2 workstation (which will be seen in the next subsection to be related to time-step effects); That difference is still relatively small, with no qualitative change in behavior predicted, and there is no corresponding visible difference in amount of hydrogen generated.

Figure 9.1.3 presents run times and time step histories for calculations on the various platforms for the SNL/IET-1 and SNL/IET-6 experiment simulations, as typical results. The three cases with no hydrogen combustion (SNL/IET-1, SNL/IET-1R and SNL/IET-5) always show the time step rising relatively smoothly to the user-defined maximum allowed value; the four cases with hydrogen combustion (SNL/IET-3, SNL/IET-4, SNL/IET-6 and SNL/IET-7) always show "sawtooth" time step histories correlated to beginnings and ends of deflagrations. The SUN and PC are always slowest in run time required; the IBM, HP and Cray are all significantly faster with the HP the fastest for these analyses.

9.2 Time Step Effects

Otherwise identical MELCOR Surtsey SNL/IET calculations were run on a SUN Sparc2 workstation with the user-input maximum allowed time step progressively set to 1s, 0.5s, 0.1s, 0.05s and 0.01s; simultaneously, the initial time step size for HPME

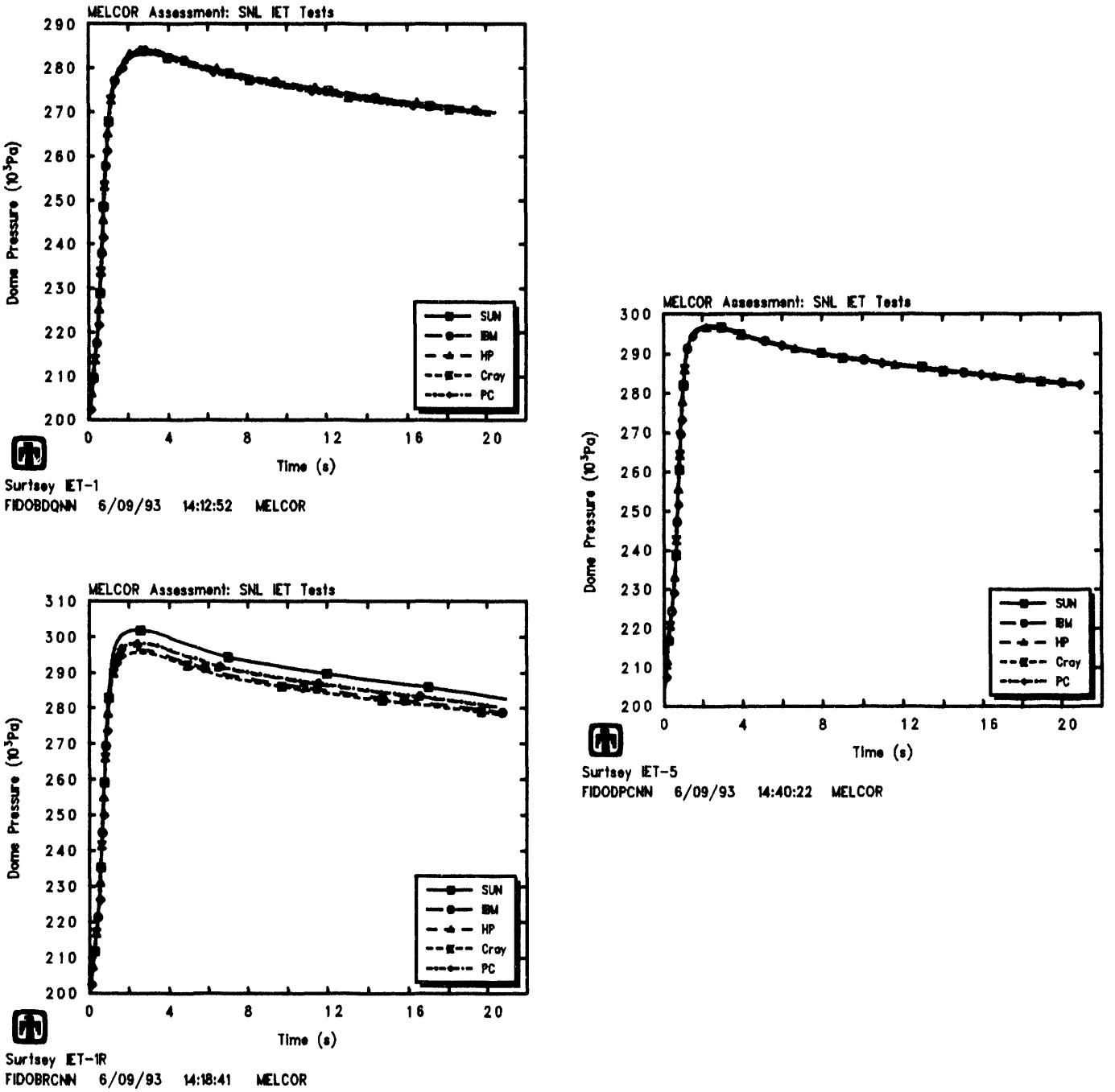

Figure 9.1.1. Vessel Pressures for Experiments SNL/IET-1 (upper left), SNL/IET-1R (lower left) and SNL/IET-5 (middle right) Machine Dependency Sensitivity Study

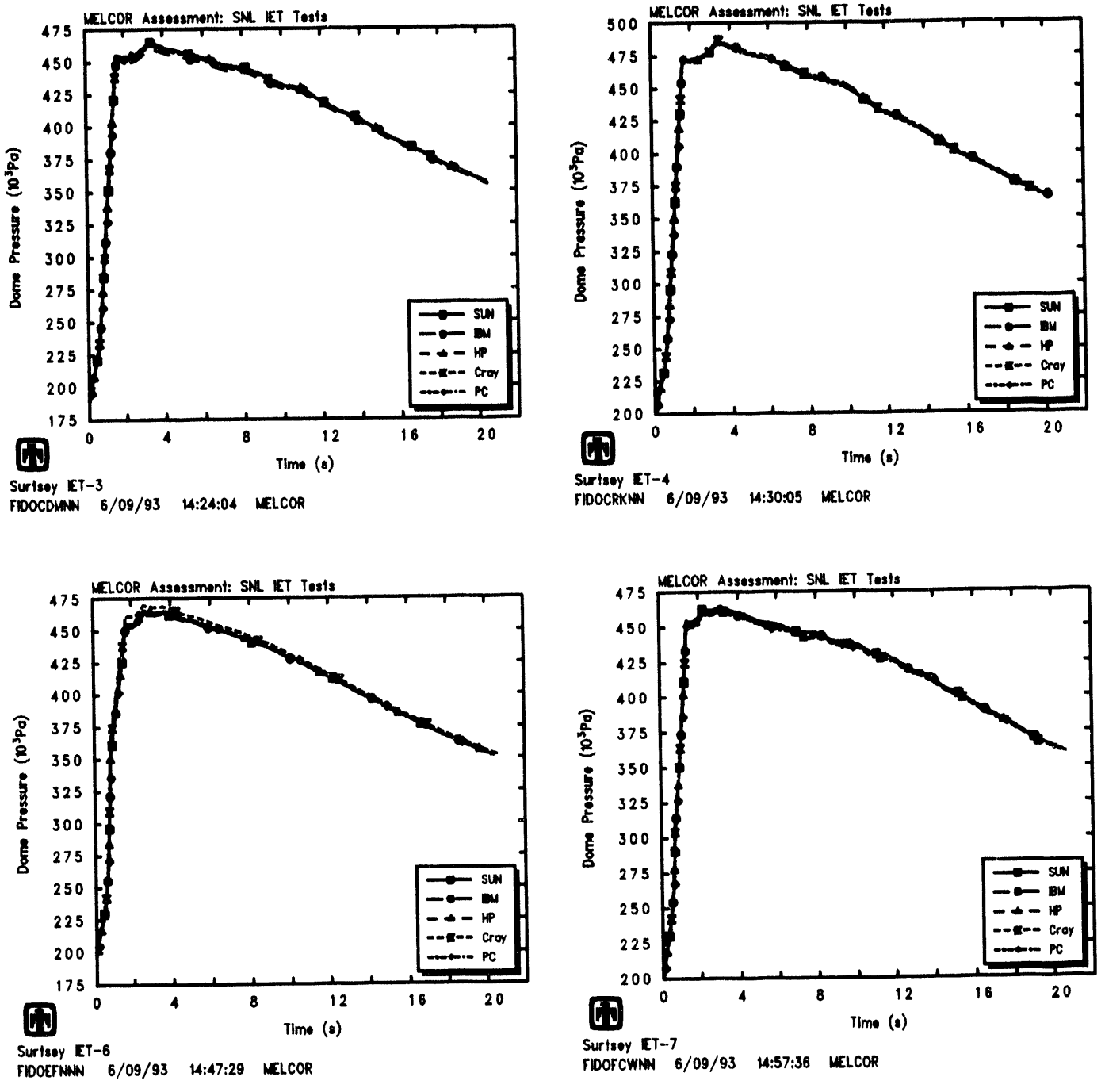

Figure 9.1.2. Vessel Pressures for Experiments SNL/IET-3 (upper left), SNL/IET-4 (upper right), SNL/IET-6 (lower left) and SNL/IET-7 (lower right) - Machine Dependency Sensitivity Study

Table 9.1.1. Hydrogen Generation for the SNL/IET Experiments Machine Dependency Sensitivity Study

Experiment	Hydrogen Produced (gm-moles)					
	Data†	MELCOR‡				
		SUN	IBM	HP	Cray	PC
IET-1	233	286/266	286/266	286/267	286/266	286/266
IET-1R	248	266/267	266/267	265/266	265/266	266/267
IET-3	227	232/352	232/350	234/353	233/351	234/353
IET-4	303	243/361	249/366	246/364	246/365	244/363
IET-5	319	240/313	242/314	240/312	240/313	240/312
IET-6	319	236/354	236/354	235/354	233/355	236/356
IET-7	274	229/351	229/349	229/350	228/349	227/348

†from gas grab bottle samples at 30min
‡(actual values at 20s)/ (assuming only steam/metal reactions)

Table 9.1.2. Machine Dependency for the SNL/IET Experiments Machine Dependency Sensitivity Study

Experiment	Hydrogen Burned (gm-moles)					
	Data†	MELCOR‡				
		SUN	IBM	HP	Cray	PC
IET-1	3	0/4	0/4	0/4	0/4	0/4
IET-1R	11	0/28	0/28	0/28	0/28	0/28
IET-3	190	188/313	186/306	189/313	187/310	188/312
IET-4	240	209/332	212/334	210/333	211/334	209/332
IET-5	53	0/91	0/91	0/91	0/91	0/91
IET-6	345	182/307	181/306	183/308	184/311	182/309
IET-7	323	223/350	223/349	223/349	222/349	221/348

†from gas grab bottle samples at 30min
‡(actual values at 20s)/ (assuming only steam/metal reactions)

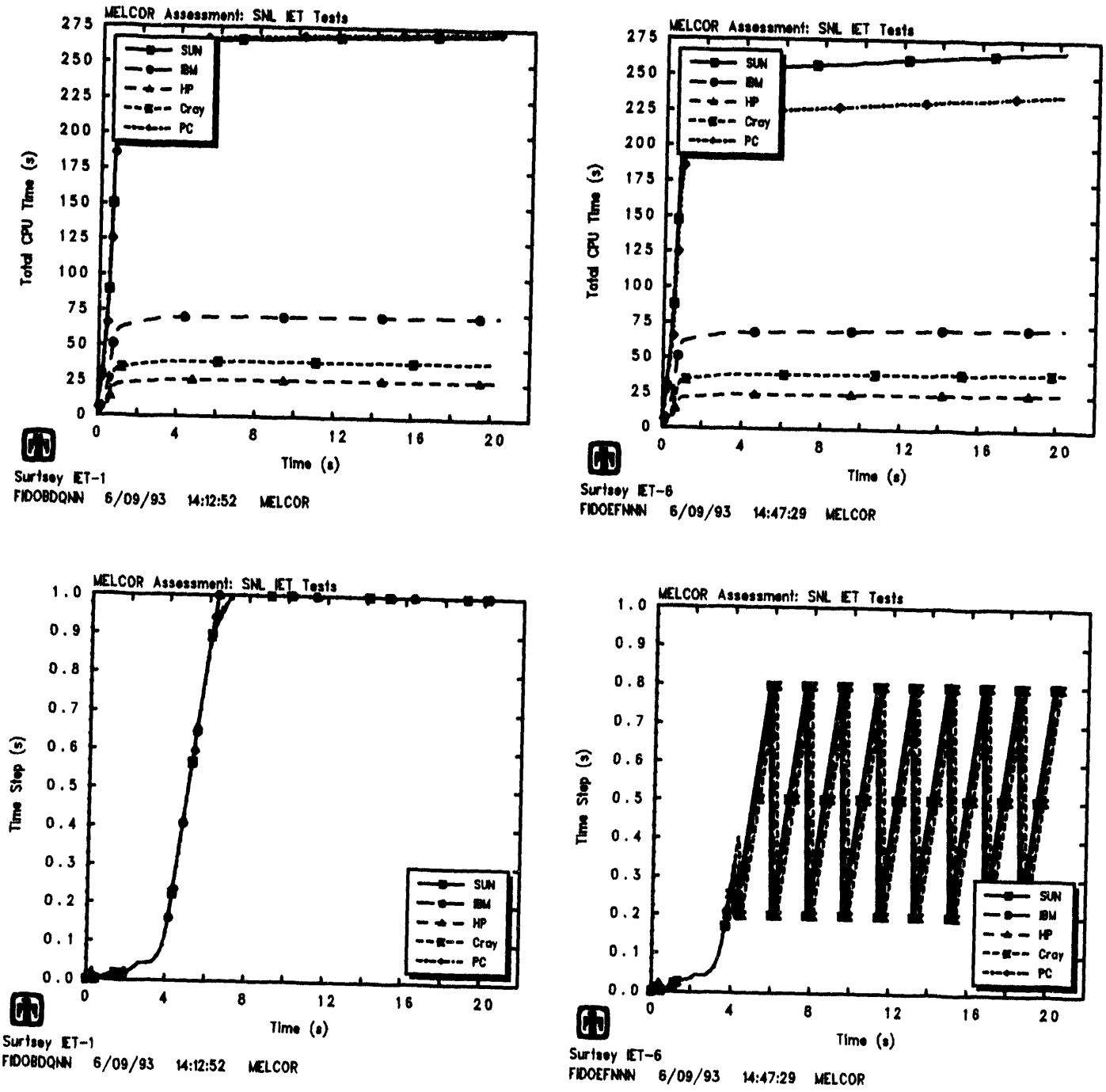

Figure 9.1.3. Total Run Times (top) and Time Step Histories (bottom) for SNL/IET-1 (left) and SNL/IET-6 (right) Experiment Analyses Machine Dependency Sensitivity Study

initiation (SC4607) was progressively set to 1×10^{-4}s (the default), 5×10^{-5}s, 1×10^{-5}s, 5×10^{-6}s, and 1×10^{-6}s. (The basecase analyses and the other sensitivity study calculations all used a user-input maximum allowed time step of 1s, and an initial time step size for HPME initiation of 1×10^{-4}s.)

The predicted vessel pressures for the basecase and reduced-timestep calculation sets are presented in Figure 9.2.1 and 9.2.2 for the tests without and with hydrogen combustion, respectively. (Test data are included for reference.)

The plot in the lower left of Figure 9.2.1 shows that the difference seen in vessel pressurization predicted for SNL/IET-1R on the SUN Sparc2 (Figure 9.1.1) is due to this particular case not having converged fully on the SUN; the reduced time step results on the SUN agree very well with the basecase results calculated on other platforms. Note that most of the other experiment analyses show results converging much better with reduced time steps, especially the no-burn cases SNL/IET-1 and SNL/IET-5.

There is somewhat more time-step dependence found in the cases with hydrogen burns occurring, as illustrated in Figure 9.2.2 (which is not surprising). The dependence seen is generally monotonic and converging with reduced time steps. Table 9.2.1 indicates that there is no significant change in hydrogen production in any case as the time step is varied, while Table 9.2.2 shows a monotonic increase in amount of hydrogen burned as the time step is decreased, except in the SNL/IET-7 case.

The qualitatively different behavior found in the total amounts of hydrogen calculated to be burned in the SNL/IET-7 analyses is also seen earlier in the HPME/DCH transient period. Figure 9.2.3 gives the time-dependent hydrogen combustion in the four cases with hydrogen burn (SNL/IET-3, SNL/IET-4, SNL/IET-6 and SNL/IET-7), and shows that the differences found in hydrogen combustion are not generated during the HPME period (from 0 to ~4s), but are due to a slowly-accumulating divergence later in time. The plots in this figure show that, in general, the runs with the larger time steps (Δt_{MAX} >0.1s) may not be converged but the runs with smaller time steps (Δt_{MAX} ≤0.1s) are converged. The SNL/IET-7 case appears to be converged even at the larger time steps allowed.

Total run times and time step histories for calculations using different time steps for the SNL/IET-1 and SNL/IET-1R experiment simulations are presented in Figure 9.2.4. (The corresponding results for SNL/IET-5 are similar to those shown.) There is no significant, overall difference visible in either run time or time step history to explain the difference in predicted vessel pressurization found in this study for the SNL/IET-1R conditions. Figure 9.2.5 gives total run times and time step histories for the SNL/IET-6 and SNL/IET-7 calculation sets. (The corresponding results for SNL/IET-3 and SNL/IET-4 are similar to those shown.) While there is no significant, overall difference visible in either run time or time step history to explain the difference in predicted hydrogen combustion found in this study for the SNL/IET-7 conditions, these plots suggest that, in three of our four "burn" cases, the time step control causing time step reduction at the start of hydrogen burns may not reduce the time step sufficiently far or long a sufficiently long period; note that the hydrogen masses predicted to be burned in the runs with smaller time step values were generally quite similar, illustrating significant convergence when the time step was reduced.

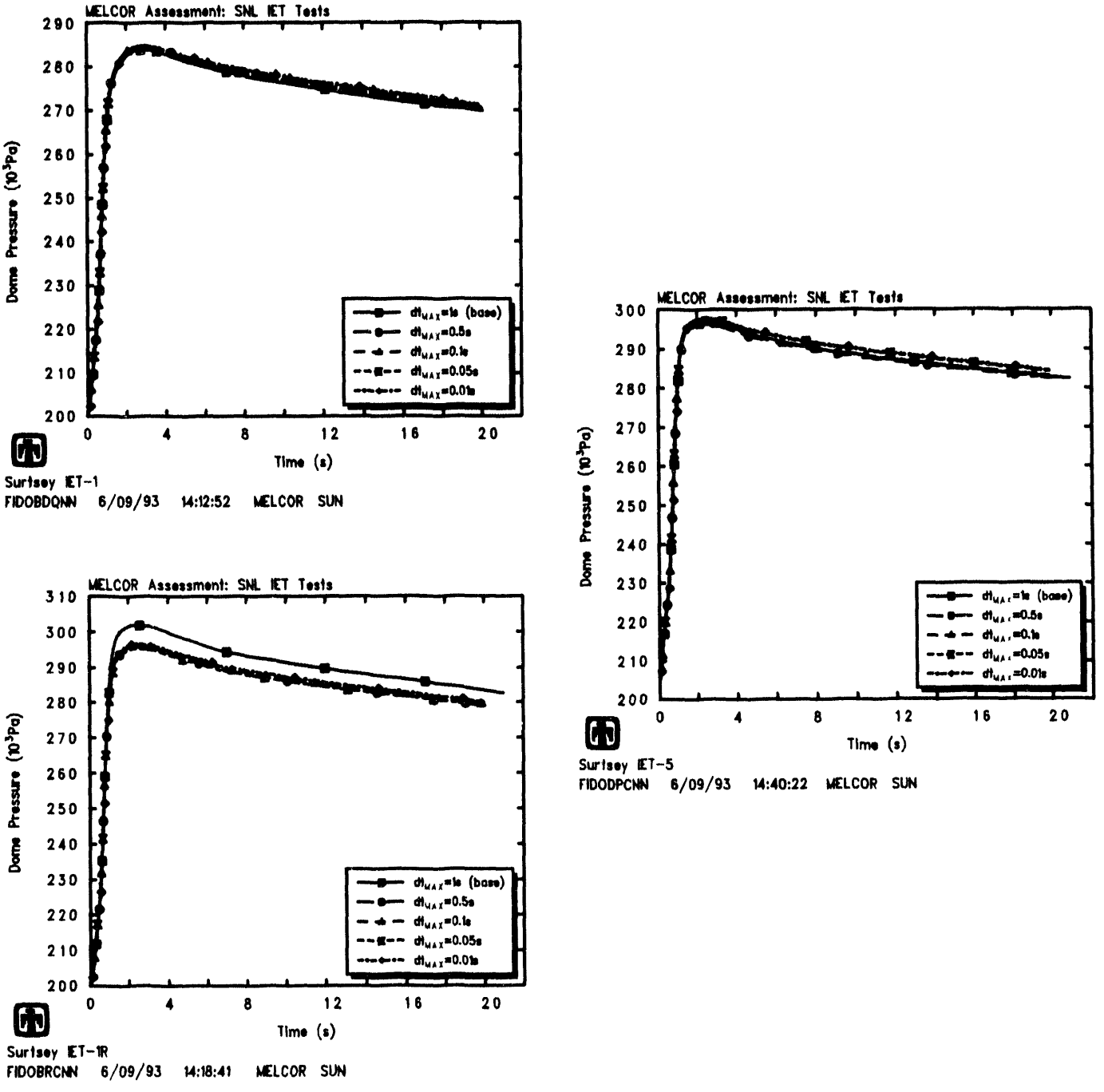

Figure 9.2.1. Vessel Pressures for Experiments SNL/IET-1 (upper left), SNL/IET-1R (lower left) and SNL/IET-5 (middle right) Time Step Sensitivity Study

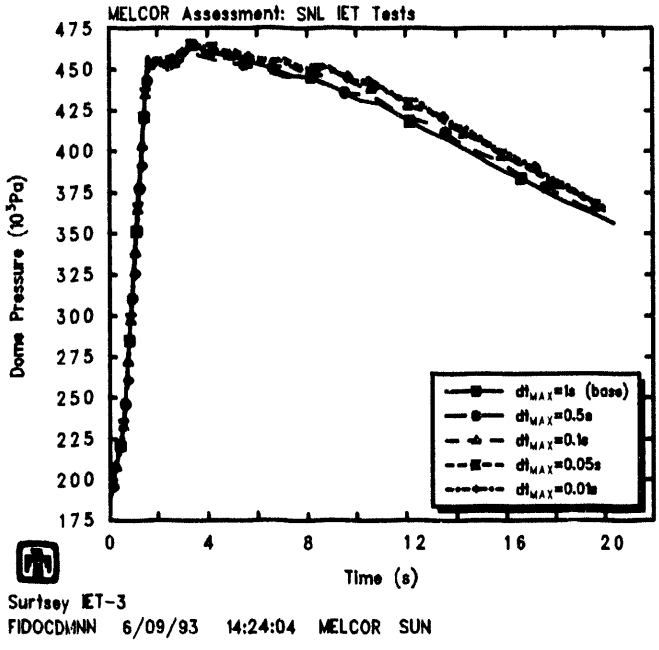

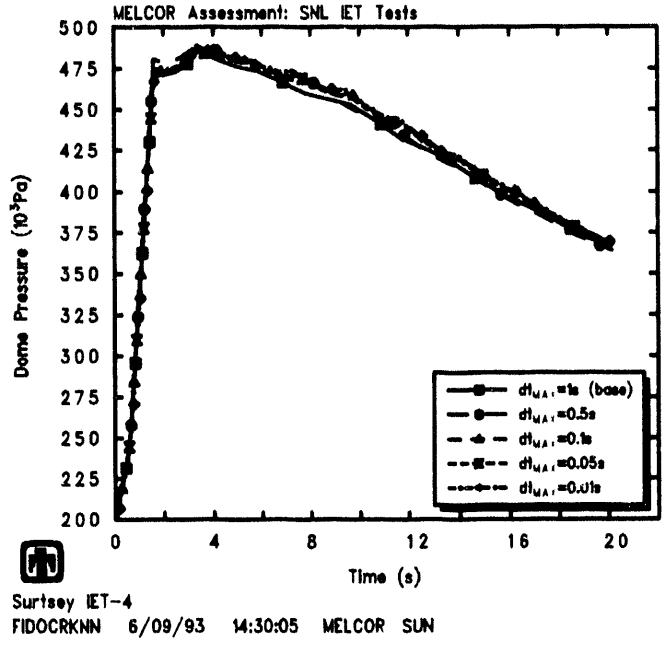

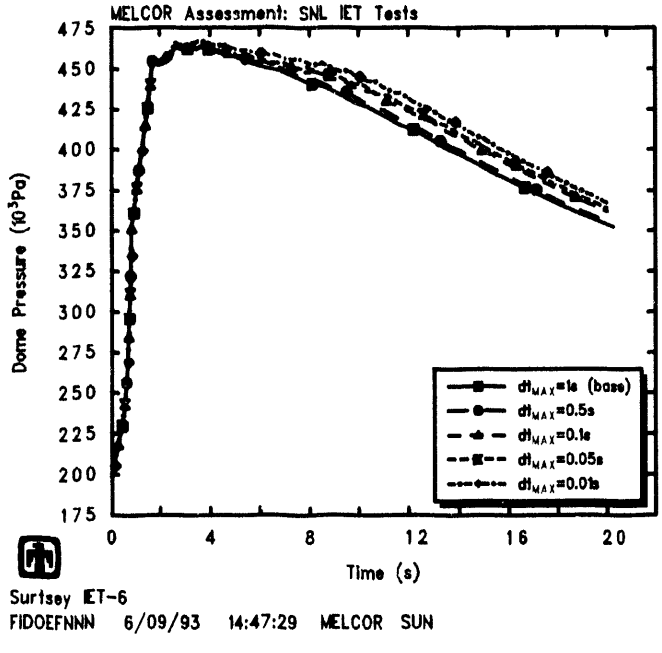

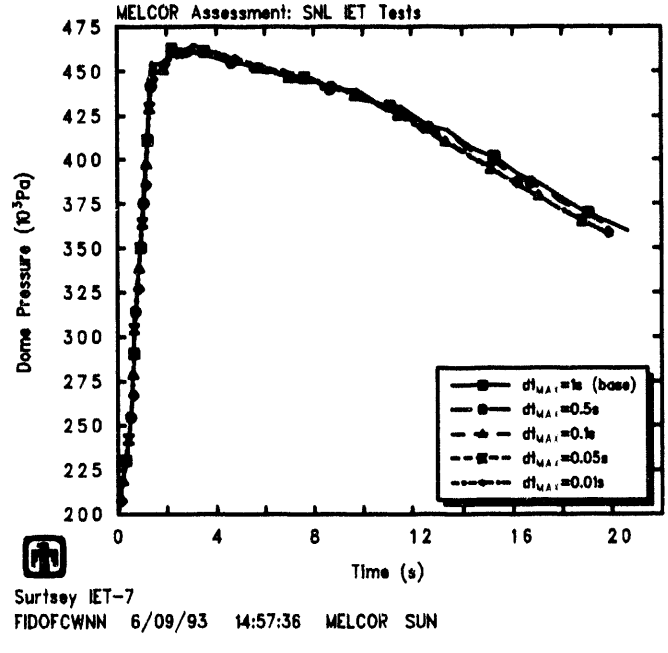

Figure 9.2.2. Vessel Pressures for Experiments SNL/IET-3 (upper left), SNL/IET-4 (upper right), SNL/IET-6 (lower left) and SNL/IET-7 (lower right) Time Step Sensitivity Study

Table 9.2.1. Hydrogen Generation for the SNL/IET Experiments – Time Step Sensitivity Study

Experiment	Hydrogen Produced (gm-moles)					
	Data†	MELCOR‡ Δt_{MAX}=				
		1s	0.5s	0.1s	0.05s	0.01s
IET-1	233	286/266	286/266	286/265	286/265	287/266
IET-1R	248	266/267	265/264	267/266	267/264	267/265
IET-3	227	232/352	231/351	233/353	232/356	233/354
IET-4	303	243/361	244/368	246/364	246/365	245/366
IET-5	319	240/313	240/312	240/313	241/312	242/313
IET-6	319	236/354	237/355	233/354	234/355	237/357
IET-7	274	229/351	227/346	226/347	229/350	227/348

†from gas grab bottle samples at 30min
‡(actual values at 20s)/ (assuming only steam/metal reactions)

Table 9.2.2. Hydrogen Combustion for the SNL/IET Experiments – Time Step Sensitivity Study

Experiment	Hydrogen Burned (gm-moles)					
	Data†	MELCOR‡ Δt_{MAX}=				
		1s	0.5s	0.1s	0.05s	0.01s
IET-1	3	0/4	0/4	0/4	0/4	0/4
IET-1R	11	0/28	0/28	0/28	0/28	0/28
IET-3	190	188/307	201/326	221/345	225/351	229/353
IET-4	240	209/332	222/349	236/358	238/361	241/365
IET-5	53	0/91	0/91	0/92	0/89	0/91
IET-6	345	182/307	185/310	210/336	215/341	224/350
IET-7	323	223/350	221/346	221/346	223/349	222/348

†from gas grab bottle samples at 30min
‡(actual values at 20s)/ (assuming only steam/metal reactions)

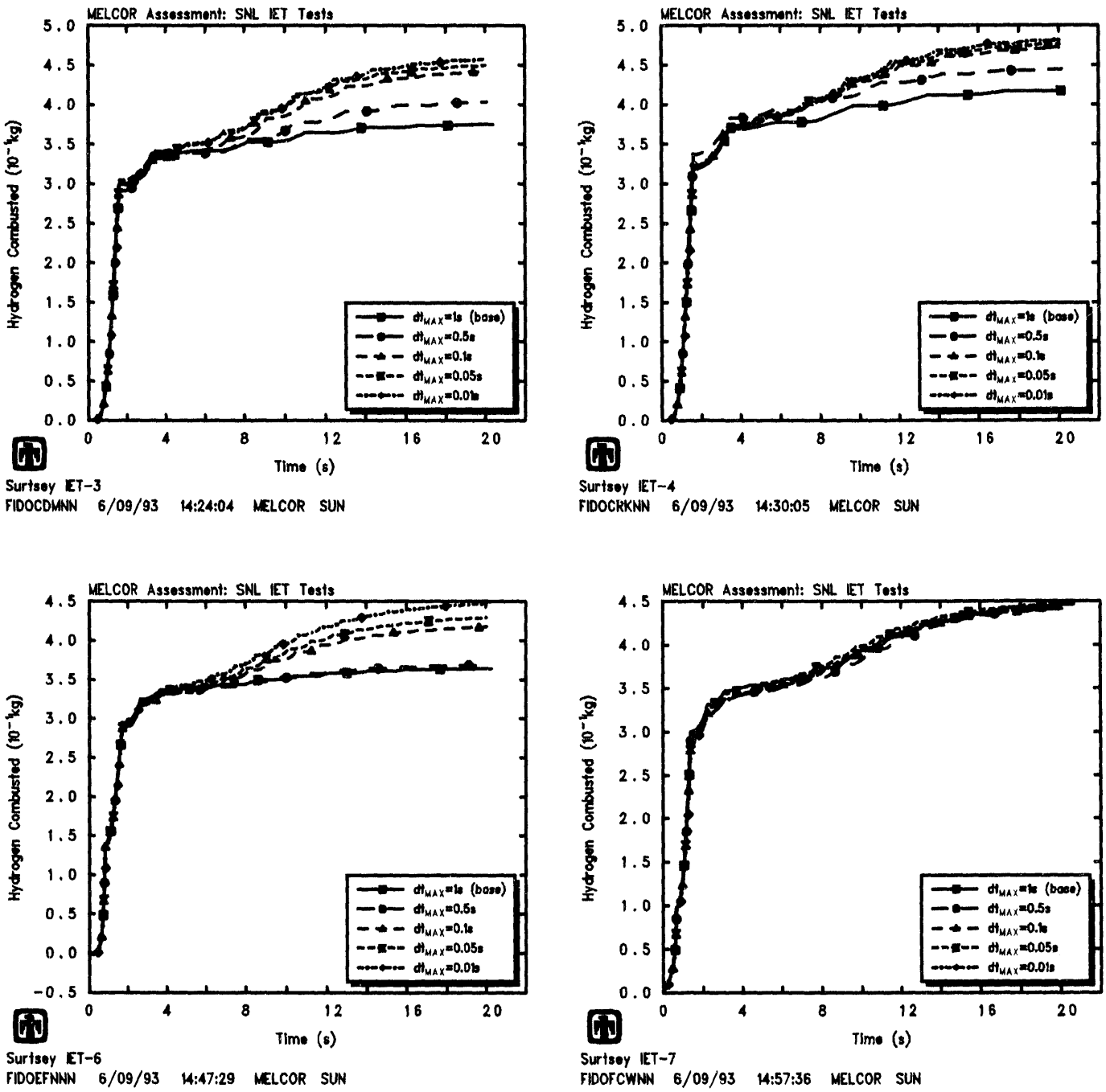

Figure 9.2.3. Hydrogen Combustion for Experiments SNL/IET-3 (upper left), SNL/IET-4 (upper right), SNL/IET-6 (lower left) and SNL/IET-7 (lower right) – Time Step Sensitivity Study

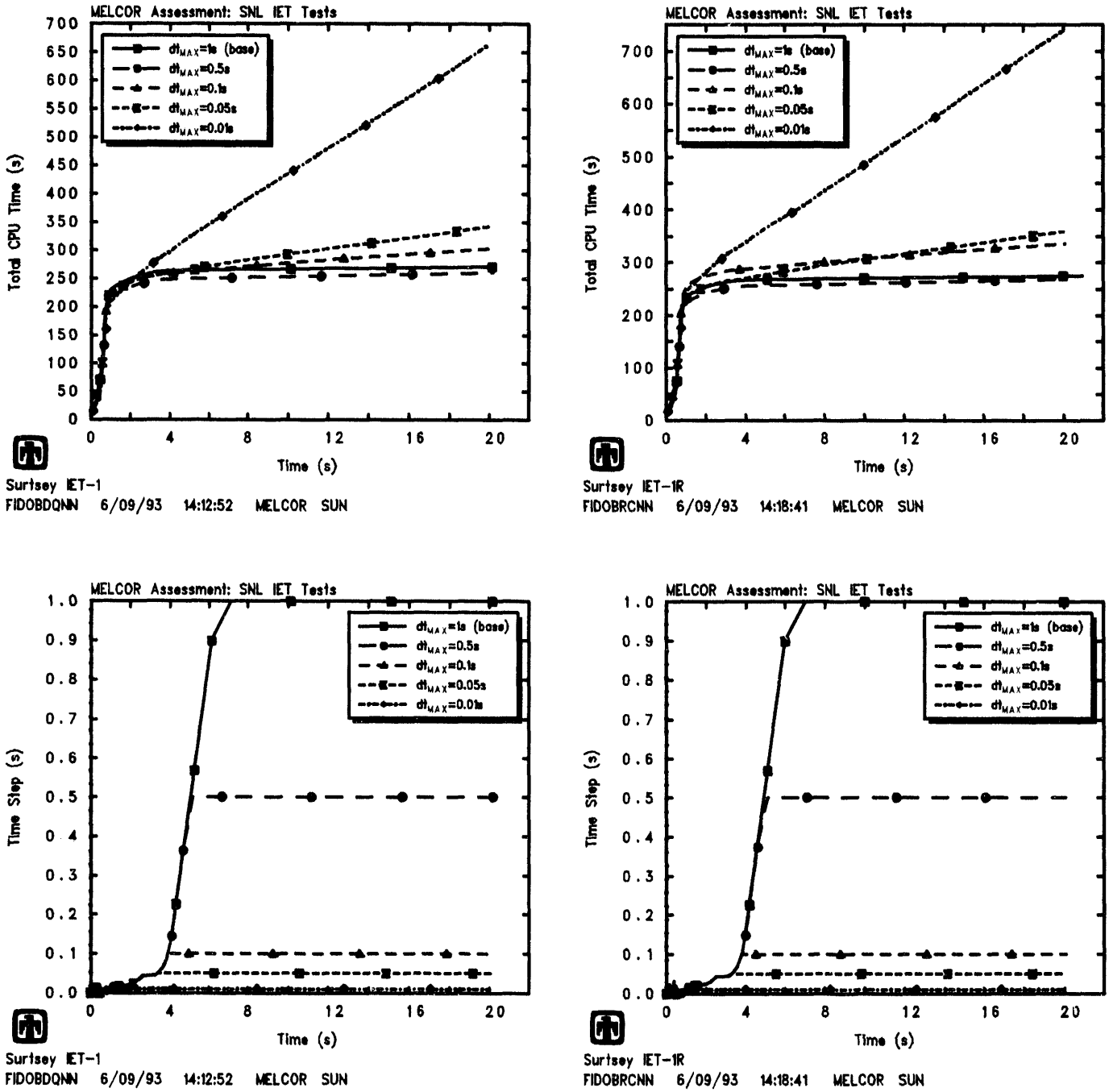

Figure 9.2.4. Total Run Times (top) and Time Step Histories (bottom) for SNL/IET-1 (left) and SNL/IET-1R (right) Experiment Analyses – Time Step Sensitivity Study

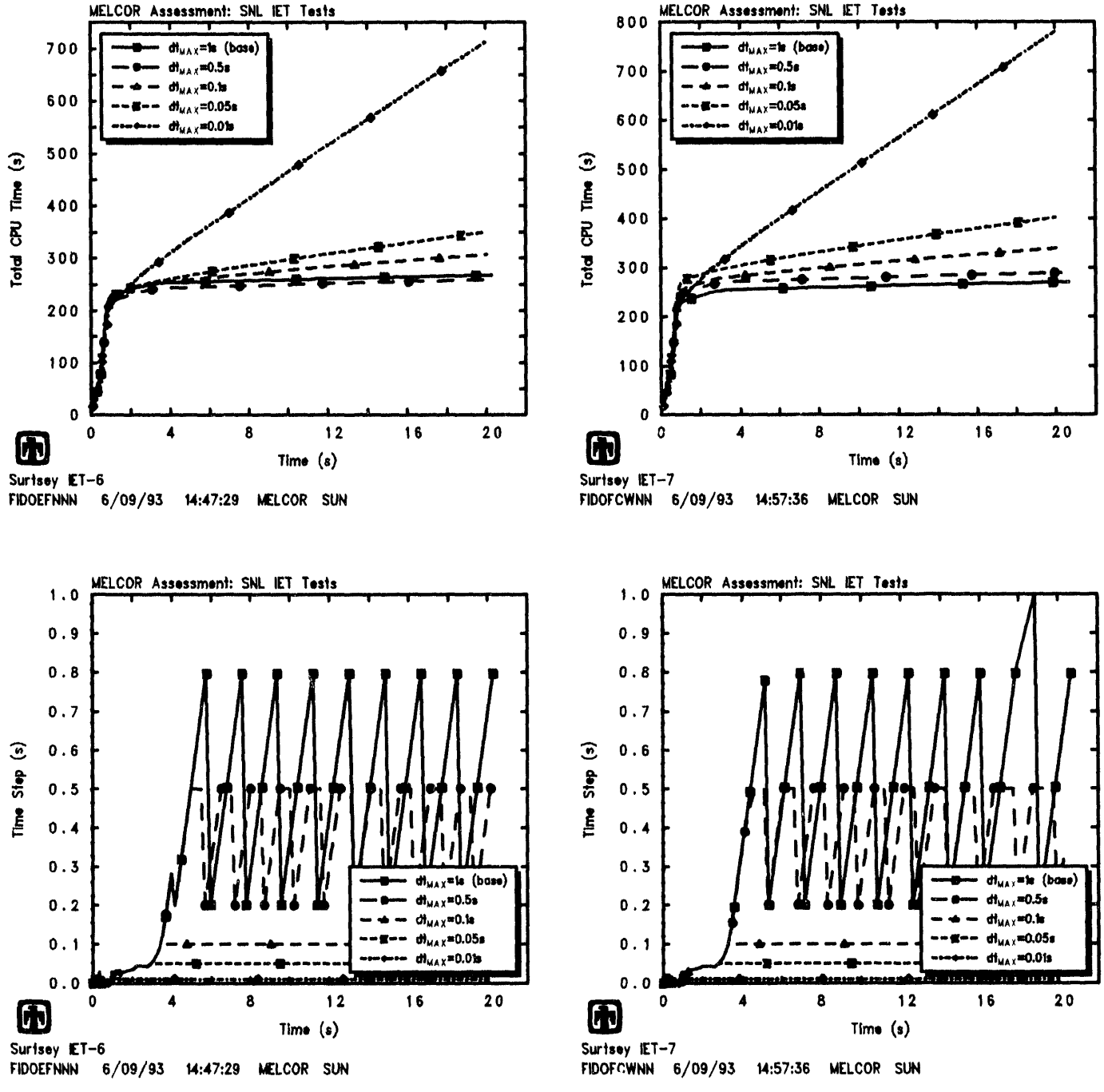

Figure 9.2.5. Total Run Times (top) and Time Step Histories (bottom) for SNL/IET-6 (left) and SNL/IET-7 (right) Experiment Analyses – Time Step Sensitivity Study

10 Comparison to CONTAIN

Several of the 1:10 linear scale SNL/IET experiments done in the Surtsey vessel have been analyzed with the CONTAIN code. The CONTAIN DCH model is quite different from the MELCOR FDI/HPME DCH model, being a more detailed, more mechanistic treatment rather than a more obviously parametric approach.

A number of CONTAIN calculations were done with evolving versions of the code. The early SNL/IET-1 and SNL/IET-1R pretest calculations were done with CONTAIN 1.12 citecontain-1-pretest,contain-1r-pretest,contain-1-posttest,contain-1-bypass. Pretest calculations were also done for SNL/IET-3 [31] and SNL/IET-5 [32] using CONTAIN 1.12 with the unconditional hydrogen burn (UCHB) model added, and SNL/IET-3 posttest calculations [33] were performed using the most recent, diffusion flame burn (DFB) and bulk spontaneous reaction (BSR), combustion models. In all cases, a number of sensitivity study calculations were done evaluating the effects of various parameters and modelling options.

More recently, several of the SNL/IET experiment simulations have been rerun, with results presented at the CONTAIN Peer Review [38]. Those results were obtained using a "standard" input prescription based upon prior experience [39]. Many inputs were defined as described in Appendix B of [29]. The new models for vessel failure and blowdown, and models for cavity entrainment and dispersal, weren't being assessed; hence, blowdown rates and debris dispersal fractions were matched to the experimental results, and debris source time-dependence was derived from the cavity pressurization history in order to uncouple uncertainties in these processes from the assessment of phenomena which were being modelled. Particle size was 1mm MMD (mass median diameter), assuming a lognormal distribution with σ_g=4. The parametric model for nonairborne debris was used in the cavity with an effective particle size of 0.01m.

A number of sensitivity study results were presented in [38]. The results presented here, on the recommendation of D. C. Williams of the CONTAIN development group [39], are those obtained using default DFB concentrations, which correctly predicted H_2 combustion for all four Zion SNL/IET tests analyzed. (However, note that H^2 combustion in other tests, especially SNL/IET-9, was underpredicted by the default model and that further refinement in combustion criteria is still needed. Also note that the "standard" case in [38] involved parameters set to make DFB almost unconditional, which wouldn't work for SNL/IET-5; this made little difference on the other Zion SNL/IET experiments simulated (*i.e.*, SNL/IET-1, SNL/IET-3 and SNL/IET-6), but did matter for SNL/IET-9.)

Table 10.1 compares measured peak vessel pressures with results calculated by both MELCOR and by CONTAIN. (The MELCOR results used in this section are those from the reference calculations described in Section 4.) Tables 10.2 and 10.3 compare measured hydrogen production and combustion, respectively, with corresponding calculated results; note that the hydrogen production and combustion for CONTAIN are estimated from hydrogen and oxygen molar balances, as is the experimental data.

Table 10.1. Peak Pressures for the SNL/IET Experiments – Code Comparison Study

Experiment	ΔP_{MAX} (kPa)		
	Data	MELCOR	CONTAIN
IET-1	98	84	70.4 [27] 92 [29] 92 [38]
IET-1R	103	102	79.5 [28]
IET-3	246	276	101.6 [31]§ 236.8 [31]¶ 199 [33]¶ 194 [33]ß 195 [38]
IET-5	103	93	75 [32] 75 [38]
IET-6	279	266	180 [38]

§using DHB (default hydrogen burn)
¶using UCHB (unconditional hydrogen burn)
ßusing DFB (diffusion flame burn)

Table 10.2. Hydrogen Generation for the SNL/IET Experiments – Code Comparison Study

Experiment	Hydrogen Produced (gm-moles)		
	Data†	MELCOR‡	CONTAIN
IET-1	233	286/266	173 [27] 238 [29] 260 [38]
IET-1R	248	266/267	220 [28]
IET-3	227	232/352	250 [31]§ 252 [31]¶ 232 [33]¶ 233 [33]ß 260 [38]ß
IET-5	319	240/313	221 [32] 257 [38]
IET-6	319	236/354	215 [38]

†from gas grab bottle samples at 30min
‡(actual values)/ (assuming only steam/metal reactions)

§using DHB (default hydrogen burn)
¶using UCHB (unconditional hydrogen burn)
ßusing DFB and BSR latest combustion models

Table 10.3. Hydrogen Combustion for the SNL/IET Experiments – Code Comparison Study

Experiment	Hydrogen Burned (gm-moles)		
	Data†	MELCOR‡	CONTAIN
IET-1	3	0/4	– [27]
			– [29]
			– [38]
IET-1R	11	0/28	– [28]
IET-3	190	209/313	37 [31]§
			250 [31]¶
			222 [33]¶
			200 [33]ß
			150 [38]ß
IET-5	53	0/91	– [32]
			3.5 [38]
IET-6	345	223/307	120 [38]

†from gas grab bottle samples at 30min
‡(actual values)/ (assuming only steam/metal reactions)

¶using DHB (default hydrogen burn)
§using UCHB (unconditional hydrogen burn)
ßusing DFB and BSR latest combustion models

The results obtained with the two code models are generally similar. In particular, a pressure rise of $\leq$100kPa is calculated for tests with no significant hydrogen combustion, and a larger pressure rise of $\sim$200-250kPa is obtained for cases with substantial hydrogen burn. Some other observations on the MELCOR-CONTAIN comparisons taken from [39] are:

1. The CONTAIN calculations indicated that, with a degree of debris-steam coherence equal to that inferred from the experimental results, CONTAIN underpredicted ΔP and H_2 production unless substantial contributions from nonairborne debris and/or co-dispersed cavity water were allowed.

2. CONTAIN sensitivity studies indicated that improved agreement could be obtained for ΔP in SNL/IET-3, SNL/IET-5 and SNL/IET-6 (but not necessarily SNL/IET-1) if increased nonairborne debris interactions (*i.e.*, in the subcompartment) or interaction with co-dispersed water were allowed, relative to the standard input set. This would overpredict H_2 in SNL/IET-1 and SNL/IET-3, but not in SNL/IET-5 and SNL/IET-6. There was no tendency of model assumptions giving good ΔP results to underpredict H_2 results; thus, the CONTAIN calculations do not support the possibility that much of the hydrogen production inferred from the gas analyses represents "late" effects occurring on time scales of minutes rather than seconds.

3. CONTAIN sensitivity studies indicated that substantial mitigation results from the combined effects of heat transfer and inability of all DCH-produced hydrogen to burn promptly due to oxygen starvation in the subcompartment; incomplete debris-gas equilibration was also a significant mitigation effect, but not as important as the heat transfer and hydrogen effects in the calculations.

4. DCH time constants calculated by CONTAIN tended to be strong functions of location and time during the event. Trapping and heat transfer time constants tended to be shorter but oxidation time constants tended to be greater than those input to MELCOR; however, the significance of longer oxidation time constants was reduced by the fact that CONTAIN still used most of the coherent steam.

5. Differences resulting from different ways of evaluating H_2 production and combustion are considerably less for CONTAIN than in MELCOR because unreacted debris in the CONTAIN model doesn't see nearly as much oxygen as in MELCOR's model.

11 Code Problems Identified

A number of code and modelling errors and inadequacies were identified and corrected during our DCH IET experiment MELCOR assessment analyses. Many of these have been mentioned throughout the text, but are summarized in this section for easy reference.

11.1 Debris Material and Source Input

The first problem encountered in beginning these DCH IET experiment MELCOR assessment analyses was that some of the required post-thermite reaction materials (Fe, Al, Cr and Al_2O_3) were not available as materials recognized by the new HPME model added recently to the FDI package in MELCOR. In the original coding, the FDI HPME model only recognized the standard COR-package materials UO_2, Zr, ZrO_2, steel, steel oxide and control rod poison. The CAV package recognizes all of the standard CORCON materials as possible inputs, including the post-thermite reaction materials, but this was of no help in modelling debris dispersal to control volume atmospheres and/or to heat structure surfaces. Therefore, Al and Al_2O_3 were added as allowed input materials in the FDI HPME model.

While Al and Al_2O_3 were added as allowed input materials in the FDI HPME model, Fe and Cr were not added as separate input materials because they could already be input as constitutive components of steel (assumed to consist of a mixture of Fe, Ni, Cr and C). For user convenience and for consistency, the optional user input specification of the composition of steel was moved from the COR package input to be MP ("material properties") input; for internal self-consistency, the oxidation reaction energy of steel is then calculated within the MP package for the composition specified.

At the same time, a "stand-alone" input capability was added to the FDI HPME model allowing specification of debris input through tabular function input in addition to the previously-available specification of debris input through TP ("transfer process") package input; the previously-available TP input assumed debris sources coming from the COR package through translation matrices or from external user-specified data sets defined using the EDF ("external data file") package in MELCOR. The stand-alone tabular-function input capability added to the FDI HPME model allows a much more user-friendly and convenient format for specification of debris input, particularly for experiment analyses such as in this study.

Our first IET experiment analyses would frequently abort with temperature convergence failures. After several patches were tried, the FDI HPME temperature convergence coding was changed to be much more robust. No code aborts due to temperature convergence failures during HPME have been seen since, despite the large number of calculations done and the wide range of conditions encountered.

These early problems were reported as DIR1097 and DIR1098, and the code modifications implemented in version 1.8MY. These modifications are therefore included in the release version of MELCOR 1.8.2 (1.8NM).

11.2 Debris Interaction with Structures

After work on these analyses had been in progress for some time, we became concerned about the interaction of debris with heat structures. In the original HPME model added to MELCOR, any debris immediately deposited onto a heat structure or later settled onto a heat structure essentially left the problem; there was no subsequent interaction of any kind for that debris, except for decay heating of the structure surface. This was identified as a major potential problem area during our MELCOR DCH analyses, especially given MELCOR's emphasis on mass and energy conservation. For example, the lack of any thermal interaction of debris with structures could adversely affect the ability to correctly predict late-time revaporization of volatile fission products. Also, the lack of any oxidation of deposited debris meant that the total amount of hydrogen producable during HPME was very highly dependent on the user-specified initial debris distribution – any debris deposited or settled could not generate any hydrogen, regardless of oxygen and/or steam availability or debris temperature and/or amount. Therefore two major effects were later added to the original HPME model: the heating of the structure surface by deposited hot debris, and the continued oxidation of the deposited debris. The heating of the structure surface by deposited hot debris is controlled by a heat transfer coefficient adjustable through sensitivity coefficient input, and the continued oxidation of the deposited debris is controlled by a user-input structure oxidation characteristic time (distinct from and usually much longer than the characteristic time input for oxidation of airborne debris). With these input and coding modifications, HPME debris deposited on structures now can continue to affect the overall system response through several potential interactions.

These model enhancements needed were reported as DIR1130, and the code modifications implemented in version 1.8NN. Note that this set of code changes is not included in the release version of MELCOR 1.8.2 (1.8NM).

11.3 Hydrogen Combustion during DCH

We found during the course of these analyses that non-default input for the BUR package was required to match the hydrogen combustion behavior observed in these experiments. While this could be done with the standard BUR package input for these experiment analyses, the same input modification could not be made in plant analyses, because the non-standard input would affect the results calculated both before and after the HPME period. (These experiments and associated analyses, in comparison, consisted of only the HPME period.) This problem was addressed by providing new, optional input parameters in the BUR package, essentially allowing the user to specify one set of input

parameters to be used during periods of HPME and another set of input parameters to be used during the remaining times. The hydrogen combustion input during HPME is default to the non-HPME values if not specified otherwise. The HPME period in any given control volume is a time period which satisfies constraints on minimum airborne debris amount and/or density, and temperature, all of which cutoff values are adjustable through sensitivity coefficient input.

This is included in DIR1130 as a FDI/HPME/DCH model enhancement, and the code modifications implemented in version 1.8NN. Note that this set of code changes are not included in the release version of MELCOR 1.8.2 (1.8NM).

11.4 Additional Output

While studying results from our various calculations, we found that there were not enough control functions and plot variables to readily analyze the hydrogen production *vs* combustion in the various cases. Reactant masses and energies for oxidation on structures were added as control functions and plot variables to the FDI package HPME model, similar to those already provided for oxidation of airborne debris; reactant masses and energies for hydrogen combustion also were added as control functions and plot variables to the BUR package, which had very limited output capabilities prior to these output enhancements. This was also included in DIR1130, and the code modifications implemented in version 1.8NN. Note that this set of code changes is therefore not included in the release version of MELCOR 1.8.2 (1.8NM).

11.5 Debris Heat Transfer

As noted in Sections 3.1 and 7.2, most of our calculations were run with control volume flow areas reduced by factors of ≥ 10 from their default values, to enhance convective heat transfer from the control volume atmospheres to the heat structure surfaces. The convective heat transfer was enhanced to account for some potential missing heat transfer mechanisms and effects:

First, preliminary calculations showed that the flow predicted through the system was primarily that associated with the steam blowdown only, flowing from the steam accumulator through the cavity and chute volumes to the subcompartments and then to the dome. The MELCOR FDI/HPME/DCH model does not model transport of debris between and through volumes but instead deposits the debris directly at its ultimate destination, using the same time-dependent deposition in all volumes regardless of their distance from the debris source. Thus, instead of debris being transported into an "upstream" volume (*e.g.*, the cavity or the subcompartments) with the blowdown steam and the resultant additional heating adding to the driving force pushing flow further "downstream" (*e.g.*, from the cavity to the chute or the subcompartments to the dome), the MELCOR logic does not represent this additional flow driving force and in contrast has debris appearing "upstream" and heating the atmosphere in upstream volumes, if

anything contributing a retarding force to the expected flow. This results in lower velocities, and is more benign than the transient HPME blowdown actually occurring in the experiments, with transport of hot debris together with the steam blowdown. Decreasing volume flow areas results in increased volume velocities more characteristic of the turbulent conditions that might be expected during HPME, and the associated turbulent forced convection heat transfer to structures.

In addition, the MELCOR FDI/HPME/DCH model does not account for any radiation directly from airborne debris to surrounding structures (or from deposited debris directly to atmosphere). There is little or no calculated atmosphere-structure radiation heat transfer early in these transients (except IET-5), because MELCOR only considers radiation heat transfer for steam and/or CO_2 in atmospheres; in most of the experiment simulations there is very little steam present early in the transient, because any blowdown steam is consumed in debris oxidation soon after arrival, and very little CO_2 present at all (except in IET-5). The lack of steam and/or CO_2 in the atmosphere would if anything enhance radiation heat transfer from airborne debris to structures because there would be little absorption in the intervening atmosphere. Hand calculations indicate that this could be a significant heat transfer mechanism, early in the transient. Because there is no way in MELCOR to model this effect, too much energy may be deposited in the atmosphere by the airborne debris; because there is no convenient way to enhance atmosphere-structure radiation heat transfer in general, we relied on increasing convective heat transfer instead to help remove that energy.

The capability to adjust the volume velocities through the control volume flow areas in order to enhance convective heat transfer to structures only during DCH was provided through new input, this time to the CVH package, adding a sensitivity coefficient that optionally multiplies the volume velocities during the HPME period only in any given control volume. This was included in DIR1130, and the code modifications implemented in version 1.8NN. Note that this set of code changes are not included in the release version of MELCOR 1.8.2 (1.8NM).

However, the capabilities of the MELCOR FDI/HPME/DCH model would be significantly enhanced in general if the following effects were added:

1. radiation heat transfer from airborne debris directly to structures,
2. radiation heat transfer from deposited debris directly to atmosphere,
3. time delays for debris deposition to account for different transit distances from the source point, and
4. fission product release from debris not deposited in or settled into a cavity (not discussed in this report, but discussed in [40], and included here for completeness.

11.6 Cavity Condensate Water

Finally, when we first tried doing machine dependency and time step calculations, we found sensitivities in the amount of hydrogen both produced and burned in several calculations. The problem was ultimately traced to occasional rapid depletion of all the condensate water in the cavity through bulk transport to the chute control volume rather than through boiloff and entrainment as expected. Once the water entered the chute volume, it remained mostly liquid, and the resulting smaller amount of steam available for oxidation explained the differences seen in hydrogen production and combustion. Three possible workarounds were identified for this problem: reducing the flow path opening height slightly, changing the flow path from a horizontal to a vertical flow path orientation, and increasing the debris-to-structure heat transfer coefficient (to boil off the water more quickly). Since the problem identified was a basic CVH problem not directly affecting the evaluation of the MELCOR FDI/HPME/DCH model, and given the facility geometry and condition uncertainties, we considered using any of these three workarounds to be acceptable. We chose to reduce the flow path opening height slightly (from 30.5cm to 29.9cm). All calculations were then rerun with this input change, and the results proved quite satisfactory. (Trying to find and fix the source of this CVH problem while significant changes are being made to the basic CVH package coding did not seem useful in the long term.)

12 Summary and Conclusions

The MELCOR computer code has been used to analyze several of the IET direct containment heating experiments done at 1:10 linear scale in the Surtsey test facility at Sandia and at 1:40 linear scale in the corium-water thermal interactions (CWTI) COREXIT test facility at Argonne National Laboratory. This report documents the results of those analyses.

Note that these MELCOR calculations were done as an open posttest study, with both the experimental data and CONTAIN results available to guide the selection of code input. Most individual parameters in our MELCOR input models were not separately adjusted in each of our MELCOR IET experiment analyses to best match data for each individual experiment. Instead, the basic control-volume/flow-path/heat-structure model was kept the same for all SNL/IET experiments analyzed, and a single set of debris source, distribution and interaction time parameters was used for all the SNL/IET experiments analyzed. The only test-specific changes made were to set the initial pressures, temperatures, gas composition, and liquid pool heights to match individual experiment initial conditions. A similar approach was taken for the ANL/IET analyses.

The processes modelled in the MELCOR FDI/HPME/DCH model include oxidation of the metallic debris components in both steam and oxygen, surface deposition of the airborne debris by trapping or settling, and heat transfer to the atmosphere; first-order rate equations with user-specified time constants for oxidation, heat transfer and settling are used to determine the rate of each process.

A single set of characteristic interaction times was specified for all the seven of the 1:10-scale tests analyzed (SNL/IET-1 through SNL/IET-7). The characteristic times for settling of debris in the control volume atmospheres onto floor heat structures were based upon free-fall times for the various volume heights, and therefore proportional to volume heights and constant in the various tests; there could be some test-to-test variations in turbulent flow circulation patterns, thermal buoyancy effects, *etc.*, but these were assumed negligible. The characteristic oxidation and heat transfer times were assumed to depend primarily on parameters such as average airborne or deposited particle concentrations, which in a given geometry should be approximately constant for identical melt debris and blowdown steam sources such as used in the tests analyzed.

The characteristic times for oxidation and heat transfer of debris in the control volume atmospheres, as well as a characteristic time for oxidation of debris deposited on heat structures, were selected after a number of iterations in sensitivity studies as giving reasonable agreement with a subset of test data (in particular, vessel pressure, subcompartment temperature and hydrogen production and combustion) in the SNL/IET experiments simulated. Note that there is no reason to assume that the debris source and interaction input parameter set used in our reference analyses is unique (*i.e.*, the only set to provide reasonable agreement with the selected test data). It is also not guaranteed that the iterative procedure followed results in an input parameter set that yields the best agreement with data, or agreement with data for the "correct" reasons (*i.e.*, representing

the actual behavior). For example, freezing some of the parameter values early in this iterative process undoubtedly affected the values assumed for other parameters. Further, experiment ambiguities may have led to incorrect modelling assumptions that would also affect the values chosen for various parameters (such as the characteristic oxidation time, as discussed below).

The results of the MELCOR reference calculations for the Surtsey 1:10-scale tests correctly reproduce the subdivision of the pressure response into two major families, caused by the effect of hydrogen combustion, as seen in the test data, with a peak pressure rise of ~100kPa due to HPME and an additional pressure rise of ~150kPa due to hydrogen combustion. The results also correctly reproduce the lack of any significant effects of presence *vs* absence of pre-existing hydrogen or presence *vs* absence of basement condensate water.

The hydrogen production and combustion calculated by MELCOR is generally in reasonable agreement with test data (after careful adjustment of the BUR package input, as described below). However, it is difficult to quantitatively compare the measured and calculated hydrogen production and combustion because of the basic assumption made by the experimenters that all oxygen depletion was due to reaction with hydrogen. The experimenters assumed in their data analysis that debris reacted only with steam, not with free oxygen, whereas MELCOR assumes that oxidation of metals with free oxygen occurs preferentially to oxidation with steam. Therefore, throughout this report, pairs of values are given for the hydrogen production and combustion calculated by MELCOR, presenting both the actual amounts of hydrogen calculated to be produced by HPME steam/metal reactions and burned, and the amounts of hydrogen produced and burned that would be calculated using the initial and final oxygen and hydrogen moles from the MELCOR analyses in the same formulae as in the experiment data analysis.

The two sets of MELCOR values differ by twice the number of moles of O_2 consumed by direct metal/oxygen reactions. There is little difference found in the hydrogen production evaluated using the experimental procedure and actually calculated by MELCOR in the tests with little or no free oxygen present (*i.e.*, SNL/IET-1 and SNL/IET-1R); however, note that, for those two tests and for SNL/IET-5, assuming all oxygen depletion was due to combustion reaction with hydrogen does result in a small mass of hydrogen calculated to be burned, similar to the experimental results. The actual moles of hydrogen produced and burned in these MELCOR analyses appear generally less than measured values, especially in the experiments with hydrogen combustion, while the hydrogen production and combustion calculated using the experimental procedure on the MELCOR results are generally greater than measured. Also, the actual amount of hydrogen calculated to be produced by MELCOR is lower in the tests with oxygen initially present (SNL/IET-3 through SNL/IET-7) than in the experiments with no significant oxygen initially present (SNL/IET-1 and SNL/IET-1R). However, deriving the amounts of hydrogen produced and burned in the MELCOR calculations by assuming that all oxygen depletion is the result of hydrogen burning yields greater hydrogen production in SNL/IET-3 through SNL/IET-7 than in SNL/IET-1 and SNL/IET-1R, reproducing the trend seen in the tabulated experimental data.

Overall, the "correct" answers are likely to lie somewhere between the two limiting assumptions. It is unlikely that there is no oxidation of metal with free oxygen at all (as assumed in the experimental analysis protocol). However, MELCOR would be expected to exaggerate the relative degree to which metal oxidizes with free oxygen *vs* with steam, because of the hierarchical assumptions in the MELCOR FDI/HPME/DCH model and because, in the experiment, the debris transport probably lags the steam/hydrogen mixture flow, so that not much of the debris gets to see much oxygen, while in the MELCOR model the debris is immediately transported to its ultimate distribution (within a user-specified time period, in this case 1s) while the steam blowdown is modelled "normally" as a transient process taking several seconds.

The quantification of hydrogen production and combustion in the SNL/IET experiments assuming that all oxygen depletion was due to reaction with hydrogen had an unforeseen effect on our MELCOR analyses. In particular, the choice of a very short time constant for airborne debris oxidation (0.025s in the reference analyses) was driven by trying to explicitly match the reported hydrogen production and combustion data; sensitivity study results show very little difference in calculated pressures or temperatures for $0.01\text{s} \leq \tau_{ox} \leq 0.1\text{s}$, because the oxidation rate is essentially limited by availability of steam and/or oxygen at the shorter characteristic interaction times, and the hydrogen production and combustion results later derived from a molar balance assuming only steam/metal reactions (as in the test data analysis) is in better agreement with test data for calculations using longer characteristic airborne-debris oxidation times ($\tau_{ox} \geq 0.1\text{s}$), which seems a more reasonable value based on physical grounds. (This does not affect any of the comparative conclusions drawn from the various other sensitivity studies.)

The hydrogen combustion observed in these tests could not be calculated using the default burn package input, because the default ignition criteria are never satisfied in these experiments. Instead, in the majority of our IET analysis calculations, the hydrogen mole fraction ignition criterion in the absence of igniters was set to 0.0, which (in the absence of CO) also gives a combustion completeness correlation value of 0.0; in addition, burn was suppressed in all control volumes except the vessel dome. This particular combination of input was found to produce reasonable agreement with test data in all cases. The combustion completeness being set to 0 prevents the burning of any pre-existing hydrogen, but allows burning of any additional hydrogen generated during the HPME. Suppressing burn except in the dome mimicked the experimental behavior of a jet flame burning at the outlet from the subcompartments to the dome; because little or no hydrogen was generated by debris oxidation in the dome in our analyses, only hydrogen advected into the dome from the subcompartments burned, and only on the time scale over which it was advected into the dome.

(While these non-standard combustion criteria could be specified with the standard BUR package input for these experiment analyses, the same input modification could not be made in plant analyses, because the non-standard input would affect the results calculated both before and after the HPME period. This problem was addressed by providing new, optional input parameters in the BUR package, essentially allowing the user to specify one set of input parameters to be used during periods of HPME and

another set of input parameters to be used during the remaining times.)

Most of our calculations were run with control volume flow areas reduced by factors of ≥ 10 from their default values, to enhance convective heat transfer from the control volume atmospheres to the heat structure surfaces. (The control volume flow areas are used only to obtain volume velocities for use in the calculation of convective heat transfer coefficients; changing control volume flow areas does not affect flow path calculations at all.) The convective heat transfer was enhanced for two reasons:

First, our preliminary calculations showed that the flow through the system in these calculations was primarily that associated with the steam blowdown only, flowing from the steam accumulator through the cavity and chute volumes to the subcompartments and then to the dome. The MELCOR FDI/HPME/DCH model does not model transport of debris between and through volumes but instead deposits the debris directly at its ultimate destination, using the same time-dependent deposition in all volumes regardless of their distance from the debris source. Thus, instead of debris being transported into an "upstream" volume with the blowdown steam and the resultant additional heating adding to the driving force pushing flow further "downstream", the MELCOR logic does not represent this additional flow driving force and in contrast has debris appearing "upstream" and heating the atmosphere in upstream volumes, if anything contributing a retarding force to the expected flow. This results in lower velocities, and is more benign than the transient HPME blowdown actually occurring in the experiments, with transport of hot debris together with the steam blowdown. Decreasing volume flow areas resulted in increased volume velocities more characteristic of the turbulent conditions that might be expected during HPME, and the associated turbulent forced convection heat transfer to structures.

In addition, the MELCOR FDI/HPME/DCH model does not account for any radiation directly from airborne debris to surrounding structures (or from deposited debris directly to atmosphere). Although radiation heat transfer was included in the MELCOR input model, there is little or no calculated atmosphere-structure radiation heat transfer early in these transients (except in IET-5), because MELCOR only considers radiation heat transfer for steam and/or CO_2 in atmospheres. In IET-5, some atmosphere-structure radiation heat transfer is calculated because of the large amount of CO_2 used to inert the system; however, in most of the experiment simulations there is very little steam present early in the transient, because any blowdown steam is consumed in debris oxidation soon after arrival, and very little CO_2 present at all. The lack of steam and/or CO_2 in the atmosphere would if anything enhance radiation heat transfer from airborne debris to structures because there would be little absorption in the intervening atmosphere. Hand calculations indicate that this could be a significant heat transfer mechanism, early in the transient. Because there is no way in MELCOR to model this effect, too much energy may be deposited in the atmosphere by the airborne debris; because there is no convenient way to enhance atmosphere-structure radiation heat transfer in general, we relied on increasing convective heat transfer instead to help remove that energy.

(Again, while this could be done with the standard CVH package input for these experiment analyses, the same input modification could not be made in plant analyses,

because the non-standard input would affect the results calculated both before and after the HPME period. This problem also was addressed through new input capabilities, adding a sensitivity coefficient to the CVH package that optionally multiplies the volume velocities in any given control volume during the HPME period only.)

The MELCOR FDI/HPME/DCH model does not model transient transport of debris into and through the system, but instead immediately places the debris at its ultimate destination. MELCOR uses a single function for the time-dependence of the melt injection in all control volumes and heat structures; in reality, the melt reaches the subcompartments later than the cavity, and the dome later than the subcompartments. The time period over which melt injection was specified to occur was varied in sensitivity study analyses, and the time-dependence of the melt addition in the MELCOR input was adjusted to match the rate of pressure and temperature increase in the vessel. Based upon results results for vessel pressure, hydrogen generation and subcompartment temperatures, our analyses were run with a melt injection period of 1s, with most of the injection occurring during the second half of that period. This $\leq$1s melt injection period is in reasonable agreement with test observations indicating molten brass, steel and thermite entering the cavity between 0 and $\sim$0.3s, and debris entrainment from the cavity into the subcompartments between about 0.4s and 0.8s.

The total debris mass collected in these experiments was usually greater than the initial thermite charge due to melting of the inner wall of the crucible, vaporization of the fusible brass plug, ablation of concrete in the cavity and structures, and oxidation of metallic debris. Thus, despite the careful duplication of the initial thermite charge, the different amounts of debris collected from the melt generator and from the vessel result in some uncertainty in the actual amount and composition of melt injected into the vessel. The majority of our MELCOR analyses simply specified the original thermite charge mass, neglecting both the retention of any debris in the melt generator and the addition of any debris due to melting, vaporization, ablation, and/or oxidation. To determine the effect of the injection mass source uncertainty, calculations were done varying the melt mass. As would be expected, the vessel pressurization increases slightly as more melt mass is injected during the HPME; there is also a small increase in both hydrogen production and combustion with increasing melt injection amount, and a small increase in subcompartment temperature.

Sensitivity studies varying the debris temperature showed, as would be expected, that increasing debris temperature increases the vessel pressures calculated, but has very little effect on either the amounts of hydrogen generated or burned. The debris temperature variation has the strongest effect on the subcompartment temperatures predicted, with a 1000K increase in debris temperature producing a $\sim$500K increase in subcompartment peak temperatures.

The MELCOR FDI/HPME/DCH model does not model transient transport of debris into and through the system, but instead immediately places the debris at its ultimate destination. The debris fractions placed in each control volume and on each heat structure are controlled solely by user input. In these IET analyses, the debris injected was all placed in various control volume atmospheres and then allowed to settle out onto floor

heat structures; no debris was specified to be deposited directly onto any heat structures. The debris distribution was kept the same in our MELCOR input for all tests analyzed, because there were only small differences in the test data debris distributions.

However, in most plant analyses, there will be no equivalent data set providing guidance on HPME melt distribution. To evaluate the effect of the debris distribution assumed on the overall DCH behavior calculated, calculations were done in which the experimental debris distribution for each test was used, and in which most of the debris was placed either in the cavity and chute or in the dome. The major difference is seen for the calculation with most of the debris specified to go into the vessel dome, a volume with a longer characteristic settling time (proportional to the volume height), which allows more time for oxidation and especially for heat transfer from airborne debris to the atmosphere; assuming most of the debris goes to the dome results in much less hydrogen production calculated for most of the tests because then most of the debris is oxidized by the relatively large amount of free oxygen available in the dome.

The effects of varying the characteristic debris interaction times were also investigated. With a very long characteristic airborne debris oxidation time, the overall pressurization, and both the hydrogen production and combustion, are all underpredicted. Using shorter characteristic airborne debris oxidation times ($\leq$0.1s) gives generally similar results because in all these cases the oxidation is mostly limited by the availability of oxygen and/or steam. As would be expected, control volume temperatures are affected most by varying the airborne debris characteristic heat transfer time; the control volume atmosphere temperatures increase as the airborne debris characteristic heat transfer time is shortened; the vessel pressurization also increases, and there is decreasing hydrogen production and combustion. The effect of increasing the airborne debris characteristic settling time is to increase the vessel pressures and temperatures calculated, as well as the amount of hydrogen both produced and burned, because this increases the available time for both oxidation and heat transfer to occur.

After work on these analyses had been in progress for some time, we became concerned about the interaction of debris with heat structures. In the original HPME model added to MELCOR, any debris immediately deposited onto a heat structure or later settled onto a heat structure essentially left the problem; there was no subsequent interaction of any kind for that debris, except for decay heating of the structure surface. This was identified as a major potential problem area, especially given MELCOR's emphasis on mass and energy conservation. For example, the lack of any thermal interaction of debris with structures could adversely affect the ability to correctly predict late-time revaporization of volatile fission products. Also, the lack of any oxidation of deposited debris meant that the total amount of hydrogen producable during HPME was very highly dependent on the user-specified initial debris distribution and on the characteristic settling time constants – any debris deposited or settled could not continue to generate hydrogen through further oxidation, regardless of oxygen and/or steam availability or debris temperature and/or amount. Therefore two effects were added to the original HPME model: heat transfer to the structure surface from deposited hot debris, and the continued oxidation of the deposited debris. The heating of the structure surface by deposited hot debris

is controlled by a heat transfer coefficient adjustable through sensitivity coefficient input, and the continued oxidation of the deposited debris is controlled by a user-input structure oxidation characteristic time (distinct from and usually much longer than the characteristic time input for oxidation of airborne debris). With these input and coding modifications, HPME debris deposited on structures now can continue to affect the overall system response through several potential interactions.

In these IET experiment analyses, there was generally little effect on either the peak or the long-term pressurization as the deposited debris characteristic oxidation time was varied. The total amount of hydrogen generated increased as the characteristic oxidation time for deposited debris decreased, as would be expected, because more hydrogen accumulates late in the transient as the debris settled and/or deposited onto structures continues to oxidize. There was little effect seen on the amount of hydrogen burned, however, because the hydrogen combustion primarily occurs early in the transient, on a time scale of a few seconds or less, as the airborne debris provides an ignition source during the high-pressure melt ejection.

Much of this "lack of effect" of deposited debris oxidation is probably due to the fact that the values of most of the other input parameters used in the MELCOR input were set in earlier sensitivity study calculations, before this effect was included in the MELCOR FDI/HPME/DCH model. A longer characteristic interaction time constant for oxidation of airborne debris (which would probably be more reasonable on physical grounds) would have left more debris unoxidized during the first few seconds of the transient and thus would allow more oxidation of deposited debris later in the transient. Oxidizing less airborne debris within the first few seconds and more deposited debris later in the transient could also potentially allow both high enough hydrogen generation and combustion and low enough vessel pressurization and subcompartment temperatures to match the measured test data, without requiring as large an increase in heat transfer to structures early in the transient.

Several counterpart tests to the IET direct containment heating experiments done at Sandia in the 1:10 linear scale Surtsey facility were performed at ANL in the 1:40 linear scale COREXIT facility, in an experimental program to investigate the effects of scale on DCH phenomena. The results of the 1:40-scale IET experiment MELCOR simulations were generally inconclusive. The vessel pressures predicted in our SNL and ANL counterpart-test calculations were quite similar when both the geometry and the characteristic interaction times in the FDI HPME input were scaled, but the test data showed a number of non-scaled effects. In particular, the results of both our limited review of the facility and data scalability and of our ANL test simulations suggest that, in the experiments, the DCH energy-transfer efficiency is greater at smaller scale, that there is less pressurization due to hydrogen combustion at smaller scale, and that there appears to be a greater effect of pre-existing hydrogen in the ANL 1:40-scale tests than in the counterpart SNL 1:10-scale tests. These scale-dependent differences are not reproduced in the corresponding MELCOR analyses. Other sensitivity studies indicated that some of the greater pressurization due to DCH at small scale observed in the experiments but "missing" in our MELCOR calculations may be due to differences in heat transfer to

structures at smaller compared to larger scale, that the pressure dropoff rate in the ANL data clearly would be matched better by assuming a recirculation flow area greater than the 10% value assumed in the SNL experiment analyses, and that the data for those tests in which hydrogen combustion occurred could not be matched by using the same, non-default hydrogen burn package input that gave good agreement with test data for the 1:10-scale test simulations.

The reference MELCOR calculations for the 1:10 linear scale IET experiments done in the Surtsey vessel have been compared to similar calculations done with the CONTAIN code, when available. The CONTAIN DCH model is quite different from the MELCOR FDI/HPME DCH model, being a more detailed, more mechanistic treatment rather than a more parametric approach. Despite these differences, the results obtained with the two code models are generally quite similar: in particular, a pressure rise of $\leq$100kPa was calculated by both for tests with no significant hydrogen combustion, and a larger pressure rise of $\sim$200-250kPa for cases with substantial hydrogen burn.

Several calculations have been done to identify whether any numeric effects exist in our DCH IET assessment analyses, producing either differences in results on different machines or differences in results when the time step used is varied. The SNL/IET reference calculations were run, using the same code version, on an IBM RISC-6000 Model 550 workstation, on an HP 755 workstation, on a SUN Sparc2 workstation, on a CRAY Y-MP8/864, and on a 50MHz 486 PC. There is generally excellent agreement among results generated on these various hardware platforms. The SUN and PC were always slowest in run time required; the IBM, HP and Cray were all significantly faster with the HP the fastest for these analyses. In addition, otherwise identical MELCOR SNL/IET calculations were run on a SUN Sparc2 workstation with both the user-input maximum allowed time step and the initial time step size for HPME initiation simultaneously reduced by factors of 2, 10, 20 and 100 from the basecase values. The results showed about half of the SNL/IET experiment analyses fully converged for all these time steps, with the other half demonstrating convergence with reduced time steps.

Bibliography

[1] R. M. Summers *et al.*,"MELCOR 1.8.0: A Computer Code for Severe Nuclear Reactor Accident Source Term and Risk Assessment Analyses", NUREG/CR-5531, SAND90-0364, Sandia National Laboratories, January 1991.

[2] C. D. Leigh, ed.,"MELCOR Validation and Verification - 1986 Papers", NUREG/CR-4830, SAND86-2689, Sandia National Laboratories, March 1987.

[3] L. N. Kmetyk, "MELCOR 1.8.1 Assessment: LACE Aerosol Experiment LA4", SAND91-1532, Sandia National Laboratories, September 1991.

[4] L. N. Kmetyk, "MELCOR 1.8.1 Assessment: FLECHT SEASET Natural Circulation Experiments", SAND91-2218, Sandia National Laboratories, December 1991.

[5] L. N. Kmetyk, "MELCOR 1.8.1 Assessment: ACRR Source Term Experiments ST-1/ST-2", SAND91-2833, Sandia National Laboratories, April 1992.

[6] L. N. Kmetyk, "MELCOR 1.8.1 Assessment: LOFT Integral Experiment LP-FP-2", SAND92-1273, Sandia National Laboratories, December 1992.

[7] R. J. Gross, "MELCOR 1.8.1 Assessment: PNL Ice Condenser Experiments", SAND92-2165, Sandia National Laboratories, June 1993.

[8] L. N. Kmetyk, "MELCOR 1.8.1 Assessment: Marviken-V Aerosol Transport Tests Att-2b/Att-4", SAND92-2243, Sandia National Laboratories, January 1993.

[9] T. J. Tautges, "MELCOR 1.8.2 Assessment: the DF-4 BWR Fuel Damage Experiment", SAND93-1377, Sandia National Laboratories, October 1993.

[10] M. D. Allen, M. Pilch, R. O. Griffith, R. T. Nichols, T. K. Blanchat, "Experiments to Investigate the Effects of 1/10th Scale Zion Structures on Direct Containment Heating (DCH) in the Surtsey Test Facility: the IET-1 and IET-1R Tests", SAND92-0255, Sandia National Laboratories, July 1992.

[11] M. D. Allen, T. K. Blanchat, M. Pilch, R. T. Nichols, "Quick-Look Report on the Second Integral Effects Test (IET-2): Thermite Temperature Measurements", Sandia National Laboratories, preliminary report, June 1992.

[12] M. D. Allen, M. Pilch, R. O. Griffith, D. C. Williams, R. T. Nichols, "The Third Integral Effects Test (IET-3) in the Surtsey Test Facility", SAND92-0166, Sandia National Laboratories, March 1992.

[13] M. D. Allen, T. K. Blanchat, M. Pilch, R. T. Nichols, "Results of an Experiment in a Zion-like Geometry to Investigate the Effect of Water on the Containment Basement Floor on Direct Containment Heating (DCH) in the Surtsey Test Facility: the IET-4 Test", SAND92-1241, Sandia National Laboratories, September 1992.

[14] M. D. Allen, T. K. Blanchat, M. Pilch, R. T. Nichols, "Experimental Results of an Integral Effects Test in a Zion-like Geometry to Investigate the Effect of a Classically Inert Atmosphere on Direct Containment Heating: the IET-5 Test", SAND92-1623, Sandia National Laboratories, November 1992.

[15] M. D. Allen, T. K. Blanchat, M. Pilch, R. T. Nichols, "An Integral Effects Test in a Zion-like Geometry to Investigate the Effects of Pre-Existing Hydrogen on Direct Containment Heating in the Surtsey Test Facility: the IET-6 Experiment", SAND92-1802, Sandia National Laboratories, January 1993.

[16] M. D. Allen, T. K. Blanchat, M. Pilch, R. T. Nichols, "An Integral Effects Test to Investigate the Effects of Condensate Levels of Water and Preexisting Hydrogen on Direct Containment Heating in the Surtsey Test Facility: the IET-7 Experiment", SAND92-2021, Sandia National Laboratories, January 1993.

[17] M. D. Allen, T. K. Blanchat, M. Pilch, R. T. Nichols, "Experiments to Investigate the Effects of Fuel/Coolant Interactions on Direct Containment Heating (The IET-8A and IET-8B Experiments)", SAND92-2849, Sandia National Laboratories, February 1993.

[18] J. L. Binder, L. M. McUmber, B. W. Spencer, "Quick Look Data Report on the Integral Effects Test 1R in the COREXIT Facility at Argonne National Laboratory, LWR-92-2, Argonne National Laboratory, May 1992 (draft).

[19] J. L. Binder, L. M. McUmber, B. W. Spencer, "Quick Look Data Report on the Integral Effects Test 1RR in the COREXIT Facility at Argonne National Laboratory, LWR-92-3, Argonne National Laboratory, May 1992 (draft).

[20] J. L. Binder, L. M. McUmber, B. W. Spencer, "Quick Look Data Report on the Integral Effects Test 2 in the COREXIT Facility at Argonne National Laboratory, LWR-92-1, Argonne National Laboratory, February 1992 (draft).

[21] J. L. Binder, L. M. McUmber, B. W. Spencer, "Quick Look Data Report on the Integral Effects Test 3 in the COREXIT Facility at Argonne National Laboratory, ANL/RE/LWR 92-7, Argonne National Laboratory, July 1992 (draft).

[22] J. L. Binder, L. M. McUmber, B. W. Spencer, "Quick Look Data Report on the Integral Effects Test 6 in the COREXIT Facility at Argonne National Laboratory, ANL/RE/LWR 92-8, Argonne National Laboratory, August 1992 (draft).

[23] J. L. Binder, L. M. McUmber, B. W. Spencer, "Quick Look Data Report on the Integral Effects Test 7 in the COREXIT Facility at Argonne National Laboratory, ANL/RE/LWR 92-9, Argonne National Laboratory, September 1992 (draft).

[24] J. L. Binder, L. M. McUmber, B. W. Spencer, "Quick Look Data Report on the Integral Effects Test 8 in the COREXIT Facility at Argonne National Laboratory, ANL/RE/LWR 92-10, Argonne National Laboratory, October 1992 (draft).

[25] R. C. Smith, "MELCOR Direct Containment Heating Model", letter report to R. B. Foulds (NRC), Sandia National Laboratories, February 10, 1992.

[26] MELCOR Code Development Group, "Fuel Dispersal Interactions (FDI) Package Reference Manual", Sandia National Laboratories, August 26, 1993.

[27] D. C. Williams, "Pretest Calculations for the First Integral Effects Experiment (IET-1) at the Surtsey and CWTI DCH Experimental Facilities (Rev.1)", letter report to A. Notafrancesco (NRC), Sandia National Laboratories, August 23, 1991.

[28] D. C. Williams, "Pretest Calculation for IET-1B", memo to M. D. Allen, Sandia National Laboratories, January 30, 1992.

[29] D. C. Williams, "Posttest Calculations for the First Integral Effects Experiment (IET-1) at the Surtsey DCH Facility", letter report to A. Notafrancesco (NRC), Sandia National Laboratories, January 22, 1992.

[30] D. C. Williams, letter to A. Notafrancesco (NRC), Sandia National Laboratories, March 3, 1992.

[31] D. C. Williams, "IET-3 Pretest Calculations", memo to M. D. Allen, Sandia National Laboratories, December 24, 1991.

[32] D. C. Williams, "Summary of CONTAIN Pretest Calculations for the IET-5 Experiment in the Surtsey DCH Experimental Facility", letter to A. Notafrancesco (NRC), Sandia National Laboratories, May 13, 1992.

[33] D. C. Williams, "Summary of CONTAIN Calculations Examining Scale Effects in Direct Containment Heating (DCH) Scenarios", letter to A. Notafrancesco (NRC), Sandia National Laboratories, May 4, 1992.

[34] D. C. Williams, "MELCOR DCH Assessment Report", Sandia National Laboratories memo to L. N. Kmetyk, August 17, 1993.

[35] Private communication from R. C. Smith, MELCOR Development Group, Sandia National Laboratories, August 31, 1993.

[36] M. M. Pilch, M. D. Allen, J. L. Binder, "Counterpart and Replicate DCH Experiments Conducted at Two Different Physical Scales: the SNL/IET-1,1R and the ANL/IET-1R,1RR Experiments", Sandia National Laboratories, draft report (dated July 15, 1992).

[37] B. E. Boyack, V. K. Dhir, J. A. Gieseke, T. J. Haste, M. A. Kenton, M. Khatib-Rahbar, M. T. Leonard, R. Viskanta, "MELCOR Peer Review", LA-12240, Los Alamos National Laboratory, March 1992.

[38] D. C. Williams, "Proposed Assessment Approach for the CONTAIN DCH Models", presented at the CONTAIN Peer Review meeting, Albuquerque, August 23-25, 1993.

[39] D. C. Williams, "MELCOR-CONTAIN Comparisons", Sandia National Laboratories memo to L. N. Kmetyk, September 1, 1993.

[40] L. N. Kmetyk, "MELCOR 1.8.2 Assessment: Surry PWR TMLB' (with a DCH Study)", SAND93-1899, Sandia National Laboratories, to be published.

A MELCOR FDI package HPME/DCH Model (excerpted from [27])

The Fuel Dispersal Interactions (FDI) package in MELCOR calculates the behavior of debris in containment from the time it is ejected from a failed reactor pressure vessel until the time it is deposited in a cavity. Both low pressure melt ejection (LPME) from the reactor vessel and high pressure melt ejection (HPME) from the reactor vessel (direct containment heating) are modelled.

The FDI package becomes active whenever debris material enters the package via the MELCOR Transfer Process (TP) package interface. Debris material typically enters the TP package in one of three ways. In a reactor plant accident calculation debris enters the TP package from the core (COR) package after failure of the reactor pressure vessel has been calculated. In a stand-alone direct containment heating (DCH) calculation debris material is sourced into the TP package from either tabular function user input or a user source file via the external data file (EDF) package interface of MELCOR.

After the introduction of debris material, the FDI package classifies the ejection event as either a low or a high pressure melt ejection event on the basis of the ejection velocity passed through the TP package or a flag set by the user for stand-alone DCH calculations.

If the velocity of the molten debris ejected from the reactor vessel exceeds a critical value prescribed by sensitivity coefficient 4602 (default value of10 m/s), or if the user has invoked the stand-alone option for high pressure melt ejection modeling, then the fuel dispersal interactions will be treated by the high pressure model instead of the low pressure model. The parametric high pressure model requires user input to control both the distribution of debris throughout the containment and the interaction of the hot debris with the containment atmosphere.

The HPME model does not include a mechanistic debris transport model; rather, the user specifies a set of debris destinations with a corresponding set of transport fractions that prescribe where the ejected debris is assumed to go. The debris destinations may include the atmosphere of any CVH control volume, the surface of any heat structure and cavities defined by the CAV package. The sum of the transport fractions over all the specified control volume atmospheres, heat structure surfaces and cavities must equal one. Transport of the ejected debris to its assumed destinations occurs instantaneously with no interactions occuring between the point of ejection and the destination sites. As long as the HPME model is active (i.e. as long as the ejection velocity exceeds the LPME/HPME transition velocity prescribed by sensitivity coefficient 4602 or if the user has invoked the stand-alone HPME model) the ejected debris will be partitioned among the destinations as specified by the transport fractions. When the ejection velocity falls below the LPME/HPME transition velocity for non-stand-alone applications, any debris subsequently ejected is passed to the LPME model, which uses LPME model input instead of the HPME transport model to determine the debris destination. However, debris that was transported to the HPME debris destinations before the model transition occured will continue to be treated by the HPME model.

The processes modeled include oxidation of the metallic components of the debris in both steam and oxygen, surface deposition by debris trapping or airborne-debris settling and heat transfer to the atmosphere and heat structure surfaces. However, debris which is transported to cavity destinations is not treated further by the FDI package; rather, subsequent treatment is provided by the CAV package. As implemented in the HPME model, surface deposition of debris can occur in two distinct ways. Ejected debris which impacts structures prior to any significant interaction with the atmosphere is sourced directly to the destination surface via the user-specified transport fraction for that surface. This process is referred to as trapping in MELCOR. Alternatively, debris which interacts significantly with the atmosphere should be sourced to the appropriate control volume, in which a user-specified settling time constant will determine the rate of deposition to the specified settling destination (either a heat structure surface or a cavity). This process is referred to as settling in MELCOR.

First order rate equations with user specified time constants for oxidation, heat transfer and settling are used to determine the rate of each process. Oxidation of airborne and deposited debris is only calculated if the debris temperature exceeds a value, $TOXMIN$, which is adjusted using sensitivity coefficient 4609 and has a default value of 600K. If a pool of water exists in the reactor cavity at the time of debris ejection, then the model ejects the water into the droplet field (fog) of the atmosphere at a rate proportional to the rate of injection of the debris into the pool. The proportionality constant is adjustable through sensitivity coefficient 4605 and has a default value of 10. When the HPME model first initiates direct containment heating in a control volume, the FDI package requests a fallback of the cycle if the time step exceeds the recommended start-up value prescribed by sensitivity coefficient 4607 (with a default value of 10^{-4}s). Experience has indicated that for most realistic scenarios the rapid excursions in pressure and temperature caused by direct containment heating dictate the use of very small time steps for several cycles following DCH initiation.

Airborne Debris

The airborne masses of UO_2 and other materials that neither oxidize nor are the products of oxidation are described by the following first order linear differential equation:

$$\frac{dM(i,k,t)}{dt} = -\frac{M(i,k,t)}{T_{ST}(i)} + S(i,k) \tag{A.1}$$

where $M(i,k,t)$ is the mass of component k in control volume i at time t, $TST(i)$ is the time constant for settling or trapping in control volume i and $S(i,k)$ is the constant mass source rate of component k in control volume i associated with the high pressure melt ejection process. The solution of Eq. A.1 is given by:

$$M(i,k,t) = [M(i,k,t_0) - S(i,k) \times T_{ST}(i)] \times exp\left(\frac{-dt}{T_{ST}(i)}\right) + S(i,k) \times T_{ST}(i) \tag{A.2}$$

where $M(i,k,t_0)$ is the mass at arbitrary initial time t_0, and dt is the difference between the final time, t, and time t_0. The airborne masses of Zr, Fe and other materials that are oxidized in the presence of oxygen or steam are described by the following first order linear differential equation:

$$\frac{dM(i,k,t)}{dt} = -\frac{M(i,k,t)}{T_{SO}(i)} + S(i,k) \tag{A.3}$$

where $T_{SO}(i)$, the time constant for simultaneous oxidation and settling/trapping, is given by:

$$\frac{1}{T_{SO}(i)} = \frac{1}{T_{ST}(i)} + \frac{1}{T_{OX}(i)} \tag{A.4}$$

where $T_{OX}(i)$ is the oxidation time constant in control volume i. The solution to Eq. A.3 is identical to Eq. A.2 except that $T_{ST}(i)$ is replaced by $T_{SO}(i)$. The airborne masses of ZrO_2 and other materials that are products of oxidation reactions are given by:

$$\frac{dM(i,k,t)}{dt} = -\frac{M(i,k,t)}{T_{ST}(i)} + R \times \frac{M(i,l,t)}{T_{OX}(i)} + S(i,k) \tag{A.5}$$

where R is the mass of product k formed by the oxidation of a unit mass of reactant l. The solution of Eq. A.5 is:

$$M(i,k,t) = [M(i,k,t_0) - C_1 - C_2] \times exp\left(\quad \right) + C_2 \times exp\left(\frac{-dt}{T_{SO}(i)}\right) + C_1 \tag{A.6}$$

where

$$C_1 = \left[\frac{S(i,k) + R \times S(i,l) \times T_{SO}(i)}{T_{OX}(i)}\right] \times T_{ST}(i)$$

and

$$C_2 = [R \times S(i,l) \times T_{SO}(i)] - M(i,l,t_0)$$

The HPME model contains two options for oxidation modeling. The user invokes the sequential oxidation option, in which the order of oxidation is Zr, Al then steel, by specifying a positive value for the oxidation time constant, $T_{OX}(i)$. For control volumes in which the user would prefer simultaneous oxidation of the metals, a negative value of $T_{OX}(i)$ is specified and the time constant will be equal to the absolute value of $T_{OX}(i)$. In the sequential oxidation model a separate oxidation rate is first calculated for each metal independently of all others with the given value of $T_{OX}(i)$. Then the mass of metal

B consumed will be converted into an equivalent mass of metal A, where metal A is assumed to oxidize in preference to metal B, until all of metal A is consumed. Hence, steel will not be consumed until all the Zr and Al have been consumed, and Al will not be consumed until the Zr is exhausted. This implies that the effective time constant for metal A oxidation when metal B is present may be significantly shorter than tau_{ox}(i). The actual values of the effective oxidation time constants will be used in determining the end of time step airborne mass inventories in Eq. A.2 and Eq. A.6 above. Of course both oxidation options are constrained by the availability of oxygen or steam. Steam oxidation will only be calculated if there is insufficient oxygen available in the control volume to support the prescribed oxidation rate. If there is insufficient oxidant to support the calculated rates of oxidation for zirconium and iron, then the zirconium will have first priority. The oxidation reactions will proceed at the initial time step values of debris temperature in each control volume, and hydrogen formed by the steam reaction will enter the atmosphere at that temperature.

The energy of the airborne debris is given by the solution of the following simple equation:

$$\frac{dH(i,t)}{dt} = \dot{E}_{OX}(i,t) - \dot{Q}_{GAS}(i,t) + S_H(i) \tag{A.7}$$

where $\dot{E}_{OX}(i,t)$ is the rate of heat generation by the oxidation reaction, $S_H(i)$ is the enthalpy source rate associated with the high pressure melt ejection source, and where the rate of heat transfer to the gas is approximated as:

$$\dot{Q}_{GAS}(i,t) = \frac{Q_g(i,t)}{T_{HT}(i)} = \frac{H(i,T_{dbr}) - H(i,T_{gas})}{T_{HT}(i)} \tag{A.8}$$

where $Q_g(i,t)$ is the energy available for transfer to the gas, where $T_{HT}(i)$ is the user specified time constant for heat transfer from the airborne debris to the atmosphere in control volume i, where $H(i,T_{dbr})$ is the energy content of the debris at its actual temperature, T_{dbr}, and $H(i,T_{gas})$ is the energy content of the debris in equilibrium with the gas at temperature, T_{gas}. The solution to Eq. A.7 is given by:

$$H(i,t) = H(i,t_0) + E_{OX}(i,t) - Q_{GAS}(i,t) \tag{A.9}$$

where $H(i,t_0)$ is the energy of the debris following the addition of the integrated enthalpy source, $S_H(i) \times dt$, and following adjustments to its composition associated with the oxidation reaction, where $E_{OX}(i,t)$ is the oxidation energy generated between times t_0 and t and where $Q_{GAS}(i,t)$ is the amount of heat transferred to the gas between times t_0 and t. QGAS(i,t) is given by:

$$Q_{GAS}(i,t) = \int_{t_0}^{t_0+dt} \left[\frac{Q_g(i,t)}{T_{HT}(i)}\right] dt \tag{A.10}$$

where $Q_g(i,t)$ satisfies:

$$\frac{dQ_g(i,t)}{dt} = -\frac{Q_g(i,t)}{T_{HT}(i)} + \left[Q_{SRC} + \frac{(E_{OX} + Q_{OX})}{dt}\right] \tag{A.11}$$

$$Q_{SRC} = S_H(i, T_{src}) - S_H(i, T_{gas})$$

is the available source enthalpy and

$$Q_{OX} = H_{OX}(i, T_{dbr}) - H_{OX}(i, T_{gas})$$

is the available enthalpy created by composition adjustments during oxidation. The solution to Eqs. A.10 and A.11 is:

$$\begin{aligned} Q_{GAS}(i,t) \;=\; & Q_{OLD} \times \left[1 - exp\left(\frac{-dt}{T_{HT}}\right)\right] + \\ & \left[Q_{SRC} + \frac{(E_{OX} + Q_{OX})}{dt}\right] \times \left\{dt - T_{HT} \times \left[1 - exp\left(\frac{-dt}{T_{HT}}\right)\right]\right\} \end{aligned} \tag{A.12}$$

where $Q_{OLD} = H(i, T(t_0)) - H(i, T_{gas})$ is the initial available energy.

The inclusion of the HPME source terms in Eqs. A.1 through A.12 eliminates time-step dependencies that would arise if the sources were added prior to the calculation of oxidation, heat transfer and settling/trapping. After the total energy at the advanced time, t, is determined, it is compared to the enthalpy corresponding to a maximum permissible temperature, H_{MAX}. If $H(i,t)$ exceeds H_{MAX}, then Eq. A.9 is solved for $Q_{GAS}(i,t)$ with $H(i,t)$ set equal to HMAX as follows:

$$Q_{GAS}(i,t) = H(i,t_0) + E_{OX}(i,t) - H_{MAX} \tag{A.13}$$

so that the heat transferred to the gas is increased sufficiently to limit the advanced time debris temperature to the maximum prescribed value, T_{MAX}. T_{MAX} is given by:

$$T_{MAX} = MAX(T_{gas}, T_{dbr}(t_0), T_{dbr}(t'), T4603) \tag{A.14}$$

where T_{gas} is the gas temperature, $T_{dbr}(t_0)$ is the debris temperature at the beginning of the time step, $T_{dbr}(t')$ is the debris temperature after addition of new source material to the initial inventory and $T4603$ is the temperature limit prescribed by sensitivity coefficient 4603, which normally exceeds the other arguments in the max function of Eq. A.14. The default value of T4603 is approximately equal to the boiling temperature

of UO_2 – temperatures much in excess of this value would likely result in very rapid fragmentation of debris droplets and significantly increased droplet-to-gas heat transfer.

After an advanced time temperature for the airborne debris has been determined, the projected change in the CVH atmosphere temperature as a result of direct containment heating during the time step is calculated. If the change exceeds a value prescribed by sensitivity coefficient 4604 (with a default value of 500K), then the FDI package requests a fallback with a decreased time step.

Following the determination of the advanced time temperature for the airborne debris, the advanced time mass equations, Eqs. A.1 through A.6, are used to determine how much material is removed from the atmosphere by settling/trapping. The settled material and its energy content are removed from the airborne inventory and deposited on the appropriate surface specified by user input. After the settling calculation has been performed, the advanced time total airborne mass in each control volume is determined by summing over all components. If the advanced time total airborne mass is insignificant compared to the total mass of material sourced into the control volume atmosphere over the duration of the DCH event, then all of the remaining airborne mass in the control volume is immediately deposited on the appropriate settling surface and a message is issued to notify the user that direct containment heating has ceased in that particular control volume. The ratio used to determine when the airborne mass has become insignificant is adjustable through sensitivity coefficient 4606 and has a default value of 0.001.

Deposited Debris

The mass of material k on surface i at time t is given by

$$M(i,k,t) = M(i,k,t_0) + S'(i,k) \times dt \tag{A.15}$$

where

$$S'(i,k) = S(i,k) + \sum_j \left[\int_{t_0}^{t_0+dt} \frac{M(j,k,t')}{T_{ST}(j)} \times dt' \right] / dt \tag{A.16}$$

and $S(i,k)$ is the constant mass source rate of component k to surface i from trapping. The second term on the right hand side of Eq. A.16 accounts for settling to the surface, and the sum is over all control volumes that have surface i as the user-specified settling surface. $M(j,k,t)$ and $T_{ST}(j)$ are the airborne mass of component k in control volume j and the settling time constant in control volume j, respectively.

For UO_2 and other materials not associated with oxidation the settling term is given by

$$\begin{aligned} \int_{t_0}^{t_0+dt} \frac{M(j,k,t')}{T_{ST}(j)} dt' &= M(j,k,t_0) \times \left[1 - exp\left(\frac{-dt}{T_{ST}(j)} \right) \right] + \\ & S(j,k) \times \left\{ dt - T_{ST}(j) \left[1 - exp\left(\frac{-dt}{T_{ST}(j)} \right) \right] \right\} \end{aligned} \tag{A.17}$$

For metals that oxidize the settling term is given by

$$\int_{t_0}^{t)0+dt} \frac{M(j,k,t')}{T_{ST}(j)}dt' = \left[\frac{T_{SO}(j)}{T_{ST}(j)}\right] \times \left\{ M(j,k,t_0) \times \left[1 - exp\left(\frac{-dt}{T_{SO}(j)}\right)\right] + S(j,k)\left[dt - T_{SO}(j)\left\{1 - exp\left(\frac{-dt}{T_{SO}(j)}\right)\right\}\right] \right\} \quad \text{(A.18)}$$

which reduces to Eq. A.17 if $T_{OX}(j) >> T_{ST}(j)$, because in that case $T_{SO}(j) \sim T_{ST}(j)$ as shown by Eq. A.4. For oxidation products the settling term is given by

$$\begin{aligned}\int_{t_0}^{t_0+dt} \frac{M(j,k,t')}{T_{ST}(j)}dt' = {} & M(j,k,t_0) \times \left[1 - exp\left(\frac{-dt}{T_{ST}(j)}\right)\right] + \\ & S(j,k)\left\{dt - T_{ST}(j)\left[1 - exp\left(\frac{-dt}{T_{ST}(j)}\right)\right]\right\} + \\ & R\left\{ \left[\frac{T_{SO}(j)}{T_{OX}(j)}\right][M(j,l,t_0) + S(j,l)\{dt - TSO(j) - T_{ST}(j)\}] - \right. \\ & [M(j,l,t_0) - S(j,l)T_{ST}(j)]exp\left(\frac{-dt}{T_{ST}(j)}\right) + \left[\frac{T_{SO}(j)}{T_{ST}(j)}\right] \times \\ & \left. [M(j,l,t_0) - S(j,l)T_{SO}(j)] \times exp\left(\frac{-dt}{T_{SO}(j)}\right) \right\} \quad \text{(A.19)}\end{aligned}$$

where material l is the metal from which the oxide is formed and R is the mass of product k formed by the oxidation of a unit mass of reactant l.

The energy of the deposited debris is calculated with equations almost identical to Eqs. A.7-A.14 except the source term $S_H(i)$ also includes the enthalpy associated with debris settling. It is assumed that the enthalpy of the settled debris is equal to the end of time step value calculated with Eq. A.9. The settled mass with the end of step enthalpy is applied to the deposition surface during the time step at a constant rate as implied by Eq. A.15. The other difference between the treatment of the energy of airborne and deposited debris concerns heat transfer. As discussed above, the user specifies a time constant for heat transfer from the airborne debris to the atmosphere. However, for heat transfer from deposited debris to the structure a different approach is taken. Because the CVH package does not recognize the deposited debris temperature as the effective surface temperature, in order to effectively simulate the heat transfer from the hot debris to the CVH pool and/or atmosphere associated with the surface it is necessary to tightly couple the debris temperature to the HS surface temperature that CVH does recognize. Accordingly, a very small time constant equal to the minimum of half the surface oxidation time constant and a value of .001s is used to calculate the amount of heat transfer from the debris to the deposition surface using the analog of Eq. A.12 for heat transfer to surfaces. The value obtained is then used to determine the average heat

transfer coefficient between the deposited debris and the surface during the time step as follows.

$$h_{SURF} = \frac{Q_{SURF}(i,t)}{A_{SURF} \times \Delta T \times dt} \tag{A.20}$$

where A_{SURF} is the surface area of the structure, ΔT is the difference between the beginning of time step debris temperature and the structure surface temperature and QSURF is the value obtained from the analog of Eq. A.12. If h_{SURF} exceeds a maximum value, $h_{SURF,max}$, specified by sensitivity coefficient 4608 (default value 1000W/m^2-K), then the value of Q_{SURF} is reduced by the ratio $h_{SURF}, max/h_{SURF}$ to limit it to the value consistent with $h_{SURF,max}$. Whenever the Q_{SURF} is limited by $h_{SURF,max}$ the direction of heat transfer (i.e. debris-to-surface or surface-to-debris) is compared to the direction from the previous time step; if the direction is alternating, that indicates that the surface temperature has probably been driven into an oscillation about the debris temperature because the time step exceeds the stability limit associated with the explicit coupling between the FDI and HS packages. In such cases, FDI requests a system fallback with the time step reduced by a factor of one half. Normally, the value of $h_{SURF,max}$ should be chosen large enough to promote rapid equilibration of the debris and surface temperatures, yet not so large as to induce instability in the surface temperature for reasonable values of the time step.

If the MELCOR Radionuclide (RN) package is active, then FDI will call RN1 anytime fuel is moved so that the associated radionuclides can be moved simultaneously. Furthermore, the decay heat associated with the radionuclides will be deposited in the appropriate location.

Specified time constants of less than 10^{-6}s will be reset to that value to avoid potential numerical problems associated with vanishing time constants. For time scales of interest, a time constant of 10^{-6}s implies an essentially instantaneous process (*i.e.*, instantaneous complete oxidation, instantaneous thermal equilibration with the atmosphere or instantaneous settling).

The simple direct containment heating model described above is not intended to predict all details of DCH events from first principles. Nodialization requirements would be much greater than normal MELCOR models. Rather, it is intended to allow users to evaluate the overall effect of varying the relative rates of the most important processes controlling DCH loads. HPME model results are sensitive to the relative values of tau_{ox}(i), tau_{ht}(i) and tau_{set}(i) specified by the user for each control volume. Reasonable values for these time constants can be obtained in basically two ways. First, results from mechanistic codes such as CONTAIN can be used to obtain appropriate values; or, second, reasonable assumptions concerning particle sizes and velocities in conjunction with simplified hand calculations can yield a range of time constants in the correct range. In most cases this second method should be adequate for parametric PRA studies.

B SNL/IET-1 Reference Calculation Input Deck

```
*
*eor* melgen
*
allowreplace
*
*******************************************************************************
*
title     'Surtsey IET-1'
*
*******************************************************************************
*
diagfile     'gen1.dia'
outputfile   'gen1.out'
plotfile     'plot1'
restartfile  'restart1'
*
*******************************************************************************
*
*  common input
*
*******************************************************************************
*
*******************************************************************************
*
*  burn package input
*
*******************************************************************************
*
bur000    0  * activate package
bur001 0.0 0.167 0.07 0.129 0.05 0.55 0.0 0.167 0.05 0.55
*bur003  1.0e-6  0.148  1.0e-6  0.125  1.0e-6  0.138  1.0e-6  0.150
burcc00  -1  -1  0.0  -1  0.0
bur100  010  86
bur101  020  86
bur102  030  86
*
*******************************************************************************
*
*  non-condensible gas input
*
*******************************************************************************
*
ncg000    n2    4
ncg001    o2    5
ncg002    h2    6
ncg003    co2   7
ncg004    co    8
ncg005    ar    9
*
*******************************************************************************
*
```

```
*  control volume and flow path
*
*************************************************************************
*
*
cv00100  accum-mg  2  2  1   * nonequil therm, vertical flow
cv001a0  3
cv001b1  0.50  0.0
cv001b2  1.50  0.308
*
fl00500  melt-plug  001  010  0.975  0.3048
fl00501  0.001282  0.1  0.0  0.10  0.10
fl00503  2.5  2.5  0.85  0.85
fl00504  0.0  0.0
fl005s1  0.001282  0.1  0.0404  16.0
fl005v1  -1  005  005
cf00500  'plug'  tab-fun  1  1.0  0.0
cf00501  0.0
cf00503  005
cf00510  1.0  0.0  time
tf00500  'plug'  2  1.0  0.0
tf00510   0.0  0.0
tf00511   2.0  1.0
*
cv01000  cavity  2  1  1   * nonequil therm, horizontal flow
cv01003  0.02
cv010a0  3
cv010b1  0.0     0.0
cv010b2  0.3048  0.100
*
fl01500  chute-inlet  010  020  0.1524  0.1524
fl01501  0.0929  2.4  1.0  0.290  0.290
fl01503  0.5  0.5
fl01504  0.0  0.0
fl015s1  0.0929  2.4  0.3048  16.0
*
cv02000  chute  2  2  1   * nonequil therm, vertical flow
cv02003  0.02
cv020a0  3
cv020b1  0.0   0.0
cv020b2  2.16  0.145
*
fl02500  chute-outlet  020  030  2.16  2.16
fl02501  0.0929  1.2  1.0  0.3048  0.76
fl02503  0.5  0.5
fl02504  0.0  0.0
fl025s1  0.0929  1.2  0.3048  16.0
fl025s2  2.7819  0.76  0.3048  16.0
*
cv03000  subcompartments  2  2  1   * nonequil therm, vertical flow
cv03003  0.025
cv030a0  3
cv030b1  2.16  0.0
```

```
cv030b2  3.68  4.65
*
fl03500  dome-inlet  030  040  3.68  3.68
fl03501  2.7819  8.25  1.0  0.76  7.5
fl03503  0.5  0.5
fl03504  0.0  0.0
fl035s1  2.7819  0.76  0.3048  16.0
fl035s2  10.125  0.76  0.3048  16.0
*
cv04000  dome  2  2  1   * nonequil therm, vertical flow
cv04003  0.1
cv040a0  3
cv040b1   2.16   0.0
cv040b2   3.68   7.54
cv040b3  12.09  85.15
*
fl04500  recirculation  040  030  9.68  2.68
fl04501  0.27819  0.75  1.0  0.75  0.75
fl04503  0.5  1.0e6
fl04504  0.0  0.0
fl045s1  0.27819  0.75  0.1048  16.0
*
*******************************************************************************
*
*  control function input
*
*******************************************************************************
*
cf01100  hydrogen  add  4  1.0  0.0
cf01110  1.0  0.0  cvh-mass.6.010
cf01111  1.0  0.0  cvh-mass.6.020
cf01112  1.0  0.0  cvh-mass.6.030
cf01113  1.0  0.0  cvh-mass.6.040
*
cf01200  al-oxid-tot  add  16  1.0  0.0
cf01210  1.0  0.0  fdi-al-oxtot.1.010
cf01211  1.0  0.0  fdi-al-oxtot.1.020
cf01212  1.0  0.0  fdi-al-oxtot.1.030
cf01213  1.0  0.0  fdi-al-oxtot.1.040
cf01214  1.0  0.0  fdi-al-sxtot.1.1.01001
cf01215  1.0  0.0  fdi-al-sxtot.1.1.01002
cf01216  1.0  0.0  fdi-al-sxtot.1.1.01003
cf01217  1.0  0.0  fdi-al-sxtot.1.1.02001
cf01218  1.0  0.0  fdi-al-sxtot.1.1.02002
cf01219  1.0  0.0  fdi-al-sxtot.1.1.02003
cf01220  1.0  0.0  fdi-al-sxtot.1.1.03001
cf01221  1.0  0.0  fdi-al-sxtot.1.1.03002
cf01222  1.0  0.0  fdi-al-sxtot.1.1.03003
cf01223  1.0  0.0  fdi-al-sxtot.1.1.04001
cf01224  1.0  0.0  fdi-al-sxtot.1.1.04002
cf01225  1.0  0.0  fdi-al-sxtot.1.1.04003
*
cf01300  ss-oxid-tot  add  16  1.0  0.0
```

```
cf01310  1.0  0.0  fdi-ss-oxtot.1.010
cf01311  1.0  0.0  fdi-ss-oxtot.1.020
cf01312  1.0  0.0  fdi-ss-oxtot.1.030
cf01313  1.0  0.0  fdi-ss-oxtot.1.040
cf01314  1.0  0.0  fdi-ss-sxtot.l.1.01001
cf01315  1.0  0.0  fdi-ss-sxtot.l.1.01002
cf01316  1.0  0.0  fdi-ss-sxtot.l.1.01003
cf01317  1.0  0.0  fdi-ss-sxtot.l.1.02001
cf01318  1.0  0.0  fdi-ss-sxtot.l.1.02002
cf01319  1.0  0.0  fdi-ss-sxtot.l.1.02003
cf01320  1.0  0.0  fdi-ss-sxtot.l.1.03001
cf01321  1.0  0.0  fdi-ss-sxtot.l.1.03002
cf01322  1.0  0.0  fdi-ss-sxtot.l.1.03003
cf01323  1.0  0.0  fdi-ss-sxtot.l.1.04001
cf01324  1.0  0.0  fdi-ss-sxtot.l.1.04002
cf01325  1.0  0.0  fdi-ss-sxtot.l.1.04003
*
cf01400  o2-oxid-tot  add  16  1.0  0.0
cf01410  1.0  0.0  fdi-o2-oxtot.1.010
cf01411  1.0  0.0  fdi-o2-oxtot.1.020
cf01412  1.0  0.0  fdi-o2-oxtot.1.030
cf01413  1.0  0.0  fdi-o2-oxtot.1.040
cf01414  1.0  0.0  fdi-o2-sxtot.l.1.01001
cf01415  1.0  0.0  fdi-o2-sxtot.l.1.01002
cf01416  1.0  0.0  fdi-o2-sxtot.l.1.01003
cf01417  1.0  0.0  fdi-o2-sxtot.l.1.02001
cf01418  1.0  0.0  fdi-o2-sxtot.l.1.02002
cf01419  1.0  0.0  fdi-o2-sxtot.l.1.02003
cf01420  1.0  0.0  fdi-o2-sxtot.l.1.03001
cf01421  1.0  0.0  fdi-o2-sxtot.l.1.03002
cf01422  1.0  0.0  fdi-o2-sxtot.l.1.03003
cf01423  1.0  0.0  fdi-o2-sxtot.l.1.04001
cf01424  1.0  0.0  fdi-o2-sxtot.l.1.04002
cf01425  1.0  0.0  fdi-o2-sxtot.l.1.04003
*
cf01500  st-oxid-tot  add  16  1.0  0.0
cf01510  1.0  0.0  fdi-st-oxtot.1.010
cf01511  1.0  0.0  fdi-st-oxtot.1.020
cf01512  1.0  0.0  fdi-st-oxtot.1.030
cf01513  1.0  0.0  fdi-st-oxtot.1.040
cf01514  1.0  0.0  fdi-st-sxtot.l.1.01001
cf01515  1.0  0.0  fdi-st-sxtot.l.1.01002
cf01516  1.0  0.0  fdi-st-sxtot.l.1.01003
cf01517  1.0  0.0  fdi-st-sxtot.l.1.02001
cf01518  1.0  0.0  fdi-st-sxtot.l.1.02002
cf01519  1.0  0.0  fdi-st-sxtot.l.1.02003
cf01520  1.0  0.0  fdi-st-sxtot.l.1.03001
cf01521  1.0  0.0  fdi-st-sxtot.l.1.03002
cf01522  1.0  0.0  fdi-st-sxtot.l.1.03003
cf01523  1.0  0.0  fdi-st-sxtot.l.1.04001
cf01524  1.0  0.0  fdi-st-sxtot.l.1.04002
cf01525  1.0  0.0  fdi-st-sxtot.l.1.04003
*
```

```
cf01600  h2-oxid-tot  add  16  1.0  0.0
cf01610  1.0  0.0  fdi-h2-oxtot.1.010
cf01611  1.0  0.0  fdi-h2-oxtot.1.020
cf01612  1.0  0.0  fdi-h2-oxtot.1.030
cf01613  1.0  0.0  fdi-h2-oxtot.1.040
cf01614  1.0  0.0  fdi-h2-sxtot.1.1.01001
cf01615  1.0  0.0  fdi-h2-sxtot.1.1.01002
cf01616  1.0  0.0  fdi-h2-sxtot.1.1.01003
cf01617  1.0  0.0  fdi-h2-sxtot.1.1.02001
cf01618  1.0  0.0  fdi-h2-sxtot.1.1.02002
cf01619  1.0  0.0  fdi-h2-sxtot.1.1.02003
cf01620  1.0  0.0  fdi-h2-sxtot.1.1.03001
cf01621  1.0  0.0  fdi-h2-sxtot.1.1.03002
cf01622  1.0  0.0  fdi-h2-sxtot.1.1.03003
cf01623  1.0  0.0  fdi-h2-sxtot.1.1.04001
cf01624  1.0  0.0  fdi-h2-sxtot.1.1.04002
cf01625  1.0  0.0  fdi-h2-sxtot.1.1.04003
*
cf01700  al-oxid-frac  equals  1  1.67785  0.0
cf01710  1.0  0.0  cfvalu.012
*
cf01800  ss-oxid-frac  equals  1  0.03795  0.0
cf01810  1.0  0.0  cfvalu.013
*
cf01900  'h2-burned'  add  2  1.0  0.0
cf01910  1.0  0.0  cfvalu.016
cf01911  -1.0  0.0  cfvalu.011
*
*******************************************************************************
*
*  tabular function input
*
*******************************************************************************
*
tf00100  debris-temp  1  1.0  0.0
tf00110  1.0  2300.0
*
tf00200  al2-o3  11  16.056  0.0
tf00210  0.0    0.0
tf00211  0.1    0.05
tf00212  0.2    0.1
tf00213  0.3    0.15
tf00214  0.4    0.2
tf00215  0.5    0.3
tf00216  0.6    0.5
tf00217  0.7    0.8
tf00218  0.8    0.9
tf00219  0.9    0.95
tf00220  1.0    1.0
*
tf00300  al  11  0.596  0.0
tf00310  0.0    0.0
tf00311  0.1    0.05
```

```
tf00312  0.2    0.1
tf00313  0.3    0.15
tf00314  0.4    0.2
tf00315  0.5    0.3
tf00316  0.6    0.5
tf00317  0.7    0.8
tf00318  0.8    0.9
tf00319  0.9    0.95
tf00320  1.0    1.0
*
tf00400  fe-cr  11  26.347  0.0
tf00410  0.0    0.0
tf00411  0.1    0.05
tf00412  0.2    0.1
tf00413  0.3    0.15
tf00414  0.4    0.2
tf00415  0.5    0.3
tf00416  0.6    0.5
tf00417  0.7    0.8
tf00418  0.8    0.9
tf00419  0.9    0.95
tf00420  1.0    1.0
*
mpmat00600  steel
* fraction     fe       cr    ni    c
mpmat00699  0.82359  0.17641  0.0  0.0
*
*****************************************************************************
*
*  dch/fdi input
*
*****************************************************************************
*
*        nfdicv  nfdcav  nfdtpi  nfdtpo
fdi0100  010     -1       1       -3
*        name
fdi0101  cavity
*        zbottm  ztop
fdi0102  0.0   0.3048
*        nfdatm  nfddep
fdi0104  4       12
*
*           matname      itable
fdi0110  aluminum-oxide    2
fdi0111  aluminum          3
fdi0112  stainless-steel   4
*
*        icvnum  idpnum  itype   frac    tauox   tauht   tausettle
fdi0150  010     01002   lhs     0.15    0.025   0.40     0.15
fdi0151  020     02002   lhs     0.10    0.025   0.40     0.35
fdi0152  030     03002   lhs     0.65    0.025   0.40     0.25
fdi0153  040     04002   lhs     0.10    0.025   0.40     0.60
*
```

```
*        idpnum  itype   frac   tsox
fdi0154  01001   lhs     0.0    600.0
fdi0155  01002   lhs     0.0    600.0
fdi0156  01003   lhs     0.0    600.0
fdi0157  02001   lhs     0.0    600.0
fdi0158  02002   lhs     0.0    600.0
fdi0159  02003   lhs     0.0    600.0
fdi0160  03001   lhs     0.0    600.0
fdi0161  03002   lhs     0.0    600.0
fdi0162  03003   lhs     0.0    600.0
fdi0163  04001   lhs     0.0    600.0
fdi0164  04002   lhs     0.0    600.0
fdi0165  04003   lhs     0.0    600.0
*
*******************************************************************************
*
*  heat structure input
*
*******************************************************************************
*
* cavity
*
hs01001000  12  1  0
hs01001001  cavity-wall
hs01001002  0.0  1.0
hs01001100  -1  1  0.0
hs01001101  0.0001  2
hs01001102  0.0003  3
hs01001103  0.0006  4
hs01001104  0.0010  5
hs01001105  0.0024  6
hs01001106  0.0050  7
hs01001107  0.0100  8
hs01001108  0.0200  9
hs01001109  0.0400  10
hs01001110  0.0900  11
hs01001111  0.1830  12
hs01001200  -1
hs01001201  concrete  11
hs01001300  0
hs01001400  1  010  int  0.0  1.0
hs01001401  0.8  gray-gas-a  0.261
hs01001500  0.779  0.3048  0.3048
hs01001600  0
*
hs01002000  12  1  0
hs01002001  cavity-floor
hs01002002  -0.1830  -1.0e-7
hs01002100  01001  1  0.0
hs01002200  01001
hs01002300  0
hs01002400  1  010  ext  0.0  1.0
hs01002401  0.8  gray-gas-a  0.261
```

```
hs01002500  0.779  0.3048  0.3048
hs01002600  0
*
hs01003000  12  1  0
hs01003001  cavity-roof
hs01003002  0.3048  0.0
hs01003100  01001  1  0.0
hs01003200  01001
hs01003300  0
hs01003400  1  010  ext  0.0  1.0
hs01003401  0.8  gray-gas-a  0.261
hs01003500  0.779  0.3048  0.3048
hs01003600  0
*
* chute
*
hs02001000  12  1  0
hs02001001  chute-wall
hs02001002  0.0  1.0
hs02001100  -1  1  0.0
hs02001101  0.0001  2
hs02001102  0.0003  3
hs02001103  0.0006  4
hs02001104  0.0010  5
hs02001105  0.0024  6
hs02001106  0.0050  7
hs02001107  0.0100  8
hs02001108  0.0200  9
hs02001109  0.0400  10
hs02001110  0.0900  11
hs02001111  0.1830  12
hs02001200  -1
hs02001201  concrete  11
hs02001300  0
hs02001400  1  020  int  0.0  1.0
hs02001401  0.8  gray-gas-a  0.261
hs02001500  1.341  2.16  2.16
hs02001600  0
*
hs02002000  12  1  0
hs02002001  chute-floor
hs02002002  -0.08022  -0.89879
hs02002100  02001  1  0.0
hs02002200  02001
hs02002300  0
hs02002400  1  020  ext  0.0  1.0
hs02002401  0.8  gray-gas-a  0.261
hs02002500  0.732  2.2  2.2
hs02002600  0
*
hs02003000  12  1  0
hs02003001  chute-roof
hs02003002  0.3048  0.89879
```

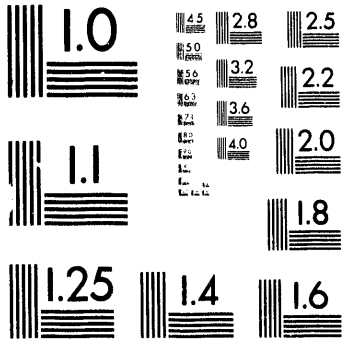
1.0
1.1
1.25
1.4
1.6
1.8
2.0
2.2
2.5
2.8
3.2
3.6
4.0
4.5
5.0
5.6
6.3
7.1

3 of 3

```
hs02003100  02001  1  0.0
hs02003200  02001
hs02003300  0
hs02003400  1  020  ext  0.0  1.0
hs02003401  0.8  gray-gas-a  0.261
hs02003500  0.6096  2.0  2.0
hs02003600  0
*
* subcompartments
*
hs03001000  12  1  0
hs03001001  subcompartments-wall
hs03001002  2.16  1.0
hs03001100  -1  1  0.0
hs03001101  0.0001  2
hs03001102  0.0003  3
hs03001103  0.0006  4
hs03001104  0.0012  5
hs03001105  0.0024  6
hs03001106  0.0050  7
hs03001107  0.0100  8
hs03001108  0.0200  9
hs03001109  0.0350  10
hs03001110  0.0650  11
hs03001111  0.1067  12
hs03001200  -1
hs03001201  concrete  11
hs03001300  0
hs03001400  1  030  int  0.0  1.0
hs03001401  0.8  gray-gas-a  0.5028
hs03001500  27.9696  0.721  0.721
hs03001600  0
*
hs03002000  11  1  0
hs03002001  subcompartments-floor
hs03002002  2.16  -1.0e-7
hs03002100  -1  1  0.0
hs03002101  0.0001  2
hs03002102  0.0003  3
hs03002103  0.0006  4
hs03002104  0.0012  5
hs03002105  0.0024  6
hs03002106  0.0050  7
hs03002107  0.0100  8
hs03002108  0.0200  9
hs03002109  0.0350  10
hs03002110  0.0508  11
hs03002200  -1
hs03002201  concrete  10
hs03002300  0
hs03002400  1  030  ext  0.0  1.0
hs03002401  0.8  gray-gas-a  0.5028
hs03002500  6.1789  0.71  0.71
```

```
hs03002600  0
*
hs03003000  10  1  0
hs03003001  subcompartments-roof
hs03003002  3.68  0.0
hs03003100  -1  1  0.0
hs03003101  0.0001  2
hs03003102  0.0003  3
hs03003103  0.0006  4
hs03003104  0.0012  5
hs03003105  0.0024  6
hs03003106  0.0050  7
hs03003107  0.0100  8
hs03003108  0.0200  9
hs03003109  0.0305  10
hs03003200  -1
hs03003201  concrete  9
hs03003300  0
hs03003400  1  030  ext  0.0  1.0
hs03003401  0.8  gray-gas-a  0.5028
hs03003500  6.4265  0.309  0.309
hs03003600  0
*
* dome
*
hs04001000  9  1  0
hs04001001  dome-wall
hs04001002  3.68  1.0
hs04001100  -1  1  0.0
hs04001101  0.0001  2
hs04001102  0.0003  3
hs04001103  0.0006  4
hs04001104  0.0012  5
hs04001105  0.0024  6
hs04001106  0.0050  7
hs04001107  0.0090  8
hs04001108  0.01588  9
hs04001200  -1
hs04001201  stainless-steel  8
hs04001300  0
hs04001400  1  040  int  0.0  1.0
hs04001401  0.8  gray-gas-a  2.489
hs04001500  135.1498  7.539  7.539
hs04001600  0
*
hs04002000  11  1  0
hs04002001  dome-floor
hs04002002  3.68  -1.0e-7
hs04002100  -1  1  0.0
hs04002101  0.0001  2
hs04002102  0.0003  3
hs04002103  0.0006  4
hs04002104  0.0012  5
```

```
hs04002105  0.0024  6
hs04002106  0.0050  7
hs04002107  0.0100  8
hs04002108  0.0200  9
hs04002109  0.0400  10
hs04002110  0.0762  11
hs04002200  -1
hs04002201  concrete  10
hs04002300  0
hs04002400  1  040  ext  0.0  1.0
hs04002401  0.8  gray-gas-a  2.489
hs04002500  10.239  1.33  1.33
hs04002600  0
*
hs04003000  9  1  0
hs04003001  dome-roof
hs04003002  12.09  0.0
hs04003100  04001  1  0.0
hs04003200  04001
hs04003300  0
hs04003400  1  040  ext  0.0  1.0
hs04003401  0.8  gray-gas-a  2.489
hs04003500  10.507  3.66  3.66
hs04003600  0
*
*******************************************************************************
*
sc42551  4255  1.0e-5  1  * reduce HS film thickness
*
sc40611  4061  0.0    1   * reduce laminar natural convection bound
sc40612  4061  0.001  2   * reduce turbulent natural convection bound
sc40641  4064  0.0    1   * reduce laminar forced convection bound
sc40642  4064  0.001  2   * reduce turbulent forced convection bound
*
sc46081  4608  1.0  1  *  reduce FDI debris-to-structure HTC
*
*******************************************************************************
*
*  test-specific input
*
*******************************************************************************
*
cv001a1  pvol  7.1e3   ph2o 7.1e6  tatm  600.0
*
cv010a1  pvol  2.0e5  ph2o  0.0  tatm  295.0  zpol 0.009
cv010a2  mlfr.4  0.9990  mlfr.5  0.0003
cv010a3  mlfr.7  0.0001  mlfr.9  0.0006
*
cv020a1  pvol  2.0e5  ph2o  0.0  tatm  295.0
cv020a2  mlfr.4  0.9990  mlfr.5  0.0003
cv020a3  mlfr.7  0.0001  mlfr.9  0.0006
*
cv030a1  pvol  2.0e5  ph2o  0.0  tatm  295.0
```

```
cv030a2  mlfr.4  0.9990  mlfr.5  0.0003
cv030a3  mlfr.7  0.0001  mlfr.9  0.0006
*
cv040a1  pvol  2.0e5  ph2o  0.0  tatm  295.0
cv040a2  mlfr.4  0.9990  mlfr.5  0.0003
cv040a3  mlfr.7  0.0001  mlfr.9  0.0006
*
*****************************************************************************
*
.
*eor* melcor
*
*****************************************************************************
*
title     'Surtsey IET-1'
*
*****************************************************************************
*
diagfile     'cor1.dia'
outputfile   'cor1.out'
messagefile  'cor1.mes'
plotfile     'plot1'
restartfile  'restart1'
*
restart -1
cymesf  100  10
dtsummary
*          tstart  dtmax    dtmin  dtedit  dtplot  dtrest
time1        0.0     1.   0.000001   10.     .001    10.
time2        0.2     1.   0.000001   10.     .01     10.
tend  20.0
cpulim  99999.
cpuleft 100.
*cvhtrace
*
.
*
*eor* hisplt
*
color,2,3,4,6,0
shade,all
gtitle,SNL Surtsey IET Tests -- SUN reference results
*
file1='plot1'
file2='plot1r'
file3='plot3'
file4='plot4'
file5='plot5'
file6='plot6'
file7='plot7'
*
startuf
uf.1 add
```

```
+ bur-h2-tot.010
+ bur-h2-tot.020
+ bur-h2-tot.030
+ bur-h2-tot.040
enduf
*
title,MELCOR Assessment: SNL IET Tests
vlabel,Accumulator Pressure (()Pa)
ulabel,Time (()s)
limits 0.0,4.0 0.0,8.0e6
plot time cvh-p.001 file=1 line=solid color=2 symbol=! legend='IET-1 (MELCOR)'
cplot time cvh-p.001 file=2 line=solid color=5 symbol=? legend='IET-1R (MELCOR)'
cplot time cvh-p.001 file=3 line=solid color=6 symbol=> legend='IET-3 (MELCOR)'
cplot time cvh-p.001 file=4 line=solid color=1 symbol=^ legend='IET-4 (MELCOR)'
cplot time cvh-p.001 file=5 line=solid color=1 symbol=_A legend='IET-5 (MELCOR)'
cplot time cvh-p.001 file=6 line=solid color=1 symbol=% legend='IET-6 (MELCOR)'
cplot time cvh-p.001 file=7 line=solid color=1 symbol=_C legend='IET-7 (MELCOR)'
data line=sdash color=3 symbol=& legend='IET-1 (Data)'
*readfile test_data pa1
data line=sdash color=3 symbol=< legend='IET-1R (Data)'
*readfile test_data pa1r
data line=sdash color=3 symbol=@ legend='IET-3 (Data)'
*readfile test_data pa3
data line=sdash color=3 symbol=\ legend='IET-4 (Data)'
*readfile test_data pa4
data line=sdash color=3 symbol=_D legend='IET-5 (Data)'
*readfile test_data pa5
data line=sdash color=3 symbol=" legend='IET-6 (Data)'
*readfile test_data pa6
data line=sdash color=3 symbol=_F legend='IET-7 (Data)'
*readfile test_data pa7
legend,ur
*
title,MELCOR Assessment: SNL IET Tests
vlabel,Vessel Pressure (()Pa)
ulabel,Time (()s)
limits 0.0,20.0 0.0,0.75e6
plot time cvh-p.040 file=1 line=solid color=2 symbol=! legend='IET-1 (MELCOR)'
cplot time cvh-p.040 file=2 line=solid color=5 symbol=? legend='IET-1R (MELCOR)'
cplot time cvh-p.040 file=3 line=solid color=6 symbol=> legend='IET-3 (MELCOR)'
cplot time cvh-p.040 file=4 line=solid color=101 symbol=^ legend='IET-4 (MELCOR)'
cplot time cvh-p.040 file=5 line=solid color=141 symbol=_A legend='IET-5 (MELCOR)'
cplot time cvh-p.040 file=6 line=solid color=1 symbol=% legend='IET-6 (MELCOR)'
cplot time cvh-p.040 file=7 line=solid color=9 symbol=_C legend='IET-7 (MELCOR)'
data line=sdash color=3 symbol=& legend='IET-1 (Data)'
*readfile test_data p1
data line=sdash color=3 symbol=< legend='IET-1R (Data)'
*readfile test_data p1r
data line=sdash color=3 symbol=@ legend='IET-3 (Data)'
*readfile test_data p3
data line=sdash color=3 symbol=\ legend='IET-4 (Data)'
*readfile test_data p4
data line=sdash color=3 symbol=_D legend='IET-5 (Data)'
```

```
*readfile test_data p5
data line=sdash color=3 symbol=" legend='IET-6 (Data)'
*readfile test_data p6
data line=sdash color=3 symbol=_F legend='IET-7 (Data)'
*readfile test_data p7
legend,ur
*
title,MELCOR Assessment: SNL IET Tests
vlabel,Hydrogen Mass Generated (()kg)
ulabel,Time (()s)
limits 0.0,5.0 0.0,1.0
plot time cfvalu.016 file=1 line=solid color=2 symbol=! legend='IET-1 (MELCOR)'
cplot time cfvalu.016 file=2 line=solid color=5 symbol=? legend='IET-1R (MELCOR)'
cplot time cfvalu.016 file=3 line=solid color=6 symbol=> legend='IET-3 (MELCOR)'
cplot time cfvalu.016 file=4 line=solid color=101 symbol=^ legend='IET-4 (MELCOR)'
cplot time cfvalu.016 file=5 line=solid color=141 symbol=_A legend='IET-5 (MELCOR)'
cplot time cfvalu.016 file=6 line=solid color=1 symbol=% legend='IET-6 (MELCOR)'
cplot time cfvalu.016 file=7 line=solid color=9 symbol=_C legend='IET-7 (MELCOR)'
vscale,2.0,0.0
data line=sdash symbol=& color=3 legend='IET-1 (Data)'
0.0,0.223
30.0,0.223
-12345,-12345
vscale,2.0,0.0
data line=sdash symbol=< color=3 legend='IET-1R (Data)'
0.0,0.252
30.0,0.252
-12345,-12345
vscale,2.0,0.0
data line=sdash symbol=@ color=3 legend='IET-3 (Data)'
0.0,0.223
30.0,0.223
-12345,-12345
vscale,2.0,0.0
data line=sdash symbol=\ color=3 legend='IET-4 (Data)'
0.0,0.297
30.0,0.297
-12345,-12345
vscale,2.0,0.0
data line=sdash symbol=_D color=3 legend='IET-5 (Data)'
0.0,0.313
30.0,0.313
-12345,-12345
vscale,2.0,0.0
data line=sdash symbol=% color=3 legend='IET-6 (Data)'
0.0,0.308
30.0,0.308
-12345,-12345
vscale,2.0,0.0
data line=sdash symbol=_F color=3 legend='IET-7 (Data)'
0.0,0.271
30.0,0.271
-12345,-12345
```

```
legend,ur
*
title,MELCOR Assessment: SNL IET Tests
vlabel,Hydrogen Mass Burned (()kg)
ulabel,Time (()s)
limits 0.0,20.0 0.0,1.0
plot time uf.1 file=1 line=solid color=2 symbol=! legend='IET-1 (MELCOR)'
cplot time uf.1 file=2 line=solid color=5 symbol=? legend='IET-1R (MELCOR)'
cplot time uf.1 file=3 line=solid color=6 symbol=> legend='IET-3 (MELCOR)'
cplot time uf.1 file=4 line=solid color=101 symbol=^ legend='IET-4 (MELCOR)'
cplot time uf.1 file=5 line=solid color=141 symbol=_A legend='IET-5 (MELCOR)'
cplot time uf.1 file=6 line=solid color=1 symbol=% legend='IET-6 (MELCOR)'
cplot time uf.1 file=7 line=solid color=9 symbol=_C legend='IET-7 (MELCOR)'
vscale,2.0,0.0
data line=sdash symbol=& color=3 legend='IET-1 (Data)'
0.0,0.001
30.0,0.001
-12345,-12345
vscale,2.0,0.0
data line=sdash symbol=< color=3 legend='IET-1R (Data)'
0.0,0.012
30.0,0.012
-12345,-12345
vscale,2.0,0.0
data line=sdash symbol=@ color=3 legend='IET-3 (Data)'
0.0,0.186
30.0,0.186
-12345,-12345
vscale,2.0,0.0
data line=sdash symbol=\ color=3 legend='IET-4 (Data)'
0.0,0.236
30.0,0.236
-12345,-12345
vscale,2.0,0.0
data line=sdash symbol=_D color=3 legend='IET-5 (Data)'
0.0,0.050
30.0,0.050
-12345,-12345
vscale,2.0,0.0
data line=sdash symbol=" color=3 legend='IET-6 (Data)'
0.0,0.335
30.0,0.335
-12345,-12345
vscale,2.0,0.0
data line=sdash symbol=_F color=3 legend='IET-7 (Data)'
0.0,0.321
30.0,0.321
-12345,-12345
legend,ur
*
title,MELCOR Assessment: SNL IET Tests
vlabel,Subcompartment Temperature (()K)
ulabel,Time (()s)
```

```
limits 0.0,5.0 0.0,1500.0
plot time cvh-tvap.030 file=1 line=solid color=2 symbol=! legend='IET-1 (MELCOR)'
cplot time cvh-tvap.030 file=2 line=solid color=5 symbol=? legend='IET-1R (MELCOR)'
cplot time cvh-tvap.030 file=3 line=solid color=6 symbol=> legend='IET-3 (MELCOR)'
cplot time cvh-tvap.030 file=4 line=solid color=101 symbol=^ legend='IET-4 (MELCOR)'
cplot time cvh-tvap.030 file=5 line=solid color=141 symbol=_A legend='IET-5 (MELCOR)'
cplot time cvh-tvap.030 file=6 line=solid color=1 symbol=% legend='IET-6 (MELCOR)'
cplot time cvh-tvap.030 file=7 line=solid color=9 symbol=_C legend='IET-7 (MELCOR)'
data line=sdash color=3 symbol=& legend='IET-1 (Data)'
*readfile test_data tsc1
data line=sdash color=3 symbol=< legend='IET-1R (Data)'
*readfile test_data tsc1r
data line=sdash color=3 symbol=@ legend='IET-3 (Data)'
*readfile test_data tsc3
data line=sdash color=3 symbol=\ legend='IET-4 (Data)'
*readfile test_data tsc4
data line=sdash color=3 symbol=_D legend='IET-5 (Data)'
*readfile test_data tsc5
data line=sdash color=3 symbol=" legend='IET-6 (Data)'
*readfile test_data tsc6
data line=sdash color=3 symbol=_F legend='IET-7 (Data)'
*readfile test_data tsc7
legend,ur
*
title,MELCOR Assessment: SNL IET Tests
vlabel,Dome Temperatures (()K)
ulabel,Time (()s)
limits 0.0,5.0 0.0,1500.0
plot time cvh-tvap.040 file=1 line=solid color=2 symbol=! legend='IET-1 (MELCOR)'
cplot time cvh-tvap.040 file=2 line=solid color=5 symbol=? legend='IET-1R (MELCOR)'
cplot time cvh-tvap.040 file=3 line=solid color=6 symbol=> legend='IET-3 (MELCOR)'
cplot time cvh-tvap.040 file=4 line=solid color=101 symbol=^ legend='IET-4 (MELCOR)'
cplot time cvh-tvap.040 file=5 line=solid color=141 symbol=_A legend='IET-5 (MELCOR)'
cplot time cvh-tvap.040 file=6 line=solid color=1 symbol=% legend='IET-6 (MELCOR)'
cplot time cvh-tvap.040 file=7 line=solid color=9 symbol=_C legend='IET-7 (MELCOR)'
legend,ur
*
title,MELCOR Assessment: SNL IET Tests
vlabel,Dome Temperature (()K)
ulabel,Time (()s)
limits 0.0,5.0 0.0,1500.0
plot time cvh-tvap.040 file=1 line=solid color=2 symbol=! legend='IET-1 (MELCOR)'
data line=ldash color=3 symbol=& legend='IET-1 (Level 1)'
*readfile test_data tl11
data line=mdash color=3 symbol=& legend='IET-1 (Level 3)'
*readfile test_data tl31
data line=sdash color=3 symbol=& legend='IET-1 (Level 5)'
*readfile test_data tl51
legend,ur
*
title,MELCOR Assessment: SNL IET Tests
vlabel,Dome Temperature (()K)
ulabel,Time (()s)
```

```
limits 0.0,5.0 0.0,1500.0
plot time cvh-tvap.040 file=2 line=solid color=5 symbol=? legend='IET-1R (MELCOR)'
data line=ldash color=3 symbol=< legend='IET-1R (Level 1)'
*readfile test_data tl11r
data line=mdash color=3 symbol=< legend='IET-1R (Level 3)'
*readfile test_data tl31r
data line=sdash color=3 symbol=< legend='IET-1R (Level 5)'
*readfile test_data tl51r
legend,ur
*
title,MELCOR Assessment: SNL IET Tests
vlabel,Dome Temperature (()K)
ulabel,Time (()s)
limits 0.0,5.0 0.0,1500.0
plot time cvh-tvap.040 file=3 line=solid color=6 symbol=> legend='IET-3 (MELCOR)'
data line=ldash color=3 symbol=@ legend='IET-3 (Level 1)'
*readfile test_data tl13
data line=mdash color=3 symbol=@ legend='IET-3 (Level 3)'
*readfile test_data tl33
data line=sdash color=3 symbol=@ legend='IET-3 (Level 5)'
*readfile test_data tl53
legend,ur
*
title,MELCOR Assessment: SNL IET Tests
vlabel,Dome Temperature (()K)
ulabel,Time (()s)
limits 0.0,5.0 0.0,1500.0
plot time cvh-tvap.040 file=4 line=solid color=101 symbol=^ legend='IET-4 (MELCOR)'
data line=ldash color=3 symbol=\ legend='IET-4 (Level 1)'
*readfile test_data tl14
data line=mdash color=3 symbol=\ legend='IET-4 (Level 3)'
*readfile test_data tl34
data line=sdash color=3 symbol=\ legend='IET-4 (Level 5)'
*readfile test_data tl54
legend,ur
*
title,MELCOR Assessment: SNL IET Tests
vlabel,Dome Temperature (()K)
ulabel,Time (()s)
limits 0.0,5.0 0.0,1500.0
plot time cvh-tvap.040 file=5 line=solid color=141 symbol=_A legend='IET-5 (MELCOR)'
data line=ldash color=3 symbol=_D legend='IET-5 (Level 1)'
*readfile test_data tl15
data line=mdash color=3 symbol=_D legend='IET-5 (Level 3)'
*readfile test_data tl35
data line=sdash color=3 symbol=_D legend='IET-5 (Level 5)'
*readfile test_data tl55
legend,ur
*
title,MELCOR Assessment: SNL IET Tests
vlabel,Dome Temperature (()K)
ulabel,Time (()s)
limits 0.0,5.0 0.0,1500.0
```

```
plot time cvh-tvap.040 file=6 line=solid color=1 symbol=% legend='IET-6 (MELCOR)'
data line=ldash color=3 symbol=" legend='IET-6 (Level 1)'
*readfile test_data tl16
data line=mdash color=3 symbol=" legend='IET-6 (Level 3)'
*readfile test_data tl36
data line=sdash color=3 symbol=" legend='IET-6 (Level 5)'
*readfile test_data tl56
legend,ur
*
title,MELCOR Assessment: SNL IET Tests
vlabel,Dome Temperature (()K)
ulabel,Time (()s)
limits 0.0,5.0 0.0,1500.0
plot time cvh-tvap.040 file=7 line=solid color=9 symbol=_C legend='IET-7 (MELCOR)'
data line=ldash color=3 symbol=_F legend='IET-7 (Level 1)'
*readfile test_data tl17
data line=mdash color=3 symbol=_F legend='IET-7 (Level 3)'
*readfile test_data tl37
data line=sdash color=3 symbol=_F legend='IET-7 (Level 5)'
*readfile test_data tl57
legend,ur
*
title,MELCOR Assessment: SNL IET Tests
vlabel,Aluminum Mass Oxidized in FDI (()kg)
ulabel,Time (()s)
limits 0.0,5.0 1.0,-1.0
plot time cfvalu.012 file=1 line=solid color=2 symbol=! legend='IET-1'
cplot time cfvalu.012 file=2 line=solid color=5 symbol=? legend='IET-1R'
cplot time cfvalu.012 file=3 line=solid color=6 symbol=> legend='IET-3'
cplot time cfvalu.012 file=4 line=solid color=101 symbol=^ legend='IET-4'
cplot time cfvalu.012 file=5 line=solid color=141 symbol=_A legend='IET-5'
cplot time cfvalu.012 file=6 line=solid color=1 symbol=% legend='IET-6'
cplot time cfvalu.012 file=7 line=solid color=9 symbol=_C legend='IET-7'
legend,lr
*
title,MELCOR Assessment: SNL IET Tests
vlabel,Fe/Cr Mass Oxidized in FDI (()kg)
ulabel,Time (()s)
limits 0.0,5.0 1.0,-1.0
plot time cfvalu.013 file=1 line=solid color=2 symbol=! legend='IET-1'
cplot time cfvalu.013 file=2 line=solid color=5 symbol=? legend='IET-1R'
cplot time cfvalu.013 file=3 line=solid color=6 symbol=> legend='IET-3'
cplot time cfvalu.013 file=4 line=solid color=101 symbol=^ legend='IET-4'
cplot time cfvalu.013 file=5 line=solid color=141 symbol=_A legend='IET-5'
cplot time cfvalu.013 file=6 line=solid color=1 symbol=% legend='IET-6'
cplot time cfvalu.013 file=7 line=solid color=9 symbol=_C legend='IET-7'
legend,lr
*
title,MELCOR Assessment: SNL IET Tests
vlabel,Oxygen Mass Consumed in FDI (()kg)
ulabel,Time (()s)
limits 0.0,5.0 1.0,-1.0
plot time cfvalu.014 file=1 line=solid color=2 symbol=! legend='IET-1'
```

```
cplot time cfvalu.014 file=2 line=solid color=5 symbol=? legend='IET-1R'
cplot time cfvalu.014 file=3 line=solid color=6 symbol=> legend='IET-3'
cplot time cfvalu.014 file=4 line=solid color=101 symbol=^ legend='IET-4'
cplot time cfvalu.014 file=5 line=solid color=141 symbol=_A legend='IET-5'
cplot time cfvalu.014 file=6 line=solid color=1 symbol=% legend='IET-6'
cplot time cfvalu.014 file=7 line=solid color=9 symbol=_C legend='IET-7'
legend,lr
*
title,MELCOR Assessment: SNL IET Tests
vlabel,Steam Mass Consumed in FDI (()kg)
ulabel,Time (()s)
limits 0.0,5.0 1.0,-1.0
plot time cfvalu.015 file=1 line=solid color=2 symbol=! legend='IET-1'
cplot time cfvalu.015 file=2 line=solid color=5 symbol=? legend='IET-1R'
cplot time cfvalu.015 file=3 line=solid color=6 symbol=> legend='IET-3'
cplot time cfvalu.015 file=4 line=solid color=101 symbol=^ legend='IET-4'
cplot time cfvalu.015 file=5 line=solid color=141 symbol=_A legend='IET-5'
cplot time cfvalu.015 file=6 line=solid color=1 symbol=% legend='IET-6'
cplot time cfvalu.015 file=7 line=solid color=9 symbol=_C legend='IET-7'
legend,lr
*
title,MELCOR Assessment: SNL IET Tests
vlabel,Hydrogen Mass Generated in FDI (()kg)
ulabel,Time (()s)
limits 0.0,5.0 1.0,-1.0
plot time cfvalu.016 file=1 line=solid color=2 symbol=! legend='IET-1'
cplot time cfvalu.016 file=2 line=solid color=5 symbol=? legend='IET-1R'
cplot time cfvalu.016 file=3 line=solid color=6 symbol=> legend='IET-3'
cplot time cfvalu.016 file=4 line=solid color=101 symbol=^ legend='IET-4'
cplot time cfvalu.016 file=5 line=solid color=141 symbol=_A legend='IET-5'
cplot time cfvalu.016 file=6 line=solid color=1 symbol=% legend='IET-6'
cplot time cfvalu.016 file=7 line=solid color=9 symbol=_C legend='IET-7'
legend,lr
*
title,MELCOR Assessment: SNL IET Tests
vlabel,Hydrogen Mole Fraction in Subcompartments
ulabel,Time (()s)
*limits 0.0,5.0 1.0,-1.0
plot time cvh-x.6.030 file=1 line=solid color=2 symbol=! legend='IET-1 (MELCOR)'
cplot time cvh-x.6.030 file=2 line=solid color=5 symbol=? legend='IET-1R (MELCOR)'
cplot time cvh-x.6.030 file=3 line=solid color=6 symbol=> legend='IET-3 (MELCOR)'
cplot time cvh-x.6.030 file=4 line=solid color=101 symbol=^ legend='IET-4 (MELCOR)'
cplot time cvh-x.6.030 file=5 line=solid color=141 symbol=_A legend='IET-5 (MELCOR)'
cplot time cvh-x.6.030 file=6 line=solid color=1 symbol=% legend='IET-6 (MELCOR)'
cplot time cvh-x.6.030 file=7 line=solid color=9 symbol=_C legend='IET-7 (MELCOR)'
data line=sdash symbol=& color=3 legend='IET-1 (Data)'
0.0,0.0003108
2.0,0.208
5.0,0.03108
30.0,0.03108
-12345,-12345
data line=sdash symbol=< color=3 legend='IET-1R (Data)'
5.0,0.03077
```

```
30.0,0.03077
-12345,-12345
data line=sdash symbol=@ color=3 legend='IET-3 (Data)'
5.0,0.0052
30.0,0.0052
-12345,-12345
data line=sdash symbol=\ color=3 legend='IET-4 (Data)'
0.0,0.0078
2.0,0.0386
5.0,0.0078
30.0,0.0078
-12345,-12345
data line=sdash symbol=_D color=3 legend='IET-5 (Data)'
5.0,0.0276
30.0,0.0276
-12345,-12345
data line=sdash symbol=% color=3 legend='IET-6 (Data)'
0.0,0.0259
2.0,0.2425
5.0,0.0221
30.0,0.0221
-12345,-12345
data line=sdash symbol=_F color=3 legend='IET-7 (Data)'
0.0,0.0397
2.0,0.3025
5.0,0.03264
30.0,0.03264
-12345,-12345
legend,next
*
title,MELCOR Assessment: SNL IET Tests
vlabel,Hydrogen Mole Fraction in Dome
ulabel,Time (()s)
*limits 0.0,5.0 1.0,-1.0
plot time cvh-x.6.040 file=1 line=solid color=2 symbol=! legend='IET-1 (MELCOR)'
cplot time cvh-x.6.040 file=2 line=solid color=5 symbol=? legend='IET-1R (MELCOR)'
cplot time cvh-x.6.040 file=3 line=solid color=6 symbol=> legend='IET-3 (MELCOR)'
cplot time cvh-x.6.040 file=4 line=solid color=101 symbol=^ legend='IET-4 (MELCOR)'
cplot time cvh-x.6.040 file=5 line=solid color=141 symbol=_A legend='IET-5 (MELCOR)'
cplot time cvh-x.6.040 file=6 line=solid color=1 symbol=% legend='IET-6 (MELCOR)'
cplot time cvh-x.6.040 file=7 line=solid color=9 symbol=_C legend='IET-7 (MELCOR)'
data line=sdash symbol=& color=3 legend='IET-1 (Data)'
0.0,0.03108
30.0,0.03108
-12345,-12345
data line=sdash symbol=< color=3 legend='IET-1R (Data)'
0.0,0.03077
30.0,0.03077
-12345,-12345
data line=sdash symbol=@ color=3 legend='IET-3 (Data)'
0.0,0.0052
30.0,0.0052
-12345,-12345
```

```
data line=sdash symbol=\ color=3 legend='IET-4 (Data)'
0.0,0.0078
30.0,0.0078
-12345,-12345
data line=sdash symbol=_D color=3 legend='IET-5 (Data)'
0.0,0.0276
30.0,0.0276
-12345,-12345
data line=sdash symbol=% color=3 legend='IET-6 (Data)'
0.0,0.0221
30.0,0.0221
-12345,-12345
data line=sdash symbol=_F color=3 legend='IET-7 (Data)'
0.0,0.03264
30.0,0.03264
-12345,-12345
legend,next
*
title,MELCOR Assessment: SNL IET Tests
vlabel,Oxygen Mole Fraction in Subcompartments
ulabel,Time (()s)
*limits 0.0,5.0 1.0,-1.0
plot time cvh-x.5.030 file=1 line=solid color=2 symbol=! legend='IET-1 (MELCOR)'
cplot time cvh-x.5.030 file=2 line=solid color=5 symbol=? legend='IET-1R (MELCOR)'
cplot time cvh-x.5.030 file=3 line=solid color=6 symbol=> legend='IET-3 (MELCOR)'
cplot time cvh-x.5.030 file=4 line=solid color=101 symbol=^ legend='IET-4 (MELCOR)'
cplot time cvh-x.5.030 file=5 line=solid color=141 symbol=_A legend='IET-5 (MELCOR)'
cplot time cvh-x.5.030 file=6 line=solid color=1 symbol=% legend='IET-6 (MELCOR)'
cplot time cvh-x.5.030 file=7 line=solid color=9 symbol=_C legend='IET-7 (MELCOR)'
data line=sdash symbol=@ color=3 legend='IET-3 (Data)'
0.0,0.0770
30.0,0.0770
-12345,-12345
data line=sdash symbol=\ color=3 legend='IET-4 (Data)'
0.0,0.0796
30.0,0.0796
-12345,-12345
data line=sdash symbol=_D color=3 legend='IET-5 (Data)'
0.0,0.0435
30.0,0.0435
-12345,-12345
data line=sdash symbol=% color=3 legend='IET-6 (Data)'
0.0,0.0739
30.0,0.0739
-12345,-12345
data line=sdash symbol=_F color=3 legend='IET-7 (Data)'
0.0,0.07330
30.0,0.07330
-12345,-12345
legend,next
*
title,MELCOR Assessment: SNL IET Tests
vlabel,Oxygen Mole Fraction in Dome
```

```
ulabel,Time (()s)
*limits 0.0,5.0 1.0,-1.0
plot time cvh-x.5.040 file=1 line=solid color=2 symbol=! legend='IET-1 (MELCOR)'
cplot time cvh-x.5.040 file=2 line=solid color=5 symbol=? legend='IET-1R (MELCOR)'
cplot time cvh-x.5.040 file=3 line=solid color=6 symbol=> legend='IET-3 (MELCOR)'
cplot time cvh-x.5.040 file=4 line=solid color=101 symbol=^ legend='IET-4 (MELCOR)'
cplot time cvh-x.5.040 file=5 line=solid color=141 symbol=_A legend='IET-5 (MELCOR)'
cplot time cvh-x.5.040 file=6 line=solid color=1 symbol=% legend='IET-6 (MELCOR)'
cplot time cvh-x.5.040 file=7 line=solid color=9 symbol=_C legend='IET-7 (MELCOR)'
data line=sdash symbol=@ color=3 legend='IET-3 (Data)'
0.0,0.0770
30.0,0.0770
-12345,-12345
data line=sdash symbol=\ color=3 legend='IET-4 (Data)'
0.0,0.0796
30.0,0.0796
-12345,-12345
data line=sdash symbol=_D color=3 legend='IET-5 (Data)'
0.0,0.0435
30.0,0.0435
-12345,-12345
data line=sdash symbol=% color=3 legend='IET-6 (Data)'
0.0,0.0739
30.0,0.0739
-12345,-12345
data line=sdash symbol=_F color=3 legend='IET-7 (Data)'
0.0,0.07330
30.0,0.07330
-12345,-12345
legend,next
*
title,MELCOR Assessment: SNL IET Tests
vlabel,Steam Mole Fraction in Subcompartments
ulabel,Time (()s)
*limits 0.0,5.0 1.0,-1.0
plot time cvh-x.3.030 file=1 line=solid color=2 symbol=! legend='IET-1'
cplot time cvh-x.3.030 file=2 line=solid color=5 symbol=? legend='IET-1R'
cplot time cvh-x.3.030 file=3 line=solid color=6 symbol=> legend='IET-3'
cplot time cvh-x.3.030 file=4 line=solid color=101 symbol=^ legend='IET-4'
cplot time cvh-x.3.030 file=5 line=solid color=141 symbol=_A legend='IET-5'
cplot time cvh-x.3.030 file=6 line=solid color=1 symbol=% legend='IET-6'
cplot time cvh-x.3.030 file=7 line=solid color=9 symbol=_C legend='IET-7'
legend,lr
*
title,MELCOR Assessment: SNL IET Tests
vlabel,Steam Mole Fraction in Dome
ulabel,Time (()s)
*limits 0.0,5.0 1.0,-1.0
plot time cvh-x.3.040 file=1 line=solid color=2 symbol=! legend='IET-1'
cplot time cvh-x.3.040 file=2 line=solid color=5 symbol=? legend='IET-1R'
cplot time cvh-x.3.040 file=3 line=solid color=6 symbol=> legend='IET-3'
cplot time cvh-x.3.040 file=4 line=solid color=101 symbol=^ legend='IET-4'
cplot time cvh-x.3.040 file=5 line=solid color=141 symbol=_A legend='IET-5'
```

```
cplot time cvh-x.3.040 file=6 line=solid color=1 symbol=% legend='IET-6'
cplot time cvh-x.3.040 file=7 line=solid color=9 symbol=_C legend='IET-7'
legend,lr
*
title,MELCOR Assessment: SNL IET Tests
vlabel,Oxygen Burned in Dome (()kg)
ulabel,Time (()s)
*limits 0.0,5.0 1.0,-1.0
plot time bur-o2-tot.040 file=1 line=solid color=2 symbol=! legend='IET-1'
cplot time bur-o2-tot.040 file=2 line=solid color=5 symbol=? legend='IET-1R'
cplot time bur-o2-tot.040 file=3 line=solid color=6 symbol=> legend='IET-3'
cplot time bur-o2-tot.040 file=4 line=solid color=101 symbol=^ legend='IET-4'
cplot time bur-o2-tot.040 file=5 line=solid color=141 symbol=_A legend='IET-5'
cplot time bur-o2-tot.040 file=6 line=solid color=1 symbol=% legend='IET-6'
cplot time bur-o2-tot.040 file=7 line=solid color=9 symbol=_C legend='IET-7'
legend,lr
*
title,MELCOR Assessment: SNL IET Tests
vlabel,Hydrogen Burned in Dome (()kg)
ulabel,Time (()s)
*limits 0.0,5.0 1.0,-1.0
plot time bur-h2-tot.040 file=1 line=solid color=2 symbol=! legend='IET-1'
cplot time bur-h2-tot.040 file=2 line=solid color=5 symbol=? legend='IET-1R'
cplot time bur-h2-tot.040 file=3 line=solid color=6 symbol=> legend='IET-3'
cplot time bur-h2-tot.040 file=4 line=solid color=101 symbol=^ legend='IET-4'
cplot time bur-h2-tot.040 file=5 line=solid color=141 symbol=_A legend='IET-5'
cplot time bur-h2-tot.040 file=6 line=solid color=1 symbol=% legend='IET-6'
cplot time bur-h2-tot.040 file=7 line=solid color=9 symbol=_C legend='IET-7'
legend,lr
*
title,MELCOR Assessment: SNL IET Tests
vlabel,Steam Generated in Burns in Dome (()kg)
ulabel,Time (()s)
*limits 0.0,5.0 1.0,-1.0
plot time bur-o2-tot.040 file=1 line=solid color=2 symbol=! legend='IET-1'
cplot time bur-o2-tot.040 file=2 line=solid color=5 symbol=? legend='IET-1R'
cplot time bur-o2-tot.040 file=3 line=solid color=6 symbol=> legend='IET-3'
cplot time bur-o2-tot.040 file=4 line=solid color=101 symbol=^ legend='IET-4'
cplot time bur-o2-tot.040 file=5 line=solid color=141 symbol=_A legend='IET-5'
cplot time bur-o2-tot.040 file=6 line=solid color=1 symbol=% legend='IET-6'
cplot time bur-o2-tot.040 file=7 line=solid color=9 symbol=_C legend='IET-7'
legend,lr
*
title,MELCOR Assessment: SNL IET Tests
vlabel,CO Used in Burns in Dome (()kg)
ulabel,Time (()s)
*limits 0.0,5.0 1.0,-1.0
plot time bur-co-tot.040 file=1 line=solid co2lor=2 symbol=! legend='IET-1'
cplot time bur-co-tot.040 file=2 line=solid co2lor=5 symbol=? legend='IET-1R'
cplot time bur-co-tot.040 file=3 line=solid co2lor=6 symbol=> legend='IET-3'
cplot time bur-co-tot.040 file=4 line=solid co2lor=101 symbol=^ legend='IET-4'
cplot time bur-co-tot.040 file=5 line=solid co2lor=141 symbol=_A legend='IET-5'
cplot time bur-co-tot.040 file=6 line=solid co2lor=1 symbol=% legend='IET-6'
```

```
cplot time bur-co-tot.040 file=7 line=solid co2lor=9 symbol=_C legend='IET-7'
legend,lr
*
title,MELCOR Assessment: SNL IET Tests
vlabel,CO2 Used in Burns in Dome (()kg)
ulabel,Time (()s)
*limits 0.0,5.0 1.0,-1.0
plot time bur-co2-tot.040 file=1 line=solid co2lor=2 symbol=! legend='IET-1'
cplot time bur-co2-tot.040 file=2 line=solid co2lor=5 symbol=? legend='IET-1R'
cplot time bur-co2-tot.040 file=3 line=solid co2lor=6 symbol=> legend='IET-3'
cplot time bur-co2-tot.040 file=4 line=solid co2lor=101 symbol=^ legend='IET-4'
cplot time bur-co2-tot.040 file=5 line=solid co2lor=141 symbol=_A legend='IET-5'
cplot time bur-co2-tot.040 file=6 line=solid co2lor=1 symbol=% legend='IET-6'
cplot time bur-co2-tot.040 file=7 line=solid co2lor=9 symbol=_C legend='IET-7'
legend,lr
*
title,MELCOR Assessment: SNL IET Tests
vlabel,BUR Power in Dome (()w)
ulabel,Time (()s)
*limits 0.0,5.0 1.0,-1.0
plot time bur-power.040 file=1 line=solid color=2 symbol=! legend='IET-1'
cplot time bur-power.040 file=2 line=solid color=5 symbol=? legend='IET-1R'
cplot time bur-power.040 file=3 line=solid color=6 symbol=> legend='IET-3'
cplot time bur-power.040 file=4 line=solid color=101 symbol=^ legend='IET-4'
cplot time bur-power.040 file=5 line=solid color=141 symbol=_A legend='IET-5'
cplot time bur-power.040 file=6 line=solid color=1 symbol=% legend='IET-6'
cplot time bur-power.040 file=7 line=solid color=9 symbol=_C legend='IET-7'
legend,lr
*
title,MELCOR Assessment: SNL IET Tests
vlabel,BUR Energy in Dome (()J)
ulabel,Time (()s)
*limits 0.0,5.0 1.0,-1.0
plot time bur-energy.040 file=1 line=solid color=2 symbol=! legend='IET-1'
cplot time bur-energy.040 file=2 line=solid color=5 symbol=? legend='IET-1R'
cplot time bur-energy.040 file=3 line=solid color=6 symbol=> legend='IET-3'
cplot time bur-energy.040 file=4 line=solid color=101 symbol=^ legend='IET-4'
cplot time bur-energy.040 file=5 line=solid color=141 symbol=_A legend='IET-5'
cplot time bur-energy.040 file=6 line=solid color=1 symbol=% legend='IET-6'
cplot time bur-energy.040 file=7 line=solid color=9 symbol=_C legend='IET-7'
legend,lr
*
```

External Distribution:

U. S. Nuclear Regulatory Commission (18)
Attn: S. Acharya, NLS-372
Y. S. Chen, NLN-344
M. A. Cunningham, NLS-372
F. Eltawila, NLN-344
R. B. Foulds, NLN-344
S. Basu, NLN-344
C. Gingrich, NLN-344
C. G. Tinkler, NLN-344
L. E. Lancaster, NLS-372
R. O. Meyer, NLS-007
J. A. Mitchell, NLS-314
C. P. Ryder, NLS-372
L. Soffer, NLS-324
B. Sheron, NLS-007
J. A. Murphy, NLS-007
L. M. Shotkin, NLN-353
N. Lauben, NLN-353
R. Landry, NLN-344
Washington, DC 20555

S. Y. Chen
Argonne National Laboratory
9700 South Cass Avenue
Argonne, IL 60439

Battelle Columbus Laboratories (3)
Attn: P. Cybulskis
M. Carmel
R. S. Denning
505 King Avenue
Columbus, OH 43201

Brookhaven National Laboratory (2)
Attn: I. K. Madni
T. Pratt
Bldg. 130
32 Lewis
Upton, NY 11973

Idaho National Engineering Laboratory (5)
Attn: A. Brown
R. J. Dallman
D. W. Golden
S. E. Reed
G. W. Johnsen
EG&G Idaho
P. O. Box 1625
Idaho Falls, ID 83404

D. Jones
EI International
P. O. Box 50736
Idaho Falls, ID 83405

Electric Power Research Institute (3)
Attn: E. Fuller
R. N. Oehlberg
B. R. Sehgal
P. O. Box 10412
Palo Alto, CA 94303

Los Alamos National Laboratory (2)
Attn: B. E. Boyack, K-551
D. R. Liles, K-553
P. O. Box 1663
Los Alamos, NM 87545

Oak Ridge National Laboratory (11)
P. O. Box 2009
Oak Ridge, TN 37831-8057
Attn: S. R. Greene, MS-8057
R. H. Morris, MS-8057
S. E. Fisher, MS-8057
R. Sanders, MS-8057
T. L. Heatherly, MS-8057
S. A. Hodge, MS-8057
C. R. Hyman, MS-8057
B. W. Patton, MS-8057
D. B. Simpson, MS-8057
R. P. Taleyarkhan, MS-8057
M. L. Tobias, MS-8088

Andrzej Drozd
Nuclear Regulatory Commission
OWFN, MS 8E1
11555 Rockville Pike
Rockville, MD 20852

W. P. Barthold
Barthold & Associates
132 Seven Oaks Drive
Knoxville, TN 37922

K. C. Wagner
Science Applications Intl. Corp.
2109 Air Park Rd. SE
Albuquerque, NM 87106

Savannah River Laboratory (2)
Attn: B. DeWald
D. Allison
Westinghouse Savannah River Co.
Bldg. 773-41A
Aiken, SC 29808-0001

Westinghouse Hanford Co. (2)
Attn: D. Ogden
O. Wang
P. O. Box 1970
Richland, WA 99352

General Electric Company (3)
Knolls Atomic Pwer Laboratory
Attn: D. F. McMullan
G. H. Epstein
E. Mennard
Bldg. F3, Room 8
P. O. Box 1072
Schenectady, NY 12301-1072

Bettis Atomic Power Laboratory (3)
Attn: Mark Riley
Jow Semanchik
Vincent Baiamonte
P. O. Box 79
West Mifflin, PA 15122

Mohsen Khatib-Rahbar
Energy Research Inc.
P. O. Box 2034
Rockville, MD 20852

V. K. Dhir
2445 22nd Street
Santa Monica, CA 90403

R. Viskanta
Purdue University
Heat Transfer Laboratory
School of Mechanical Engineering
West Lafayette, IN 47907

Dr. Jim Gieseke
Battelle Memorial Institute
505 King Ave.
Columbus, Ohio 43201

M. A. Kenton
Gabor, Kenton & Associates
770 Pasquinelli Drive
Suite 426
Westmont, IL 60559

University of California (2)
Attn: W. H. Amarasooriya
T. Theofanous
ERC-CRSS
Santa Barbara, CA 93106

F. E. Haskin
University of New Mexico
Department of Chemical and Nuclear Engineering
Albuquerque, NM 87131

J. C. Lee
University of Michigan
Dept. of Nuclear Engineering
Cooley Building, North Campus
College of Engineering
Ann Arbor, MI 48109-2104

University of Wisconsin (2)
Dept. of Nuclear Engineering
Attn: M. L. Corradini
G. A. Moses
Engineering Research Building
1500 Johnson Drive
Madison, WI 53706

Ramu K. Sundaram
Manager, LOCA Analysis Group
Nuclear Engineering
Yankee Atomic Electric Company
580 Main Street
Bolton, MA 01740

John Bolin
CEGA
P. O. Box 85608
San Diego, CA 92186-9784

M. Plys
Fauske & Associates
16W070 West 83rd Street
Burr Ridge, IL 60521

Nick Trikouros
GPU Nuclear Corporation
One Upper Pond Road
Parsippany, NJ 07054

B. Raychaudhuri
Nebraska Public Power District
PRA & Engineering Review Group
P. O. Box 499
Columbus, NE 68601

Frank Elia
Stone & Webster Engineering Corp.
245 Summer Street
Boston, MA 02210

Samir S. Girgis
Atomic Energy of Canada Limited
CANDU Operations
Sheridan Park Research Community
Mississagua, Ontario
CANADA L5K1B2

Paul J. Fehrenbach
Chalk River Nuclear Laboratories
Fuel Engineering Branch, RSR Division
Chalk River, Ontario
CANADA KOJ1J0

Dr. Bohumír Kujal
Department of Reactor Technology
Nuclear Research Institute Řež plc
250 68 Řež
CZECH REPUBLIC

Andrej Mitro
Institute of Radioecology and Applied Nuclear Techniques
Garbiarska 2
P. O. Box A-41
040 61 Košice
CHECHOSLOVAKIA

Shih-Kuei Cheng
Institute of Nuclear Energy Research
P. O. Box 3-3
Lung-Tan, Taiwan
REPUBLIC OF CHINA

Technical Research Centre of Finland (3)
Nuclear Engineering Laboratory
Attn: Lasse Mattila
Ilona Lindholm
Esko Pekkarinen
P. O. Box 208 (Tekniikantie 4)
SF-002151 Espoo
FINLAND

Jorma V. Sandberg
Finnish Center Radiation & Nucl. Safety,
Dept. of Nuclear Safety
P. O. Box 268
SF-00101 Helsinki
FINLAND

Akihide Hidaka
Safety Research Department
Reactor Accident Studies and Modelling Branch
DRS/SEMAR
Cadarache Nuclear Center
13108 Saint-Paul-Lez-Durance Cedex
FRANCE

Dr. Lothar Wolf
Battelle Institute EV
AM Romerhof 35
D-6000
Frankfurt/Main90
GERMANY

Gesellschaft fur Anlagen- und Reaktorsicherheit (3)
Attn: Ulrich Erven
Walter Erdmann
Manfred Firnhaber
Schwertnergasse 1
D-5000 Koln 1
GERMANY

Kernforschungzentrum, Karlsruhe (3)
Attn: P. Hofmann
Werner Scholtyssek
Philipp Schmuck
P. O. Box 3640
D-7500 Karlsruhe 1
GERMANY

Udo Brockmeier
University of Bochum
Energietechnik
IB-4-128
D-4630 Bochum
GERMANY

György Gyenes
Central Research Institute for Physics
Institute for Atomic Energy Research
H-1525 Budapest, P. O. Box 49
HUNGARY

Joint Research Center
Commission of the European Communities
Attn: Alan Jones
Iain Shepherd
Safety Technology Institute
21020 Ispra (Va)
ITALY

Giovanni Saponaro
ENEA
Natl. Comm. for R&D of Nuclear Energy
Via Vitaliano Brancati, 48
00144 Rome
ITALY

Japan Atomic Energy Research Institute (3)
Attn: Kunihisa Soda
Jun Sugimoto
Norihiro Yamano
Tokai-mura, Naka-gun, Ibaraki-ken
319-11, JAPAN

Dr. Masayoshi Shiba, Director General
Institute of Nuclear Safety
Nuclear Power Engineering Corporation
Fujita Kankou Toranoman Bldg. 7F
3-17-1, Toranoman
Minato-Ku, Tokyo, 105
JAPAN

Masao Ogino
Mitsubishi Atomic Power Industries
4-1 Shibakoen 2-Chome
Minatoku Tokyo
JAPAN

Hidetoshi Okada
Nuclear Power Engineering Corporation
3-17-1, Toranomon Bldg. 5F
Minato-ku, Tokyo 105
JAPAN

Hirohide Oikawa
Toshiba Corporation
8, Shin-Sugita, Isogo-ku
Yokohama
JAPAN

Korea Atomic Energy Research Inst. (3)
Attn: Kun-Joong Yoo
Song-Won Cho
Dong-Ha Kim
P. O. Box 7, Daeduk Danji
Taejon
SOUTH KOREA 305-353

Jae Hong Park
Safety Assessment Department
Korea Atomic Energy Research Institute
P. O. Box 16, Daeduk-Danji
Taejon
SOUTH KOREA 305-353

Netherlands Energy Research Foundation (2)
Attn: Karel J. Brinkmann
E. J. Velema
P. O. Box 1
1755 ZG Petten
THE NETHERLANDS

Dr. Valery F. Strizhov
Russian Academy of Science
Institute of Nuclear Safety
Moscow, G. Tulsky, 52
113191, RUSSIA

Universidad Politecnica de Madrid (2)
Attn: Augustin Alonzo Santos
Francisco Martin
E.T.S. Ingenieros Industriales
Jose Gutierrez Abascal, 2
28006 Madrid
SPAIN

Juan Bagues
Consejo de Seguridad Nuclear
Justo Dorado, 11
28040, Madrid
SPAIN

Oddbjörn Sandervåg
Statens Kärnkraftinspektion
Swedish Nuclear Power Inspectorate
Box 27106 102 52 Stockholm
SWEDEN

L. Hammar, Director
Division of Research
Swedish Nuclear Power Inspectorate
Statens Karnkraftinspektion
Sehlstedtsgatan 11
Box 27106
S-102-50 Stockholm
SWEDEN

Swiss Federal Nuclear Safety Inspectorate (4)
Attn: S. Chakraborty
Sang Lung Chan
U. Schmocker
H. P. Isaak
CH-5232 Villigen-HSK
SWITZERLAND

United Kingdom Atomic Energy Agency (3)
Winfrith Technology Center
Attn: T. Haste
S. R. Kinnersley
D. W. Sweet
Winfrith, Dorchester, Dorset
UNITED KINGDOM, DTS 8DH

United Kingdom Atomic Energy Authority (2)
Safety & Reliability Directorate
Attn: M. I. Robertson
C. Wheatley
Wigshaw Lane, Culcheth, Warrington
Cheshire, WA3 4NE
UNITED KINGDOM

Geoffrey A. Brown
Manager, Safety and Accident Analysis
AEA Technology, (SRD)
Thomson House, Risley, Warrington
Cheshire, WA3 6AT
UNITED KINGDOM

Internal Distribution:

6400 N. R. Ortiz
6403 W. A. von Riesemann
6404 D. A. Powers
6412 A. L. Camp
6412 S. E. Dingman
6413 F. T. Harper
6414 J. E. Kelly
6418 S. L. Thompson (10)
6418 R. K. Cole
6418 A. A. Elsbernd
6418 L. N. Kmetyk (10)
6418 R. C. Smith
6418 D. S. Stuart
6418 R. M. Summers
6418 T. J. Tautges
6422 M. D. Allen
6422 T. K. Blanchat
6422 M. Pilch
6429 K. E. Washington
6429 D. C. Williams
7141 Technical Library (5)
7151 Technical Publications
7613-2 Document Processing for DOE/OSTI (10)
8523-2 Central Technical Files

☆ U.S. GOVERNMENT PRINTING OFFICE 1993—774-122/80261

DATE
FILMED
1/27/94
END